Interactions between Respiratory Syncytial Virus and Cell Surface Nucleolin

by

Cameron David Griffiths

A thesis submitted in partial fulfillment of the requirements for the degree of

Doctor of Philosophy

in

Virology

Department of Medical Microbiology and Immunology
University of Alberta

Abstract

Respiratory syncytial virus (RSV) is a ubiquitous respiratory pathogen that infects almost everyone by the age of two. In high-risk populations, such as infants and elderly individuals, RSV can infect the lower respiratory tract and cause severe symptoms, such as bronchiolitis or pneumonia. As a result, RSV is a leading cause of infant hospitalization. Despite the prevalence of RSV and the severity of infection, many questions remain about the basic biology of the virus. In particular, the RSV entry process has not been completely elucidated. In this thesis, I explored the RSV entry mechanism and how RSV interacts with a critical cell surface receptor, nucleolin (NCL). In normal cells, NCL is primarily found in the nucleus and the levels of NCL on the cell surface are very low, which is uncharacteristic for an important viral receptor. While examining cell surface NCL, I created a series of NCL truncation mutants and used them to characterize the NCL domains that are required for surface expression. I found that some domains of NCL were needed for surface expression, while the presence of others restricted surface expression. Nuclear trafficking of NCL was dispensable for surface expression. I also identified a novel phenomenon of NCL transferring between the surface of cells in a contact-dependent manner. To understand how NCL was acting as an RSV receptor, I measured the levels of NCL on the cell surface and surrounding viral particles during RSV entry. Using cellular fractionations and flow cytometry, I found that NCL translocated from the nucleus to the cell surface during the RSV entry process. I then used live cell imaging and imaging flow cytometry to show that the recruitment of NCL to the cell surface was focused around RSV particles, as viral fusion with the host cell plasma membrane occurred. Using inhibitors of cellular kinases and cell surface receptors, I found that both insulin-like growth factor (IGF1R) signaling and protein kinase C zeta isoform (PKCζ) activity played an important role in RSV entry. I then used imaging flow cytometry to show that PKCζ activity was a critical mediator

of the RSV-induced recruitment of NCL to the cell surface. Using an *in vitro* kinase assay, I found that IGF1R was an upstream regulator of PKCζ activity. Furthermore, I observed that stimulation of IGF1R caused an increase in cell surface NCL expression. In addition to initiating a signaling cascade during RSV entry, I characterized IGF1R as a novel RSV receptor that played a role in RSV binding to host cells. Taken together, my results identified a novel RSV entry mechanism, where RSV first binds to IGF1R. This activates IGF1R, which subsequently signals through PKCζ to induce cell surface trafficking of NCL. On the cell surface, NCL then accumulates around RSV particles, at which point viral fusion occurs.

Preface

A portion of the introduction (Chapter 1) of this thesis, specifically parts of sections 1.1 – 1.3, was previously published in a review article as Griffiths C., Drews S., Marchant D. "Respiratory Syncytial Virus: Infection, Detection, and New Options for Prevention and Treatment." Clin. Microbiol. Rev. 2017, 30(1): 277-319[1]. In this manuscript, all three authors were jointly responsible for planning sections to include, writing, and editing.

Portions of Chapter 4, specifically involving Figures 4.3 and 4.16, have been previously published as Bilawchuk L., Griffiths C., Jensen L., Elawar F., Marchant D. "The Susceptibility of Respiratory Syncytial Virus to Nucleolin Receptor Blocking and Antibody Neutralization Depends on the Method of Virus Purification." Viruses. 2017, 9(8): 207[2]. In this manuscript, I was jointly responsible for conceiving of the study, by developing the new purification technique for respiratory syncytial virus. Throughout the study, I performed purifications, as well as experiments involving imaging flow cytometry. I was also jointly responsible for writing and editing the manuscript.

Parts of Chapter 3 were completed with Aleks Stojic, an undergraduate student under my supervision. In particular, Aleks Stojic assisted with Figures 3.4a, 3.5b, and 3.9 – 3.14. In this section, I mentored Aleks Stojic and we worked together to plan, perform, and analyze experiments.

Chapters 4 and 5 are the product of a joint effort between me and the Marchant Lab manager, Leanne Bilawchuk. We worked closely together to plan, perform, and analyze almost all experiments in the project. As a result, Leanne Bilawchuk is responsible for performing Figures 4.2b, 4.3bcd, 4.6, 4.7, 5.2b, 5.5, 5.8, 5.9, and 5.11, where I had significant input into the experimental design. Furthermore, I performed the Figure 4.11 together with Leanne Bilawchuk. Figures 4.4 and 4.5 were performed without my direct input by Dr. David Marchant and Leanne Bilawchuk, respectively.

Acknowledgements

This thesis could not have been completed without the support, encouragement, and fashion-related guidance from my supervisor, David "The Big M" Marchant. I truly appreciated his open-door policy when it came to discussing results or planning new experiments. Throughout this project, I worked side by side with Leanne Bilawchuk. The endless conversations that we had about experimental details and how to approach problems transformed this thesis. I would also like to thank Lionel Jensen and Farah Elawar, who supported me both scientifically and by being great friends. I could not have asked for better lab mates. I would like to thank Aleks Stojic for being a fantastic mentee. Her strong work ethic and experimental ability made a real impact on my project. It is important that I also thank my committee members, Dr. Edan Foley and Dr. Tom Hobman. Their keen insight and helpful guidance provided new perspectives on my project and enabled me to become a more well-rounded scientist. I would also like to thank the Medical Microbiology and Immunology administrative staff, in particular Tabitha Vasquez and Debbie Doudiet, for their behind-the-scenes work. Throughout my project, they were always willing to help when I had administrative issues and they kept me accountable to program deadlines. There are numerous other past and present members of the Medical Microbiology and Immunology department that had a substantial impact during my project. I would like to thank Drs. Aja Rieger and Steve Ogg for their experimental guidance. I would like to thank Dr. Kim Ellison for her wisdom and expertise related to teaching. I would also like to thank David Fast, Brittany Umer, Ben Kostiuk, Brienne McKenzie, Adriana Airo, Connie Le, Chris Morcos, Ninad Mehta, Marianne Ngure, Anil Kumar, Adil Mohamed, Daniel Unterweger, Amanda Scott, and Dominic Golec for their support and experimental suggestions, along with the thoughtful discussions that we had. I will truly miss the Medical Microbiology and Immunology community. I want to acknowledge the financial support that I received from The Lung Association during my project. I would also like to thank the University of Alberta Fencing Club, in particular Filmer Chu, Anton Poon, and Janna Fung, for the years of fun and exercise we had together. I would like to thank my family and friends outside of academia. Namely, Dustin "Tintin" Brossart, Daniel "Laffy" Lafreniere, and Raymond Ma. I would also like to thank my parents for their endless patience and support. Finally, I would like to thank my wife, Tiffany Griffiths, who was my best friend and biggest cheerleader during this project. This work would not have been possible without her.

Table of Contents

List of Tables

List of Figures

List of Abbreviations

1HAEo-	– human airway epithelial cell line
AB	– acidic/basic domain of NCL
Ab	– antibody
ABC	– ATP-binding cassette
ADP	– adenosine diphosphate
AGC	– PKA, PKG, and PKC family of serine/threonine kinases
ANOVA	– analysis of variance
APM	– Alberta Proteomics and Mass Spectrometry
Arp2/3	– actin related proteins 2 & 3
ATP	– adenosine triphosphate
ATP1A1	– alpha-1 subunit of the Na+ K+-ATPase
BSA	– bovine serum albumin
C	– conserved domain of PKC
Cas9	– CRISPR associated protein 9
CAV1	– caveolin 1
Cdc42	– cell division control protein 42 homolog
cDNA	– complementary DNA
CMV	– cytomegalovirus
CoA	– coenzyme A
CRISPR	– clustered regularly interspaced short palindromic repeats
CRM1	– chromosomal maintenance 1
CX3CR1	– CX3C chemokine receptor 1
CXCR4	– CXC chemokine receptor 4
DAMP	– damage associated molecular pattern
DAPI	– 4′,6-diamidino-2-phenylindole
DiD	–1,1'-Dioctadecyl-3,3,3',3'-Tetramethylindodicarbocyanine, 4-Chlorobenzenesulfonate Salt
DMEM	– Dulbecco's modified Eagles medium
DMSO	– dimethyl sulfoxide
DNA	– deoxyribonucleic acid

DTT – dithiothreitol
EDTA – ethylenediaminetetraacetic acid
EGF – epidermal growth factor
EGFR – epidermal growth factor receptor
EGTA – ethylene glycol-bis(2-aminoethylether)-N,N,N’,N’-tetraacetic acid
EM – emission filter
ER – endoplasmic reticulum
ErbB – avian erythroblastosis oncogene B homolog receptor family
ERK1/2 – extracellular signal-regulated kinase 1 & 2
EV – extracellular vesicle
EX – excitation laser
FACS – fluorescence activated cell sorting
FBS – fetal bovine serum
FGFR – fibroblast growth factor receptor family
Flow – flow cytometry
FPLC – fast protein liquid chromatography
FSC – forward scatter
FSC-A – forward scatter area
FSC-H – forward scatter height
GAB1 – GRB2-associated binder 1
GAR – glycine/arginine rich domain of NCL
GBF1 – Golgi-specific brefeldin A-resistance guanine nucleotide exchange factor 1
GDP – guanosine diphosphate
GE – gene end
GFP – green fluorescent protein
GPI – glycosylphosphatidylinositol
GRB2 – growth factor receptor binding protein 2
GS – gene start
GTP – guanosine triphosphate
HDGF – hepatoma-derived growth factor
HEK-293T – human embryonic kidney 293 cells with SV40 large T antigen

HeLa – Henrietta Lacks cells
HEp-2 – human epithelial 2 cell line (HeLa contaminant)
HEPES – 4-(2-hydroxyethyl)-1-piperazineethanesulfonic acid
HIV-1 – human immunodeficiency virus 1
HPRT – Hypoxanthine-guanine phosphoribosyltransferase
HRP – horseradish peroxidase
HSC70 – heat shock cognate 70
HSP70 – heat shock protein 70
HSP90 – heat shock protein 90
HSPG – heparan sulfate proteoglycan
ICAM-1 – intercellular adhesin molecule 1
ICC – immunocytochemistry
ICTV – International Committee on Taxonomy of Viruses
IDEAS – Image Data Exploration and Analysis Software
IFC – imaging flow cytometry
IGF1 – insulin-like growth factor 1
IGF1R – insulin-like growth factor 1 receptor
IgG – immunoglobulin G
IKK-β – inhibitor of nuclear factor kappa-B kinase beta subunit
IL – interleukin
IP – immunoprecipitation
IR – insulin receptor
IRS – insulin receptor substrate
IU – infectious units
IκBα – phosphorylates the inhibitor of kappa B alpha subunit
K_D – Dissociation constant
KIR – killer Ig-like receptor
KO – knockout
LM – light microscopy
LPS – lipopolysaccharide
mAb – monoclonal antibody

MAPK – mitogen-activated protein kinase
MARK2 – microtubule affinity regulating kinase 2
MEK1/2 – MAPK/ERK kinase 1 & 2
MEM – minimum essential medium
MFI – mean fluorescence intensity
MHC – major histocompatibility complex
MOSLB – modified oncogene science lysis buffer
mRNA – messenger RNA
mTORC2 – mammalian target of rapamycin complex 2
MVA – modified vaccinia Ankara
MyH9 – non-muscle myosin heavy chain 9
N.S. – non-significant
NCL – nucleolin
NES – nuclear export signal
NET – neutrophil extracellular trap
NF-κB – nuclear factor kappa-light-chain-enhancer of activated B cells
NGF – nerve growth factor
NHBE – primary normal human bronchial epithelial cells
NLS – nuclear localization signal
NT – NaCl and Tris buffer
pAb – polyclonal antibody
Par-3 – partitioning defective protein 3
Par-6 – partitioning defective protein 6
PARP1 – poly (ADP-ribose) polymerase 1
PB1 – Phox and Bem 1 domain
PBS – phosphate buffered saline
PCR – polymerase chain reaction
PDGF – platelet-derived growth factor
PDGFR – platelet-derived growth factor receptor family
PDPK1 – 3-phosphoinositide-dependent protein kinase 1
PEG – polyethylene glycol

PFA – paraformaldehyde

PI3K – phosphoinositide 3-kinase

PIP_3 – phosphatidylinositol-3, 4, 5-triphosphate

PKA – protein kinase A

PKC – protein kinase C

PKG – protein kinase G

qRT-PCR – quantitative reverse transcription polymerase chain reaction

Rac1 – Ras-related C3 botulinum toxin substrate 1

RACK1 – receptor for activated C kinase 1

Raf1 – rapidly accelerated fibrosarcoma

Ras – rat sarcoma protein

RIPA – radioimmunoprecipitation assay lysis buffer

RMS – root mean square

RNA – ribonucleic acid

RRM – RNA recognition motif of NCL

rRNA – ribosomal RNA

RSV – respiratory syncytial virus

RSV-F – RSV fusion protein

RSV-G – RSV attachment glycoprotein

RSV-L – RSV large polymerase protein

RSV-M – RSV matrix protein

RSV-M2-1 – RSV M2 open reading frame 1 protein

RSV-M2-2 – RSV M2 open reading frame 2 protein

RSV-N – RSV nucleoprotein

RSV-NS1 – RSV non-structural protein 1

RSV-NS2 – RSV non-structural protein 2

RSV-P – RSV phosphoprotein

RSV-SH – RSV small hydrophobic protein

RT – room temperature

RTK – receptor tyrosine kinase

SDF-1 – stromal cell-derived factor 1

SDS – sodium dodecyl sulfate

SDS-PAGE – SDS polyacrylamide gel electrophoresis

SHC – Src homology and collagen protein

SOD1 – Superoxide dismutase 1

SOS1 – son of sevenless 1

SSC-A – side scatter area

SV40 – simian virus 40

TAE – tris, acetic acid and EDTA buffer

TAM – Tyro-3, Axl, and Mer

TBS-T – tris-buffered saline with Tween

TE – tris and EDTA buffer

TfR – transferrin receptor

TGF-α – transforming growth factor alpha

TLR4 – toll-like receptor 4

TNFR – tumor necrosis factor receptor

TNFα – tumor necrosis factor alpha

Trk – tropomyosin receptor

UV – ultraviolet

V – variable domain of PKC

VEGF – vascular endothelial growth factor

VEGFR – vascular endothelial growth factor receptor family

VSV – vesicular stomatitis virus

WB – western blot

X-Gal – 5-bromo-4-chloro-3-indolyl-β-D-galactopyranoside

YT – yeast extract and tryptone buffer

Chapter 1: Introduction

1.1 What is Respiratory Syncytial Virus (RSV)?

1.1.1 RSV discovery

Respiratory syncytial virus (RSV) was discovered in 1955[3,4], and its impact on pediatric populations was subsequently realized[5]. In subsequent decades, the importance of RSV infection was recognized for the elderly population[6,7] and immunocompromised individuals[8]. The virus itself is named based on its preferential infection of the respiratory tract and its ability to cause infected cells in culture to fuse into large multinuclear syncytia[4]. However, the formation of syncytia *in vivo* is much less common and is usually only observed in the most severe cases[9].

RSV is an enveloped virus of the *Mononegavirales* order, meaning that it has a single-stranded negative-sense RNA genome. In 2015, the International Committee on Taxonomy of Viruses (ICTV) reclassified RSV out of the *Paramyxoviridae* family and created the brand new *Pneumoviridae* family[10]. In the process, RSV was also placed within the *Orthopneumovirus* genus and renamed *Human orthopneumovirus*. Phylogenetically, RSV is most closely related to other members of the *Orthopneumovirus* genus: *Bovine orthopneumovirus* (bovine RSV) and *Murine orthopneumovirus* (pneumonia virus of mice). The only other genus within the *Pneumoviridae* family is the *Metapneumovirus* genus.

RSV itself has only one serogroup, with two antigenic subtypes (A and B). The antigenic subgroups are differentiated based on the reactivity of monoclonal antibodies targeting the RSV attachment glycoprotein (RSV-G)[11,12]. RSV type A is typically more prevalent and replicates to higher titres within infected individuals[13-15]. However, RSV type B dominant seasons have also been reported[14].

1.1.2 Who is susceptible to RSV infection?

RSV is a ubiquitous pathogen that infects almost everyone by two years of age[16]; however, RSV infection does not grant lifelong immunity[17]. In healthy adults, RSV primarily infects the upper respiratory tract and causes symptoms indistinguishable from the common cold[18]. However, in high-risk populations, RSV is capable of spreading to the lower respiratory tract and causing more severe symptoms such as bronchiolitis or pneumonia[5].

The most well recognized risk factor for RSV infection is age. Children under 6 months of age are at high risk for severe RSV infection, and as a result, up to 2% of all infants will be hospitalized due to RSV infection[19]. One of the main reasons that young infants are at high risk for severe RSV infection is the relatively high surface area to volume ratio of developing airways. Since humans are born with almost all of their terminal bronchi[20], the airway diameter in young infants is comparatively much smaller than that of an adult. Therefore, infant airways are more prone to obstruction, which is a hallmark of severe RSV lower respiratory tract infection[9,21-23]. Other risk factors that increase the likelihood of severe RSV infection in infants include premature birth, low birthweight, overcrowding, exposure to smoke, evidence of asthma in the mother, and lower socio-economic status[24-28]. Infants with Down Syndrome or congenital defects in heart and/or lung structure are also at a higher risk[29].

The two other populations with increased susceptibility to RSV infection are immunocompromised individuals[8] and those aged 65 years and older[6]. In elderly populations, RSV is one of the most prevalent causes of influenza-like-illness and subsequent hospitalization[6,30]. The increased susceptibility of elderly individuals to severe RSV infection is likely related to a declining immune system and reduced RSV-specific antibody titres[31,32].

1.1.3 RSV transmission

1.1.3.1 RSV seasonality

The best data on worldwide RSV seasonality trends comes from a recent meta-analysis that combines data from 183 sites[33]. However, these data are still an accumulation of separate studies and are limited by different sampling and testing methodologies used at each site. To provide a more standardized surveillance program, the World Health Organization has recently examined the possibility of adding RSV surveillance to the existing worldwide influenza surveillance program[34]. Implementation of such a program is essential to understand the burden of RSV on society and to measure the impact of a vaccine or therapeutic, once one is released.

Each year, RSV infections around the world tend to concentrate during specific seasons. In temperate climates within the northern hemisphere, the RSV season coincides with the influenza season, with a peak in January or February[33]. However, the RSV season and the influenza season tend to be offset by 1-2 months, depending on the location[33]. In more tropical climates, the RSV season tends to start and end earlier, with a peak in September or October[33]. A similar trend occurs

in the southern hemisphere, however, the tropical RSV season peaks in March or April, while the temperate RSV season peaks in June or July[33]. In general, low temperatures and high humidity are correlated with increased RSV activity[33]. A possible reason for this temperature-dependence of RSV infections is that cold temperature reduces the host's nasal epithelial immune response (in the mouse model) and could potentially render individuals more susceptible to RSV infection[35].

1.1.3.2 Modes of transmission

RSV is typically transmitted from infected individuals to susceptible hosts via large droplets, direct contact, or fomite intermediates[36]. More recently, the potential for RSV transmission via aerosols in a hospital setting has also been described[37]. Outside of the body, RSV can survive for up to 6 hours on hard surfaces, or up to 30 min on hands[36]. However, the survival of RSV is temperature dependent, as RSV becomes less stable at higher temperatures[36,38]. This temperature dependence could be one of the reasons why RSV infections are more prevalent during winter months in temperate climates.

When encountering a susceptible host, RSV has been documented to infect through the nose or the eye, with a similar incubation period observed for either route of entry[39]. In these cases, RSV would initially replicate in the upper respiratory tract, then migrate to the lower respiratory tract in the case of more severe infections. Although the mechanism of RSV transmission from the upper to lower respiratory tract has not been fully defined, one possibility is that it occurs by sloughing of infected epithelial cells in the upper respiratory tract[40]. However, the report that RSV can be found in aerosols[37] opens the possibility of RSV directly reaching the lower respiratory tract, since inhaled droplets smaller than 5 μm in diameter are more likely to reach lower airways as opposed to impacting in the nose[41]. Initially replicating in the upper respiratory tract, then migrating to the lower tract, or directly infecting the lower respiratory tract are very different routes to a severe RSV infection and would have different implications for RSV prevention and treatment. Furthermore, due to differences in cell type and tissue temperature[35], there may be differences in the RSV life cycle when infecting the upper versus lower respiratory tract.

1.1.4 RSV burden of disease

Due to its prevalence, RSV causes a substantial burden of disease in pediatric populations. In the USA, RSV is the leading cause of infant hospitalization[42]. On a worldwide level, RSV infects about 33 million children under 5 years of age each year, causing approximately 3.2 million

hospitalizations and 118 000 deaths[43]. However, the majority of these deaths occur in developing countries, where the in-hospital case fatality rate is approximately 2%[43]. This is in comparison to industrialized countries where the case fatality rate in-hospital is less than 1%. However, RSV still causes a large financial burden in industrialized countries. In Canada, the estimated yearly cost of RSV infection in children to the health care system is $18 million[44]. In the USA this cost is much higher, as it is estimated to be over $600 million[45].

In adults over 65 years of age, the prevalence of RSV infection is much lower than in children, with approximately 1.5 million infections per year (0.67% of the population) in developed countries[46]. However, these infections are associated with a much higher hospitalization rate of 14.5% and a 1.6% case fatality rate[46]. On a global scale, RSV infection hospitalizes about 252 000 older adults, resulting in approximately 14 100 deaths[46].

The burden of disease due to RSV infection is not limited only to acute infections. There is growing evidence of an association between severe RSV infection in early childhood and subsequent asthma or chronic wheeze[47]. Furthermore, several birth cohort studies have found that severe RSV infection early in life correlates with an overall decreased in lung function through teenage years, into adulthood[48-50]. However, it remains to be determined if RSV itself is truly causing recurrent wheeze/asthma to appear later in life or if individuals who are prone to develop recurrent wheeze/asthma are more susceptible to severe RSV infection.

1.1.5 RSV treatments

The only approved antiviral drug for an ongoing RSV infection is ribavirin. However, questionable efficacy and teratogenicity concerns have resulted in it only being recommended for severe RSV infection in immunocompromised patients[51]. The only efficacious treatment available is a prophylactic, called palivizumab. Palivizumab is a humanized monoclonal antibody that targets the RSV fusion (RSV-F) protein[52]. When given to high-risk infants during the RSV season, palivizumab treatment results in a 50-75% reduction in hospitalizations, depending on the at-risk population[53]. However, due to a relatively short half-life, palivizumab must be given as monthly intramuscular injections to be effective[52]. Palivizumab is also very expensive, costing more than $10 000 USD per season to treat a single infant[54]. Therefore, palivizumab is typically only given to infants born prematurely (≤ 32 weeks gestation) or those with chronic lung disease or congenital heart disease[55]. However, palivizumab is extremely expensive. When the efficacy of palivizumab

and the hospitalization rate of high-risk infants are taken into account, palivizumab costs approximately $300 000 per hospitalization avoided[54]. By preventing severe RSV infections, palivizumab also substantially reduces the occurrence of wheezing during the first year of life[56], which supports the hypothesis of RSV being a causative agent of recurrent wheeze/asthma.

Due to the substantial burden of disease posed by RSV infection and the scarcity of efficacious treatments, significant effort has been made over the past decade to develop novel vaccines and antivirals[57]. The most common targets of antivirals in development are the RSV F protein, to prevent RSV entry into host cells, or the RSV large polymerase (L) protein, to inhibit viral transcription/replication. There are also numerous vaccine candidates in various stages of clinical development[58]. Some of the most promising vaccine candidates are derived from RSV-F, stabilized in the pre-fusion conformation[59]. Since there is a considerable number of potential RSV vaccines and therapeutics in the pipeline that target the RSV entry process, it is imperative that we have a comprehensive understanding of the basic biological questions underlying RSV entry.

1.2 RSV Biology

1.2.1 RSV virion structure

RSV is an enveloped negative-sense RNA virus with a 15.2 kb genome within a helical nucleocapsid[60]. Unlike other *Mononegavirales* members, RSV doesn't follow the rule of six; the need for a multiple of six nucleotides in the genome in order for the virus to replicate[61]. The virus itself is typically observed as a spherical shape with a diameter between 100 nm and 1 μm[62]. Asymmetric particles and filamentous species, capable of reaching several μm in length, have also been observed[62,63]. Both spherical and filamentous forms of RSV are infectious[64-66].

RSV is not a lytic virus and during infection new RSV particles bud from the surface of infected cells. However, the release of RSV particles is not efficient, and a large portion of RSV particles remain cell-associated[67]. Accumulating evidence has shown that RSV likely buds from the host cell surface in a filamentous form, with multiple genomes within each filament[64,67]. It has been proposed that over time, or during purification, the filaments lose their structure or pinch off into several spherical particles[62,67].

1.2.2 RSV proteins

The non-segmented negative-sense RNA genome of RSV contains 10 genes that encode 11 proteins[60] (**Figure 1.1**), three of which are transmembrane glycoproteins found in the envelope of the virion: fusion (F), glycoprotein (G) and small hydrophobic (SH). These glycoproteins are inserted in the viral membrane and form the first point of contact when RSV encounters a human cell. The G and SH proteins are not essential for infectivity in cell culture[68], however deletion of the G protein results in partial attenuation since it enhances attachment to host cells[69]. RSV-SH has been shown to assemble into pentamers and act as a pH-dependent ion channel[70], though no entry-related role has been ascribed to RSV-SH.

Figure 1.1 RSV genome organization. The negative sense RSV genome is shown in the order which genes are transcribed, from 3′ to 5′. Immune evasion genes are shown in orange, surface glycoprotein genes are in green, and genes encoding the replication complex and other structural proteins are shown in blue. The M2 gene has two open reading frames that encode M2-1 and M2-2 respectively.

Two other essential RSV structural proteins are the matrix (M) and nucleoprotein (N). RSV-M proteins line the underside of the viral envelope and play an important role in viral budding[71]. The amount of RSV-M within a virion also likely determines the shape, since large amounts of RSV-M are associated with tubular RSV particles, while spherical particles have less membrane associated RSV-M[63]. Oligomers of RSV-N bind to and encapsidate the RSV genome. Each RSV-N binds to 7 nucleotides of RSV RNA, forming a left-handed helical nucleocapsid[62,72]. However, the interaction between RSV-N and the genome is sequence non-specific and has been proposed to be able to shift up or down the RNA strand to enable the RSV polymerase to read the RSV genome without physically displacing the RSV-N protein from the strand. An ability for RSV-N protein to shift on the RSV strand could explain why unlike other members of the *Mononegavirales* order, RSV is not bound by the rule of six[61]. Transient unencapsidation of the RSV genome would also explain why adding more than 5 nucleotides to the 3′ end of the genome strongly inhibits RSV RNA synthesis[73]. In this case, the region near the 3′ terminus may be more transiently bound by

RSV-N, but adding more nucleotides 'buries' this sequence, making it difficult for the polymerase complex to bind.

Three non-structural RSV proteins that make up the polymerase complex are the large (L), phosphoprotein (P), and the first open reading frame of M2 (M2-1). RSV-L is an RNA-dependent RNA polymerase that functions to both transcribe RSV mRNAs and replicate full-length genomes/anti-genomes[74]. Like other viral RNA-dependent RNA polymerases, RSV-L lacks any proof-reading function. RSV-P is a highly phosphorylated protein that directly interacts with RSV-L to function as a polymerase co-factor[75]. Although not essential for polymerase activity, RSV-M2-1 plays an important role as an elongation factor that prevents premature polymerase termination[76]. RSV-M2-1 also functions as a connector between RSV-M and the viral genome during assembly and budding[63]. The second M2 open reading frame (M2-2) regulates the RSV polymerase switch from transcribing mRNAs to replicating full genomes/anti-genomes[77].

The final two RSV proteins are non-structural 1 (NS1) and non-structural 2 (NS2). These two proteins play semi-redundant roles in evading the host innate immune system. Specifically, NS1 and NS2 shut down the host interferon response by targeting the pathway at multiple points (reviewed in [78]). NS2 also plays a role in causing RSV-infected bronchial epithelial cells to slough into the airway lumen, which results in airway clogging and may impact RSV transmission to the lower respiratory tract[40]. The crystal structure of NS1 was recently solved, and the authors discovered a striking similarity between NS1 and RSV-M[79]. The authors then speculate that NS1 may be a result of an RSV-M duplication event followed by divergent evolution, since the regions of NS1 that are dissimilar from RSV-M are also essential for immune suppression[79]. Since both the NS1 and NS2 proteins are not present in other *Mononegavirales* members, it is possible that NS2 may have also arisen from a similar acquisition event.

1.2.3 RSV replication

Upon completion of entry, the contents of the infecting viral particle are released into the host cell cytoplasm. The viral replication complex then forms on internal cellular membranes[80] and consists of viral and certain host cell proteins[81]. The RSV-L, RSV-P, and RSV-M2-1 proteins, along with viral genomic RNA encapsidated by RSV-N protein, are carried in the particle and coalesce to form a replication complex. Host cell proteins are likely contributed by the autologous infected cell but may also be carried in the virus particle from the donor cell from the prior round of

replication[82]. Proteins involved in virus transcription must be carried in the virus particle to the target cell because RSV is a negative sense RNA virus and the genomic RNA alone is not infectious, unlike many positive-sense RNA viruses[83]. The RSV RNA-dependent RNA polymerase plays a dual role, capable of both transcribing viral mRNA transcripts and synthesizing full length, positive sense antigenomes[74].

The RSV genome contains non-coding regions in the 3′ and 5′ termini, called the leader and trailer regions, respectively. Within the 3′ leader sequence, the individual nucleotides important for both replication and transcription have been finely mapped using mutagenesis[74,84]. There is a great deal of similarity in the nucleotides needed for the polymerase to perform replication and transcription[28,55]. The leader sequence itself can be split into 3 regions going from 3′ to 5′: polymerase initiation site (nucleotides 1-15), the RSV-N encapsidation and elongation signal (nucleotides 16-34), and transcription signal (nucleotides 36-43)[84]. This provides support for a model where the polymerase must always initiate at the 3′ end, regardless of whether transcription or replication is taking place (as opposed to internal entry to a gene promoter site during transcription). The 5′ trailer region plays a role in inhibiting the formation of cellular stress granules during RSV replication[85]. When the trailer region is replicated into positive-sense RNA, the trailer complement is a powerful promoter, similar to the leader region, which drives replication of antigenomes back into negative-sense genomes[86].

During viral transcription, the polymerase complex starts from the 3′ terminus. It then sequentially transcribes each of the individual viral genes from their own promoters called gene start (GS) sequences, with transcription ending at the gene end (GE) sequence. This occurs in a serial stop-start fashion where the polymerase scans the intergenic sequence after a GE signal, before initiating transcription on the next GS signal[87,88]. Similar to host mRNAs, the viral transcripts are capped and polyadenylated before release. The host cell ribosome complex then translates proteins from the viral mRNA transcripts as they would translate cellular mRNAs. After an accumulation of viral proteins occurs and through a not completely elucidated mechanism, likely involving the RSV-M2-2 protein[77], the viral polymerase switches from transcribing individual genes to replicating full length, encapsidated antigenomes where the polymerase is no longer directed by GS and GE signals. Using the trailer complement as a promoter, the RSV polymerase complex

then replicates the antigenomes into full length negative-sense genomes, for viral assembly and release[86].

The RNA-dependent replication cycle of RSV lacks a proofreading mechanism, which means that incorrect bases introduced by the polymerase during replication become mutations. A study examining another *Mononegavirales* member, vesicular stomatitis virus (VSV), found that its RNA-dependent RNA polymerase has an average error rate of 2.5×10^{-4} to 3.8×10^{-4} errors per base pair[89]. Assuming that RSV has a similar mutation rate, each genome replication would have an average of 3 – 6 mutations incorporated. When taken into consideration that up to 150 viable RSV particles can be produced from a single infected cell[90], this would give a possible maximum of 900 mutant bases after infection of a single cell. However, the rate that each mutation takes hold in the RSV quasi-species is limited by the mutation's effect on viral fitness. This rapid mutational rate allows for the generation of a wide variety of single nucleotide polymorphisms in the RSV genome during a single round of RSV replication, which has the potential to alter experimental results. This also enables RSV to respond quickly to selective pressures such as vaccines or antivirals. For instance, RSV is capable of developing resistance to fusion inhibitors targeting RSV-F within 3 passages of the virus[91]. However, the resistant mutants are usually not as fit as the wildtype virus. For example, RSV overcomes the stabilizing effect of fusion inhibitors by mutating RSV-F to be less stable, though this instability has the downside of causing RSV-F to trigger prematurely[92].

1.3 RSV Entry

1.3.1 RSV-F

RSV-F is initially translated as a 70 kDa immature pro-protein (F_0), which is then N-glycosylated at 5 sites, for strain A2[93]. After translation, RSV-F is cleaved by furin-like proteases, in the *trans*-Golgi network, into three pieces, F_1, F_2, and p27[94]. The 27 amino acid fragment, p27, dissociates from the protein, while F_1 and F_2 attach using two disulphide bonds to create an RSV-F protomer[95]. Three RSV-F protomers come together to form the active trimer. The structure of RSV-F, along with its major antigenic sites, has been elucidated[96,97], and it bears a striking resemblance to other viral type I transmembrane fusion proteins, such as influenza hemagglutinin. Prior to fusion between the viral and cellular membranes, RSV-F exists as a "spring-loaded" trimer with the

fusion peptide buried within the protein[96]. RSV-F then mediates fusion between the viral envelope and the cellular membrane, making it essential for RSV infectivity[98].

Enveloped viruses require fusion proteins to overcome the "hydration force" that normally prevents the merging of the two opposing virus and host cell phospholipid membranes[99,100]. Membrane mixing permits the delivery of the viral capsid into the host cell due to the formation of a fusion pore. By the very nature of phospholipid bilayer mixing during fusion, the phospholipid constituents of the viral membrane, and any membrane-bound proteins, become interspersed throughout the fabric of the host cell membrane[99,100]. When RSV-F triggers, it undergoes a dramatic conformational shift to a prehairpin intermediate form, with the fusion peptide extended fully outward, presumably inserted into an adjacent membrane[101]. The insertion of the fusion peptide into the host cell membrane causes destabilization necessary to permit membrane mixing. The RSV-F conformational shift additionally forces the viral and host membranes into close contact. A successful fusion event would require the combined force of multiple RSV-F conformational shifts to overcome the "hydration force" and establish a fusion pore to permit the delivery of viral nucleocapsid into the cytoplasm.

After RSV-F triggers, it forms a highly stable post-fusion conformation, with the fusion peptide inserted into the membrane right beside the transmembrane domain[97]. Due to the meta-stable nature of pre-fusion RSV-F, the protein spontaneously triggers over time. Therefore, both pre-fusion and post-fusion RSV-F can be found in viral stocks[62]. This triggering is accelerated by heat, formaldehyde, or exposure to low molarity buffer (10mM)[102-104]. RSV-F triggering also alters the antigenic sites exposed on the surface of the protein. The dominant neutralizing site, Ø, is only present on the pre-fusion RSV-F conformation[96]. Based on the knowledge of the pre-fusion RSV-F structure, RSV-F mutants have been created that are stabilized in the pre-fusion conformation[59]. Currently in clinical trials, pre-fusion stabilized RSV-F mutants are leading vaccine candidates[58]. Interestingly, palivizumab binds to an antigenic site (site II), which is conserved between the pre-fusion and post-fusion RSV-F conformations[96,105].

1.3.2 RSV-G

RSV-G is the other major RSV glycoprotein involved in viral entry. Unlike RSV-F, the primary role of RSV-G is attachment to host cells[69], and it is not essential for RSV infection in cell culture[68]

or *in vivo*[106]. Although RSV-G is dispensable for infection in immortalized cells, the attachment protein plays an important role when RSV infects well-differentiated primary bronchial epithelial cells[106-108] and in the mouse model of RSV infection[106]. RSV-G itself is a type II transmembrane glycoprotein that has a molecular weight of 80 – 90 kDa, depending on the extent of O-linked glycosylation[109]. The extensive glycosylation of RSV-G accounts for approximately 60% of the mass of the protein[109]. The ectodomain of RSV-G contains a highly conserved central domain with 4 cysteine residues that form a noose shape, stabilized by disulphide bonds[110]. Two of the cystines are arranged in a CX3C motif, similar to that of fractalkine[111]. Adjacent to the conserved domain is a heparin-binding domain that mediates binding of RSV particles to heparan sulfate proteoglycans (HSPGs)[112]. Flanking the conserved domain and heparin binding domain are two heavily glycosylated mucin-like domains[109].

RSV-G is the most variable RSV protein, and differences in monoclonal antibodies binding to RSV-G is what differentiates the RSV antigenic subgroup A from B[11,12]. The highly variable nature of RSV-G is highlighted by the identification of two RSV strains with separate duplications in the C-terminal region of RSV-G[13,113]. RSV-G can also be expressed in an alternate open reading frame that begins at amino acid 48[114]. This truncated RSV-G lacks a portion of its transmembrane domain, and the remainder of the domain is proteolytically cleaved off[114,115]. The result is a soluble form of RSV-G that is secreted from infected cells[115] and is believed to play a role as a decoy for antibodies targeting RSV-G[116].

1.3.3 RSV receptors

In order to infect a host cell, a virus must first bind to and enter the target cell. Initial binding to the cell surface is mediated by receptors or attachment factors on the cell surface. These receptors and attachment factors are proteins, lipids, carbohydrates, or combinations thereof that are expressed by the host cell. Although both receptors and attachment factors bind to incoming viruses, they differ in that receptors play an active role in mediating viral entry, while attachment factors serve to enhance viral binding but do not play an active role. As defined by Fields Virology[60], a viral receptor must bind to the virus and perform at least one of three active roles: 1. Induce a conformational change in the virus or a viral protein, including triggering fusion itself. 2. Transmit a signal into the host cell that enhances viral entry/replication. 3. Guide the virus to an

endocytic route. When a virus interacts with multiple receptors, the first one contacted is referred to as the receptor, while all subsequent receptors contacted are referred to as co-receptors[60].

There have been many candidate cell surface receptors and attachment factors identified for RSV, including annexin II[117], CX3C chemokine receptor 1 (CX3CR1)[106,107,111,118], epidermal growth factor receptor (EGFR)[119-121], calcium-dependent lectins[117], toll-like receptor 4 (TLR4)[122-124], intercellular adhesion molecule 1 (ICAM-1)[125], nucleolin (NCL)[2,117,126-128], and HSPGs[112,129-131]. Some receptors, like EGFR, are purportedly used by only certain strains of RSV[119]. It is also interesting that of these receptors, annexin II, HSPGs, and C-type lectins (including surfactant proteins A and D, which are soluble and bind to RSV prior to cellular attachment) have been implicated in binding the carbohydrate-rich regions of the RSV-F and -G proteins. This is of particular importance to consider prior to experimentation because culturing RSV in different cell lines (Vero versus HEp-2) can alter the glycosylation patterns of RSV-F and -G, which in turn alters the infectivity both *in vitro* and *in vivo*[108,132,133]. None of the proposed RSV receptors so far have been directly characterized as a functional receptor, that promote RSV entry through one of the three mechanisms. Due to the large number of reported receptors, some likely work together to stabilize RSV attachment, transmit cellular signals, or trigger the RSV-F conformational shift. Alternatively, some receptors may play redundant roles depending on RSV strain or the cell type being infected.

In 2011, NCL was reported as an RSV receptor that binds directly to RSV-F[128]. Expression of human NCL on insect cells that are not normally infectable by RSV made them susceptible to infection[128]. Conversely, blocking the interaction between RSV-F and cell surface NCL using αNCL antibodies, recombinant NCL, or anti-NCL siRNA reduces RSV infectivity in cell culture and the mouse model of RSV infection[2,127,128]. Although NCL is a predominantly nucleolar protein, a small fraction can be found on the cell surface *in vitro*[134] and *in vivo*[135]. After the identification of NCL as an RSV receptor, a report by Holguera and colleagues supported the interaction[126]. However, this report showed that the interaction between RSV and NCL could be blocked by pre-treating the virus with heparin[126], which was not observed the original report identifying NCL as an RSV receptor[128]. The discrepancy between reports could be a result of using different RSV strains. Holguera *et al.* used the RSV Long strain[126], while Tayyari *et al.* used the A2 strain[128]. Aligning the amino acid sequences of the fusion proteins from these two strains reveals a 98.1 %

sequence identity. One of the few obvious differences is a charged arginine in the Long strain versus a serine in the A2 strain at position 213 of the RSV-F protein. Of note, this arginine is also present in RSV type B strains[96]. Since arginine is positively charged, it is more likely to bind the negatively charged heparin, compared to an uncharged serine residue. Furthermore, amino acid position 213 on RSV-F is located at the tip of the RSV-F protein, in site Ø[96], which is distal from the viral membrane and thus more likely to interact with a cellular receptor. A comparison of the results from these two papers[126,128] may therefore suggest that the NCL and heparin-binding sites on RSV-F are adjacent or overlapping, depending on the strain of the virus. Similar strain-specific interactions, dependent on only a few amino acids, have been observed between RSV-F and EGFR[119].

1.3.4 Mechanism of RSV fusion

During RSV entry, the viral particle first contacts the host cell surface by using viral envelope glycoproteins to bind cell surface receptors and attachment factors. This initial binding takes place on cholesterol-rich lipid rafts and removing cholesterol from the cell membrane blocks RSV entry[65,121,136]. RSV binding is followed by either pH-independent[137,138] fusion on the cell surface[64-66], or macropinocytosis and fusion in early endosomes prior to acidification[120,121,139] (**Figure 1.2a** and **b**). The ability of RSV-infected cells to fuse with neighbouring cells, forming syncytia, indicates that cell surface viral fusion can occur. However, this is not definitive evidence that cell surface fusion is the major route of entry. Surface fusion and macropinocytosis may be distinct RSV entry routes that each account for a proportion of productive infections. Alternatively, a combination of surface fusion and macropinocytosis could occur, where hemi-fusion (mixing of one layer of each phospholipid bilayer) occurs on the cell surface, followed by complete fusion and nucleocapsid delivery in endosomes, as suggested by San-Juan-Vergara and colleagues[65] (**Figure 1.2c**). A similar two-step viral fusion process, with a long hemi-fusion intermediate stage, has been described for human immunodeficiency virus 1 (HIV-1)[140]. Furthermore, studies of RSV entry are complicated by the possibility of macropinocytosis occurring after complete surface fusion. In this case, the RSV glycoproteins remaining on the surface after fusion would be endocytosed and appear in macropinosomes (**Figure 1.2a**). Regardless of the method of fusion, RSV surface proteins eventually proceed through the endocytic system and accumulate in perinuclear lysosomes[123,136]. One important aspect to note about the RSV entry process is the relatively long period of time RSV spends on the cell surface before entry by endocytosis/fusion

(20 – 60 min), especially when compared to influenza, which enters the nucleus within 5 minutes of binding[90,120,123,138].

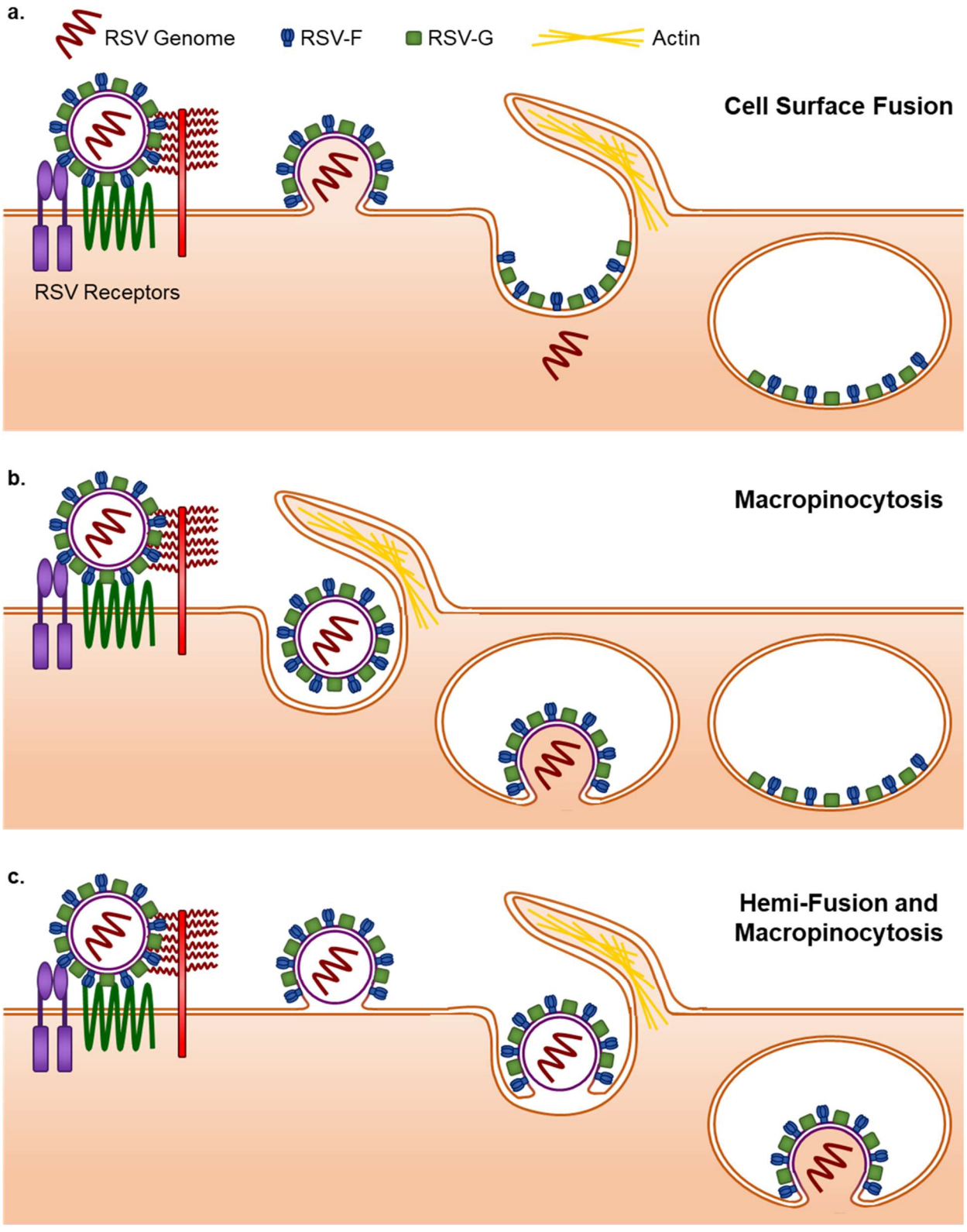

Figure 1.2 Schematic of possible RSV mechanisms of entry. RSV first binds to cell surface receptors, then one of three possible fusion mechanisms occurs. **a)** Complete cell surface fusion followed by macropinocytosis of RSV surface glycoproteins left on the surface. **b)** Macropinocytosis, with complete fusion within a macropinosome. **c)** Hemi-fusion on the cell surface followed by macropinocytosis and complete fusion within a macropinosome.

1.3.5 RSV-induced cell signals

Many viruses activate cellular signaling cascades to promote viral entry and subsequent replication (reviewed in [141]). RSV is no exception, as it potently activates multiple signaling cascades during the first few minutes after binding to a target cell. In particular, RSV activates both the p38 and extracellular signal-regulated kinase 1 & 2 (ERK1/2) mitogen-activated protein kinase (MAPK) pathways[123,142,143]. In addition to being activated during the RSV entry process, p38 and ERK1/2 have a second activation later during RSV replication[123,142,143]. Both p38 and ERK1/2 activity support RSV infection, since inhibiting either reduces RSV protein expression and progeny production[123,144,145]. The second ERK1/2 activation has been mechanistically shown to play a role in efficient assembly and budding of new RSV particles[146]. Phosphoinositide 3-kinase (PI3K) is another kinase that is activated by RSV binding/entry. However, unlike p38 and ERK, PI3K remains active up to 6 hours post-infection[147]. PI3K activity plays a role in RSV-induced macropinocytosis, and inhibiting PI3K activity effectively blocks RSV infection[120]. PI3K activity during RSV infection also supports viral replication by preventing premature apoptosis[147]. RSV entry also activates the protein kinase C (PKC) ζ and α isoforms, while the PKC β1, ε, and μ isoforms are activated later during infection[143,148]. Similar to p38 or ERK1/2, PKCδ is biphasically activated by RSV[143]. Pan-specific PKC inhibitors are effective at blocking RSV infection, and PKCα activity has been implicated in RSV entry[120,148,149]. Furthermore, PKCζ acts upstream of the RSV-induced early ERK1/2 activation[143]. However, the individual roles played by the other isoforms during RSV infection have not been thoroughly investigated.

Although RSV binding to host cells is known to activate several kinases, less is known about which cell surface receptors actually mediate the activation of these kinases. Besides NCL, the best characterized RSV receptors are EGFR[119-121], TLR4[122-124], CX3CR1[106,107,111,118], and HSPGs[112,129-131]. However, HSPGs are thought to predominantly be an attachment factor, rather than a functional receptor[101]. Furthermore, there is conflicting evidence if HSPGs are even present on the apical surface of bronchial epithelial cells[107,150], the primary host cell type infected by RSV[22,151].

RSV-induced cell signaling events play a central role in **Chapter 5**. Therefore, the potential roles of EGFR, TLR4, and CX3CR1 as RSV signaling receptors are explored below.

1.3.5.1 Epidermal growth factor receptor (EGFR)

EGFR is well known for its essential role during mammalian development and the numerous cell signaling roles it plays in human cancers (reviewed in [152]). In an RSV context, EGFR is activated by RSV within 15-30 min of binding[119,120]. Furthermore, EGFR is capable of binding directly to RSV-F and increasing the rate of fusion, though the strength of this interaction largely depends on the strain of RSV-F[119]. RSV activation of EGFR by RSV-F may also be indirect, through actions of the alpha-1 subunit of the Na^+ K^+-ATPase (ATP1A1)[121]. The RSV-induced EGFR activation has mainly been attributed to inducing macropinocytosis in the host cell, dependent on downstream PI3K activity[120,121]. EFGR activation by RSV has also been linked to decreasing apoptosis in infected cells[153], through downstream ERK1/2 activation, along with increasing mucin expression in the airway[119]. Reports of inhibiting EGFR signaling during RSV infection have shown conflicting results. The reports range from showing a drastic decrease in RSV infection [120], showing a moderate decrease[121], or showing no decrease at all[153]. These differences are likely due to the studies using different cell types. Alternatively, slight differences in RSV-F sequence within viral stocks, as small as 2 amino acids[119], can drastically alter the interaction between RSV-F and EGFR. Given the error-prone nature of viral RNA-dependent RNA-polymerases[89] it is possible that such small differences could arise during viral propagation.

1.3.5.2 Toll-like receptor 4 (TLR4)

TLR4 binding RSV-F was the first identification of a human pattern recognition receptor recognizing a viral protein[122]. The most well-known TLR4 agonist is lipopolysaccharide (LPS) from Gram-negative bacteria (reviewed in [154]). Furthermore, TLR4 activation is typically thought to induce a pro-inflammatory response[154]. To be activated efficiently by either LPS or RSV-F, TLR4 must first form a complex with CD14 and MD2[155]. In some cell types, such as macrophages, TLR4 stimulation by RSV-F causes the production of proinflammatory cytokines such as interleukin (IL) -6 and IL-8[122,156]. RSV-F stimulation of TLR4 in neutrophils causes a different proinflammatory response, where the neutrophils eject their genomic DNA to form neutrophil extracellular traps (NETs)[157]. These NETs serve to sequester and inactivate pathogens, including

RSV[157,158]. However, the viscous, DNA-rich nature of NETs can also exacerbate lower respiratory tract obstructions[158].

Conversely, TLR4 stimulation by RSV-F also activates p38[123] and nuclear factor kappa-light-chain-enhancer of activated B cells (NF-κB)[155,159]. These signaling molecules play an important role in RSV infection, since inhibiting the activity of either p38[123,144] or NF-κB[149] reduces RSV replication. Furthermore, blocking RSV binding to TLR4 also reduces infection[123,124]. This indicates that, in certain circumstances, TLR4 may act as an RSV signaling receptor.

1.3.5.3 CX3C chemokine receptor 1 (CX3CR1)

CX3CR1 is a G-protein coupled receptor for the chemokine, fractalkine[160]. Although CX3CR1 is typically expressed on immune cells, it has also been observed in the cilia of bronchial epithelial cells[106,161], including in primary pediatric lung tissue[118]. As an RSV receptor that binds RSV-G[111], CX3CR1 plays a redundant role to HSPGs during RSV infection in immortalized cells[106]. However, in cells lacking HSPGs, CX3CR1 plays an important attachment role for RSV[106,107,118]. This is of significance since it is unclear if HSPGs are expressed on the surface of bronchial epithelial cells in the lung[107,150]. When tested *in vivo*, mice deficient for CX3CR1 are significantly less susceptible to RSV infection[106]. RSV-G stimulation of CX3CR1 is capable of inducing leukocyte chemotaxis[111,162] and influencing the production of cytokines by airway epithelial cells[107]. These interactions indicate that RSV-G binding to CX3CR1 is capable of stimulating a cellular response, meaning that CX3CR1 has the potential to be an RSV signaling receptor.

1.3.5.4 Lipid rafts as signaling platforms

Lipid rafts are membrane microdomains that are enriched in sterols and sphingolipids[163]. Functionally, lipid rafts concentrate certain transmembrane proteins together through protein-protein and protein-lipid interactions[163]. Although lipid rafts are typically very small (10 – 200 nm in diameter), activation of receptors within the raft can cause multiple rafts to aggregate and form a signaling platform to potentiate a stronger signal[163,164]. During the entry process, RSV particles initially dock on lipid raft domains within the plasma membrane[65,121,136]. This is interesting since TLR4[165], EGFR[166,167], and insulin-like growth factor 1 receptor (IGF1R)[168] all localize to lipid rafts. IGF1R, as an RSV receptor, is explored in **Chapter 5**. The presence of these receptors in lipid rafts is also functionally critical for their efficient signaling[165,167,168]. For instance, if

cholesterol is depleted from the membrane, insulin-like growth factor 1 (IGF1) stimulation still causes IGF1R autophosphorylation, but downstream signaling events do not occur[168].

1.4 Nucleolin (NCL) Structure and Function

1.4.1 NCL structure

NCL is a highly abundant protein that was first described in 1973 in nucleoli purified from rat liver cells[169]. In the study, nucleolar proteins were analyzed by two-dimensional polyacrylamide gel electrophoresis[169]. After electrophoresis, the gel was divided into 3 regions (A, B, and C), and protein spots were named in decreasing order of electrophoretic mobility, with A1 being the fastest and C27 being the slowest. NCL was originally named protein C23, based on its slow mobility[169]. In 1986, C23 was renamed NCL, based on its nucleolar localization and to provide consistency in the literature between all of the proteins identified in other species that are homologous to C23[170].

Human NCL contains 710 amino acids and migrates at approximately 105 kDa due to its extensive phosphorylation[171]. The primary structure of NCL is comprised of three major domains (**Figure 1.3**). On the N-terminus are a series of highly acidic stretches[172], interspersed with basic residues, called the acidic/basic (AB) domain. The central globular domain contains 4 RNA recognition motifs (RRMs), that each fold into different secondary structures and preferentially bind different RNA sequences[173,174]. On the C-terminus is a domain with a series of arginine-glycine-glycine repeats, known as the glycine/arginine rich (GAR) domain[170]. A powerful bipartite nuclear localization signal (NLS) located between the AB domain and the first RRM causes NCL to be imported into the nucleus after translation, while interactions with nucleolar proteins and rRNA are the reason for nucleolar localization[175]. The AB and GAR domains are both highly involved in mediating protein-protein interactions[176-180]. The GAR domain is also able to non-specifically bind to nucleic acids and stabilize the interaction between the RRMs and RNA[181].

Figure 1.3 Primary structure of NCL. The primary structure of NCL is shown with the N-terminus on the left and the C-terminus on the right. Starting on the N-terminus is the disordered acidic/basic (AB) domain, followed by the bipartite nuclear localization signal (NLS), the central

globular domain with 4 RNA recognition motifs (RRMs), and the disordered glycine/arginine rich (GAR) domain.

1.4.2 NCL post-translational modifications

During protein maturation, NCL can undergo several post-translational modifications. The most well-characterized are NCL phosphorylation[182] and glycosylation[183,184], though methylation[170,185] and ADP ribosylation[186] have also been described. The methylation of NCL occurs extensively in the GAR domain and may influence the interaction between NCL and nucleic acids[187]. NCL has several O-glycosylation sites in the AB domain that may overlap and compete with phosphorylation sites[183]. NCL also has two verified N-glycosylation sites on N317 (RRM1) and N492 (RRM3), which arise through an unknown biosynthesis pathway[183]. The N-glycosylation impacts the ability of NCL to translocate to the cell surface[188,189] and to form oligomers[184].

The NCL AB domain is heavily phosphorylated by cyclin-dependent kinase 1[190] and casein kinase II[191]. However, NCL can also be phosphorylated by PKCζ[192] or casein kinase-like ectoprotein kinase[193]. NCL phosphorylation alters the cellular localization of the protein. For instance, phosphorylation during mitosis by cyclin-dependent kinase 1 blocks the NCL NLS and causes a primarily cytoplasmic localization[190], while PKCζ phosphorylation has been implicated in surface trafficking[176,192]. Besides cell cycle, NCL phosphorylation is also increased by stimulation with growth factors such as vascular endothelial growth factor (VEGF)[194], nerve growth factor (NGF)[192], or epidermal growth factor (EGF) and insulin together[195]. Furthermore, NCL phosphorylation is correlated with cell proliferation, since actively dividing[196] or cancerous[197] cells have higher levels of NCL phosphorylation compared to normal tissue cells.

1.4.3 NCL functions in the nucleus

Within the nucleus, NCL primarily localizes to the dense fibrillar component of nucleoli[198]. The dense fibrillar component is a nucleolar substructure that forms a shell around fibrillar centers, which are the site of rRNA transcription (reviewed in [199]). After transcription, rRNA is processed in the dense fibrillar component of the nucleoli[199]. Within the dense fibrillar component, NCL plays an essential role in rRNA processing, which is mediated by the AB domain[200]. Likely due to its role in ribosome biogenesis, NCL plays an essential role in cell survival. When NCL is knocked out, cells stop growing and begin apoptosis[201,202]. In the nucleus, NCL also mediates chromatin remodeling[177,203] and may play a functional role during mitosis[204]. In addition to RNA, NCL binds

strongly to guanosine-rich DNA sequences[205]. This DNA-binding characteristic of NCL has been utilized to develop a guanosine rich DNA aptamer (AS1411) that targets cell surface NCL[206]. AS1411 has completed several Phase I and Phase II clinical trials as an anti-cancer therapeutic, based on its ability to inhibit the functions of cell surface NCL[206,207]. The roles NCL plays in promoting cancer is further described in section 1.5.4.

1.4.4 NCL functions in the cytoplasm

Although NCL levels are lower in the cytoplasm than in the nucleus, NCL has been observed to actively shuttle between these two compartments[208]. The shuttling itself may indicate that NCL can act as a chaperone or influence the transport of other proteins within the cell. Within the cytoplasm, NCL utilizes its RNA binding capabilities to influence the stability of mRNAs. NCL plays a role in stabilizing some mRNA transcripts, such as *bcl-2* [209], *β-globin*[210], and *GADD45α*[211], by binding to the 3′ or 5′ untranslated region of the transcript. NCL also prevents translation of other mRNA transcripts, such as *p53*[212], by binding to the 5′ untranslated region.

1.5 Cell Surface NCL

NCL was first observed on the cell surface in 1981 as a phosphorylated protein with a molecular weight of 105 kDa[213]. This phosphorylated protein was subsequently confirmed to be NCL in 1990[214]. In 2003, NCL was first observed on the surface of cells *in vivo*[215]. However, the fraction of NCL on the cell surface is very small, even compared to the cytoplasmic fraction, which contains approximately 9 times more NCL[134]. The difference in amounts of NCL between the surface and the nucleus is so large that cell surface NCL cannot readily be observed in permeabilized cells using microscopy. To overcome this challenge, non-permeabilized cells are used to observe cell surface NCL[216]. However, cell surface NCL is dynamic and has a rapid rate of turnover[188,213]. On the cell surface, NCL is found in lipid rafts[217] and has been observed as a part of a large protein complex, including proteins implicated in cell signaling and proliferation[218].

1.5.1 Unconventional secretion of NCL

Unlike most proteins found on the cell surface[219], NCL does not have a signal peptide or transmembrane domain that mediates translation into the endoplasmic reticulum lumen for subsequent secretion. Like other unconventionally secreted proteins, the expression of NCL on the cell surface occurs independently of the Golgi apparatus[220]. One of the unanswered questions

regarding the translocation of NCL to the cell surface is how such a large, highly charged protein crosses the membrane. Other unconventionally secreted proteins rely on specialized pores or re-directing autophagy pathways[219], which may also occur in the case of NCL.

Despite many outstanding questions regarding the surface expression of NCL, there have been a few insights into the mechanism over the past 20 years. For instance, NCL interacting with heat shock cognate 70 (HSC70) is important for surface expression[176]. HSC70 is a chaperone protein that is highly similar to heat shock protein 70 (HSP70), however, HSC70 is constitutively expressed while HSP70 is typically expressed as a response to stress[221]. Interestingly, heat shock protein 90 (HSP90), which is functionally related to HSP70/HSC70, plays a critical role in the unconventional secretion of IL-1β[222]. In the study, IL-1β was shown to translocate across the membrane of a forming autophagosome prior to secretion, in a HSP90-dependent manner[222]. A similar mechanism may be utilized during the unconventional secretion of NCL to the cell surface, especially since cytoplasmic vesicles containing NCL have been observed fusing with the cell surface[220]. Furthermore, NCL has been observed in preparations of extracellular vesicles, however, it was not determined if NCL is on the inside or outside of these vesicles[223-225]. Conversely, other proteins may play a role in restricting the surface expression of NCL. For example, retinoblastoma protein is a tumor suppressor that binds to NCL and encourages strict nucleolar localization[226].

Although the levels of cell surface NCL are typically very low, external stimuli can induce recruitment of intracellular NCL to the cell surface[227]. Several stimuli are capable of inducing this recruitment, including fresh serum[220,228], VEGF[194,227,228], hepatoma-derived growth factor (HDGF)[229], pleiotrophin[228], or fibronectin[227]. Since phosphorylation of NCL by casein kinase II or PKCζ plays a functional role in NCL surface trafficking, one of these kinases may act downstream of the external stimuli to induce translocation of NCL to the cell surface. Furthermore, phosphorylated NCL has been observed on the cell surface[213], which supports phosphorylation as a signal to induce NCL surface expression. The translocation of NCL itself to the cell surface is an active process that relies on nonmuscle myosin heavy chain 9[176,227]. Furthermore, NCL closely associates with the actin cytoskeleton and inhibiting actin polymerization drastically disrupts the organization of NCL on the cell surface[220].

1.5.2 Functions of cell surface NCL

Although NCL was first observed on the cell surface almost 40 years ago, its function on the cell surface of normal cells is still not completely characterized. The main reason for this is that cell surface NCL has been mainly studied in the context of cancerous cells, where it is expressed to much higher levels[188]. Despite this, cell surface NCL is primarily believed to act as a scavenger receptor on normal cells. Binding of ligands to cell surface NCL causes NCL to form clusters on the surface, and the ligand is then internalized via endocytosis[180,188,215,230,231]. Antibodies targeting NCL cause similar clustering and are likewise internalized[220,232]. Cell surface NCL can bind to a wide variety of endogenous ligands including endostatin[180,233], urokinase-type plasminogen activator[231], hepatocyte growth factor[234], HDGF[229], P-selectin[235], factor J[236], low-density lipoproteins[214], midkine[230,237], and lactoferrin[238].

On the cell surface, NCL also plays a role in signal transduction[235,239-242]. Although NCL does not have any described kinase activities itself, it interacts with several cell surface signaling proteins that do have kinase activities, and NCL is thought to act as a signaling co-factor. NCL has been shown to bind to and play a signaling co-factor role with EGFR[240,243], urokinase plasminogen activator receptor[180], CXC chemokine receptor 4 (CXCR4)[179,242], low-density lipoprotein receptor-related protein[230], and several integrins[180,217,228]. Furthermore, ligand binding to cell surface NCL directly induces a calcium influx from the extracellular environment, indicating that cell surface NCL may play a role in calcium signaling[189].

1.5.3 Cell surface NCL as a pathogen receptor

In addition to being a cell surface receptor for RSV[128], NCL has been described as a receptor, co-receptor, or attachment factor for multiple other viruses. The viruses that bind to cell surface NCL include both enveloped viruses such as human parainfluenza virus type 3[244], influenza A virus[245], Crimean-Congo hemorrhagic fever virus[246], and HIV-1[247,248], as well as non-enveloped viruses such as group B coxsackievirus[249], adeno-associated virus type 2[250], and enterovirus 71[251]. Furthermore, some bacteria, such as *Francisella tularensis*[252] and enterohemorrhagic *Escherichia coli* O157:H7[253], also bind to cell surface NCL to initiate internalization (*F. tularensis*) or stabilize adhesion to the cell surface (*E. coli*).

There are several possible reasons why NCL is an attractive pathogen receptor. One reason could be the presence of the highly charged N-terminal domain with acidic stretches or the arginine-rich

C-terminal domain. Both of these domains are highly involved in protein-protein interactions with endogenous proteins[176-180], so it is reasonable that they could also bind proteins on the surface of invading pathogens. Another possible reason that NCL shows up frequently as a pathogen receptor is that it forms a complex with numerous cell surface proteins[179,180,217,218,228,230,242,243] that may be the primary receptor for the pathogen. In this case, NCL would act as a co-receptor that could enhance the formation of a receptor cluster underneath the bound pathogen. A final attractive property of NCL as a cell surface receptor for multiple pathogens is that ligation of cell surface NCL induces endocytosis[180,188,215,230,231]. This is pertinent because endocytosis is a commonly utilized entry pathway for pathogens that bypasses the cortical actin cytoskeleton and removes foreign antigen from the cell surface[60].

1.5.4 Cell surface NCL in cancer

The majority of research on cell surface NCL has been regarding the roles it plays in cancer. The main reason for this is that actively dividing cells express high levels of NCL on the cell surface, while quiescent cells express low or undetectable amounts[220]. Furthermore, several studies have shown a correlation between high levels of extranuclear NCL and poor clinical prognosis[194,228,240]. Cell surface NCL's functional role in cell transformation and tumor growth is likely due to the ligands it binds and its interaction with other cell surface proteins. For instance, growth factors and growth factor receptors (like EGFR) play well-characterized roles in cell transformation, especially when their regulation is altered by mutation[152].

Cell surface NCL has also been shown to play a functional role in angiogenesis. The formation of new blood vessels is a critical component to tumor growth, which is highlighted by its inclusion in the list of the original six hallmarks of cancer[254]. When examined *in vivo*, NCL is readily observed on the surface of tumor blood vessels but is not found on the surface of blood vessels in healthy tissues[215]. Furthermore, inhibiting cell surface NCL prevents tumor blood vessel formation *in vitro* and *in vivo*[227,255]. In addition to the growth of primary tumors, cell surface NCL also impacts the ability of transformed cells to metastasize and invade new tissues. Similar to angiogenesis, inhibiting cell surface NCL can also block tumor cell migration and colony formation *in vitro*[194,227,228,242,255]. NCL's direct or indirect interaction with the extracellular matrix[227], integrins[180,217,228], and cytoskeletal proteins[176,220] may play a role in metastasis and

angiogenesis, which both require active cellular movement. However, the role of cell surface NCL for angiogenesis during normal growth and development has not been determined.

Due to its functional role in cancer progression, targeting cell surface NCL is a promising anti-cancer therapeutic strategy. One cell surface NCL-targeting compound that has received particular attention is a DNA aptamer called AS1411, which is a guanosine-rich oligonucleotide, with the following sequence: 5′ – GGTGGTGGTGGTTGTGGTGGTGGTGG. Instead of the traditional DNA duplex structure, AS1411 forms a variety of quadruplex structures in solution[256]. AS1411 is internalized into cancer cells by macropinocytosis and subsequently increases the rate of macropinocytosis in a NCL-dependent manner[257]. By accumulating in cancer cells, AS1411 destabilizes *bcl-2* mRNA, which normally plays an anti-apoptotic role[209,258]. AS1411 may also cause more direct cytotoxicity when accumulated in cancer cells[206,258]. In humans, AS1411 has been through phase I and II clinical trials, with low toxicity[207]. However, response rates to AS1411 are very low, and the aptamer has a short half-life in plasma (1.71 hours)[207]. More recently, the NCL-targeting properties of AS1411 have been utilized to specifically deliver nanoparticles, oligonucleotides and small molecules into cancer cells[206]. Attaching fluorophores to AS1411 has also been used to image tumors *in vivo*[206].

1.6 Protein Kinase C (PKC) Signaling

The PKC family of kinases is a subgroup within the larger AGC group of serine/threonine kinases, which contains protein kinase A (PKA), protein kinase G (PKG), and PKC[259]. PKCs mediate a wide variety of cellular processes, including cellular differentiation, proliferation, and survival, as well as immune cell activation (reviewed in [260] and [261]). The PKC family itself contains nine genes, which can be divided into three subfamilies, called conventional, novel, and atypical. The division between each subfamily is based on structural similarity and sensitivity to activators. In **Chapter 5** of this thesis, I identified PKCζ as a critical kinase that mediates RSV-induced cell surface trafficking of NCL. Due to the importance of PKCζ for my thesis, I have included an introduction into PKCζ biology, and how it fits into the PKC family of kinases.

1.6.1 Conventional and novel PKC isoforms

The conventional PKCs were the first to be discovered, and the subfamily contains the alpha (α), beta (β), and gamma (γ) isoforms[262,263]. The next PKC subfamily to be discovered was the novel

PKCs, which contain the delta (δ), epsilon (ε), eta (η), and theta (θ) isoforms[264-267]. The final PKC subfamily to be discovered was the atypical PKCs, which contain the zeta (ζ)[265] and iota/lambda (ι/λ)[268,269] isoforms. ι is the isoform found in humans, while λ is found in mice. It is also worth noting that the PKC β[270] and δ[271] isoforms have additional splice variants, which expand the PKC family.

Structurally, conventional PKCs contain four conserved (C) domains, with five variable (V) domains in between the C domains and on either end[262]. The N-terminal half of the protein is a regulatory region, containing C1 and C2, while the C-terminal catalytic region contains C3 and C4. The V3 domain divides the regulatory and catalytic regions. The C1 domain contains two zinc finger-like regions and is responsible for binding to diacylglycerol or phorbol esters, which are the primary activators for conventional and novel PKCs[272]. On the N-terminal side of the C1 domain is a pseudosubstrate sequence that mimics an endogenous substrate, except it has an alanine in the position of the serine/threonine that would normally be phosphorylated[273]. The C2 domain binds to calcium as a secondary signal that mediates activation and membrane translocation[272]. The C3 domain binds ATP, while the C4 domain contains the catalytic active site[262,274]. The V3 domain acts as a hinge[274], allowing the protein to fold over and the pseudosubstrate to bind and inhibit the active site. Novel PKCs are very similar to conventional PKCs, except the C2-like domain in novel PKCs does not bind calcium, making this subfamily calcium insensitive[264]. Furthermore, the C1 and C2-like domains in novel PKCs are in reversed order compared to conventional PKCs[275]. Novel PKCs make up for this calcium insensitivity by binding to diacylglycerol with much higher affinity[276].

In order to activate, conventional and novel PKCs are first primed by phosphorylation events within the C4 domain. The activation loop, adjacent to the active site, is directly phosphorylated by 3-phosphoinositide-dependent protein kinase 1 (PDPK1)[277-279]. The other two important motifs for PKC activity are the turn motif and the hydrophobic motif, which are located near the C-terminus. These two sites are either autophosphorylated[277,278] or phosphorylated in a manner dependent on the mammalian target of rapamycin complex (mTORC2)[279,280]. Once primed, conventional PKCs are then activated by diacylglycerol/phorbol esters and calcium[272], while novel PKCs are activated by diacylglycerol/phorbol esters alone[264]. Diacylglycerol is a secondary messenger that is produced transiently in cells by phospholipase C, which activates conventional

and novel PKCs[261]. On the other hand, phorbol esters are synthetic or derived from plants and do not normally exist in mammalian cells[281]. As a result, mammalian cells lack a mechanism to break down phorbol esters. Therefore, phorbol ester treatment of cells leads to constitutive activation of conventional and novel PKCs, which results in their proteolytic degradation[282]. Phorbol esters are an effective secondary stimulus (after an initiating carcinogen) to cause spontaneous tumor formation in mice[281,283]. This led to the hypothesis that conventional and novel PKCs are oncogenes. However, more recent evidence has shown that conventional and novel PKCs are actually tumor suppressors, and it is their eventual degradation that results in tumor formation due to phorbol ester treatment[261,284].

1.6.2 Atypical PKC isoforms

The catalytic region of atypical PKC isoforms is structurally similar to that which is found in conventional and novel PKCs, however, the regulatory region is substantially different (**Figure 1.4**). The atypical PKC C1-like domain contains only one zinc finger and does not bind to diacylglycerol or phorbol esters[285]. As a result, prolonged phorbol ester treatment does not cause atypical PKCs to degrade. Atypical PKCs also lack a C2 domain, making them calcium insensitive[285]. Instead, these isoforms have a Phox and Bem 1 (PB1) domain, near the N-terminus, that mediates binding to other proteins containing a PB1 domain[286,287], including forming homodimers. In humans, PKCι is widely expressed in many tissues, while PKCζ is expressed at low levels in most tissues, except the lungs, brain, and testes, where it is expressed at high levels[288].

Figure 1.4 Primary structure atypical PKC isoforms. The primary structure of atypical PKC isoforms is shown, with the N-terminus on the left and the C-terminus on the right. The N-terminal regulatory region consists of a Phox and Bem 1 (PB1) domain, a pseudosubstrate sequence (PS), and a C1-like domain. The C-terminal catalytic region contains an ATP-binding C3 domain and a C4 catalytic domain. The protein is capable of folding at the hinge, so that the pseudosubstrate can bind to and inhibit the C4 domain (**Figure 1.5a**).

One PKC isoform that is activated by RSV during the entry process is PKCζ[143], which is consistent with its high expression in lung tissue[288]. Like other PKCs, PKCζ has a pseudosubstrate sequence adjacent to its C1-like domain that intramolecularly binds to the catalytic site and inhibits kinase

activity[286] (**Figure 1.5a**). However, the resting activity of purified PKCζ is about 40 times lower than that of purified conventional PKCs, which is attributed to more efficient inhibition by the PKCζ pseudosubstrate[286,289]. Like other PKCs, the PKCζ C1-like domain plays a role in regulating kinase activity[286]. However, it also contains non-classical NLS and nuclear export signal (NES) sequences for nuclear shuttling[290]. Nuclear accumulation of PKCζ is regulated simultaneously with activation, in that the NLS sequence is masked when the pseudosubstrate is bound to the active site and becomes unmasked when the pseudosubstrate leaves the active site[290]. Like conventional and novel PKCs, PKCζ can be phosphorylated in its activation loop (threonine 410) and turn motif (threonine 560)[289]. However, the PKCζ hydrophobic motif has a phospho-mimetic glutamate occupying the phosphorylation site. As a result, PKCζ only needs to be phosphorylated at two sites (410 and 560) to be primed for activity[289].

1.6.3 PKCζ activation and regulation

PKCζ activation typically occurs as a downstream response to the ligation of immune receptors or growth factor receptors. Regarding immune receptors, stimulation of CXCR4 with stromal cell-derived factor 1 (SDF-1)[291], tumor necrosis factor receptor (TNFR) with tumor necrosis factor alpha (TNFα)[292] or TLR4 with LPS[293] all activate PKCζ. Treating cells with growth factors such as EGF[294], IGF1[295,296], insulin[297], VEGF[298], platelet-derived growth factor (PDGF)[299], or NGF[192] also increases PKCζ activity.

PKCζ threonine 560 is co-translationally phosphorylated by mTORC2, meaning that PKCζ in resting cells is already phosphorylated at one of the two required sites (Thr 410 and Thr 560)[289]. Therefore, PKCζ activity has typically been described to be regulated by threonine 410 phosphorylation by PDPK1, which occurs downstream of PI3K[300,301]. However, a recent report has shown that about 50% of PKCζ is phosphorylated at both sites in resting cells[289]. Combined with previous evidence, this has provided a PI3K independent model of PKCζ activity, where PKCζ activity is instead determined by protein binding partners, which stabilize PKCζ in a conformation with the pseudosubstrate domain away from the catalytic site[286,287] (**Figure 1.5b**). Partitioning defective protein-6 (Par-6) and p62 (also known as Sequestosome-1 or zeta interacting protein) are both PB1 containing proteins that activate PKCζ when bound[286,287,302]. However, Par-6 is more effective than p62 at stabilizing PKCζ in an active conformation[287], which provides evidence that the scaffolding protein bound to PKCζ can determine the strength of the subsequent

signal. Furthermore, other signaling proteins also join the PKCζ scaffolding complex to enhance signaling capabilities. For instance, PKCζ bound by Par-6 also recruits small GTPases, called Ras-related C3 botulinum toxin substrate 1 (Rac1) and cell division control protein 42 homolog (Cdc42), to influence cellular polarity[303,304]. Scaffolding proteins also have the ability to sequester PKCζ away from certain substrates to preferentially phosphorylate others. After insulin or IGF1 stimulation, phosphorylated insulin receptor substrate 1 (IRS-1) forms a complex with p62 and PKCζ[287,305]. The formation of this complex reduces PKCζ-mediated phosphorylation of microtubule affinity regulating kinase 2 (MARK2)[287] and increases phosphorylation of vimentin[305].

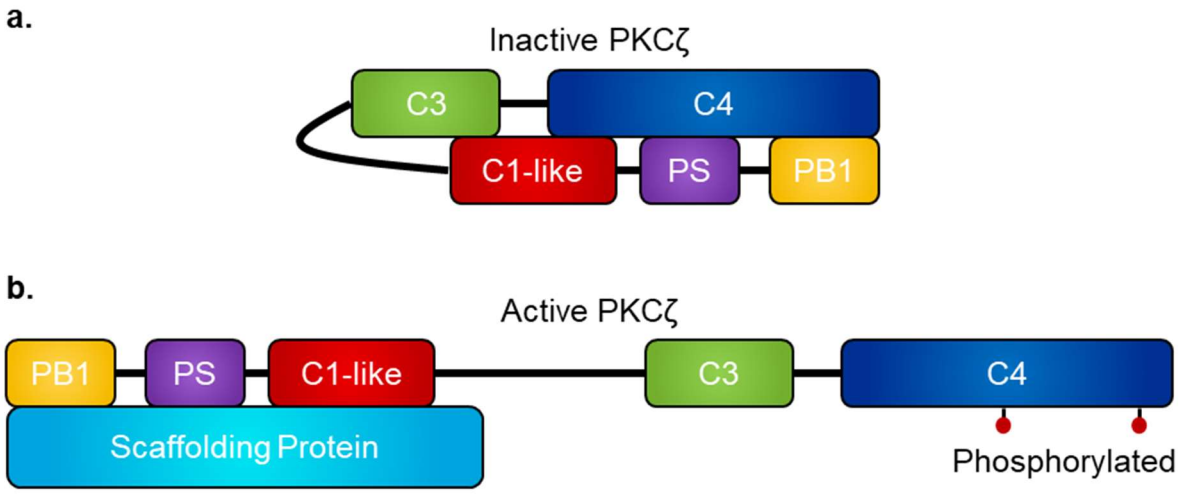

Figure 1.5 Schematic of PKCζ activation. a) Inactive PKCζ is shown, with the protein folded at the hinge. The pseudosubstrate sequence (PS) is bound to and inhibits the activity of the catalytic site in the C4 domain. **b)** Active PKCζ is shown, with the protein unfolded at the hinge, in an open conformation. The PS is away from the catalytic site, allowing for kinase activity. This active conformation of PKCζ is stabilized by phosphorylation at threonine residues 410 and 560, along with scaffolding proteins bound to the PB1 and/or C1-like domains.

Binding of acidic lipids, such as phosphatidyl serine, arachidonic acid, phosphatidic acid, cardiolipin, oleic acid, linoleic acid, linolenic acid, or phosphatidylinositol-3, 4, 5-triphosphate (PIP_3, produced by PI3K) to the PKCζ C1-like domain increases kinase activity by helping stabilize the active conformation[285,289,306]. Similarly, acidic proteins, such as 14-3-3, can also bind to PKCζ and enhance its activity[307]. In cells, the level of PKCζ activity is likely a result of both proteins scaffolds and the presence of acidic lipids. For instance, the ability of phosphatidyl serine

to increase PKCζ activity means that a PKCζ scaffold would have enhanced activity when adjacent to a membrane[289].

1.6.4 Downstream effects of PKCζ activity

Activated PKCζ influences several cellular pathways, with the most well-described role in influencing cellular polarity. In this regard, a protein complex including PKCζ, Par-6, Cdc42, and partitioning defective protein-3 (Par-3) plays a critical role in asymmetric cell division, tight junction formation, and maintenance of apical/basolateral polarity. The PKCζ/Par-6/Cdc42/Par-3 complex influences polarity by localizing to the apical or basolateral plasma membrane, then phosphorylating target proteins to exclude them from this membrane (reviewed in [308]). It is noteworthy that polarized bronchial epithelial cells are only susceptible to RSV infection from the apical surface[149], which opens up the possibility that PKCζ may play a role in this polarity specificity of infection. The other major role ascribed to PKCζ is being an upstream signaling regulator, capable of activating NF-κB[292] and ERK1/2[293,309]. PKCζ activates NF-κB by directly phosphorylating the inhibitor of nuclear factor kappa-B kinase beta subunit (IKK-β)[292], which in turn phosphorylates the inhibitor of kappa B alpha subunit (IκBα), freeing NF-κB to enter the nucleus and act as a transcription factor. When activating ERK1/2, PKCζ bypasses the rat sarcoma protein (Ras) and rapidly accelerated fibrosarcoma protein 1 (Raf1), to directly phosphorylate the mitogen-activated protein kinase kinase, MEK1/2 (MAPK/ERK kinase 1 & 2)[293,309], which is directly upstream of ERK1/2. PKCζ activity is also capable of mediating cellular differentiation[305]. In connection with my project, PKCζ has been observed to enter the nucleus and directly phosphorylate NCL on a serine residue[192]. Furthermore, knocking down the expression of PKCζ or treating cells with a non-specific protein kinase inhibitor both reduce the surface expression of NCL[176].

1.7 Growth Factor Receptors

Humans have 58 identified receptor tyrosine kinases (RTKs), that can be divided into 20 families[310]. Each family is grouped based on similar structure and specificity for related ligands. Notable families include the avian erythroblastosis oncogene B homolog (ErbB, which includes EGFR) family, the insulin receptor family (which includes IGF1R), the vascular endothelial growth factor receptor (VEGFR) family, the platelet-derived growth factor receptor (PDGFR)

family, the fibroblast growth factor receptor (FGFR) family, and the tropomyosin receptor kinase (Trk, which binds NGF) family. All RTKs share a similar structure, with an extracellular ligand-binding domain, a single transmembrane pass, a juxtamembrane regulatory segment, a tyrosine kinase domain, and a C-terminal tail[310]. In **Chapter 5** of this thesis, I described a novel role of IGF1R as an RSV receptor. The only other RTK described as an RSV receptor is EGFR[119-121]. Therefore, an introduction into some of the similarities and differences between EGFR and IGF1R activation and signaling is included.

1.7.1 Epidermal growth factor receptor (EGFR)

EGFR, also known as ErbB1, is an RTK of the ErbB family, which includes three other members (ErbB2-4)[310]. In its inactive state, EGFR exists as a single-chain monomer on the cell surface[311]. The extracellular region of EGFR is responsible for ligand binding and initiating dimerization[310,311]. EGF is the best-described ligand for EGFR, however, numerous other ligands have been described, including tumor growth factor alpha (TGF-α), amphiregulin, epiregulin, betacellulin, heparin-binding EGF-like growth factor, and epigen[312]. Upon ligand binding, EGFR forms a homodimer or heterodimer with another ErbB family member[152,311]. During dimerization, the tyrosine kinase domains form an asymmetric dimer, where the C-terminal lobe of one domain binds to the N-terminal lobe of the other domain, which results in the transactivation of the dimer[313].

Once activated, EGFR is capable of initiating several kinase cascades, resulting in a plethora of cellular responses, including proliferation, survival, and differentiation[152,314]. The two most well-described downstream pathways of EGFR are Ras/Raf/MEK/ERK and PI3K/Akt[152,310]. However, EGFR stimulation also activates other signaling pathways, such as Src[315] and PKCζ[294], through less well-defined mechanisms. To activate the Ras pathway, growth factor receptor binding protein 2 (GRB2) and Src homology and collagen (SHC) are both recruited to activated EGFR[316], which directly phosphorylates SHC[317]. SHC then binds to GRB2, and son of sevenless 1 (SOS1) is recruited to GRB2[318]. SOS1 switches the GDP in Ras for a GTP, which activates Ras[318]. Ras then recruits Raf1 to the membrane[166], where it is activated and subsequently activates MEK1/2 via phosphorylation[319]. This is then followed by MEK1/2 activating ERK1/2[319]. Similar to Ras, activation of PI3K by EGFR begins with GRB2 binding to activated EGFR. GRB2-associated binder 1 (GAB1) binds to GRB2, then subsequently recruits and activates PI3K[320]. Active PI3K

then catalyzes the formation of PIP_3, which activates PDPK1 and its downstream substrate, Akt[321,322].

Under normal circumstances, EGFR signaling plays essential roles during mammalian development[323]. However, dysregulation of EGFR signaling is associated with uncontrolled proliferation and development of cancer[152]. As a result, numerous EGFR inhibitors have been tested as anti-cancer therapies[152]. When identified as an RSV signaling receptor, the PI3K pathway was described to be involved in RSV entry via macropinocytosis[120], as described in section 1.3.4.

1.7.2 Insulin-like growth factor receptor (IGF1R)

IGF1R is an RTK that is closely related to the insulin-like growth factor 2 receptor (IGF2R) and the insulin receptor (IR)[310]. IGF1R and EGFR have several structural and functional similarities, allowing the two receptors to form heterodimers in some cancers[324]. However, unlike EGFR, IGF1R is proteolytically cleaved during maturation into an α (ligand binding) and β (tyrosine kinase) chain[325]. During maturation, the α and β chains re-attach via a disulphide bond[325]. Furthermore, two IGF1R monomers (or an IGF1R monomer and an IR monomer[326]) bind using a disulphide bond between the α chains, prior to ligand binding[325]. The primary ligand for IGF1R is IGF1, however, IGF2 and insulin are also able to bind with lower affinities[325,327]. Upon ligand binding, the internal IGF1R tyrosine kinase domains within the dimer phosphorylate each other at tyrosine 1135, followed by tyrosine 1131, then tyrosine 1136[328]. Tyrosine residues 1131, 1135, and 1136 are in the IGF1R activation loop (A-loop), which normally acts like a pseudosubstrate to block signaling, until ligand binding causes the tyrosine residues to become phosphorylated and leave the active site[328]. These phosphorylations shift IGF1R into an active form that has a 120-fold increased catalytic ability for binding and phosphorylating substrates[328].

Like EGFR, the primary signaling pathways downstream of IGF1R are Ras/Raf/MEK/ERK and PI3K[296,329]. To activate Ras, IGF1R can utilize SHC, GRB2, and SOS1, similar to EGFR[318,330,331]. Alternatively, IGF1R recruits and phosphorylates IRS proteins[332], which can take the place of SHC in the pathway leading to activated Ras[330,331]. As substrates of IGF1R, the IRS proteins play a multifunctional role and bind to PI3K, leading to its activation and downstream signaling[332]. Several other signaling pathways are also activated downstream of IGF1R, including PKCζ[295,296]. The downstream signaling cascade of IGF1R plays a critical role during mammalian development. As such, IGF1R knockout causes severe growth defects (45% of normal birthweight) and usually

results in neonatal lethality[333]. After development, most circulating IGF1 is produced in the liver, under the regulation of growth hormone[334]. However, some tissues are capable of producing IGF1 to induce local signaling cascades. For instance, when alveolar macrophages encounter IL-4, IL-13, or apoptotic cells, they produce IGF1, which subsequently binds to and stimulates bronchial epithelial cells[335]. This indicates that bronchial epithelial cells express functional IGF1R on the apical surface. Since IGF1R has similar downstream effects compared to EGFR, it has also gained substantial attention in the field of oncology[336].

1.8 Research Project Aims and Hypotheses

Despite the prevalence of RSV[16] and its importance as a human pathogen[19,42,43,46], important biological questions remain about the RSV life cycle. In particular, the relative roles of different RSV cell surface receptors and RSV-induced signaling events have not been fully elucidated. Answering these questions about the RSV entry process is both interesting from a biological standpoint and has the potential to open new drug targets for therapeutic intervention during infection. The main goal of this thesis was to investigate the interactions between RSV and cell surface NCL during RSV entry.

1.8.1 Chapter 3

The primary goal of **Chapter 3** was to examine the nature of cell surface NCL. This involved examining which domains of the protein play a role in surface expression and testing the hypothesis that NCL is tethered to the cell surface via palmitoylation. A secondary goal of this chapter was to characterize a novel phenomenon of NCL transferring from the surface of one cell to another.

1.8.2 Chapter 4

NCL is known to be an important RSV receptor[128], however, levels of NCL on the cell surface are low[134]. The main objective of **Chapter 4** was to test the hypothesis that NCL translocates from the nucleus to RSV particles on the cell surface during RSV entry. A secondary objective was to build a new laboratory stock of RSV and examine alternative methods of RSV purification.

1.8.3 Chapter 5

In **Chapter 4**, NCL was observed translocating to RSV particles during viral entry. The primary aim of **Chapter 5** was to test the hypothesis that RSV binding to a cell surface receptor sends a downstream signal required for this translocation of NCL. A secondary aim of the chapter was to characterize the interaction between RSV and a newly identified cell surface receptor, IGF1R.

Chapter 2: Materials and Methods

2.1 Buffers and Solutions

Table 2.1 Buffers and solutions prepared in lab.

Buffer	Purpose	Composition
ÄKTA protein binding buffer (A)	Purifying protein by FPLC	20 mM disodium phosphate, 100 mM sodium chloride, pH 7, 0.2 µm filtered
ÄKTA protein elution buffer (B)	Purifying protein by FPLC	0.1 M glycine-HCl, pH 2.7, 0.2 µm filtered
ÄKTA virus running buffer (A)	Purifying RSV by FPLC	NT buffer + 1% sucrose, pH 7.4, 0.2 µm filtered
ÄKTA virus wash buffer (B)	Purifying RSV by FPLC	1 N sodium hydroxide, 30% isopropanol, 0.2 µm filtered
FACS buffer	Flow cytometry wash buffer	5 mM EDTA, 25 mM HEPES, 1% FBS in PBS, pH 7
Kinase activity buffer	PKCζ *in vitro* kinase assay	10 µM ATP, 200 µg/mL CREBtide, 20 mM magnesium chloride, 0.1 mg/mL BSA, 50µM DTT, 40 mM Tris, pH 7.5
Laemmli sample buffer (6x)	SDS-PAGE	375 mM Tris pH 6.8, 12% SDS, 60% glycerol, 0.06% bromophenol blue
MOSLB	Cell lysis buffer	10 mM HEPES, 50 mM sodium pyrophosphate tetrabasic decahydrate, 50 mM sodium fluoride, 50 mM sodium chloride, 5 mM EDTA, 5 mM EGTA, 1 mM sodium orthovanadate, 0.5% Triton X-100, pH 7.4
NT buffer	Purifying/storing RSV	150 mM sodium chloride, 50 mM Tris, pH 7.4
PBS	Wash buffer	137 mM sodium chloride, 10 mM disodium phosphate, 2.7 mM potassium chloride, 1.8 mM monopotassium phosphate, pH 7.4

SDS-PAGE Tris-glycine running buffer	SDS-PAGE	25 mM Tris, 192 mM glycine, 0.1% SDS
TAE buffer	Agarose gel electrophoresis	40 mM Tris, 20 mM acetic acid, 1 mM EDTA, pH 8.0
TBS-T	Western blot wash buffer	25 mM Tris, 2 mM potassium chloride, 150 mM sodium chloride, 0.1% Tween, pH 7.4-7.6
TBTA (20x)	Palmitoylation assay click reaction	2 mM TBTA in tert-butanol:H_2O (4:1), must be in glass bottle
TCEP (250x)	Palmitoylation assay click reaction	250 mM TCEP-HCl in H_2O
TE buffer	Resuspending DNA	10 mM Tris, 1 mM EDTA, pH 8.0
Tris-glycine transfer buffer	SDS-PAGE	25 mM Tris, 192 mM glycine, 10% methanol, pH 8.1-8.4
Weak RIPA lysis buffer	Cell lysis buffer for palmitoylation assay	50 mM HEPES, 150 mM sodium chloride, 0.5% sodium-deoxycholate, 2 mM magnesium chloride, 0.5% Triton X-100 pH 7.4
X-Gal (100x)	β-galactosidase activity	50 mg/mL X-Gal in DMSO
Yellow substrate solution	β-galactosidase activity	3 mM potassium ferricyanide III, 3 mM potassium ferrocyanide trihydrate, 1 mM magnesium chloride hexahydrate, in PBS
YT agar	Growing RSV cDNA plasmids	85.56 mM sodium chloride, 8 g/L tryptone, 5 g/L yeast extract, 1.7 g/L bacto agar, pH 7.2
YT buffer	Growing RSV cDNA plasmids	85.56 mM sodium chloride, 8 g/L tryptone, 5 g/L yeast extract, pH 7.2

Abbreviations: yeast extract and tryptone (YT); phosphate buffered saline (PBS); Tris, acetic acid, and EDTA (TAE); ethylenediaminetetraacetic acid (EDTA); Tris and EDTA (TE); modified oncogene science lysis buffer (MOSLB); 4-

(2-hydroxyethyl)-1-piperazineethanesulfonic acid (HEPES); ethylene glycol-bis(2-aminoethylether)-*N,N,N',N'*-tetraacetic acid (EGTA); radioimmunoprecipitation assay (RIPA); sodium dodecyl sulfate (SDS); SDS polyacrylamide gel electrophoresis (SDS-PAGE); tris-buffered saline with Tween (TBS-T); Tris(benzyltriazolylmethyl)amine (TBTA); tris(2-carboxyethyl)phosphine (TCEP); NaCl and Tris (NT); 5-bromo-4-chloro-3-indolyl-β-D-galactopyranoside (X-Gal); dimethyl sulfoxide (DMSO); fetal bovine serum (FBS); fluorescence activated cell sorting (FACS); fast protein liquid chromatography (FPLC); adenosine triphosphate (ATP); bovine serum albumin (BSA); dithiothreitol (DTT).

2.2 Cell Culture

Primary normal human bronchial epithelial cells (NHBE), acquired as a generous gift from Dr. Harissios Vliagoftis (University of Alberta) and Dr. David Proud (University of Calgary), were grown in Lonza BEGM Bulletkit media (CC-3170) containing retinoic acid, passaged no more than four times. 1HAEo- cells[337] (gift from Dr. D. Gruenert, University of California) are a human airway epithelial cell line, that were previously immortalized using SV-40. Both 1HAEo- cells and HEK-293T cells[338] were grown in MEM with 10% heat-inactivated FBS. HeLa cells[339] were grown in DMEM, with L-glutamine, high glucose, sodium bicarbonate, and 10% heat-inactivated FBS. All mammalian cell types were grown in a humidified incubator at 37ºC, with 5% CO_2. Cell and RSV stocks were routinely screened for Mycoplasma using the MycoAlert mycoplasma detection kit (Lonza #LT07-118).

Cell stocks were stored in the vapor phase of a liquid nitrogen tank in normal growth media + 10% DMSO. Cells were thawed rapidly in a 37ºC water bath, then immediately diluted 1:10 in fresh growth media and seeded into a culture flask. The next day, the media on the cells was changed to remove the remaining DMSO. Before experimentation, cells were grown for a minimum of one week after thawing. To prevent overgrowth, cells were split 2-3 times per week before becoming confluent. During splitting, cells were washed with PBS, lifted using 0.25% trypsin-EDTA, and resuspended in growth media. Cells were then diluted between 1:5 and 1:8 into fresh growth media and re-seeded. During experiments, cells were counted using a hemacytometer prior to seeding in well plates.

2.3 RSV Reverse Genetics, Propagation, and Purification

The laboratory adapted RSV type-A2 strain expressing green fluorescent protein (rgRSV RW30[340]) was a gift from Dr. Mark Peeples (Nationwide Children's Hospital, Columbus, Ohio).

Full-length rgRSV RW30 cDNA was rescued to infectious virus in HeLa cells. Briefly, sub-confluent HeLa cells were transfected with rgRSV RW30, 4 support plasmids (RSV N, P, L, and M2-1), and T7 RNA polymerase (a gift from Benhur Lee; Addgene plasmid #65974, in place of vaccinia virus MVA-T7[341]) using *Trans*IT-HeLa MONSTER (Mirus Bio, MIR 2900). Successful rescue was confirmed by imaging GFP expression, using the EVOS FL Auto Cell Imaging System. During the initial passages post rescue, RSV yield was maximized by scraping infected cells, vortexing to release cell-associated virus, then centrifuging to pellet cell debris. After rescue, RSV was propagated in T75 flasks of HeLa cells and harvested as cell-free (clarified) RSV-conditioned DMEM with 10% FBS. To create purified RSV stocks, RSV was first precipitated from conditioned media by stirring with 10% polyethylene glycol (PEG)-6000 for 90 min on ice, then pelleted by centrifugation at 4300× g at 4ºC for 30 min. The pellets were resuspended in NT buffer and overlaid on a discontinuous sucrose gradient (35%, 45%, 60% sucrose in NT Buffer), as described previously[2]. The sucrose-purified RSV band was harvested after a 4 hour spin at 217,290× g at 4ºC, then aliquoted and stored in liquid nitrogen. All RSV infections were at an MOI of ~1 unless otherwise noted.

2.4 Plasmids and Cloning

The human NCL gene was cloned from a previously used[128] NCL construct in pCMV6-XL6 by PCR amplification, using Platinum Taq DNA Polymerase (Thermo Fisher #10966034). The NCL PCR product was then inserted into CT-GFP Fusion TOPO (Thermo Fisher #K482001), which adds green fluorescent protein (GFP) in frame to the C-terminus (in the pcDNA3.1 vector). The GFP only vector provided in the CT-GFP Fusion TOPO Kit was used as a negative control. The NCL ΔGAR, ΔAB, ΔABΔGAR, core, ΔABΔRRM12, and GAR mutants (**Figure 3.1**) were also created using PCR amplification, followed by insertion into the CT-GFP Fusion TOPO Kit. The NCL NLS reverse and C543S mutants were created using the QuikChange II Site Directed Mutagenesis Kit (Agilent #200523). NCL-FLAG was also created using the QuikChange II kit to replace the GFP tag with a FLAG tag. To create NCL C543S-FLAG, NCL was replaced with NCL C543S in the FLAG construct using restriction digest by NotI-HF (New England BioLabs #R3189S) and KpnI-HF (New England BioLabs #R3142S) enzymes, followed by ligation using the NEB Quick Ligation Kit (New England BioLabs #M2200S).

The original versions of each NCL-GFP construct (and NCL-FLAG) were lacking 6 amino acids on the C-terminus, compared to the NCL reference sequence. These 6 amino acids were added back to each construct by PCR using the NEB Q5 High-Fidelity DNA Polymerase (New England BioLabs #M0491S). The PCR fragments were then re-ligated using the NEB HiFi DNA Assembly Master Mix (New England BioLabs #E2621S). Using NCL-GFP as a template, the ΔRRM234, ΔRRM134, ΔRRM124, and ΔRRM123 constructs were created by PCR, using the NEB Q5 High-Fidelity DNA Polymerase, followed by ligation of the PCR products using the NEB HiFi DNA Assembly Master Mix. To create transferrin receptor-GFP (TfR-GFP), TfR-pHuji[342] was obtained as a gift from David Perrais (Addgene plasmid #61505). TfR was then amplified by PCR, using the NEB Q5 High-Fidelity DNA Polymerase, followed by ligation into the GFP vector (pcDNA3.1 backbone) using the NEB HiFi DNA Assembly Master Mix.

To create RSVF-Fc, RSV-F (A2 Long strain[343]) was first obtained as a gift from Dr. Thomas Grunwald (Ruhr-Universität Bochum, Germany). RSV-F was PCR amplified using Platinum Taq DNA Polymerase (including adding a 5′ HindIII cut site), then inserted into the pGEM T Easy vector (Promega #A1360) following the manufacturer's protocol. RSV-F was excised by restriction digest, using HindIII-HF (New England BioLabs #R3104S) and NotI-HF restriction enzymes. RSV-F was then ligated, using the NEB Quick Ligation Kit, into the pCMV6-AC-FC-S vector (Origene # PS100054), which had been digested using the same enzymes. To improve the pCMV6-AC-FC-S vector, the QuikChange II Site Directed Mutagenesis Kit was used to remove the stop codon in the original multiple cloning site and add an additional multiple cloning site to the 3′ end of the Fc region, thereby creating pCMV6-FCV2-S. To create Fc-RSVG, RSV-G was obtained as a gift from Dr. Thomas Grunwald[343]. RSV-G was then PCR amplified using the NEB Q5 High-Fidelity DNA Polymerase and ligated into pCMV6-FCV2-S (using the NEB Quick Ligation Kit), which had been digested by PmeI (New England BioLabs #R0560S). PmeI forms blunt ends after restriction digest, which allow ligation of PCR products. To improve ligation efficiency, the RSV-G PCR product ends were phosphorylated using T4 polynucleotide kinase (ThermoFisher # EK0031) and the FCV2 vector was dephosphorylated using the FastAP alkaline phosphatase (ThermoFisher #EF0654).

To create RSVΔG, rgRSV RW30 was digested using ApaI (New England BioLabs #R0114S) and SacII (New England BioLabs #R0157S) restriction enzymes. The ApaI and SacII cut sites are

found in the intergenic regions adjacent to the RSV-G gene. A section of the multiple cloning site in the pGEM T Easy vector was then amplified by PCR, using Platinum Taq DNA Polymerase. The PCR product was purified using the MinElute PCR purification kit (Qiagen #28004), then digested using ApaI and SacII. After digestion, the 35 bp fragment was ligated (using the NEB Quick Ligation Kit) into the rgRSV RW30 backbone, in the place of RSV-G. RSVΔG was rescued from cDNA into live virus as described above.

During cloning, plasmids were transformed into Top10 (ThermoFisher #C4040-10), XL-1 Blue (Agilent # 200236), or NEB-10β (New England BioLabs #C3019H) chemically competent cells. Bacteria were grown at 37ºC on Difco LB agar plates (BD #244520) or in Difco LB broth (BD # 244620), containing either 100 µg/mL ampicillin (Sigma #A0166-5G) or 50 µg/mL kanamycin (ThermoFisher #11815024). Due to the large plasmid size and to minimize random mutations, bacteria containing the RSV reverse genetics cDNA plasmids were instead grown sub-optimally at 30ºC on YT agar plates or in YT broth, supplemented with 100 µg/mL tetracycline. Stocks of transformed bacteria were stored in 20% glycerol at -80ºC. Plasmids were harvested from bacterial cultures using the QIAprep Spin Miniprep Kit (Qiagen #27106) or the HiSpeed Plasmid Maxi Kit (Qiagen #12662).

Agarose gel electrophoresis was used to check plasmid sizes and purify DNA fragments after restriction digest or PCR. Gels were made using 0.5-2% UltraPure Agarose (Invitrogen #16500-500) in TAE buffer and were run until the dye front reached ~2/3 of the way down the gel. DNA was stained using SYBR safe (Invitrogen #S33102) and gels were images using a BioRad GelDoc XR+ imager. When appropriate, gel slices were excised using a razor blade and DNA was extracted using the QIAEX II Gel Extraction Kit (Qiagen #20021). All DNA concentrations were determined using a NanoDrop 8000 spectrophotometer (ThermoFisher #ND-8000-GL). All plasmids were confirmed by sanger sequencing using the University of Alberta Applied Genomics Core.

2.5 Primers

Table 2.2 List of primers used. Overhanging bases are bold, mutations/insertions are underlined, and deletion borders are divided.

Name	Sequence	Resulting Plasmids
NCL-F	GCCATCATGGTGAAGCTCGCG	NCL-GFP, ΔGAR

NCL-R	GTGGCTTGTGGTCACCTCCTCCT	NCL-GFP, ΔAB, ΔABΔRRM12, GAR
NCLcore-F	**GCCATCATG**GTCAAAGAAGCACCTGG	ΔAB, ΔABΔGAR, Core
NCLcore-R	**G**GCCATTTTGGTTCTGGGGTACTT	Core
RRM4-R	**G**ACCTTCACCCTTAGGTTTGGCCC	ΔGAR, ΔABΔGAR
RRM3-F	**GCCATCATG**TCAAAAACTCTGGTTTT AAGCAACC	ΔABΔRRM12
GAR-F	**GCCATCATG**GGTGGCTTCGGGG	GAR
C543S-F	CTAAAGAAGCTTTAAATTCCTCTAATA AAAGGGAAATTGAGGG	C543S
C543S-R	CCCTCAATTTCCCTTTTATTAGAGGAA TTTAAAGCTTCTTTAG	C543S
NLSrev-1-F	CCTGTCAAAGAAGCACCTGGAAAAAA AAGGAAGGAAATGGCCAAAC	NLS reverse
NLSrev-1-R	GTTTGGCCATTTCCTTCCTTTTTTTTCC AGGTGCTTCTTTGACAGG	NLS reverse
NLSrev-2-F	GCTCCTGAAGCCAAGCAAAAGAAAG TGGAAGGCACAG	NLS reverse
NLSrev-2-R	CTGTGCCTTCCACTTTCTTTTGCTTGG CTTCAGGAGC	NLS reverse
FLAG-1-F	GGCGGCCGCTC|TAATGAATTAAACCCGC	NCL-FLAG
FLAG-1-R	GCGGGTTTAATTCATTA|GAGCGGCCGCC	NCL-FLAG
FLAG-2-F	GGCGGCCGCTCGATTACAAGGACGACGA TGACAAGTAATGAATTAAACCCGC	NCL-FLAG
FLAG-2-R	GCGGGTTTAATTCATTACTTGTCATCGTC GTCCTTGTAATCGAGCGGCCGCC	NCL-FLAG
NCL+6-F	**GGAAAGAAGACGAAGTTTGAA**GGGCA ATTCTGCAG	Adding 6 C-terminal amino acids to NCL
NCL+6-R	**TTCAAACTTCGTCTTCTTTCC**TTGTGGC TTGTGG	Adding 6 C-terminal amino acids to NCL

pcDNA-F	CAAGGCGAGTTACATGATC	All NCL+6 and ΔRRM constructs
pcDNA-R	GATCATGTAACTCGCCTTG	All NCL+6 and ΔRRM constructs
ΔRRMG-F	GGTGGCTTCGGG	ΔRRM234, ΔRRM134, ΔRRM124
ΔRRMA-R	TGTGCCTTCCACTTTC	ΔRRM134, ΔRRM124, ΔRRM123
RRM2A-F	**GAAAGTGGAAGGCACA**AAGAAAGAGC GAGATGC	ΔRRM134
RRM3A-F	**GAAAGTGGAAGGCACA**GGAAAGAATA GCACTTGGA	ΔRRM124
RRM4A-F	**GAAAGTGGAAGGCACA**GCCAGAAGCC AGC	ΔRRM123
RRM1G-R	**GACCCCCGAAGCCACC**ACTGTCTTTTC CTTTTGGTT	ΔRRM234
RRM2G-R	**GACCCCCGAAGCCACC**ACCTCTATAGT CTTGATTTTGAC	ΔRRM134
RRM3G-R	**GACCCCCGAAGCCACC**ATTAGGTGATC CCCTGG	ΔRRM124
TfR-F	**GTGGAATTGCCCTTGCCAT**CATGGATCA AGCTAGATCAG	TfR-GFP
TfR-R	**GGATATCTGCAGAATTG**CCCAAACTCAT TGTCAATGT	TfR-GFP
GFP-Topo-F	GATGGCAAGGGCAATTCC	TfR-GFP
GFP-Topo-R	GGGCAATTCTGCAGATATC	TfR-GFP
RSVF-F	**AAGCTT**CAGAACATCACCGAGGAGTTC	RSVF-Fc
RSVF-R	**G**GTTGGTGGTGCTCTTGCCG	RSVF-Fc
FCV2-1-F	CTTGTCACGAATTC|CGCGGCCGCTC	pCMV6-FCV2-S
FCV2-1-R	GAGCGGCCGCG|GAATTCGTGACAAG	pCMV6-FCV2-S
FCV2-2-F	CTTGTCACGAATTCCGTACGATATCCGCG GCCGCTCG	pCMV6-FCV2-S
FCV2-2-R	CGAGCGGCCGCGGATATCGTACGGAATT	pCMV6-FCV2-S

	CGTGACAAG	
FCV2-3-F	CCCGGACTCCGGGTAAGCTTGTTTAAACG GCCGGCCG	pCMV6-FCV2-S
FCV2-3-R	CGGCCGGCCGTTTAAACAAGCTTACCCGG AGTCCGGG	pCMV6-FCV2-S
RSVG-F	CCAACCACAAGGTGACCCTGACC	Fc-RSVG
RSVG-R	**AAAC**TCACTGCCGGGTGGTGTTG	Fc-RSVG
TEasy-MCS-F	GCGCGTAACCACCACACCC	RSVΔG
TEasy-MCS-R	CTGTTGTTGGCGGCAGGGG	RSVΔG

2.6 Chemical Inhibitors

Table 2.3 List of cell transport and cellular kinase inhibitors used.

Inhibitor name	**Target protein**	**Concentration**	**Supplier**
Cytochalasin D	Actin	8 μM (DMSO)	Tocris #1233
Jasplakinolide	Actin (stabilizer)	200 nM (DMSO)	Tocris #2792
CK666	Arp2/3	30 μM (DMSO)	Tocris #3950
(S)-(-)-Blebbistatin	Myosin II	40 μM (DMSO)	Tocris #1852
Nocodazole	β-tubulin	5 μM (DMSO)	Sigma #M1404
Brefeldin A	GBF1 (ER-Golgi transport)	1 μg/mL (DMSO)	Cell Signaling Technology #9972
Tunicamycin	N-glycosylation	3 μg/mL (DMSO)	Sigma #T7765
Leptomycin B	Nuclear export	20 nM (ethanol)	Tocris #1987
GO 6976	PKCα/β	500 nM (DMSO)	Tocris #2253
SB203580	p38	20 μM (DMSO)	Tocris #1202
U0126	MEK1/2 (upstream of ERK1/2)	10 μM (DMSO)	Tocris #1144
Salirasib	Ras	20 μM (DMSO)	Tocris #4989
PP2	Src kinase	10 μM (DMSO)	Tocris #1407
LY294002	PI3K	20 μM (DMSO)	Tocris #1130

PKCζ pseudosubstrate	PKCζ	3 μM (PBS)	Tocris #1791
Antennapedia	PKCζ control	1.5 μM (PBS)	Novus # NBP2-29334-5mg

Abbreviations: dimethyl sulfoxide (DMSO); actin related proteins 2 & 3 (Arp2/3); Golgi-specific brefeldin A-resistance guanine nucleotide exchange factor 1 (GBF1); protein kinase C (PKC); MAPK/ERK kinase 1 & 2 (MEK1/2); extracellular signal regulated kinase 1 & 2 (ERK1/2); rat sarcoma protein (Ras); phosphoinositide 3-kinase (PI3K); phosphate buffered saline (PBS).

Table 2.4 List of cell surface receptor inhibitors used.

Inhibitor name	**Target protein**	**Concentration**	**Supplier**
PQ401	IGF1R	30 μM (DMSO)	Tocris #2768
IGF1	IGF1R (activator)	500 ng/mL (H_2O)	Thermo Fisher #PHG0078
AS1411 (5′ GGT GGT GGT GGT TGT GGT GGT GGT GG 3′)	NCL	5 μM (H_2O)	IDT
CRO (5′ CCT CCT CCT CCT TCT CCT CCT CCT CC 3′)	AS1411 control	5 μM (H_2O)	IDT
αTLR4 IgA	TLR4	5 μg/mL	Invivogen #maba2-htlr4
Isotype IgA	IgA control	5 μg/mL	Invivogen #maba2-ctrl
C34	TLR4	20 μM (PBS)	Tocris #5373
LPS	TLR4 (activator)	200 ng/mL (PBS)	Sigma
AEE788	EGFR	2 μM (DMSO)	Tocris #5318
αCX3CR1 antibody	CX3CR1	20 μg/mL	Biolegend #149011
Isotype antibody	αCX3CR1 control	20 μg/mL	Biolegend #400264
AZD8797	CX3CR1	5 μM (DMSO)	Axon Medchem #2255-2

AMD3465	CXCR4	1 μM (PBS)	Axon Medchem #1930-5
R428	Axl	5 μM (PBS)	Axon Medchem #1946-1
UNC569	Mer	1 μM (DMSO)	Axon Medchem #2086-5
LCKLSL	Annexin II	40 μM (DMSO)	APM
LGKLSL	LCKLSL control	40 μM (DMSO)	APM

Abbreviations: insulin-like growth factor receptor (IGF1R); dimethyl sulfoxide (DMSO); insulin-like growth factor (IGF1); nucleolin (NCL); Integrated DNA Technologies (IDT); toll-like receptor 4 (TLR4); immunoglobulin A (IgA); phosphate buffered saline (PBS); lipopolysaccharide (LPS); epidermal growth factor receptor (EGFR); CX3C chemokine receptor (CX3CR1); CXC chemokine receptor 4 (CXCR4); Alberta Proteomics and Mass Spectrometry (APM).

2.7 Antibodies

Table 2.5 List of primary antibodies used.

Target Protein	Source Species	Assay/Dilution	Distributor
NCL [H-250]	Rabbit pAb	WB – 1:2000 ICC – 1:500 IP – 1:20 IFC – 1:100	Santa Cruz #sc-13057
NCL [D-6]	Mouse mAb	Flow – 1:500 WB – 1:3000	Santa Cruz #sc-17826
GFP	Rabbit pAb	WB – 1:2000	ThermoFisher #A6455
GFP	Rabbit mAb	Flow – 1:200 ICC – 1:200	Thermo Fisher #G10362
GFP	Goat pAb	IP – 1:400	Gift from Dr. Luc Berthiaume
Streptavidin-HRP	N/A	WB – 1:20 000	Gift from Dr. Luc Berthiaume

FLAG	Rabbit pAb	IP – 1:33	Cell Signaling Technology #2368
RSV	Goat pAb	LM – 1:1000 WB – 1:2000	Meridian #B65860G
RSV-F [2F7]	Mouse mAb	IP – 1:200 ICC – 1:500	Abcam #ab43812
RSV -F, -N, -P	Mouse 4 mAb blend	ICC – 1:400 IFC – 1:400	Novocastra #NCL-RSV3
β-actin	Rabbit pAb	WB – 1:5000	Abcam #ab8227
SOD1 [FL-154]	Rabbit pAb	WB – 1:1000	Santa Cruz #sc-11407
PARP1 [H-250]	Rabbit pAb	WB – 1:1000	Santa Cruz #sc-7150
Caveolin-1	Rabbit pAb	WB – 1:1000	Cell Signaling Technology #3238
PKCζ [H-1]	Mouse mAb	WB – 1:5000 IP – 1:20	Santa Cruz #sc-17781
p-PKCζ	Rabbit pAb	WB – 1:1000	Cell Signaling Technology #9378
IGF1R-β [D23H3]	Rabbit mAb	WB – 1:1000 ICC – 1:200	Cell Signaling Technology #9750
p-IGF1R-β [DA7A8]	Rabbit mAb	WB – 1:1000	Cell Signaling Technology #3918

Abbreviations: nucleolin (NCL); western blot (WB); immunoprecipitation (IP); immunocytochemistry (ICC); imaging flow cytometry (IFC); flow cytometry (Flow); light microscopy (LM); monoclonal antibody (mAb); polyclonal antibody (pAb); green fluorescent protein (GFP); Respiratory Syncytial Virus (RSV); RSV fusion protein (RSV-F), RSV nucleoprotein (RSV-N), and RSV phosphoprotein (RSV-P); superoxide dismutase 1 (SOD1); Poly (ADP-ribose) polymerase 1 (PARP1); insulin like growth factor receptor β chain (IGF1R-β); phosphorylated insulin like growth factor receptor (p-IGF1R-Tyr1135); protein kinase C, zeta isoform (PKCζ); phosphorylated protein kinase C, zeta/lambda isoform (p-PKCζ-Thr410/403).

Table 2.6 List of secondary antibodies used. Note: Secondary antibodies for flow cytometry, imaging flow cytometry, or immunocytochemistry used at half of the dilution of the primary antibody (ex. 1^o = 1:200, 2^o = 1:400)

Target Protein	Source Species	Conjugation	Assay/Dilution	Distributor
Rabbit IgG light chain	Mouse	HRP	WB – 1:10 000	Jackson ImmunoResearch #211-032-17
Mouse IgG light chain	Goat	HRP	WB – 1:10 000	Jackson ImmunoResearch # 115-035-174
Goat IgG light chain	Mouse	HRP	WB – 1:10 000	Jackson ImmunoResearch # 205-032-176
Mouse IgG heavy & light chain	Goat	HRP	WB – 1:10 000	Jackson ImmunoResearch # 115-035-062
Rabbit IgG	Goat	Alexa-568	Flow, ICC	Thermo Fisher #A11011
Rabbit IgG	Donkey	Alexa-647	Flow, IFC, ICC	Thermo Fisher #A31573
Mouse IgG	Goat	Alexa-568	Flow	Thermo Fisher #A11004
Mouse IgG	Goat	Alexa-488	ICC, IFC	Thermo Fisher #A11001
Mouse IgG	Goat $F(ab')_2$ Fragment	Alexa-647	Flow compensations	New England BioLabs #4410S
Goat IgG	Rabbit	β-galactosidase	LM – 1:2000	Abcam # ab136712

Abbreviations: Immunoglobulin G (IgG); horseradish peroxidase (HRP); western blot (WB); immunocytochemistry (ICC); imaging flow cytometry (IFC); flow cytometry (Flow); light microscopy (LM).

2.8 Microscopy

1HAEo- cells were grown on Labtek II chambered coverslips (Thermo Fisher #12565338). The cells were then cooled on ice for 15 min and RSV infections were synchronized on ice for 1 hour, before warming for the indicated time. Cells were fixed with 4% paraformaldehyde (PFA), blocked with PBS + 1% FBS, then stained with primary antibody for 1 hour at RT or at 4^oC overnight,

followed by secondary antibody for 1 hour at room temperature (RT). To permeabilize cells (if required), 0.3% Triton X-100 was added to antibody, blocking, and wash buffers. Actin staining was done using ActinGreen 488 ReadyProbes (Thermo Fisher #R37110) and cell nuclei were stained with DAPI (0.33 µg/mL in water) at RT for 2 min. After staining, cells were stored in Vectashield (Vector Labs, H-1000) at -20°C. Images were acquired using Volocity software (PerkinElmer) on a spinning disc confocal microscope (Wave FX #2, Quorum Technologies), using a 100x lens, in the Cell Imaging Centre at the University of Alberta.

On the Wave FX#2, the following lasers (EX) and filters (EM) were used for each fluorescent target: DAPI or Alexa 405 - EX 44mW 405nm, EM 460/50 nm; GFP, ActinGreen, or Alexa 488 - EX 50mW 491nm, EM 525/50 nm; Alexa 568 - EX 50mW 561nm, EM 620/60 nm; Alexa 647 - EX 45mW 642nm, EM 700/75 nm. Images were analyzed using Volocity software.

To examine RSV-F on DiD-RSV particles, 1HAEo- cells were grown on Labtek II chambered coverslips. The cells were then cooled and DiD-RSV infection was synchronized for 1 hour on ice. Without warming, the cells were fixed and stained (without permeabilization) as described above. The cells were then imaged on an OMX super resolution microscope (Applied Precision), using solid state conventional illumination, similar to what was used to image DiD-RSV in live cells (see below).

2.9 Live Cell Microscopy

HEK-293T cells were subcultured on Labtek II chambered coverslips. Two days later, the cells were transfected using FuGENE 6 Transfection Reagent (Promega #E2691) with NCL-GFP truncation mutants, TfR-GFP, or GFP alone. 48 hours after transfection, the cells were labeled with NucBlue Live ReadyProbes Reagent (Hoechst 33342 derivative - Thermo Fisher #R37605) and CellMask Deep Red (Thermo Fisher #C10046 – CellMask is an amphipathic dye that stains membranes and has been engineered to remain at the cell surface for longer than traditional lipophilic dyes), following manufacturer's instructions. The cells were then imaged live on the Wave FX#2 spinning disk confocal microscope at 37°C, with 5% CO_2.

To image nuclear accumulation of NCL-GFP NLS reverse, HEK-293T cells were grown under normal conditions to 50-60% confluence. The cells were then transfected with NCL-GFP or NCL-GFP NLS reverse using FuGENE6 Transfection Reagent. Every day after transfection, brightfield

and green fluorescence images were taken using the EVOS FL Auto Cell Imaging System (Invitrogen). These experiments did not involve a nuclear stain or a cell membrane stain.

To image RSV entry in living cells, 1HAEo- cells were subcultured on Labtek II chambered coverslips. Two days later, the cells were transfected using FuGENE 6 Transfection Reagent with NCL-GFP or GFP alone. 48 hours after transfection, the cells were labeled with DAPI (1:1000 in growth media) for 1 hour at 37°C, 5% CO_2, humidified. To prepared DiD-RSV, sucrose-purified RSV was labeled with DiD (1,1'-Dioctadecyl-3,3,3',3'-Tetramethylindodicarbocyanine, 4-Chlorobenzenesulfonate Salt dissolved in DMSO – Thermo Fisher #D7757) for 1 hour at RT, at a final DiD concentration of 45μM. Cells were washed with PBS and cooled on ice, while free label was separated from DiD-labeled virus particles using a PD Spintrap G-25 Sephadex Column (GE Healthcare, 28-9180-04). The DiD-RSV was diluted 1 to 1 with growth media, then added to cells and the infection was synchronized on ice for 1 hour as above. The live-cell infection was imaged at 37°C, with 5% CO_2, using an Applied Precision OMX super-resolution microscope (Cell Imaging Centre, University of Alberta). DAPI, GFP, and DiD (Cy5) fluorophores were excited using conventional LEDs and complete Z-stacks for each were imaged every 2 min. Videos were edited using Volocity software.

2.10 Flow Cytometry

To measure cell surface NCL-GFP, HEK-293T cells were grown under normal conditions to 50-60% confluence, then transfected with NCL-GFP truncation mutants using FuGENE 6 Transfection Reagent (Promega, E2691). 48 hours later, the cells were cooled on ice, washed with PBS, and detached using 10mM EDTA in PBS, followed by scraping. Cells were blocked with 5% FBS in PBS for 30 min on ice, stained for surface NCL-GFP with a rabbit anti-GFP monoclonal antibody (1:200 dilution) for 30 min on ice, then stained with a secondary donkey anti-rabbit-Alexa 647 (1:400 dilution) antibody for 30 min on ice. Ghost Dye Violet 450 viability stain (Tonbo #13-0863-T500) was also used. GFP expression, Ghost Dye staining, and Alexa 647 staining was measured on a BD LSR Fortessa SORP Cell Analyzer in the University of Alberta Flow Cytometry Core Laboratory (GFP - EX 488 nm, EM 530/30 nm; Ghost Dye - EX 405 nm, EM 450/50 nm; Alexa 647 - EX 640, EM 670/14). Data analysis and spectral overlap compensations were completed using FlowJo version 10.

To measure IGF1 induced changes in surface NCL-GFP, HEK-293T cells were transfected with NCL-GFP as described above. 48 hours later, the cells were treated with 500 ng/mL IGF1 for 1 hour or left untreated. The cells were then harvested, stained, and analyzed as described above.

To measure cell surface NCL, cells were grown under normal conditions to 70-80% confluence. If applicable, RSV infections were synchronized by cooling the cells for 15 min on ice, replacing growth media with virus-containing media, incubating for 1hr on ice to synchronize infection, then warming to 37ºC, with 5% CO_2, humidified. At the appropriate time points, the cells were then harvested and stained as described above. Mouse monoclonal anti-C23 antibodies (1:500 dilution) and goat anti-mouse Alexa 568 (1:1000 dilution) antibodies were used to detect cell surface NCL. Alexa 568 staining was measured on a BD LSR Fortessa SORP Cell Analyzer in the University of Alberta Flow Cytometry Core Laboratory (EX 561 nm, EM 610/20 nm). Data analysis was completed using Flowing Software (Perttu Terho, Cell Imaging Core, Turku Centre for Biotechnology, Finland).

2.11 Co-Culture

HEK-293T or 1HAEo- 'donor' cells were transfected with NCL-GFP, a NCL-GFP mutant construct, TfR-GFP, or GFP alone. HEK-293T 'recipient' cells were transfected with mCherry. If 1HAEo- cells were used as 'recipient' cells, they were instead stained with CellTracker Orange CMRA (ThermoFisher #C34551) for 45 min, immediately before co-culture. 24 hours after transfection, donor and recipient cells were lifted with 0.25% trypsin-EDTA and resuspended in growth media. The cells were then mixed together and re-seeded in a larger well. Successful transfection and CellTracker staining were confirmed with fluorescence microscopy, using the EVOS FL Auto Cell Imaging System. After 48 hours of co-culture, the cells were harvested without permeabilization using 10 mM EDTA, stained for cell surface GFP, and analyzed by flow cytometry as described above. In addition to Ghost Dye and cell surface GFP, CellTracker staining (EX 561 nm, EM 586/15 nm) and mCherry expression (EX 561 nm, EM 610/20 nm) were measured on the BD LSR Fortessa SORP Cell Analyzer during flow cytometry.

To test contact-dependence of the co-culture, 'donor' and 'recipient' HEK-293T cells were instead seeded into a ThinCert transwell dish (Grenier), with 400 nm pores. The 'donor' HEK-293T cells were seeded into the upper chamber, while the 'recipients' were seeded into the lower chamber. Alternatively, 'donor' HEK-293T cells were transfected, then had their media replaced 24 hours

later. The conditioned media produced between 24 and 48 hours after transfection was collected, then used to treat 'recipient' HEK-293T cells for 24 hours, without dilution. For these contact-dependence experiments, only 'recipient' HEK-293T cells were harvested. Staining for cell surface GFP and analysis by flow cytometry occurred as described above.

2.12 Flow Cytometry Data Analysis

Cell surface NCL-GFP gates: FSC-A vs SSC-A to gate cells away from debris/clumps. FSC-A vs FSC-H to gate single cells from doublets. Ghost dye viability stain vs FSC-A to gate living cells away from dead cells. GFP intensity histogram used to gate only GFP+ cells. Surface NCL-GFP positive cells were then gated using a histogram for surface GFP intensity.

Cell surface NCL-GFP gates (with HEK-293T – HEK-293T co-culture and media transfer): FSC-A vs SSC-A to gate cells away from debris/clumps. FSC-A vs FSC-H to gate single cells from doublets. Ghost dye viability stain vs FSC-A to gate living cells away from dead cells. mCherry vs GFP used to gate donor cells (GFP-positive, mCherry-negative) from recipient cells (GFP-negative, mCherry-positive). Surface NCL-GFP positive cells were then gated using a histogram for surface GFP intensity.

Cell surface NCL-GFP gates (with HEK-293T – 1HAEo- or 1HAEo- – 1HAEo- co-culture): FSC-A vs SSC-A to gate cells away from debris/clumps. FSC-A vs FSC-H to gate single cells from doublets. Ghost dye viability stain vs FSC-A to gate living cells away from dead cells. CellTracker Orange vs FSC-A used to gate donor cells (CellTracker-negative) from recipient cells (CellTracker-positive). Within donor cells, GFP intensity histogram used to gate GFP+ cells. Surface NCL-GFP positive cells were then gated using a histogram for surface GFP intensity.

Cell surface NCL-GFP gates (with HEK-293T – HEK-293T co-culture in a transwell dish): FSC-A vs SSC-A to gate cells away from debris/clumps. FSC-A vs FSC-H to gate single cells from doublets. Ghost dye viability stain vs FSC-A to gate living cells away from dead cells. Surface NCL-GFP positive cells were then gated using a histogram for surface GFP intensity.

Endogenous cell surface NCL gates: FSC-A vs SSC-A to gate cells away from debris and clumps. FSC-A vs FSC-H to gate single cells from doublets. A surface NCL intensity histogram or surface NCL vs SSC-A was then used to gate cells positive for surface NCL.

2.13 Immunoprecipitation

Cells were cooled, washed with PBS, then harvested in MOSLB lysis buffer, including 1X cOmplete-Mini Protease Inhibitor Cocktail (Millipore Sigma #04693159001). Lysates were then spun at 16 000 x g for 10 min at 4ºC to pellet cell debris and supernatants were collected. Antibody was added and bound by rotating lysate overnight at 4ºC. Lysate with antibody was then used to resuspend Protein G conjugated Dynabeads (Life Technologies #10004D), creating a slurry. Antibodies were bound to the beads by rotation at 4ºC for at least 2hr. Beads were then washed three times using lysis buffer and protein was eluted with 50 mM HEPES, 1% SDS, including protease inhibitor by heating to 80ºC for 15 min.

2.14 SDS-PAGE and Western Blot

Cells were cooled, washed with PBS, and then lysed with either MOSLB buffer or as the supplied protocol outlines using the NE-PER (ThermoFisher #89842) or mem-PER (ThermoFisher #89842) fractionation kits. Harvested protein lysates (or immunoprecipitation eluates) were boiled for 5 min with 1x Laemmli sample buffer including 2.5% 2-mercaptoethanol as a reducing agent. Samples were then run on precast Mini-PROTEAN TGX polyacrylamide gradient gels (Biorad) at 150V for 1hr in tris-glycine-SDS running buffer. Coomassie gels were stained with 3 g/L Brilliant Blue R-250 in 45% methanol, 45% water, and 10% acetic acid (v/v/v). Gels were subsequently destained with 45% methanol, 45% water, and 10% acetic acid (v/v/v), then imaged using a BioRad GelDoc XR+ imager.

For western blot, separated proteins in a polyacrylamide gel were wet-transferred onto a nitrocellulose membrane at 100V for 1hr at 4ºC, bathed in tris-glycine transfer buffer including 10% methanol. Membranes were washed with tris-buffered saline containing 0.1% Tween (TBS-T), blocked with 5% BSA in TBS-T, and probed with primary then secondary-HRP antibodies in TBS-T containing 1% BSA. ECL2 substrate (Pierce pi80196) was added to blots for 5 min at RT, then removed for blots to be imaged. Blots were imaged using a GE ImageQuant LAS 4000, detecting HRP using the Cy2 filter and markers using the Cy5 filter. Images were cropped and edited for brightness and contrast using Adobe Photoshop or ImageJ.

2.15 Palmitoylation Assay

HeLa cells were transfected using FuGENE 6 transfection reagent. Depending on the experiment, the transfected plasmids were N-Ras-GFP, K-Ras-GFP, NCL-GFP, NCL C543S-GFP, NCL-FLAG, or NCL C543S-FLAG. The media on all wells was replaced 24 hours after transfection. 48 hours after transfection, the cells were washed with warm PBS and DMEM + 1% fatty acid free BSA (or 5% charcoal stripped FBS for **Figures 3.17** and **3.18**) was added to each well for 1 hour to starve the cells of fatty acids. During this hour, 50 mM alkynyl-palmitate was saponified at 65ºC for 5 min, using 60 mM sodium hydroxide. 25 volumes of DMEM + 20% fatty acid free BSA was then added to the alkynyl-palmitate to conjugate the fatty acids, which were then incubated at 37ºC for at least 15 min. The DMEM + alkynyl-palmitate + 20% fatty acid free BSA was then added to the HeLa cells to a final concentration of 100 µM alkynyl-palmitate. The cells were incubated with alkynyl palmitate for 3-5 hours at 37ºC, washed with cold PBS, then lysed in weak RIPA buffer + cOmplete-Mini Protease Inhibitor Cocktail. An immunoprecipitation was then performed using antibodies against GFP, FLAG, or NCL (depending on the transfected construct, or if the cells were left untransfected). Weak RIPA buffer + cOmplete-Mini Protease Inhibitor Cocktail was used during the wash steps.

After eluting the immunoprecipitated proteins from the Dynabeads, a Click reaction was performed to attach a biotin to each alkynyl-palmitate. This involved sequentially adding 100 µM TBTA, 1 mM copper(II) sulfate, 1 mM TCEP, then 100 µM azido-biotin (final concentrations shown). The click reaction was then incubated for 30 min in darkness at 37ºC, followed by adding 10 volumes of ice-cold acetone to stop the reaction and precipitate the protein. After an overnight incubation at -20ºC, the samples were pelleted at 16 000 x g for 10 min at 4ºC. The acetone was then removed, and the samples were resuspended in 1x Laemmli sample buffer, with 20 mM DTT (instead of 2-mercaptoethanol). The samples then underwent a western blot, as described above. Streptavidin-HRP was used to detect the biotin-palmitate, in place of primary and secondary antibodies.

2.16 Purification of RSV by Fast Protein Liquid Chromatography (FPLC)

The PEG-precipitated RSV resuspended in NT was filtered through an ÄKTA Start FPLC system (GE Healthcare Life Sciences, Mississauga, ON, Canada) stored within a biosafety cabinet, as described previously[2]. The instrument was equipped with a HiTrap Capto Core 700 column (GE

Healthcare Life Sciences #17-5481-51) with a 1 mL bed volume. The matrix beads of the column bind small impurities while allowing large molecules to pass through the column (molecular weight > 700,000 kDa). ÄKTA Running Buffer A was comprised of NT buffer +1% sucrose, pH 7.4, 0.2 µm filtered, and ÄKTA Elution Buffer B was 1N sodium hydroxide in 30% isopropanol, 0.2 µm filtered. The system and column were washed with sterile filtered distilled water at 5 mL/min. The column was primed and equilibrated with 5 mL of Buffer A running at 1 mL/min. The 2-mL injection loop was flushed with buffer A and then loaded with the PEG-precipitated virus resuspended in NT buffer. Fractionation was set to collect 1 mL fractions as soon as the sample was injected onto the column at 0.5 mL/min, collecting 5 mL total throughout the absorbance peak at 250 nm. Isocratic elution was set at 100% Buffer B to remove the impurities bound to the column to allow for re-use. The column was stored at 4ºC in 20% ethanol.

2.17 RSV Infectivity Quantification

RSV infectivity was measured by infecting confluent cells with a serial dilution of sucrose purified virus for 2-4 hours at 37ºC, 5% CO_2, humidified. Cells were then washed, fresh growth media was added, and cells were incubated for another 14-16 hours. Cells were then fixed and permeabilized with methanol:acetone (1:1), blocked with PBS + 5% FBS, and stained with goat polyclonal anti-RSV antibody (1:1000 dilution), followed by an anti-goat secondary antibody conjugated to beta-galactosidase (1:2000 dilution). X-Gal substrate (5-bromo-4-chloro-3-indoyl-β- galactopyranoside in PBS containing 3 mM potassium ferricyanide, 3 mM potassium ferrocyanide, and 1 mM magnesium chloride) was then added. X-Gal substrate cleavage by β-galactosidase creates an insoluble blue color, indicating RSV infection. Blue cells were manually counted as RSV infectious units (IU) by light microscopy using the EVOS FL Auto Cell Imaging System (Invitrogen). It is important to note that this technique quantifies infected cells during the first round of RSV infection and requires only viral protein expression to occur. This is in contrast to a typical plaque assay which requires the entire viral life cycle, including assembly and budding, to form plaques.

To examine the effects of cellular inhibitors on RSV entry, confluent 1HAEo- cells were pre-treated with inhibitor for 1 hour, then infected with RSV. 4 hours after infection, the cells were acid-washed with 3 M glycine to remove virus that has not yet entered. The cells were then washed

with media 3 times, incubated for another 14-16 hours, then fixed, stained, and counted as described above.

2.18 Quantitative reverse transcription PCR (qRT-PCR)

RNA was harvested from cell monolayers, spiked with 25µg of salmon sperm DNA (Life Technologies 15632-011) and 2% 2-mercaptoethanol, using the E.Z.N.A. Total RNA Kit 1 (Omega Bio-tek, R6834-01). Reverse-transcription and amplification were both performed in the same reaction using Quanta qScript XLT One-Step RT-qPCR ToughMix, low ROX reference dye (95134-100). TaqMan primer/probes (FAM) were purchased from Life Technologies: human NCL Hs01066668_m1, human HPRT housekeeping control Hs02800695_m1. The RNA was run on a CFX96TM Real-Time system, C1000 Touch Thermal Cycler by Bio-Rad, with cycling conditions as follows: cDNA synthesis at 50ºC for 10 min, initial denaturation at 95ºC for 1 min, and 45 amplification cycles (95ºC for 10 sec, then 60ºC for 60 sec). NCL RNA was quantified relative to HPRT.

2.19 Imaging Flow Cytometry

1HAEo- cells were grown under normal conditions to 95% confluence. When applicable, the cells were pre-treated with an inhibitor for 1 hour at 37ºC and inhibitor concentration was maintained until detachment of the cells. RSV infections were synchronized by cooling the cells for 10 min on ice, replacing growth media with media containing RSV at an MOI of 1, and incubating for 1 hour on ice. The media was then replaced with fresh 37ºC media and the cells were incubated for the indicated time at 37ºC, 5% CO_2, humidified. The cells were then washed with 4ºC PBS and detached using 10mM EDTA in PBS on ice, followed by scraping. The cells were blocked with 5% FBS in PBS for 30 min on ice, stained for surface NCL with rabbit polyclonal anti-C23 antibody (1:100 dilution) and stained for RSV using the mouse anti-RSV 4 monoclonal blend (RSV3 - 1:400 dilution) for 30 min on ice. The cells were then stained with a secondary donkey anti-rabbit Alexa 647 antibody (1:200 dilution) and a secondary goat anti-mouse Alexa 488 antibody (1:800 dilution) for 30 min on ice. Cells were fixed in 4% PFA and stained with DAPI for 5 min on ice, followed by acquisition of at least 100 000 single cells using the Amnis Mark II ImageStream (405 nm, 488 nm, and 642 nm excitation lasers, 60x magnification). Data analysis was performed using IDEAS software (Amnis).

2.20 Imaging Flow Cytometry Data Analysis

Data analysis was done on IDEAS software, with all gate values empirically pre-set for unbiased analysis of samples. FSC area vs FSC aspect ratio intensity was used to gate single cells from beads and doublets/clumps. An FSC gradient RMS histogram was then used to gate in-focus single cells (high FSC gradient RMS). A DAPI (405nm) aspect ratio histogram was used as a further quality control step, to remove cells with fragmented nuclei (high DAPI aspect ratio events were gated). Since the proportion of NCL on the cell surface is very low compared to cytoplasmic and nuclear regions, a NCL (642 nm) area histogram, followed by an intensity histogram were used to gate non-permeable cells (low NCL area/intensity). RSV-positive cells were then gated using an RSV (488 nm) max pixel intensity histogram (low max pixel cells removed). The number of viral particles attached to each cell was then counted using a spot count, detecting bright spots with a 4 to 1 spot to background ratio, a minimum width of 3 pixels, a maximum area of 250 μm^2, and a minimum intensity similar to the RSV-positive gate. Cells with 1-5 viral particles bound were then gated for further analysis. Cell surface NCL was detected using a threshold 80% mask (removes the lower 20% of pixels) with a minimum intensity. Overlap between RSV and NCL (patching mask) was detected using the virus spot mask, that had been dilated 2 pixels, in conjunction with the cell surface NCL mask. Cells with an RSV-NCL patching event were then selected using a patching area histogram (remove low patching area). The NCL intensity within the patching mask was then recorded. Gate summary: Singlets, In Focus, Nuclear Shape, Non-Permeable-1, Non-Permeable-2, RSV Positive, 1-5 Virus Spots, Patching Positive. Total surface NCL and RSV levels were recorded after the Non-Permeable-2 gate (before the RSV Positive gate).

2.21 Purification of Fc-Proteins

To create purified versions of RSVF-Fc, Fc-RSVG, and Fc alone, each construct was transfected into four T175 flasks of HEK-293T cells, using FuGENE 6 transfection reagent. 24 hours after transfection, the media on each flask was replaced with MEM + 2% FBS. Every 12 hours thereafter (from 36 to 120 hours post transfection) the culture supernatant was collected, spun down to pellet any cells, then pooled based on the construct transfected. Using an ÄKTA Start FPLC system (within a biosafety cabinet to maintain sterility), a 1 mL HiTrap protein G HP column (ThermoFisher #45000053PM) was first equilibrated with 5 mL of MEM. The culture supernatants were then run past the HiTrap protein G HP column at a 0.5 – 1 mL/min flow rate, to bind Fc-containing proteins. After running all of the culture supernatant, the column was washed with 10

mL of ÄKTA protein binding buffer (A). The bound proteins were then eluted using a linear gradient of 10-100% ÄKTA protein elution buffer (B), over 18 mL. 5 mL of elution buffer was then run past the column to elute any remaining proteins. Fractions were collected every 0.5 mL throughout the elution and 15-30 µL of 1 M Tris-HCl (pH 9) was added to each eluted fraction to stabilize the pH. Elution peaks were observed from 50-100% elution buffer, depending on the Fc-protein. Eluted protein concentrations were determined using the Qubit Protein Assay Kit (ThermoFisher #1657803) on a Qubit 3.0 fluorometer (ThermoFisher).

2.22 PKCζ *In Vitro* Kinase Assay

1HAEo- cells were grown under normal conditions to 95% confluence. If applicable, the cells were pre-treated with an inhibitor for 1 hour at 37ºC and inhibitor concentration was maintained until the cells were harvested. RSV infections were synchronized by cooling the cells for 10 min on ice, replacing growth media with virus-containing media, incubating for 1hr on ice, then warming at 37ºC, 5% CO_2, humidified. At the appropriate time points, cells were cooled on ice, washed with 4ºC PBS, and lysed using MOSLB including 1X cOmplete-Mini Protease Inhibitor Cocktail. An immunoprecipitation for PKCζ was then performed using a mouse α PKCζ monoclonal antibody (Santa Cruz #sc-17781). After incubation with the Dynabeads, the samples were washed twice with MOSLB and twice with PBS, then the PKCζ kinase reaction was performed on the beads for 1 hour at RT with 10µM ATP and 200µg/mL CREBtide (PKCζ substrate) in 40mM Tris pH 7.5, 20mM $MgCl_2$, 0.1mg/mL BSA, and 50µM DTT. The Promega ADP-Glo Kit (#V9101) was then used to quantify the ATP used during the kinase assay, with each experiment compared to a standard ADP/ATP 10µM dilution series. The luminescence was then quantified using the GloMax Explorer plate reader (Promega). This assay was adapted from the Promega PKCζ Kinase Enzyme System (#V2781), which is used to screen for specific inhibitors of PKCζ.

2.23 Microscale Thermophoresis (MST)

DS-Cav1 protein (gift from Dr. Jason McLellan, University of Texas at Austin) or RSV-G protein (Acro Biosystems RSG-V5221-50UG) were labeled with NT-647 dye, as recommended with the Monolith His-Tag Labeling Kit RED-tris-NTA (NanoTemper Technologies, MO-L008). Labeled protein (50 nM, final concentration) was then added to a dilution curve of IGF1R protein (Novus Biologicals, 391-GR-050) in PBS + 0.05% Tween-20 ranging from 1 µM to 15.3 pM, final concentrations. DS-Cav1-red + IGF1R samples were run in standard capillaries (NanoTemper

Technologies, MO-K022) and RSV-G-red + IGF1R samples were run using premium capillaries (NanoTemper Technologies, MO-K025). MST was completed in 5 independent repeat experiments on a Monolith NT.115 instrument (NanoTemper Technologies), running MO.Control software with settings at 60-70% excitation power, 40% MST power at 27°C. K_D calculations were completed using MO.Affinity Analysis software.

2.24 RSV Fusion Assay

To measure RSV fusion on a per-well basis, instead of a per-particle basis, a protocol was adapted from Srinivasakumar and colleagues[138]. 1HAEo- cells (or IGF1R KO 1HAEo- cells) were subcultured in a 96-well plate, with black wells and a clear bottom (Greiner CELLSTAR #655090). Two days later, the cells were pre-treated with inhibitors for 1 hour, cooled on ice for 15 min, then DiD-RSV infections were synchronized on ice for 1 hour. Each well was washed 5x with growth media, then the media was replaced with clear FluoroBrite DMEM + 10% FBS (Thermo Fisher #A1896701). The initial DiD fluorescence in each well was measured using the GloMax Explorer Plate Reader (Promega - EX 627 nm, EM 690/60 nm). The cells were then incubated at 37oC, with 5% CO_2, humidified, with DiD fluorescence readings taken every 15 min, for 2 hours. At the end of the assay, Triton X-100 was added to each well, to a final concentration of 1%. The addition of detergent unquenches all remaining DiD within the well and the DiD fluorescence provides a measure of total DiD-RSV bound in each well[138]. Fluorescence values from uninfected wells were subtracted from the DiD-RSV-infected wells to account for background cellular autofluorescence. Inhibitors were present throughout the assay.

2.25 Statistical Analysis

All statistical analyses were performed using GraphPad Prism 8 software. Unless otherwise indicated, results are expressed as mean +/- SEM. I compared means of two groups using a two-tailed Student's t-test. When comparing three or more groups with a single independent variable, I used a one-way analysis of variance (ANOVA) with Tukey's, Dunnett's, or Sidak's post hoc test, depending on the experiment, comparing each group to the appropriate control. When comparing three or more groups with more than one independent variable, I used a two-way ANOVA with Tukey's post hoc test, comparing each group to its cognate control. For experiments with two timecourses, multiples t-tests (one per timepoint) were used to compare the timecourses to one another, taking into account false discovery rate using the method by Benjamini, Krieger, and

Yekutieli. Linear regression with an F-test to compare the slope of the line to zero was used for timecourse experiments without a cognate control. All tests were two tailed, unless otherwise indicated. I considered a p value of less than or equal to 0.05 to be statistically significant.

Chapter 3: Subcellular Localization and Intercellular Transfer of NCL

3.1 Introduction

NCL is an abundant protein that primarily resides in the nucleolus, making up about 10% of all protein content within the nucleolus[185]. Within the cell, NCL plays a multifunctional role and its nuclear role has been extensively characterized. Included in NCL's functions are ribosome biogenesis, chromatin remodeling, and cell cycle regulation (Reviewed in [344]). Likely due to the various functions it plays in the nucleus, NCL is an essential cellular protein[201,202]. NCL itself can be divided into 3 main domains (**Figure 1.3**). On the N-terminus is a series of acidic/basic segments (AB), followed by a central domain containing 4 RNA recognition motifs (RRMs), and on the C-terminus is a glycine/arginine rich (GAR) domain. Nuclear import of NCL is mediated by a bipartite NLS located between the AB domain and the first RRM.

Besides being found in the nucleus, NCL is also present in lower levels in the cytoplasm[208] and on the cell surface[134,213,214,216]. The mechanism by which NCL translocates to the cell surface remains unclear, though it has been suggested to involve phosphorylation of NCL[176]. To mediate this active transport throughout the cell, NCL closely associates with non-muscle myosin heavy chain 9 (MyH9)[176,227] and the actin cytoskeleton[220]. Despite these insights, investigations into NCL surface trafficking have been hindered by the fact that NCL lacks a conventional signal peptide and translocates to the surface using a pathway independent of the Golgi apparatus[220]. Furthermore, the level of NCL on the cell surface is typically very low, though the levels can be enhanced by the binding of extracellular ligands[194,227,228].

On the cell surface, NCL acts as a scavenger receptor by binding various ligands, including several growth factors, then mediating their internalization via endocytosis[180,230,231]. Cell surface NCL may also influence cell signaling events[189,235,239-242] and NCL has been reported to interact (directly or indirectly) with a number of cell surface proteins including EGFR[243], urokinase plasminogen activator receptor[180], CXCR4[179,242], low-density lipoprotein receptor-related protein[230], and several integrins[180,217,228]. Many of these interactions are mediated by the GAR domain at the C-terminal end of NCL. Furthermore, high levels of cell surface NCL are correlated with cell proliferation[220] and is a marker of some malignant cancers[194,215,228,240,345]. For these reasons, cell surface NCL has garnered substantial interest in the field of oncology. Additionally, cell surface NCL is important

in the field of infectious disease, since it is a receptor or co-receptor for a number of viral and bacterial pathogens[128,345]. Cell surface NCL as a receptor for RSV will be explored further in **Chapter 4** and **Chapter 5**.

How NCL remains attached to the cell surface is unknown, since NCL does not possess a transmembrane domain and does not have a glycosylphosphatidylinositol (GPI) anchor. Besides transmembrane domains and GPI anchors, the post-translational addition of fatty acid groups is another mechanism that proteins use to tether to membranes[346]. The most common fatty acylation modifications are S-palmitoylation, N-myristoylation, S-farnesylation, and S-geranylgeranylation. As the most common fatty acylation, palmitoylation involves the reversible attachment of a 16-carbon fatty acid to a cysteine within the target protein via a thioester linkage[347]. This process is typically mediated by palmitoyl transferase. A few mass spectrometry screens have picked up NCL as a palmitoylated protein, however, this has not been validated and none of the screens have directly picked up the palmitoylated peptide[348-352]. NCL contains only one cysteine, at position 543 (…CNKRE…), which does not fit the consensus sequence for farnesylation or geranylgeranylation (CaaX or CC/CXC), making these modifications unlikely[347]. Myristoylation typically occurs on the N-terminus of a protein with a glycine at position 2, where methionine at position 1 is removed and the myristate is attached to the glycine at position 2[353]. The first glycine in NCL is at position 8 (MVKLAKAG…), rather than position 2, making myristoylation as the NCL membrane tethering mechanism unlikely.

In this chapter, I explored the NCL domains required for cell surface expression. I established an overexpression system where HEK-293T cells were transfected with green fluorescent protein tagged NCL (NCL-GFP). I then measured the expression of NCL-GFP on the cell surface by non-permeabilized flow cytometry using anti-GFP antibodies. An advantage of this system is that it permitted testing a series of NCL truncation mutants that I made to determine if they had an altered ability to translocate to the cell surface. Since many of NCL's post-translational modifications have been mapped out, these truncation mutants have the added benefit of indirectly informing which modifications may be important for cell surface expression. I then examined an interesting phenomenon of NCL transferring between the surfaces of different cells, which has not been described previously. Finally, I attempted to shed light on the mechanism that NCL uses to remain attached to the cell surface by examining if NCL is palmitoylated. Together, these experiments

explored basic cell biology questions of a protein that plays important roles in the fields of cancer and infectious disease.

3.2 Results

3.2.1 Creating and characterizing a library of NCL-GFP truncation mutants

3.2.1.1 Overview and rationale behind NCL-GFP constructs

Although NCL is essential for cell survival and its nuclear roles have been well characterized[177,200-203], many questions remain about the function of cell surface NCL and its secretion pathway. To begin characterizing the roles each domain of NCL plays in surface expression, I created a library of truncation mutants, each with GFP fused to the C-terminus (**Figure 3.1**). Since the N-terminal AB domain of NCL and the C-terminal GAR domain mediate protein-protein interactions, mutants lacking each or both of these domains were created. Furthermore, a construct containing only the GAR domain and a construct with the last two RRMS and the GAR domain were also created. Previously, an antibody raised against the first two and a half RRMs of NCL was shown to block RSV infection[128], which implies that this core region of the protein may play an important role on the cell surface. Therefore, a mutant composed of only the NCL core was created.

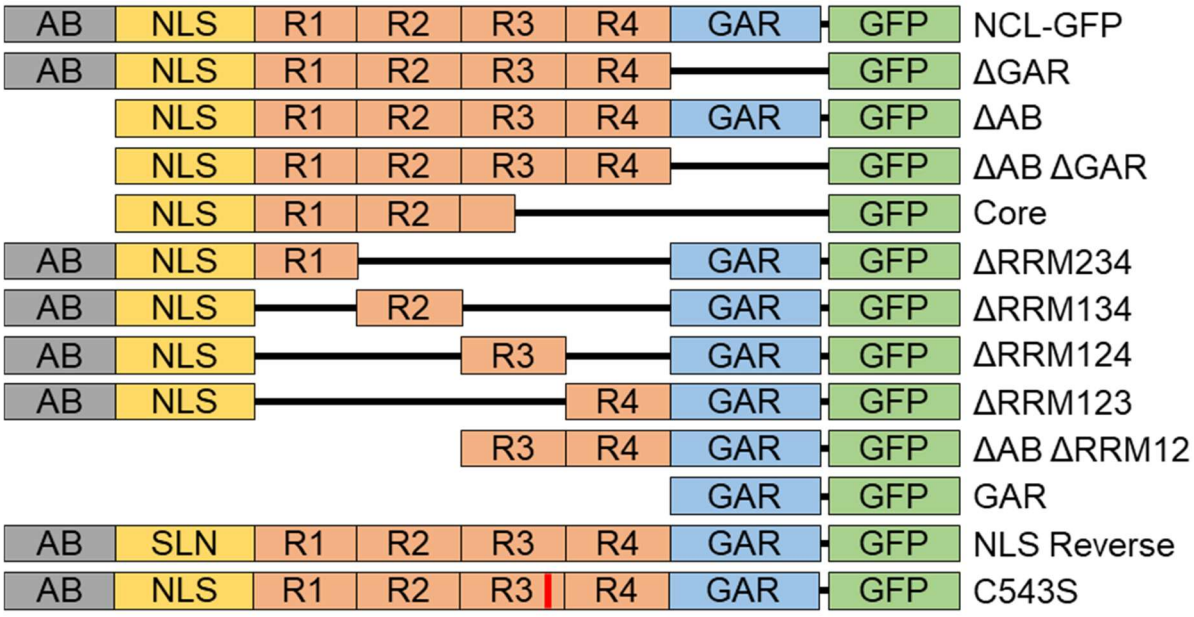

Figure 3.1 Schematic diagram of NCL-GFP truncation mutants. Full length NCL-GFP and a series of truncation mutants were created in the pcDNA3.1 vector, under a CMV promoter. NCL domains removed include the N-terminal acidic/basic (AB) domain, multiple RNA recognition

motifs (RRMs), and the C-terminal glycine/arginine repeat (GAR) domain. The NLS reverse construct has the bipartite nuclear localization signal reversed to prevent nuclear import of the NCL construct. Cysteine 543 was mutated to serine using site directed mutagenesis to investigate potential palmitoylation of NCL.

A major obstacle when studying cell surface NCL is that the roles NCL plays within the nucleus are essential for cell survival. Therefore, *NCL* gene knockout experiments are impossible. However, although the AB and GAR domains are critical, the RRMs of NCL are redundant to one another[201]. The RRM domains also contain two N-glycosylation sites – N317 in RRM1 and N492 in RRM3[183]. This is of note since cell surface NCL has been described to be glycosylated at these sites and the glycosylation plays an important role in NCL oligomerization[183,184]. However, the glycosylation biosynthesis pathway that NCL follows is unknown. To investigate the RRM redundancy and the roles of these glycosylation sites, four NCL mutants lacking all RRMs except one were created.

NCL utilizes a bipartite NLS to mediate entry into the cell nucleus[175]. To examine the role of this NLS, a NCL-GFP mutant was created with each section of the NLS reversed to eliminate binding to nuclear import proteins, while maintaining the overall charge of NCL. Site directed mutagenesis was used to mutate the first part of the NLS, KRKK (AA 279-282), to KKRK. Similarly, the second half of the NLS, KKQK (AA 294-297), was mutated to KQKK. This NLS reverse mutant was expected to be excluded from the nucleus of cells, which is supported by the fluorescent localization of the mutant (**Figure 3.2**).

Finally, a NCL-GFP construct with a cysteine to serine point mutation at residue 543 (C543S) was created using site directed mutagenesis. This construct was used to examine potential palmitoylation of NCL, since palmitate is typically attached to a cysteine residue and NCL contains only one cysteine. The cysteine was mutated to serine since serine is a similar amino acid that lacks the sulphur atom required for the thioester linkage and therefore cannot be palmitoylated[354]. The potential palmitoylation of NCL will be elaborated upon further in section 3.2.3.

3.2.1.2 Expression and localization of NCL-GFP and mutant proteins

Each of the NCL-GFP mutant constructs were transfected into HEK-293T cells and imaged live using fluorescent confocal microscopy (**Figure 3.2**). As expected, the full length NCL-GFP primarily localized to nucleoli and similar strict nucleolar localization was observed for the mutant

lacking the AB domain[201] and NCL-C543S. Each of the mutants lacking 3 RRMs also had nucleolar localization, though more of the protein could be observed throughout the rest of the nucleus[201]. Similar to what has previously been observed[175,201], in the 3 mutants lacking the GAR domain (ΔGAR, ΔABΔGAR, and Core), a diffuse nuclear localization was observed, with some accumulation of protein in the nucleoli. Since it lacks an NLS, the ΔABΔRRM12 mutant was largely excluded from the nucleus and seemed also to be excluded from the endoplasmic reticulum/Golgi apparatus (based on intense membrane stain adjacent to the nucleus). However, the mutant protein containing only the GAR domain fused to GFP was able to enter and accumulate within the nucleus. As expected[175], the NLS reverse mutant primarily localized to the cytoplasm and was excluded from the nucleus. In addition to cytoplasmic localization, the NLS reverse mutant was also observed in the nucleus of some cells, which has been reported previously[201]. When imaged daily after transfection, the amount of NLS reverse mutant localized to the cell nucleus seemed to increase over time (**Figure 3.3**).

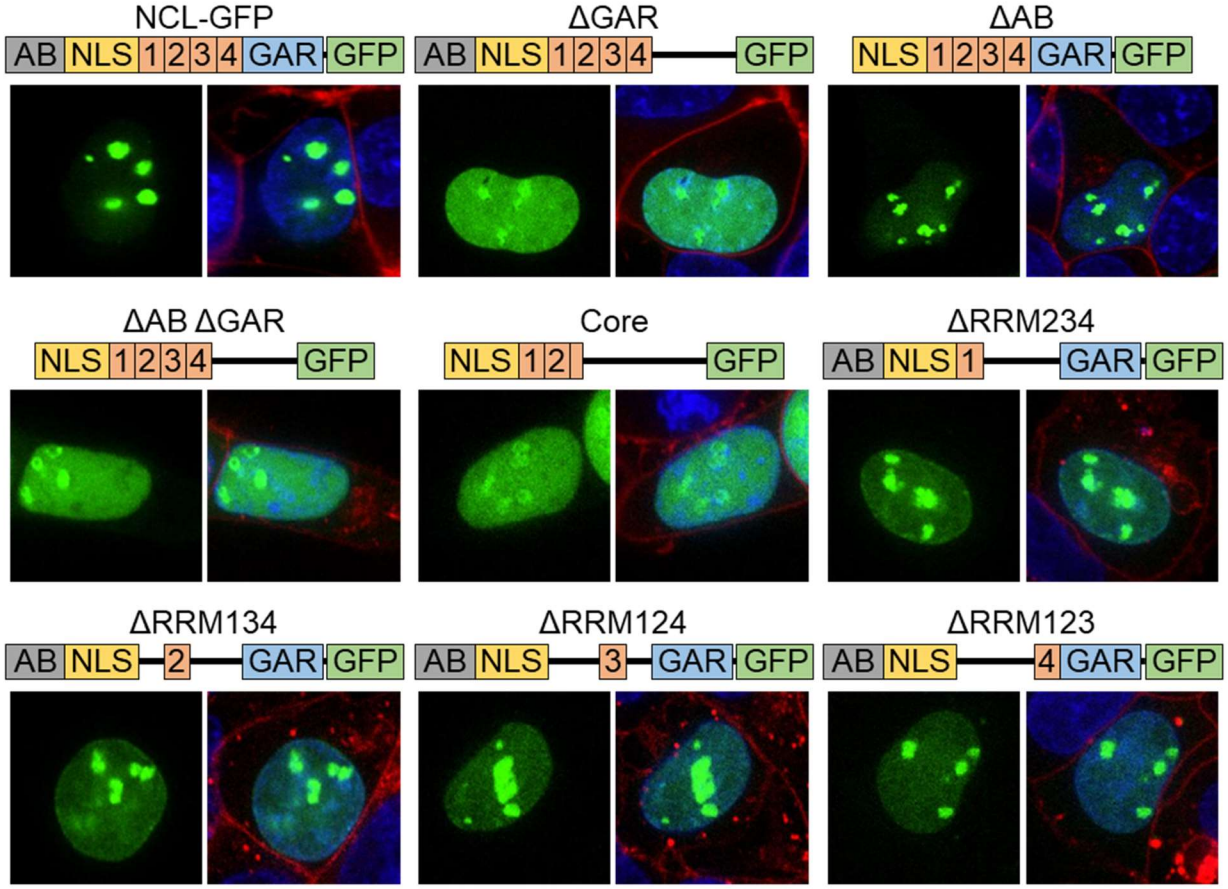

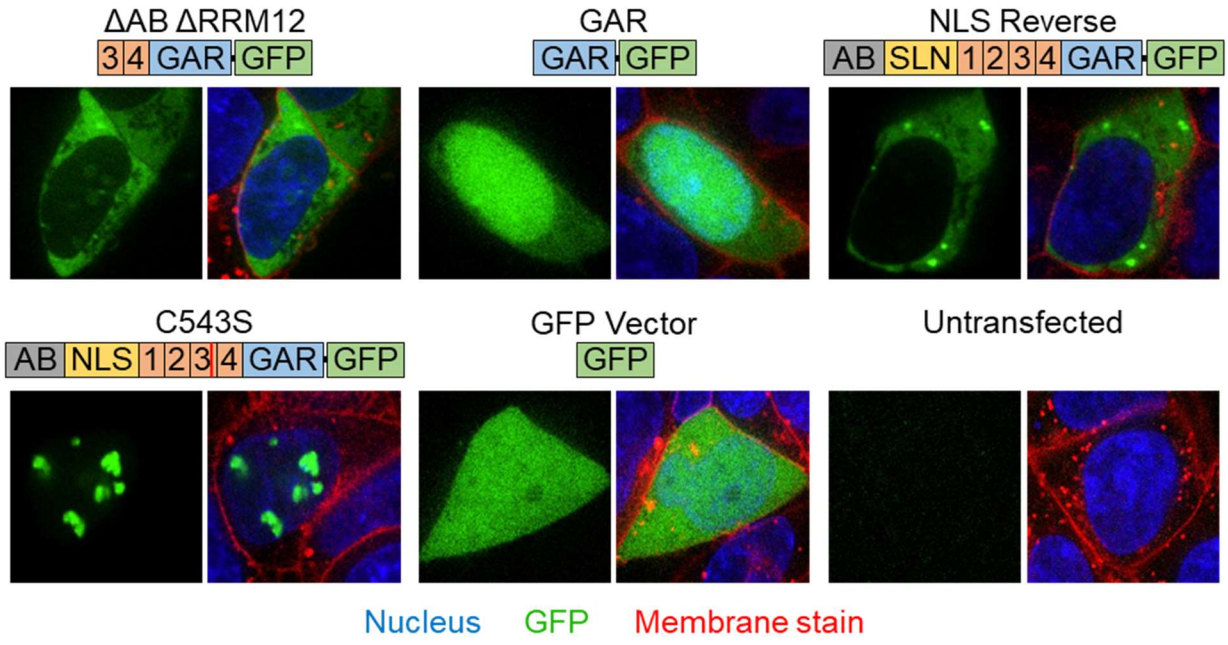

Figure 3.2 Cellular localization of NCL-GFP mutant proteins. Each NCL-GFP construct was transiently transfected into HEK-293T cells using FuGENE 6 transfection reagent. 48 hours later, the cell membranes were stained with CellMask Deep Red and the nuclei were stained with NucBlue Live ReadyProbes Reagent. The cells were then imaged live on a spinning disk confocal microscope in a chamber heated to 37°C, with 5% CO_2. For each mutant protein, the GFP channel alone is shown on the left, while a merged image with GFP, membrane stain, and nuclear stain is shown on the right.

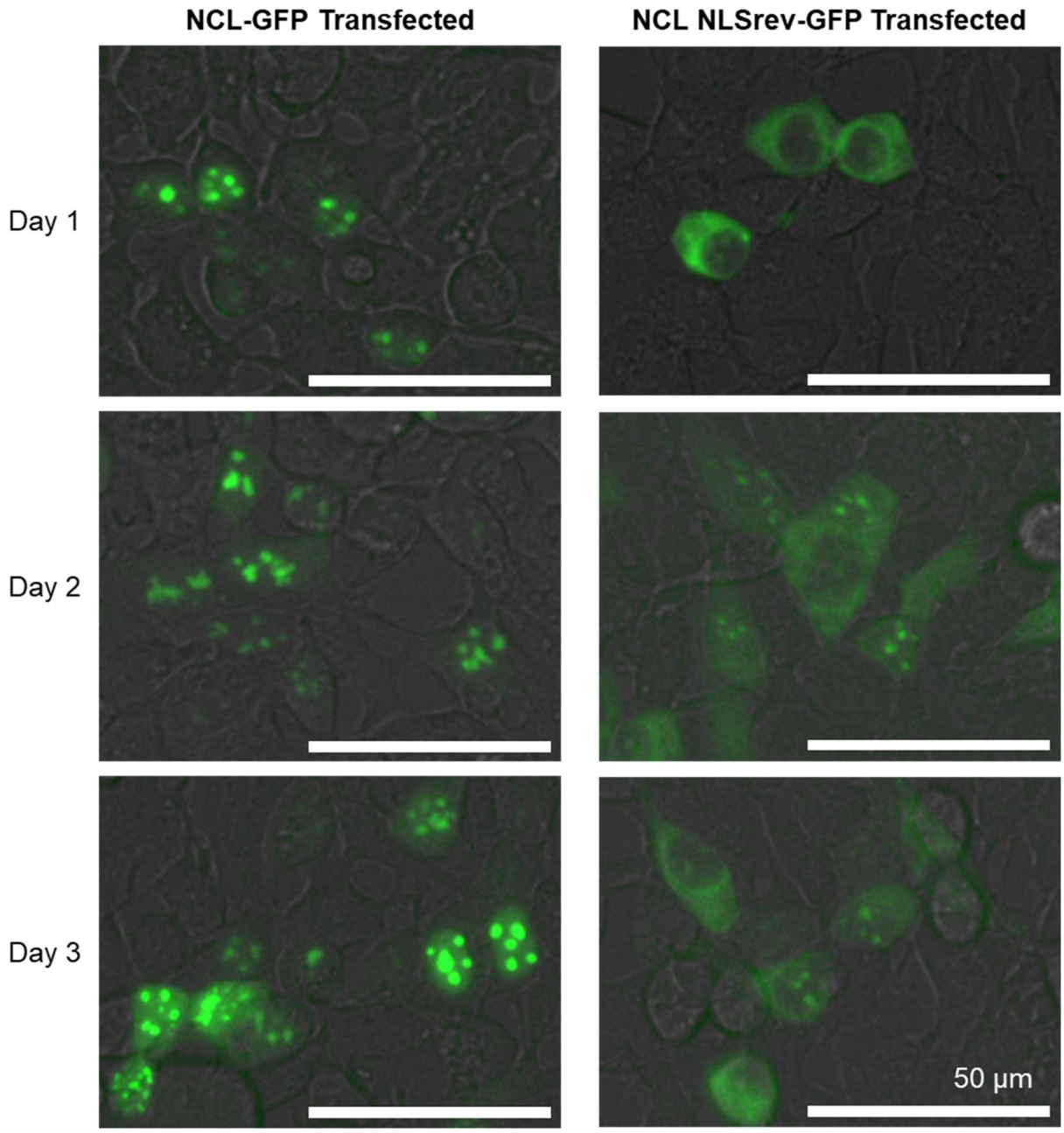

Figure 3.3 Time course of NCL-GFP and NCL NLS-reverse-GFP expression. NCL-GFP and NCL NLS-reverse-GFP were transfected into HEK-293T cells using FuGENE6 transfection reagent. At 1, 2, and 3 days post transfection, the cells were imaged using the EVOS FL-Auto fluorescent microscope. Images are shown with green fluorescence overlaid on to transillumination.

Similar to the above imaging analysis, I transfected each NCL-GFP construct into HEK-293T cells. However, instead of imaging, I collected whole cell lysate using MOSLB lysis buffer and examined the mutant proteins by western blot using antibodies against NCL and GFP (**Figure 3.4**).

In all samples, I observed endogenous NCL at approximately 100 kDa, and the addition of the GFP tag increased the molecular weight of NCL by about 25 kDa. The anti-NCL antibody was raised against a peptide containing the first 2 and a half RRMs, therefore, it is not expected to efficiently recognize the ΔABΔRRM12, GAR, or mutant proteins lacking 3 RRMs. Removing portions of the protein decreased the molecular weight of the mutant protein as expected. The largest reduction of molecular weight was observed when the AB domain was removed, since this region contains 272 out of 710 residues, along with numerous phosphorylation sites. Removing other regions similarly decreased the molecular weight of the mutant protein, though to lesser degrees, since each RRM is approximately 75 amino acids long and the GAR domain contains 53 amino acids. Although each RRM is approximately the same size, the mutant proteins lacking RRMs 134 and 123 migrated slightly slower than the mutant proteins lacking RRMs 234 and 124. Of note, the 25 kDa free form of GFP could not readily be detected in any of the lysates containing the NCL-GFP mutant proteins, with the exception of a minor amount in the lysate containing the GAR domain only mutant protein. This indicates that the GFP is not cleaved from the protein during maturation.

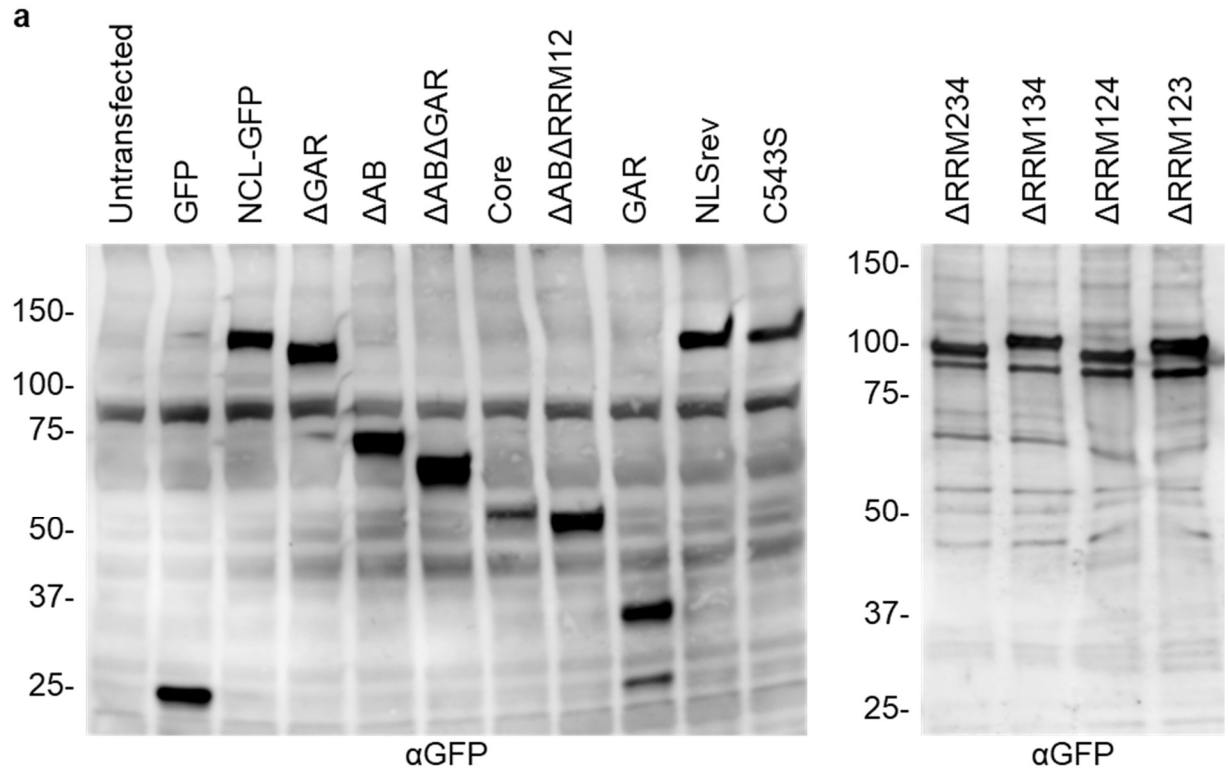

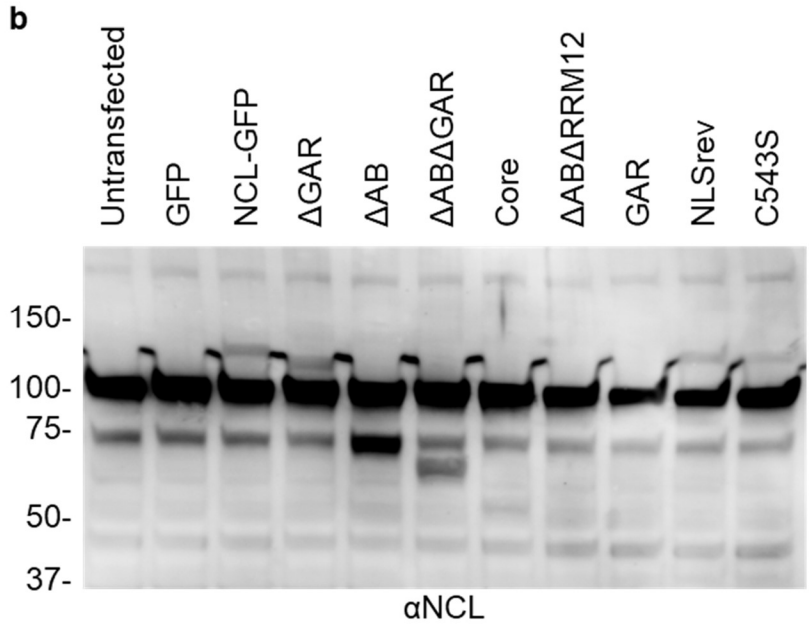

Figure 3.4 Western blot of NCL-GFP mutant proteins. Each NCL-GFP construct (**Figure 3.1**) was transfected into HEK-293T cells using FuGENE 6 transfection reagent. 48 hours later, the cells were lysed using MOSLB lysis buffer, including cOmplete mini protease inhibitor, then analyzed by western blot using antibodies against GFP **(a)** and NCL **(b)**. Panel **a** done with Aleks Stojic.

3.2.1.3 Cell surface expression of NCL-GFP mutant proteins

Although the nuclear localization of various NCL truncation mutants has been described previously[175,201], the ability of each truncation mutant to be expressed on the cell surface has not. To test this, I transfected the NCL-GFP truncation mutants into HEK-293T cells and harvested the cells without permeabilization 48 hours later. I detected the presence of each mutant protein on the cell surface using anti-GFP antibodies and analyzed the cells by flow cytometry (**Figure 3.5**). As expected, very little GFP could be detected on the surface of cells transfected with GFP alone. However, a significant proportion of NCL-GFP transfected cells were positive for surface GFP, indicating that the NCL-GFP mutant protein is expressed on the cell surface.

When the truncation mutants were examined, there were a few noticeable trends (**Figure 3.5**). Each NCL mutant lacking the GAR domain had impaired expression on the cell surface, compared to a similar mutant with the GAR domain – NCL-GFP vs ΔGAR and ΔAB vs ΔABΔGAR. Conversely, each NCL mutant lacking the AB domain had enhanced surface expression – NCL-GFP vs ΔAB and ΔGAR vs ΔABΔGAR. Despite the apparent role GAR plays in the surface

expression of NCL, GAR alone is not sufficient to mediate surface expression. This is likely due to role played by the RRMs in NCL surface expression. Each mutant protein lacking RRMs (Core, ΔABΔRRM12, GAR, ΔRRM234, ΔRRM134, ΔRRM124, and ΔRRM123) also had reduced cell surface expression compared to a full length NCL-GFP. The C543S mutant protein was capable of making it to the cell surface, albeit a bit less efficiently compared to wildtype NCL (though not statistically significant). Despite localizing to a different cellular compartment, compared to wildtype NCL (**Figure 3.2)**, the NLS reverse mutant was also observed on the cell surface.

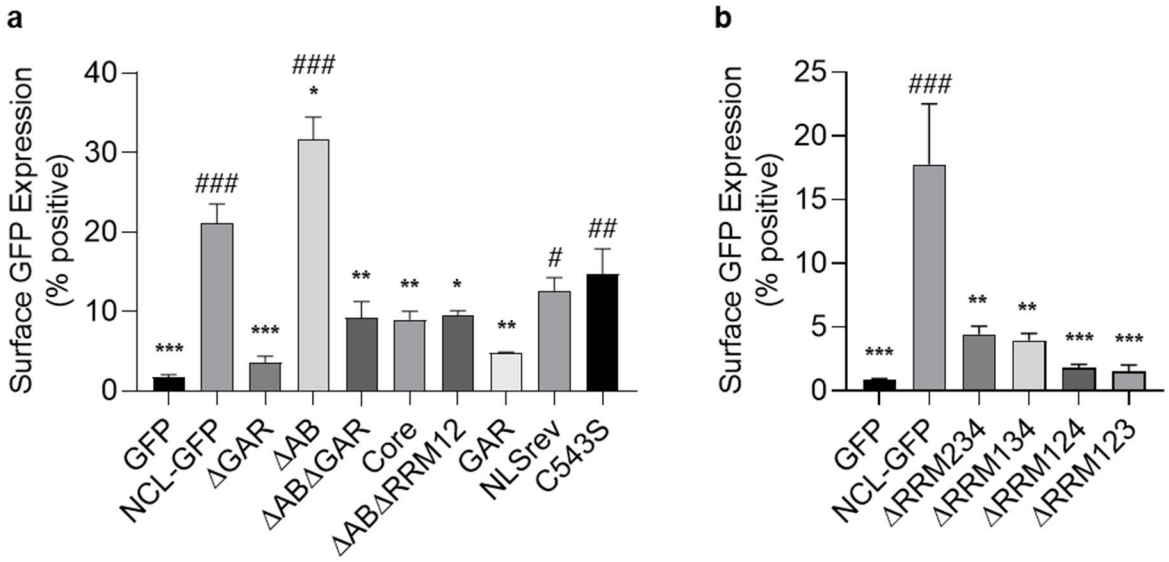

Figure 3.5 Surface expression of NCL-GFP mutant proteins. Each NCL-GFP construct (**Figure 3.1**) was transfected into HEK-293T cells using FuGENE6 transfection reagent. 48 hours later, the cells were harvested without permeabilization using ice-cold 10mM EDTA. The cells were then stained for surface GFP and analyzed by flow cytometry. Single cells were gated from doublets/clumps and GFP-positive cells were analyzed for surface GFP expression. Data in panel **a** was derived from three independent experiments, while panel **b** was derived from two independent experiments, with two biological replicates per experiment (four data points per bar). The data was statistically analyzed by one-way ANOVA followed by Tukey's post hoc test. * indicates comparison to NCL-GFP, # indicates comparison to GFP. */#; $p < 0.05$, **/##; $p < 0.01$, ***/###; $p < 0.001$. Panel **b** done with Aleks Stojic.

3.2.2 Cell-to-cell transfer of surface NCL

3.2.2.1 Surface NCL-GFP expression on untransfected HEK-293T cells

When transiently transfecting cells, the distribution of plasmid-containing transfection complexes is random, and therefore a proportion of cells does not uptake plasmid. These untransfected cells therefore don't express the desired gene. In the case of NCL-GFP, the untransfected cells can be

differentiated from transfected cells by GFP fluorescence. When examining the surface expression of NCL-GFP, I noticed that a large proportion of untransfected (GFP-negative) cells stained positive for surface NCL-GFP (**Figure 3.6**, right panel, bottom-right quadrant). Furthermore, the level of surface GFP expression did not correlate with the intensity of GFP expression within the cells. This led me to hypothesize that NCL-GFP may be transferring from the surface of transfected cells to the surface of untransfected cells.

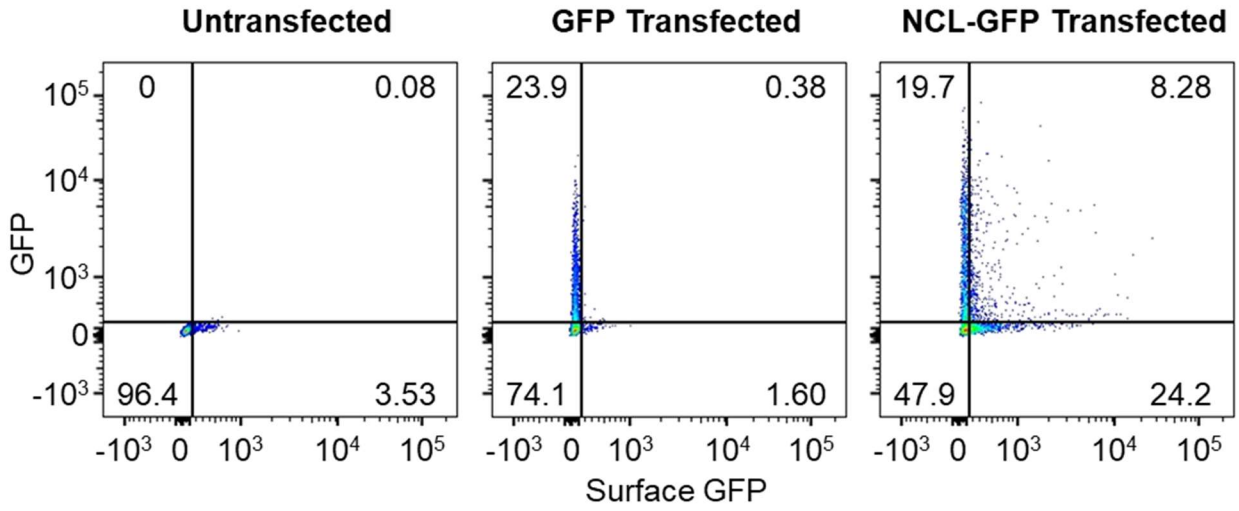

Figure 3.6 NCL-GFP is expressed on the surface of GFP-negative cells. Using the same experimental setup as **Figure 3.5**, transfected HEK-293T cells were analyzed by flow cytometry for GFP expression and stained to detect surface GFP. Cells were treated with transfection reagent alone (left), transfected with GFP (middle), or transfected with NCL-GFP (right). The expression of cell surface GFP was then graphed against GFP expression using FlowJo software (version 10). The bottom-right quadrant of the right panel shows cells that were negative for NCL-GFP expression, but positive for cell surface GFP.

3.2.2.2 Transfer of NCL-GFP mutant proteins between the surface of HEK-293T cells

To directly test if NCL-GFP was indeed transferring from the surface of one cell to another, I set up a co-culture system. A population of HEK-293T 'donor' cells were transfected with NCL-GFP or GFP alone, while a population of HEK-293T 'recipient' cells were transfected with mCherry. 24 hours later, the cells were trypsinized, combined, and co-cultured for 48 hours (**Figure 3.7**). The cells were then harvested, stained for surface GFP, and analyzed by flow cytometry. GFP expression was used to detect donor cells, while mCherry expression was used to differentiate recipient cells (**Figure 3.8**). Similar to detecting GFP on the surface of untransfected cells, GFP was detected on the surface of mCherry expressing cells. Unexpectedly, the proportion of cells

expressing surface GFP was similar between GFP-positive and mCherry-positive cells (**Figure 3.9**, NCL-GFP bars). This is counter-intuitive since one would expect that the GFP-positive cells producing NCL-GFP should have more cell surface GFP, with less surface GFP observed on the mCherry-positive cells, which can only obtain cell surface GFP via transfer. Instead the equal amount of cell surface GFP on donor and recipient cells indicates that cell surface GFP is readily shared to form an equilibrium.

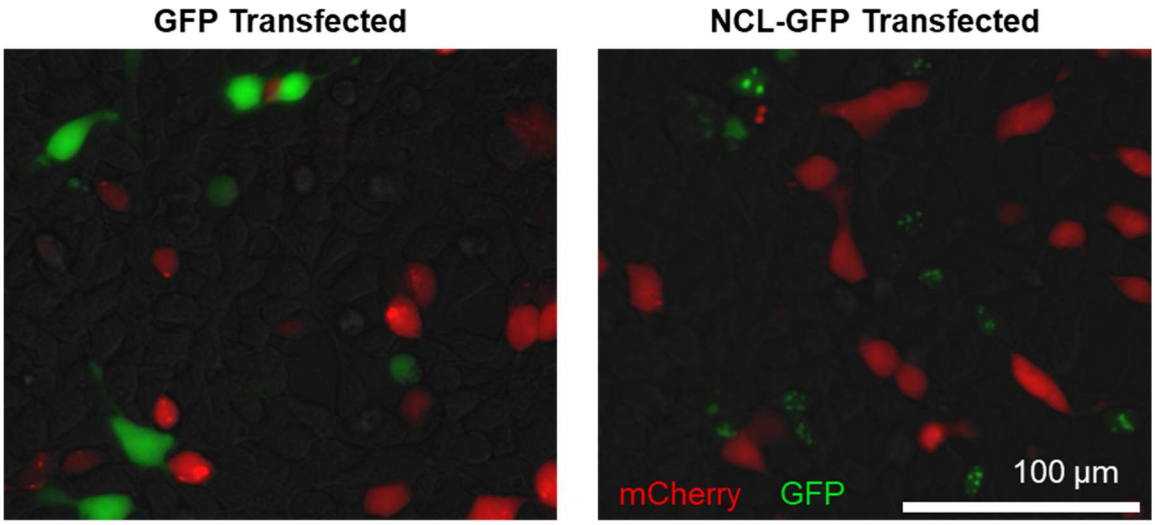

Figure 3.7 Co-culture of donor and recipient HEK-293T cells. Donor HEK-293T cells were transfected with NCL-GFP or GFP alone and recipient HEK-293T cells were transfected with mCherry. The cells were then co-cultured for 48 hours and imaged using the EVOS FL-Auto fluorescent microscope. Images are shown with red and green fluorescence overlaid on to transillumination.

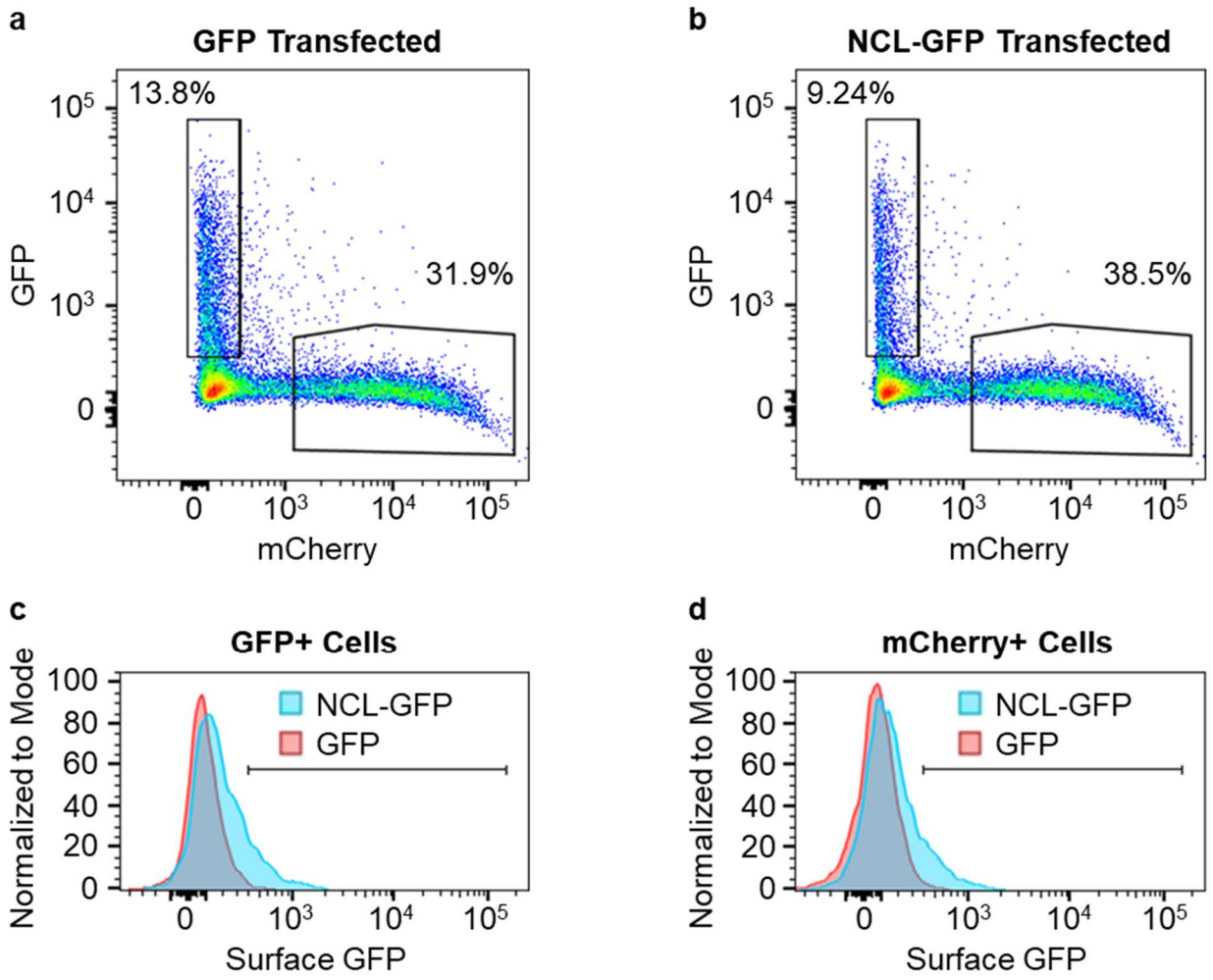

Figure 3.8 Transfer of NCL-GFP to mCherry expressing HEK-293T cells. HEK-293T donor cells were transfected with NCL-GFP or GFP, while HEK-293T recipient cells were transfected with mCherry. The donors and recipients were then co-cultured for 48 hours and surface GFP was measured by flow cytometry. Representative flow plots from co-cultures where the donors were transfected with GFP (**a**) or NCL-GFP (**b**) are shown. GFP-positive cells within the gates shown were used to create panel **c**, while mCherry-positive cells were used to create panel **d**. Representative flow plots showing cell surface GFP on donor cells (GFP-positive, panel **c**), and recipient cells (mCherry-positive, panel **d**). Note that both donors and recipients from the NCL-GFP transfected co-culture express surface GFP. The mCherry vs GFP graphs and surface GFP histograms were made using FlowJo software (version 10). Quantification for NCL-GFP surface transfer is shown in **Figure 3.9**.

Using the same experimental setup, the NCL-GFP truncation mutants from section 3.2.1 (**Figure 3.1**) were tested for their ability to transfer between cells. Each NCL-GFP construct was transfected into the HEK-293T donor cells, while transfection of mCherry into the recipients remained constant. The cells were then analyzed by flow cytometry for surface GFP expression

(**Figure 3.9**). Compared to the NCL-GFP mutant protein surface expression characterized in **Figure 3.5**, a similar trend was observed among the GFP-positive donor cells. However, the ΔABΔGAR and ΔABΔRRM12 mutant proteins were no longer expressed significantly less than full length NCL-GFP on the surface of cells. This could be attributed to the longer timeframe of the experiment due to the addition of the co-culture.

Interestingly, an almost identical trend was observed was observed in the mCherry-positive recipient cells, which implies that requirements for surface expression and cell-to-cell transfer of NCL-GFP are the same (**Figure 3.9**). Furthermore, no significant differences between the surface expression of each mutant protein on the surface of GFP-positive and mCherry-positive cells could be observed. This indicates that over the 48-hour co-culture period, the surface-expressed NCL-GFP mutant proteins are readily shared and form an equilibrium among donor and recipient cells.

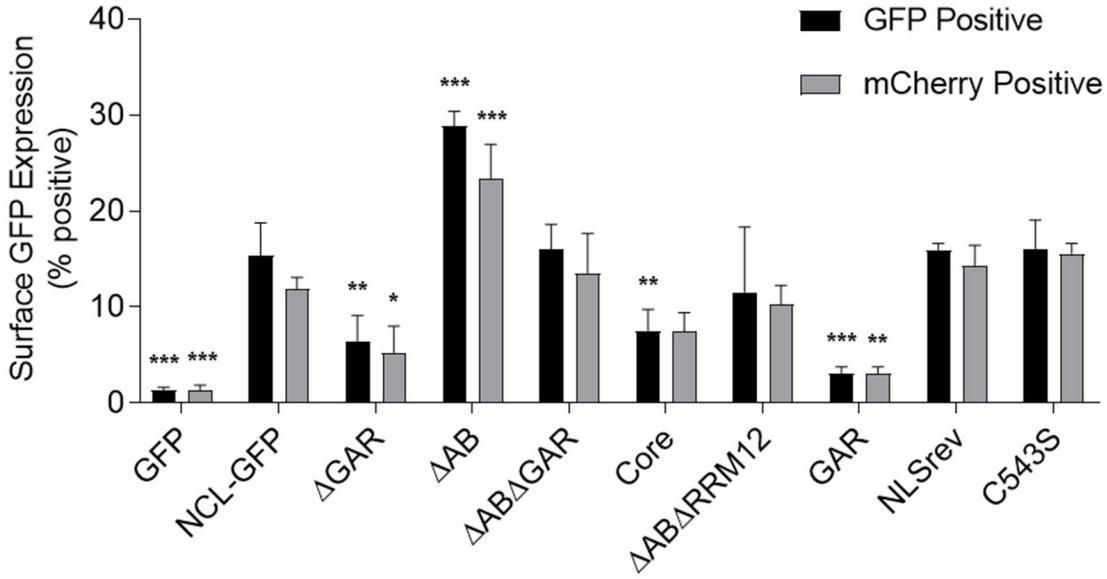

Figure 3.9 Transfer of NCL-GFP mutant proteins between the surface of HEK-293T cells. HEK-293T donor cells were transfected with NCL-GFP constructs (**Figure 3.1**) and recipient cells were transfected with mCherry. The cells were then co-cultured for 48 hours and surface GFP expression was analyzed by flow cytometry. Data was derived from three independent experiments, with two biological replicates per experiment. The biological replicates were averaged, and each bar represents of three data points. The data was statistically analyzed by 2-way ANOVA. Sidak's post hoc was used to compare GFP-positive and mCherry-positive cells for each mutant protein (non-significant). Dunnett's post hoc was used to compare each mutant protein to NCL-GFP within the same population (GFP-positive compared to GFP-positive and mCherry-positive compared to mCherry-positive). *; $p < 0.05$, **; $p < 0.01$, ***; $p < 0.001$. Experiment done with Aleks Stojic.

3.2.2.3 Contact dependence of surface NCL-GFP transfer

Since NCL-GFP could readily be detected on the surface of recipient cells during co-culture, I then sought to further probe the mechanism by which the NCL-GFP is transferring. One possibility is that the transfer is mediated by extracellular vesicles (EVs). EVs are a well characterized contact-independent mechanism of intercellular protein transfer, which are of particular interest since NCL has been observed in preparations of EVs[223-225]. However, it hasn't been determined if NCL is inside the EVs or attached to the outside. Attachment to the outside of EVs would be required for direct transfer of NCL to the surface of a recipient cell. Since NCL does not have a transmembrane domain, another contact-independent possibility is that soluble NCL is released from donor cells and binds to the surface of recipient cells. To investigate these contact-independent possibilities, GFP, NCL-GFP, or ΔAB was transfected into donor HEK-293T cells. The donors were co-cultured with recipient HEK-293T cells in a transwell dish, separated by a membrane with 400 nm pores, which are of sufficient size to permit exosomes and other small EVs to pass through. The ΔAB mutant was included since it consistently has higher levels of surface expression and intercellular transfer, compared to full length NCL-GFP. The GFP surface expression on the recipient cells was then measured by flow cytometry (**Figure 3.10a**). HEK-293T cells transfected with NCL-GFP were used as a positive control and HEK-293T cells transfected with GFP were used as a negative control. GFP was not observed on the surface of any recipient cell populations within the transwell dish, indicating that NCL-GFP was not transferred across the membrane. To further examine contact dependence, HEK-293T donor cells were transfected with NCL-GFP or GFP, then 48 hours later the conditioned media from the transfected cells was applied to mCherry-transfected recipient HEK-293T cells for 24 hours. The mCherry-positive recipient cells were then analyzed by flow cytometry (**Figure 3.10b**). No significant levels of GFP were detected on the surface of recipient cells after media transfer. Donor and recipient HEK-293T cells directly co-cultured were used as positive (NCL-GFP transfected) and negative (GFP transfected) controls for NCL-GFP transfer. Together, these data indicate that the transfer of cell surface NCL-GFP is cell-cell contact dependent.

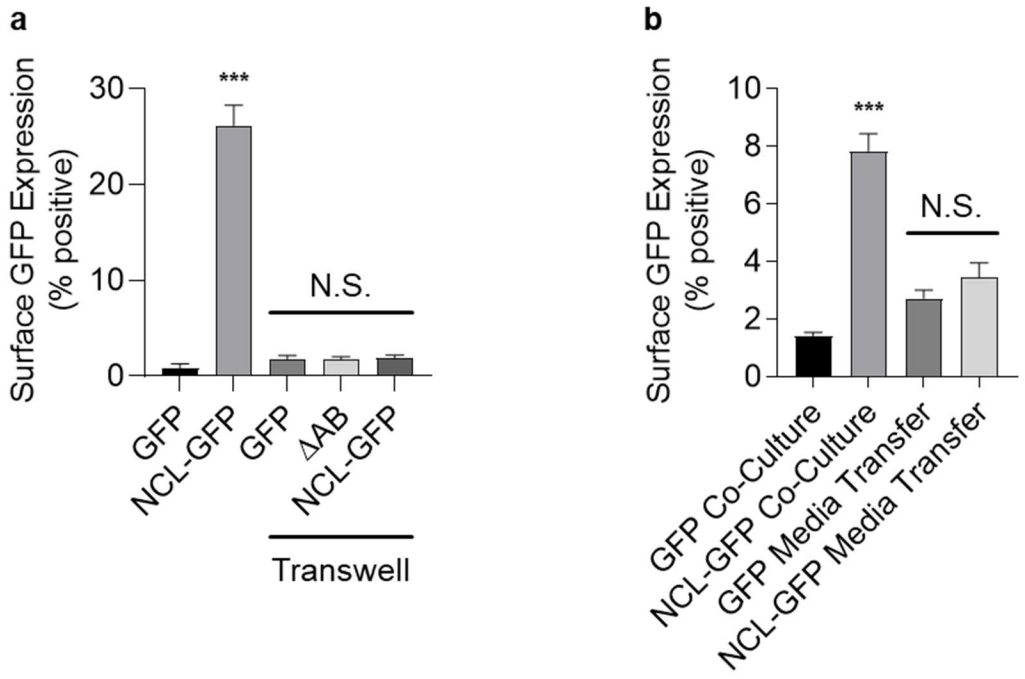

Figure 3.10 Contact dependence of NCL-GFP surface transfer. a) HEK-293T donor cells were transfected with NCL-GFP, ΔAB, or GFP then co-cultured with untransfected HEK-293T cells in a transwell dish, separated by a membrane with 400 nm pores. Surface GFP expression was then quantified by flow cytometry. HEK-293T cells transfected with NCL-GFP or GFP, without co-culture, are used a positive and negative controls respectively. Data was statistically analyzed by one-way ANOVA, with Tukey's post hoc, comparing each mutant protein to GFP within the same group (transwell or without co-culture). **b)** HEK-293T donor cells were transfected with NCL-GFP or GFP. Recipient cells transfected with mCherry were then co-cultured with donor cells for 48 hours or were incubated in conditioned media from donor cells for 24 hours. Surface GFP on the mCherry-positive recipient cells was then quantified by flow cytometry. Data was statistically analyzed by one-way ANOVA and Sidak's post hoc comparing GFP to NCL-GFP for each group (co-culture or media transfer). N.S.; non-significant, ***; $p < 0.001$. Data in both panel **a** and **b** was derived from two independent experiments, with three biological replicates per experiment (six data points per bar). Experiment done with Aleks Stojic.

3.2.2.4 Transfer of cell surface NCL-GFP between different cell types

To determine if the transfer of NCL-GFP between the surface of cells is specific to cell type, I tested if the transfer could occur using HEK-293T cells as donors and 1HAEo- bronchial epithelial cells as recipients. 1HAEo- cells were chosen as recipients since they endogenously express low levels of NCL and I utilized them extensively as a model cell line for RSV infection in **Chapter 4** and **Chapter 5**. Since 1HAEo- cells do not efficiently transfect, I stained them with CellTracker Orange CMRA to differentiate them from donor cells. Similar to previous experiments, I detected surface GFP expression using antibodies against GFP since it differentiates surface from internal

GFP (**Figure 3.6**). Using primary antibodies against GFP followed by fluorophore-conjugated secondary antibodies also greatly enhances the fluorescent signal (**Figure 3.11**). After co-culturing the donor and recipient cells, I analyzed the surface expression of NCL-GFP by flow cytometry. Similar to the co-culture between HEK-293T cells (**Figure 3.8**), I found that surface NCL-GFP was found in similar levels in both CellTracker-negative HEK-293T cells and CellTracker-positive 1HAEo- cells (**Figure 3.12**).

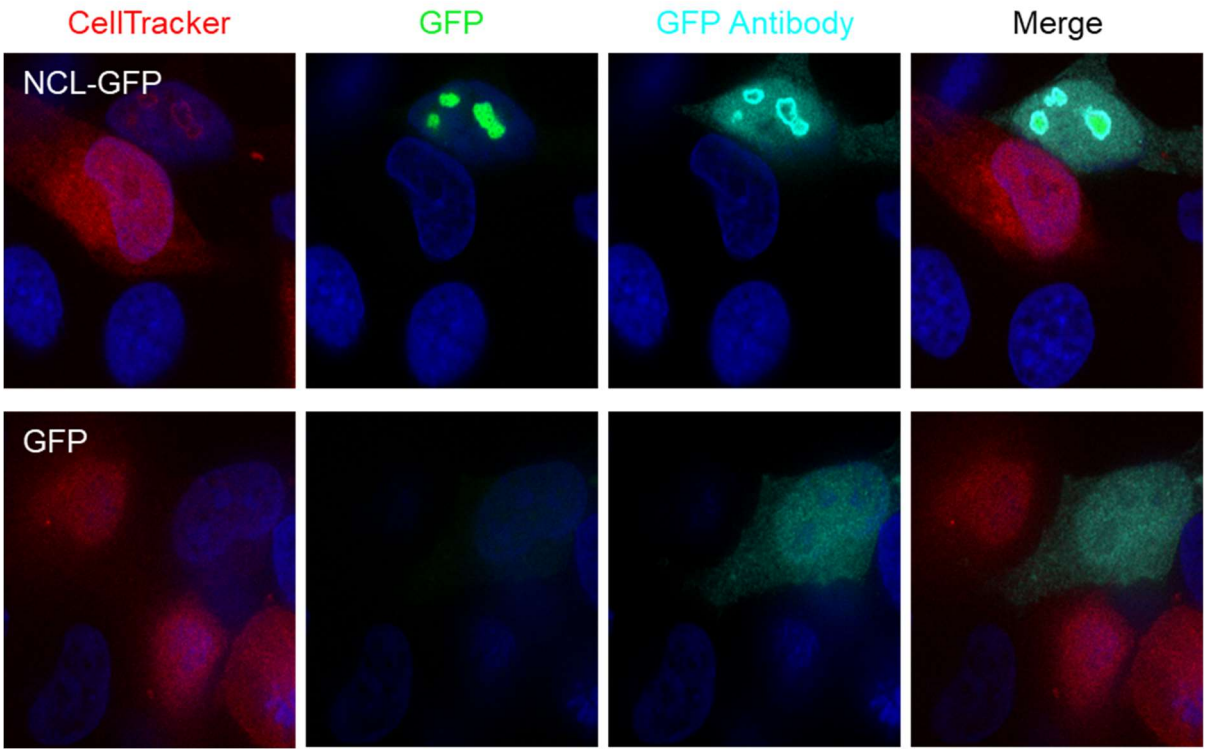

Figure 3.11 Co-culture of donor HEK-293T cells and recipient 1HAEo- cells. HEK-293T cells transfected with NCL-GFP or GFP were co-cultured for 48 hours with 1HAEo- cells stained with CellTracker Orange CMRA. The cells were then fixed, permeabilized, and stained with anti-GFP primary antibodies, followed by Alexa 647-conjugated secondary antibodies. The cells were then imaged on a spinning disk confocal microscope. Nuclei were stained with NucBlue Fixed ReadyProbes Reagent (DAPI derivative). Experiment performed with Aleks Stojic.

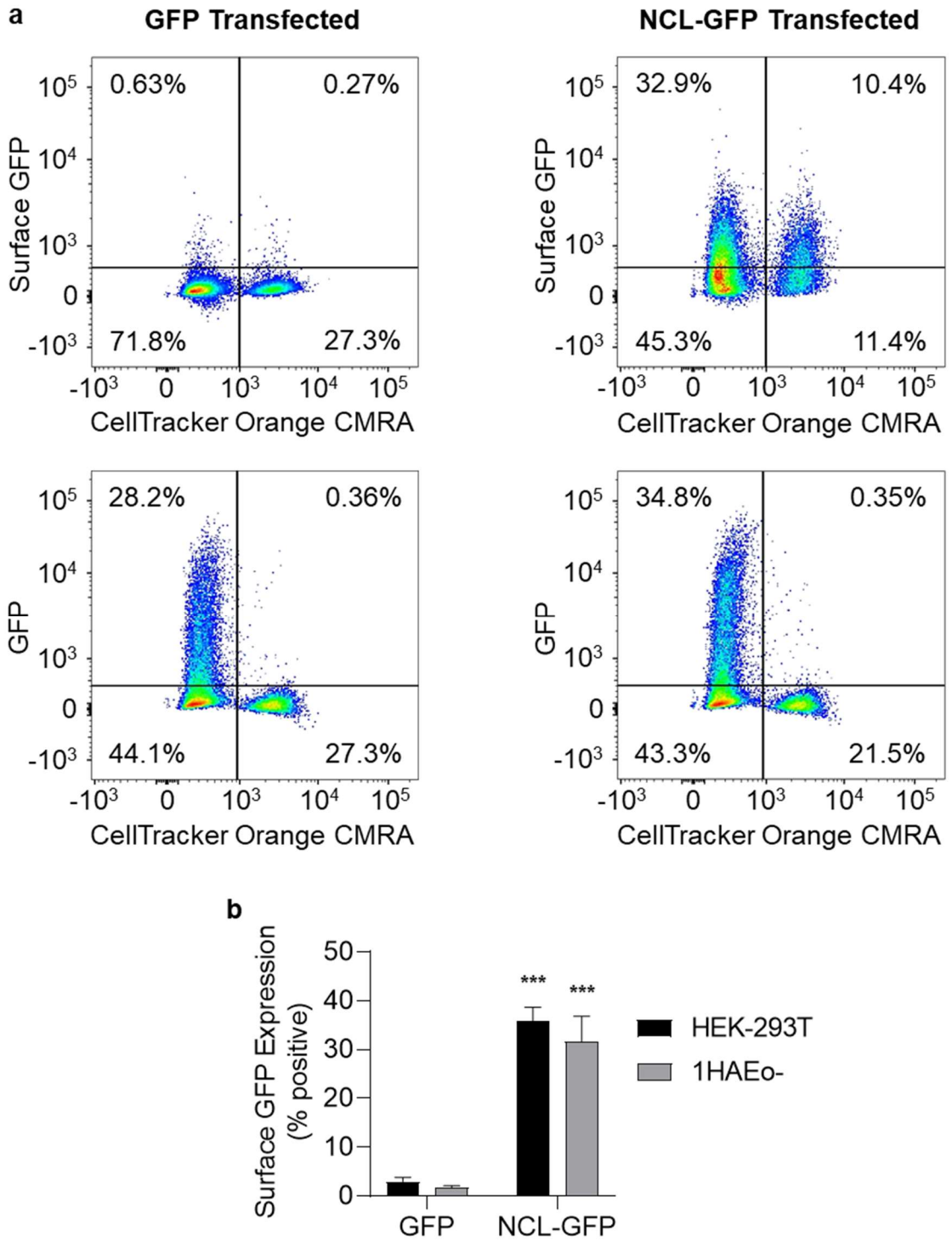

Figure 3.12 Transfer of NCL-GFP from HEK-293T cells to 1HAEo- cells. HEK-293T donor cells were transfected with NCL-GFP or GFP alone and co-cultured with 1HAEo- recipient cells that were stained with CellTracker Orange CMRA. 48 hours later, the cells were harvested, stained for surface GFP, and analyzed by flow cytometry. **a)** Representative flow plots showing GFP and surface GFP expression in the HEK-293T donor cells (CellTracker-negative) and 1HAEo- recipient cells (CellTracker-positive) were generated using FlowJo (version 10). The top row

shows surface GFP expression in all donor and recipient cells, where donor cells were transfected with GFP (left) or NCL-GFP (right). The upper right quadrants show recipient cells that have received cell surface GFP. The bottom row shows total GFP expression in all donor and recipient cells, where donor cells were transfected with GFP (left) or NCL-GFP (right). Note that the recipient cell populations do not have detectable total GFP levels (upper right quadrant). **b)** Quantification of the surface GFP expression for the HEK-293T and 1HAEo- cells. Data was derived from three independent experiments, with three biological replicates per experiment (nine data points per bar). The data was statistically analyzed by 2-way ANOVA. Sidak's post hoc was used to compare HEK-293T cells and 1HAEo- cells for each mutant protein (non-significant). Sidak's post hoc was also used to compare each GFP to NCL-GFP within the same population (HEK-293T compared to HEK-293T and 1HAEo- compared to 1HAEo-). ***; $p < 0.001$. Experiment done with Aleks Stojic.

To test if the transfer of cell surface NCL was specific to the donor cell type, 1HAEo- cells were used as both donors and recipients. Similar to **Figure 3.12**, donor cells were transfected with NCL-GFP or GFP and recipient cells were stained with CellTracker Orange CMRA. To improve transfection efficiency in the 1HAEo- cells, jetPRIME was used instead of FuGENE6 to transfect the cells. However, even with this improved transfection reagent, the overall transfection efficiency was very low (~2-3%). The background GFP fluorescence was also much higher and the cell viability upon analysis was lower compared to the HEK-293T cells. This is likely due to the greater adherence of 1HAEo- cells to the tissue culture plate, which are not efficiently removed by the 10mM EDTA, compared to the HEK-293T cells. Despite the low level of surface NCL-GFP, it still efficiently transferred from donor cells to recipient cells (**Figure 3.13**).

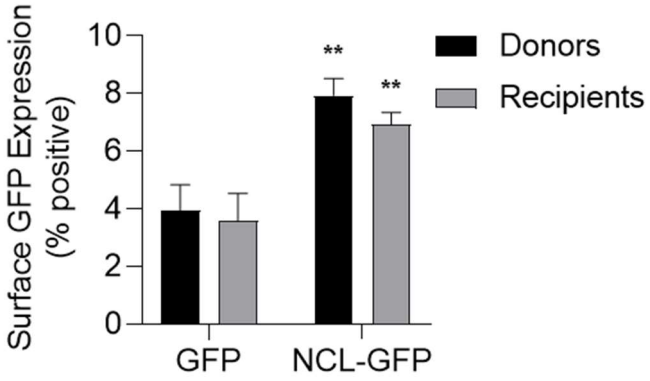

Figure 3.13 Transfer of NCL-GFP between 1HAEo- cells. Donor 1HAEo- cells were transiently transfected with GFP or NCL-GFP using jetPRIME transfection reagent. Recipient 1HAEo- cells were stained with CellTracker Orange CMRA. The cells were then co-cultured for 48 hours and surface GFP was examined by flow cytometry. The data was derived from two independent experiments, with three biological replicates per experiment (six data points per bar). The data was

statistically analyzed by 2-way ANOVA. Sidak's post hoc was used to compare donor and recipient cells for each mutant protein (non-significant). Sidak's post hoc was also used to compare each GFP to NCL-GFP within the same population (donors compared to donors and recipients compared to recipients). **; $p < 0.01$. Experiment done with Aleks Stojic.

3.2.2.5 Efficient transfer of surface proteins is specific to NCL

To test if other surface proteins are transferred in this surface GFP model, I examined an unrelated cell surface protein, transferrin receptor (TfR). TfR is a cell surface receptor that normally plays a role in iron uptake by inducing receptor-mediated endocytosis when bound by iron-containing transferrin (reviewed in [355]). TfR exists as a homodimer and contains a single transmembrane domain. To create a TfR-GFP construct, I first started with a TfR construct that encodes a functional form of TfR, with a fluorescent protein tag, that has previously been used to study endocytosis[342]. Next, I replaced the pH sensitive fluorescent protein (pHuji) with GFP (**Figure 3.14a**). I then compared the abilities of TfR-GFP and NCL-GFP to transfer from HEK-293T cells to 1HAEo- cells, using the same procedure as in **Figure 3.12**. Since a much greater proportion of TfR protein is expressed at the cell surface compared to NCL, I examined the surface GFP fluorescence intensity of recipient cells (GFP-negative HEK-293T and 1HAEo-) as a ratio of the donor cell surface GFP intensity (**Figure 3.14b**). Similar levels of surface GFP were observed between NCL-GFP transfected HEK-293T cells (GFP-positive), untransfected HEK-293T cells (GFP-negative), and 1HAEo- cells. However, in the TfR-GFP transfected culture, very little surface GFP was observed on untransfected HEK-293T cells or 1HAEo- cells. This provides evidence that the transfer of NCL-GFP between the surface of cells is not simply an artifact of over expressing a GFP-tagged surface protein.

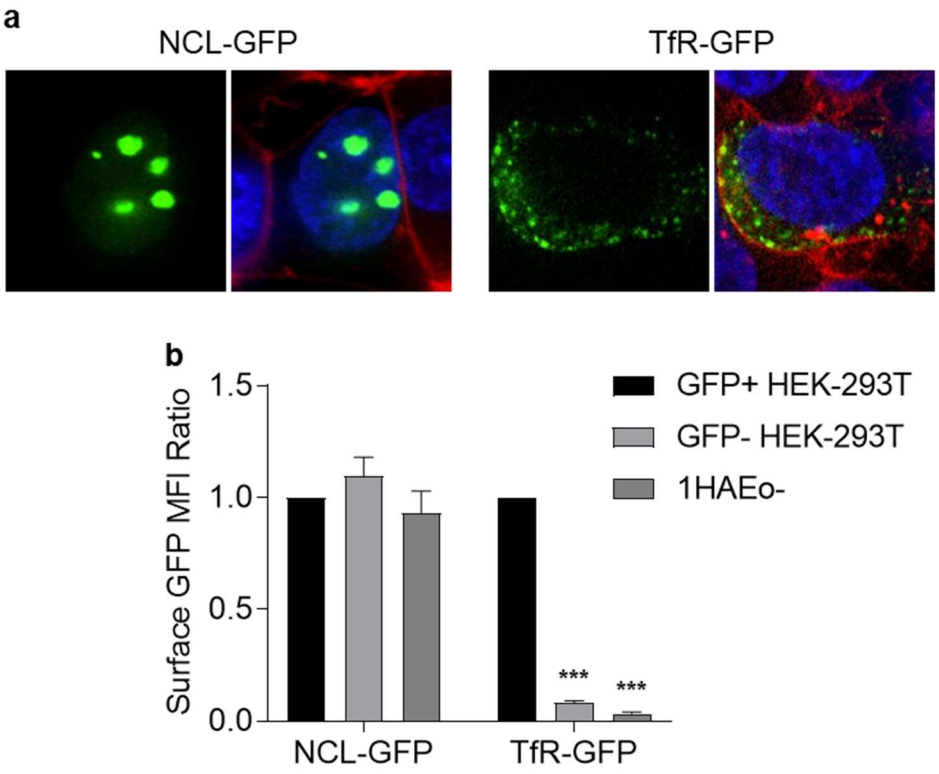

Figure 3.14 Comparing surface transfer of NCL-GFP to TfR-GFP. a) HEK-293T cells were transiently transfected with either NCL-GFP or TfR-GFP and imaged live 48 hours later. The NCL-GFP image is duplicated from **Figure 3.2** for reference. Cell membranes were stained with CellMask Deep Red and the nuclei were stained with NucBlue Live ReadyProbes Reagent. The GFP channel alone is shown on the left, while a merged image with GFP, membrane stain, and nuclear stain is shown on the right. **b)** HEK-293T cells were transfected with either NCL-GFP or TfR-GFP and co-cultured for 48 hours with 1HAEo- cells stained with CellTracker Orange CMRA. The cells were then harvested, stained for surface GFP expression, and analyzed by flow cytometry. GFP-positive HEK-293T cells are those that were successfully transfected, GFP-negative HEK-293T cells are those that did not uptake plasmid (untransfected), and CellTracker-positive 1HAEo- cells are the recipients. The surface GFP mean fluorescence intensity (MFI) for each population is shown as a ratio of the transfected donor HEK-293T cells (GFP-positive). The data was derived from two independent experiments, with three biological replicates per experiment (six data points per bar). The raw data was statistically analyzed by a 2-way ANOVA, with Tukey's post hoc test comparing each treatment to all other treatments within the same transfected group (NCL-GFP compared to NCL-GFP and TfR-GFP to TfR-GFP). Statistical significance was only found comparing GFP-negative HEK-293T cells and 1HAEo- cells to GFP-positive HEK-293T cells in the TfR transfected group. ***; $p < 0.001$. Panel **b** performed with Aleks Stojic.

3.2.3 Investigating NCL palmitoylation

3.2.3.1 Testing palmitoylation of NCL-GFP

Although NCL has been observed on the surface of cells from various tissues, it is unknown how the protein remains attached. Unlike most surface proteins, NCL does not have a transmembrane domain or GPI anchor to remain attached. An alternative mechanism that enables proteins to remain attached to membranes is post-translational attachment of a fatty acid group such as palmitate[346].

Mass spectrometry screens for palmitoylated proteins have identified NCL as potentially palmitoylated[348-352]. Since the addition of a palmitate group typically occurs on a cysteine residue, I mutated the only cysteine (C543) in NCL to a serine to create a mutant lacking the proposed palmitoylation site[354]. I then transfected NCL-GFP, NCL C543S-GFP, N-Ras-GFP, and K-Ras-GFP into HeLa cells to test if the NCL proteins are palmitoylated. N-Ras-GFP and K-Ras-GFP were gifts from Dr. Luc Berthiaume (University of Alberta). N-Ras is used as a positive control for palmitoylation, while K-Ras is used as a negative control[356]. Next, I starved the cells of fatty acids for 1 hour and subsequently treated them with alkynyl-palmitate for 3-5 hours (**Figure 3.15a**). I then immunoprecipitated the transfected proteins using anti-GFP antibodies and performed a copper-catalyzed click chemistry reaction on the immunoprecipitated proteins to covalently attach azido-biotin to the alkyne palmitate[356] (**Figure 3.15b**). The presence of biotin on the immunoprecipitated proteins was then detected using western blot with a streptavidin-HRP probe. Palmitoylation was detected on N-Ras, the positive control, but not on the negative control, K-Ras (**Figure 3.16**). However, a non-specific band at 125 kDa prevented identification of NCL palmitoylation. Alkyne groups are rare in nature, so it is unlikely that the non-specific band is due to the click reaction, however, cells contain several endogenously biotinylated proteins that would be detected if they were non-specifically immunoprecipitated.

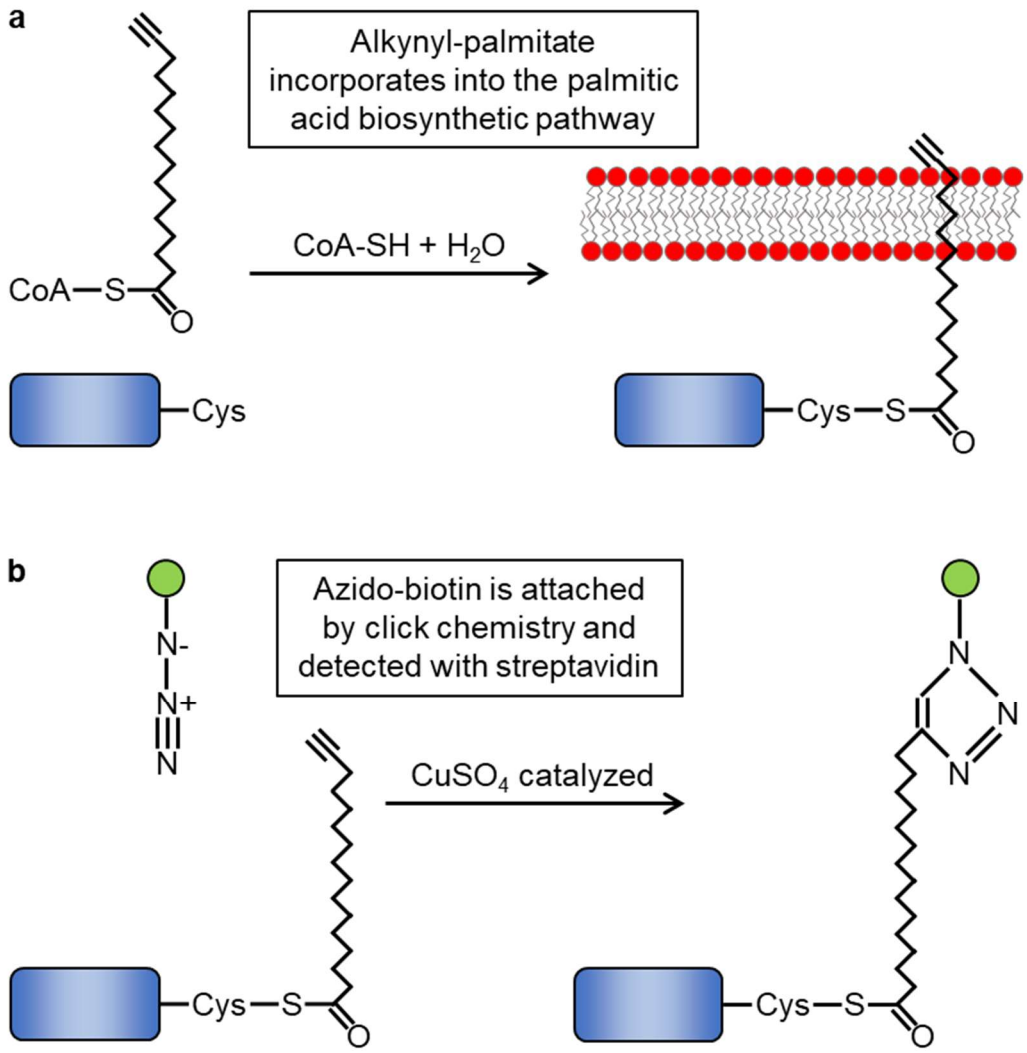

Figure 3.15 Palmitoylation assay schematic. a) HeLa cells are starved of fatty acids for 1 hour, then treated with alkynyl-palmitate for 3-5 hours. The alkynyl-palmitate incorporates into the palmitic acid biosynthetic pathway and palmitoyl transferase attaches the alkynyl-palmitate to a cysteine residue on a substrate protein. The alkynyl-palmitate then functions as a normal palmitate, inserting into a membrane. **b)** The cells are lysed, and the target proteins are immunoprecipitated. Azido-biotin is then covalently attached to the alkyne group in the palmitate by a copper-catalyzed click reaction. Streptavidin is used to detect the presence of the biotin on the palmitoylated protein.

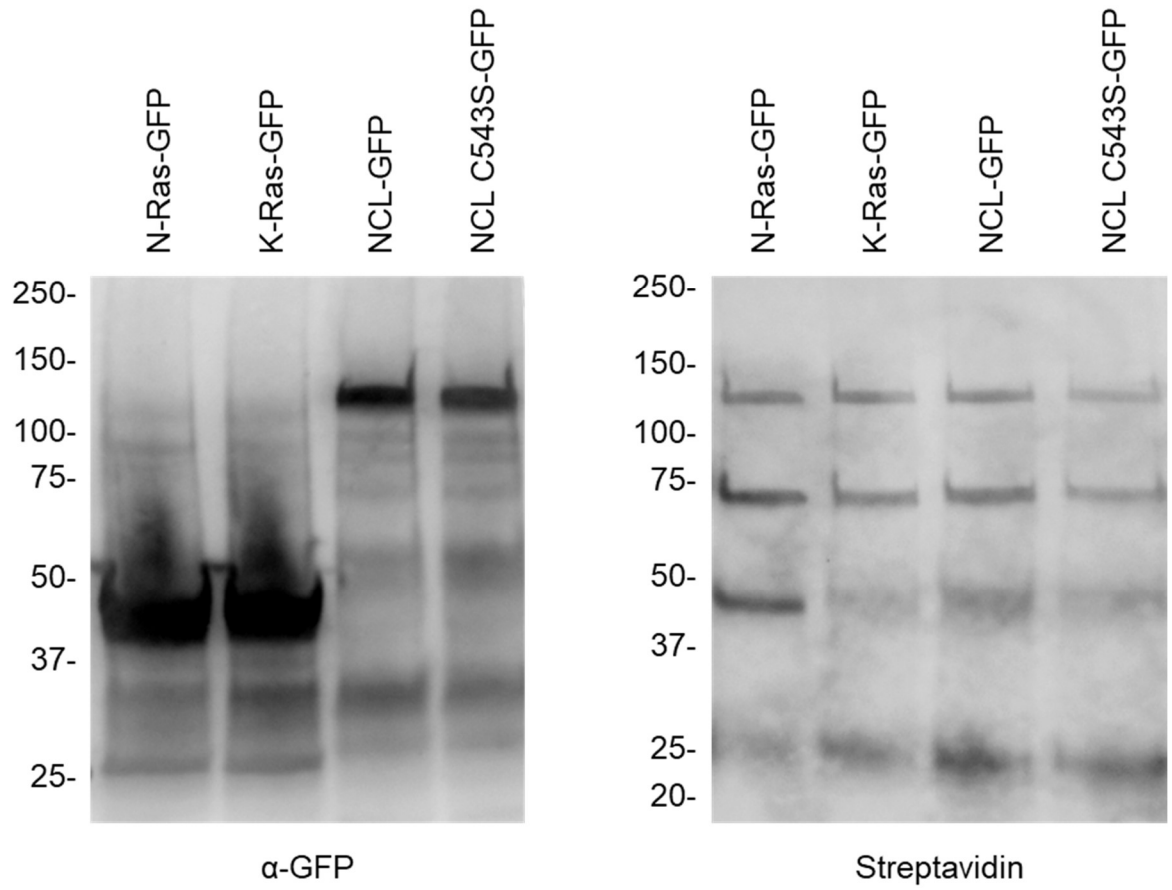

Figure 3.16 Detection of N-Ras palmitoylation. HeLa cells were transfected with N-Ras-GFP, K-Ras-GFP, NCL-GFP, or NCL C543S-GFP. 48 hours after transfection, the cells were starved of fatty acids for 1 hour, then treated with alkynyl-palmitate for 3-5 hours. The cells were lysed and immunoprecipitated using anti-GFP antibodies. A copper-catalyzed click reaction was then used to covalently attach azido-biotin to the alkynyl-palmitate. The click-reaction was halted by precipitating the proteins in ice-cold acetone. The samples were then analyzed by western blot, using anti-GFP antibodies and streptavidin-HRP to detect biotin. Molecular weight markers shown in kDa.

3.2.3.2 Testing palmitoylation of NCL-FLAG

I replaced the GFP tag on the NCL and NCL C543S constructs with a FLAG tag to decrease the molecular weight of the mutant proteins to ~100 kDa and avoid the non-specific band previously observed. I then repeated the experiment in **Figure 3.16**, using NCL-FLAG and NCL C543S-FLAG constructs, immunoprecipitated with anti-FLAG antibodies, instead of GFP-tagged NCL constructs. Furthermore, I also included non-transfected HeLa cells +/- alkynyl-palmitate and used anti-NCL antibodies to immunoprecipitate endogenous NCL (**Figure 3.17**). Similar to **Figure 3.16**, N-Ras palmitoylation was detected, while no palmitoylation was detected for either NCL-

FLAG protein or endogenous NCL. Of note, non-specifically immunoprecipitated protein band was recognized by streptavidin at approximately 150 kDa in the NCL immunoprecipitation lanes. This protein is likely endogenously biotinylated, since it is recognized by streptavidin in the absence of alkyne palmitate.

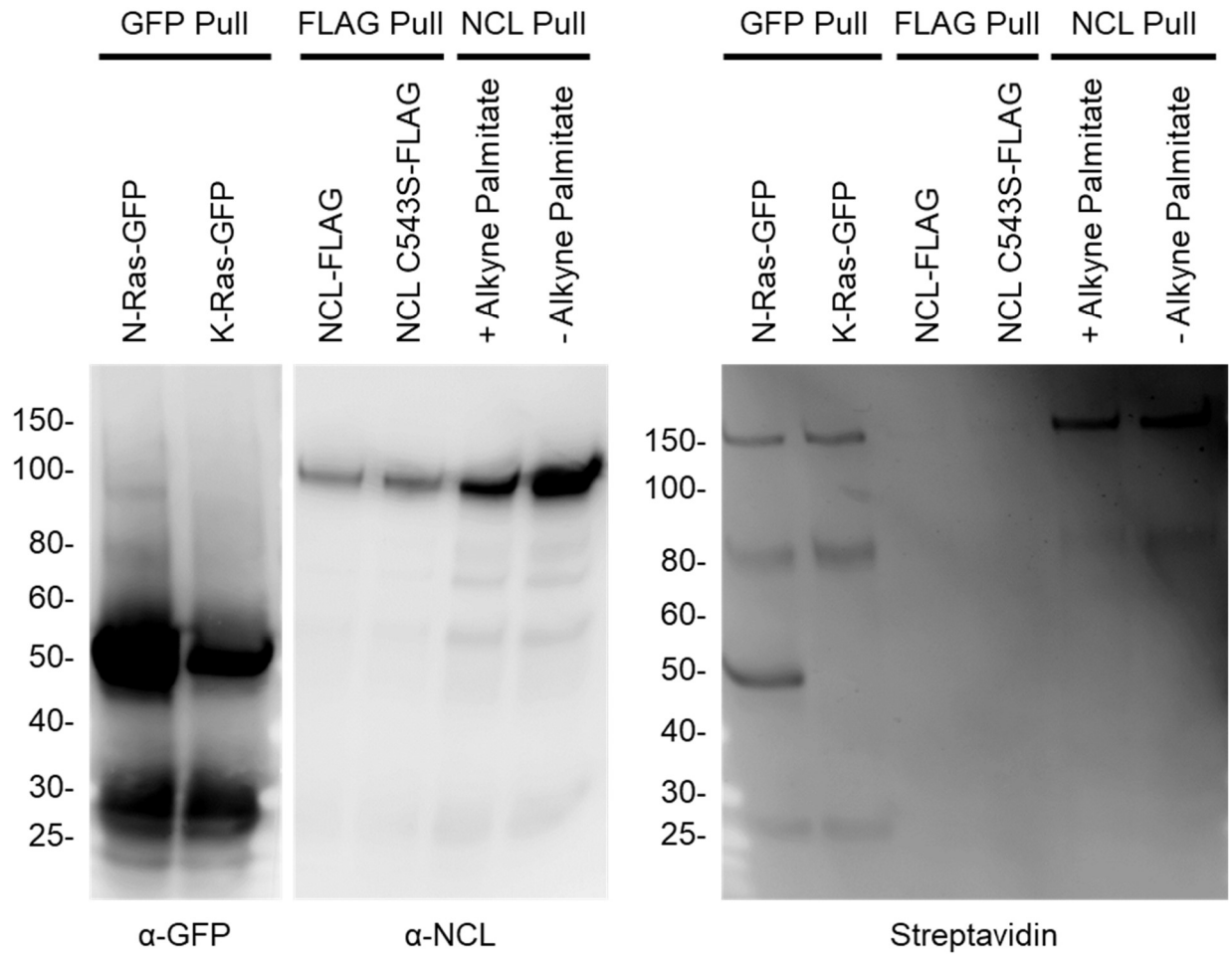

Figure 3.17 Examining potential palmitoylation of NCL-FLAG and endogenous NCL. Similar to **Figure 3.16**, HeLa cells were transfected then treated with alkynyl-palmitate. Untransfected HeLa cells +/- alkynyl-palmitate were included to examine endogenous NCL. Ras-GFP, NCL-FLAG, and endogenous NCL were immunoprecipitated by anti-GFP antibodies, anti-FLAG antibodies, and anti-NCL antibodies respectively. After the click reaction, the samples were analyzed by western blot, using anti-GFP and anti-NCL antibodies, along with streptavidin-HRP to detect biotin. Molecular weight markers shown in kDa.

3.2.3.3 Testing palmitoylation of membrane-associated NCL-GFP

Since the fraction of NCL that is found on the cell surface is a very small portion of the total NCL pool, it is possible that the lack of palmitoylation signal is due to the nuclear and cytoplasmic NCL

overwhelming the experiment. The **Figure 3.16** experiment was then repeated, with the alkynyl-palmitate treatment extended from 3-5 hours to 1 day to increase the likelihood of incorporation. A membrane isolation kit (MEM-PER) was used to harvest membrane-associated proteins before immunoprecipitation using anti-GFP antibodies. NCL-GFP transfected HeLa cells, treated with unlabeled palmitate, were used as a negative control. As above, the immunoprecipitated proteins underwent a click reaction and were analyzed by western blot (**Figure 3.18**). No detectable palmitoylation was observed in cells transfected with NCL-GFP or NCL C543S-GFP. However, a small ~40 kDa protein appeared to co-immunoprecipitate with both NCL-GFP proteins and was absent from the NCL-GFP lane lacking alkynyl-palmitate (**Figure 3.18**, arrowhead). This ~40 kDa band is likely another palmitoylated protein, since NCL is known to bind to palmitoylated proteins, including both N-Ras and H-Ras[357]. Due to its ability to bind NCL, it is possible that this palmitoylated protein plays a role in transporting NCL to the surface or tethering it to the membrane via protein-protein interactions.

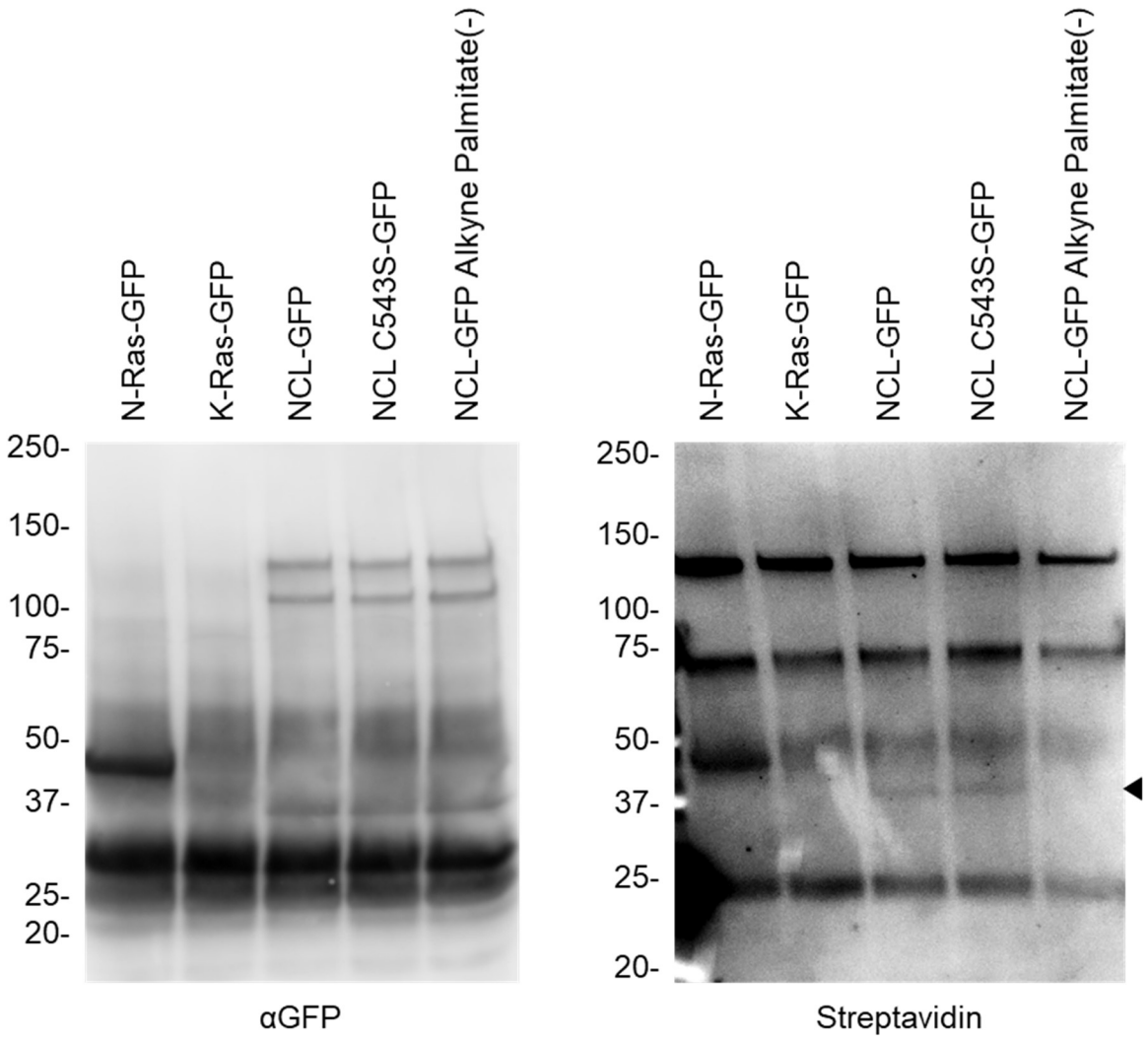

Figure 3.18 Examining palmitoylation after membrane isolation. Similar to **Figure 3.16**, HeLa cells were transfected with NCL-GFP, NCL C543S-GFP, N-Ras-GFP, or K-Ras-GFP. The cells were then starved of fatty acids for 1 hour, treated with alkynyl-palmitate (or unlabeled palmitate) for 1 day, and a membrane isolation kit (MEM-PER) was used to harvest membrane-associated proteins. The transfected proteins were then immunoprecipitated using anti-GFP antibodies and a click reaction was used to attach biotin to palmitoylated proteins. The proteins were then analyzed by western blot using anti-GFP antibodies and streptavidin-HRP. A ~40 kDa palmitoylated protein that co-immunoprecipitated with NCL-GFP and NCL C543S-GFP is marked with an arrowhead. Molecular weight markers shown in kDa.

3.3 Discussion

These results describe a series of GFP-tagged NCL truncation mutants, with the goal of elucidating the roles major NCL domains play in determining protein localization and intercellular exchange of NCL between cells. The GAR and RRM domains are the major determinants of cell surface

localization, while the presence of the AB domain restricts NCL surface expression. However, nuclear localization does not influence cell surface localization. NCL was observed to efficiently transfer between the surface of cells, with similar domain requirements as NCL surface expression. Furthermore, I could not find any support for direct palmitoylation as a mechanism of NCL membrane-tethering.

3.3.1 Cellular localization of NCL-GFP mutants

The NCL mutants were fused to GFP on the C-terminus to confirm successful transfection and examine cellular localization. Attaching GFP to the C-terminus, as opposed to the N-terminus, was chosen since the N-terminal AB domain contains several post-translational cleavage sites[220,358]. Surprisingly, the ΔRRM234 and ΔRRM124 mutant proteins appeared to have a lower molecular weight compared to the ΔRRM134 and ΔRRM123 mutant proteins. Based on the identified N-glycosylation sites in RRM1 and RRM3, I predicted that the relative sizes would be opposite what was observed[183]. This discrepancy could be explained by the presence of not yet described post-translational modification sites in RRM2 and RRM4, or that the N-glycosylation prevents the addition of post-translational modifications at other sites. The cellular localization of each NCL mutant protein agrees with previous reports of similar truncation mutants[175,201]. In general, removing the GAR or RRM domains caused a more diffuse nucleoplasmic localization of the mutant protein, while removing the AB domain or mutating C543S did not have any noticeable effect.

When examining the NLS reverse mutant, the mutant protein had a primarily cytoplasmic localization, as expected. However, it was interesting to note that some of the mutant protein entered the nucleus and this nuclear protein seemed to accumulate over time. A similar observation of partial nuclear accumulation was reported by other groups, who were examining chicken NCL with a mutated/deleted NLS[175,201]. The explanation for this nuclear accumulation, provided by Schmidt-Zachmann and Nigg[175], is that the NCL with the mutant NLS "piggy-backs" on wildtype NCL by binding to the endogenous NCL during nuclear import. Alternatively, I hypothesize that the mutant NLS NCL could enter the nucleus by binding to nucleolar proteins as the nuclear envelope reforms after mitosis.

3.3.2 The NCL GAR and RRM domains are required for surface expression

The ability of each mutant protein to be expressed on the cell surface was then tested by flow cytometry. This experiment revealed that removing the N-terminal AB domain enhanced surface expression of the NCL mutant protein. A possible explanation for this result is that interactions between the NCL AB domain and other nuclear proteins, such as histones[177,203], retains NCL within the nucleus and reduces the amount present on the cell surface. In agreement with my results, Ding and colleagues found that removing the NCL AB domain enhanced its interaction with HSC70, a chaperone protein[176]. The group also found that NCL's interaction with HSC70 was important for the cell surface expression of NCL.

Conversely, any NCL mutant proteins lacking the GAR domain had decreased expression on the cell surface. This could be explained by protein folding issues with constructs that lack the GAR domain. However, this is unlikely since the GAR domain is predicted to be largely disordered and the mutants lacking the GAR domain still effectively enter the nucleus (as opposed to accumulating in cytoplasmic protein inclusions). Alternatively, this could be explained by protein-protein interactions between the NCL GAR domain playing a role in translocation to the surface or interactions with surface proteins retaining NCL on the surface. For instance, the NCL GAR domain interacts with MyH9 and the interaction between NCL and MyH9 plays a role in NCL surface expression[176,227]. On the cell surface, the NCL GAR domain has been implicated in binding to several receptors including urokinase plasminogen activator receptor[180] and CXCR4[179,242]. This interaction with other surface proteins could stabilize cell surface NCL or act as a tethering mechanism, since NCL lacks a transmembrane domain or GPI anchor. However, the GAR domain alone is not sufficient for cell surface expression.

Despite the dramatic difference in cellular localization, the NCL mutant with a reversed NLS did not have significantly different surface expression compared to wildtype NCL-GFP. Originally, I hypothesized that since this NLS reverse mutant protein largely localizes to the cytoplasm, it would also have much greater levels of expression on the cell surface. However, the cell surface expression of NCL NLS reverse is comparable to wildtype NCL-GFP, if not slightly lower. A possible explanation for this could be that NCL must first enter the nucleus before translocating to the cell surface, which the NLS reverse mutant is capable of doing, albeit to a lesser extent. This

is supported by reports that PKCζ phosphorylates NCL in the cell nucleus[192] and that PKCζ is important for cell surface expression of NCL[176].

Removing multiple RRMs also negatively impacted the surface expression of the mutant NCL proteins. A potential reason for this is that removing multiple RRMs would also result in the deletion of one or both or NCL's N-glycosylation sites, N317 (RRM1) and N492 (RRM3)[183]. NCL expressed on the cell surface is normally glycosylated, through an unknown biosynthesis pathway, and inhibiting N-glycosylation decreases the surface expression of NCL[188,189]. The RRM domains and N-glycosylation sites also play a role in the oligomerization of NCL[184], which may impact translocation throughout the cell and surface expression. The finding that NCL lacking multiple RRMs is unable to be expressed on the cell surface opens new possibilities for studying cell surface NCL. Previously, it was impossible to knock out NCL from a cell line without killing the cells, due to NCL's essential nuclear functions. NCL lacking the AB or GAR domain is not able to perform its essential functions, however, the RRMs are redundant and cells lacking up to 3 RRMs are still viable[201]. Therefore, if endogenous NCL is replaced by a mutant lacking 3 RRMs, it would create a cell line that has functional nuclear NCL but lacks surface NCL. This mutant cell line would be a useful tool to study cell surface NCL in the context of cancer or infectious disease.

3.3.3 No evidence of NCL palmitoylation

NCL lacks a transmembrane domain or GPI anchor to remain attached to the cell surface, therefore, I investigated palmitoylation as a potential mechanism of tethering. Since NCL has shown up in several mass spectrometry-based screens of palmitoylated proteins[348-352], I hypothesized that NCL was palmitoylated on the only cysteine (C543) in the protein. Through several experiments, I could not find evidence that NCL is palmitoylated. However, it is still possible that a palmitoylated species of NCL exists, at a level below my assay's limit of detection. It is worth noting that palmitoylation screens with NCL as a hit did not directly find a palmitoylated NCL peptide and did not validate NCL as a hit. Instead, it is likely that NCL showed up as a hit since it binds directly to known palmitoylated proteins, such as Ras[357]. In fact, evidence of NCL binding to another palmitoylated membrane protein was observed. It would be interesting to identify this new NCL-binding palmitoylated protein since it may play a role in NCL surface trafficking or tethering NCL to the membrane. Alternative fatty acylation modifications such as farnesylation or geranylgeranylation are unlikely since NCL lacks the consensus sequence for attachment[347].

Likewise, myristoylation is unlikely since it occurs on the N-terminus of proteins, most often when the second amino acid is glycine[353], and the first glycine in NCL occurs at position 8. Furthermore, myristoylation at the N-terminus would enhance membrane association and removing the NCL N-terminus (ΔAB) enhances cell surface expression instead of inhibiting it. As it stands, the mechanism NCL uses to remain attached to the cell surface is unclear. However, the NCL GAR domain interacts with several surface proteins[179,180]. Furthermore, cell surface NCL can be purified as part of a ~500 kDa protein complex[218]. Therefore, I speculate that these protein-protein interactions likely mediate NCL tethering to the cell surface.

3.3.4 Contact-dependent transfer of NCL-GFP between the surface of cells

While testing NCL-GFP expression on the cell surface, I observed that a portion of untransfected (GFP-negative) cells stained positive for GFP on the cell surface. Furthermore, the expression level of GFP within the cells did not correlate to the level of GFP on the cell surface. This led me to hypothesize that cell surface NCL was being transferred from the surface of transfected cells to neighboring untransfected cells. I supported this hypothesis using co-culture experiments to show that NCL-GFP was capable of transferring between HEK-293T cells, from HEK-293T cells to 1HAEo- cells, and between 1HAEo- cells. I then tested the ability of the various NCL-GFP truncation mutants to transfer between cells and found a very similar pattern between donor and recipient cells for each mutant. This indicates that the same domains are required for surface expression and transfer between cells. It is likely that once a mutant protein makes it to the cell surface, transfer between cells occurs freely, as indicated by similar levels of NCL-GFP on the surface of donors and recipients. Despite the efficient transfer of NCL-GFP from donor to recipient cells, no increase in GFP fluorescence is observed in the recipient cells, compared to those co-cultured with donors expressing GFP only. This is likely due to the relatively low level of NCL-GFP found on the surface, compared to the large amount in the nucleus of donor cells. An important follow-up experiment would be to test if endogenous NCL can similarly be donated from cells with high surface expression to cells with low surface expression.

The three best described methods for cell-to-cell transfer of surface proteins are EVs, tunneling nanotubes, and trogocytosis[359]. NCL has previously been observed in EV preparations[223-225], which initially led me to hypothesize that EVs are the mechanism of NCL-GFP transfer between cells. However, using a transwell dish and conditioned media transfer, I showed that the transfer of NCL-

GFP between cells is contact dependent. These experiments effectively rule out soluble NCL or EVs as the mechanism of NCL-GFP transfer. Furthermore, reports of soluble NCL in conditioned media describe it as present transiently or undetectable[220,258]. Alternatively, tunneling nanotubes are actin-dependent protrusions extending between cells that can transfer cytoplasmic and surface proteins between cells, including large cargo such as mitochondria[360]. However, tunneling nanotubes are unlikely to be the mechanism of surface NCL-GFP transfer since they are known to mediate transfer of other surface proteins, such as TfR-GFP[361], which is not observed to the same extent as NCL-GFP. Due to their small size relative to cells, extracellular vesicles and tunneling nanotubes typically transfer small amounts of protein and are not efficient enough to establish an equilibrium of NCL-GFP between donor and recipient cells. Trogocytosis involves one cell "taking a small bite" out of another cell and acquiring some of its membrane in the process[362]. Although originally identified as a process specific to immune cells forming a synapse[362,363], trogocytosis has recently been observed in other cell types, including intestinal cells[364]. The mechanism of trogocytosis is actin-dependent and appears related to phagocytosis[362-364]. This is of note since bronchial epithelial cells are non-professional phagocytes, capable of phagocytosing apoptotic cells and debris[335]. Furthermore, transfer of membrane proteins by trogocytosis is relatively efficient. For instance, natural killer cells transfer about 4% of all surface killer Ig-like receptors (KIRs) to target cells expressing major histocompatibility complex (MHC) class II within 2 hours of co-culture[363]. As such, trogocytosis is a possible mechanism behind the transfer of NCL between the surface of cells. Since trogocytosis typically relies on strong protein-protein interactions between cells, it would also be pertinent to examine if other cell surface proteins are transferred along with NCL. Alternatively, I propose a 'handoff' as the transfer mechanism for surface NCL-GFP, where NCL binds to surface proteins on adjacent cells simultaneously via protein-protein interactions. The attachment/dissociation of NCL with cell surface binding partners would then allow NCL to freely move from cell to cell. If this is the case, only NCL would transfer between cells and equal sharing of membrane between donor and recipient cells would not be observed. Of course, this hypothesis would have to be validated experimentally.

3.3.5 Implications of the intercellular transfer of cell surface NCL

When considered in a broader context, the transfer of surface NCL between cells alters our view of cell theory and the fluid mosaic model of cell surface membranes. Traditionally, proteins in the cell surface can move laterally with varying degrees of freedom, but are restricted to the plane of

the membrane, making each cell an individual unit. Practically, this approach is very effective, as evidenced by the widespread use of surface markers to characterize cells. The transfer of NCL between the surface of cells presents an exception to this rule, where a protein seems to have unrestricted freedom to form an equilibrium between adjacent cells. In the context of an organism or tissue, it is possible that cells with high levels of surface NCL donate some of this NCL to cells with lower levels of expression. For example, human alveoli within the lung stop developing around age two[365]. Since surface NCL is directly correlated to cell proliferation[188], after age 2 most lung cells would have low levels of surface NCL. However, some lung cells, like fibroblasts, continue to proliferate and could present a supply of surface NCL for donation. This would then alter the recipient cells' susceptibility to pathogens or ability to uptake growth factors. The situation of terminally differentiated cells no longer proliferating is not unique to the lung and this situation could occur in a number of tissues. However, the *in vivo* relevance of the transfer of NCL between cells remains to be elucidated.

Chapter 4: NCL Trafficking During RSV Entry

4.1 Introduction

RSV is an enveloped, single stranded, negative sense RNA virus that infects almost everyone by the age of two[16]. Despite being a prevalent human pathogen, many fundamental questions remain regarding the cellular replication cycle of RSV. In particular, the specific molecular events occurring during the RSV cell-entry process have not yet been fully elucidated.

There have been many candidate cell surface receptors described for RSV entry, including annexin II[117] and CX3CR1[106,107,111,118], which bind to RSV-G. Potential RSV receptors that bind to RSV-F include, TLR4[122,123], EGFR[119-121], ICAM-1[125], and NCL[2,117,126-128]. In addition, both RSV-G and RSV-F can bind to HSPGs[112,129-131], though RSV lacking RSV-G is less dependent on binding to HSPGs[366]. However, there are conflicting reports of whether HSPGs are present on the apical surface of ciliated epithelial cells[107,150], which are the primary target of RSV infection in the lungs[22,151]. Interestingly, ligands binding to NCL[257] or EGFR[367] stimulates macropinocytosis, similar to RSV binding to host cells[120,121]. Of the identified cell surface receptors for RSV, only NCL is critical for RSV entry[128]. In this study, NCL was shown to bind directly to RSV-F and colocalize with viral particles during RSV entry[128]. Furthermore, ectopic NCL expression rendered RSV-resistant insect cells susceptible to infection, while blocking the interaction between RSV and cell surface NCL *in vitro* or *in vivo* decreased RSV infectivity[128]. Since RSV has numerous identified cell surface receptors, it is conceivable that some may work to mediate virus particle attachment and signaling events, while others trigger the conformational change in RSV-F to mediate the fusion of viral and cellular membranes.

NCL has been shown to be an entry receptor for several different viral and bacterial pathogens, including HIV[247,248], parainfluenza virus[244], Crimean-Congo hemorrhagic fever virus[246], Group B coxsackievirus[249], enterohemorrhagic *Escherichia coli*[253], and *Francisella tularensis*[252]. When NCL binds to ligands on the cell surface, it forms clusters in lipid rafts[220,248]. After clustering, NCL induces the endocytosis of these ligands, including antibodies that bind to NCL[188,215,220,230]. However, NCL is a primarily nucleolar protein, with low levels of expression on the surface of cells that are not actively dividing[188]. This is in contrast to most receptors for viruses, which are typically major determinants of viral tropism, based on their pre-existing high surface expression[60]. Since NCL has been found on the surface in greater quantities on actively dividing cells[188], this

may play a role in the preference of RSV to infect the lower respiratory tract in young children because alveoli continue to grow until about 2 years of age[365]. After the age of 2, hospitalizations due to RSV infection decline significantly[368].

Studying cell surface NCL as a pathogen receptor is complicated by the essential role NCL plays in cells[201,202], which prevents the creation of NCL knockout animals or cell lines. Furthermore, the mechanisms by which NCL translocates to the cell surface and then remains functionally attached to the plasma membrane remain unknown, as NCL lacks a signal peptide required for secretion and it does not have a transmembrane domain (explored in **Chapter 3**).

In this chapter, I investigated the biology of NCL as an RSV receptor. Specifically, how a primarily nucleolar protein, with low levels of surface expression, can play an essential role for RSV entry on the cell surface. To do this, I first grew a new laboratory stock of RSV to test and investigate alternate methods of purifying RSV stocks. I then examined the intracellular movement of NCL during RSV entry and the specific interaction between RSV and NCL on the cell surface. This was accomplished using a variety of techniques, including cellular protein fractionations, live cell imaging, and imaging flow cytometry. Together, these techniques showed active translocation of NCL to the cell surface during RSV entry, where it acted as a receptor by accumulating around bound RSV particles.

4.2 Results

4.2.1 RSV reverse genetics system

4.2.1.1 Switching modified vaccinia virus for a T7 expressing plasmid

In order to study the RSV entry process, I first worked to establish a new laboratory stock of RSV to test. To do this, we collaborated with Dr. Mark Peeples (Nationwide Children's Hospital, Columbus, Ohio), who with Dr. Peter Collins (National Institutes of Health, Bethesda, Maryland) developed a reverse genetics system for RSV (rgRSV)[369-371]. The rgRSV system was generated using the RSV A2 strain[369] and has GFP inserted upstream of the first RSV gene (NS1) to permit easy tracking of successful viral infection[370,371]. The system works by transfecting HeLa cells with a full-length RSV-GFP antigenome cDNA, along with 4 helper plasmids – RSV-N, RSV-P, RSV-L, and RSV-M2-1. The helper plasmids encode the RSV RNA-dependent RNA polymerase, along

with co-factor proteins that together form the RSV polymerase complex[74,81]. Unlike many positive sense viral genomes[83], the negative sense RSV genome is not infectious on its own and requires a viral polymerase complex to produce viral mRNAs[369,372].

Since RSV is a negative sense RNA virus, the antigenome is used in the reverse genetics system to make genetic manipulation easier to plan. Furthermore, the antigenome must be first replicated back to the negative sense genome before viral genes can be expressed. This means that if GFP expression is observed during rescue from cDNA, the virus has successfully undergone both replication and transcription. Due to the cytoplasmic localization of RSV replication, polyadenylation signals and cryptic splice sites have accumulated within RSV genes, making nuclear expression via CMV promoter impossible without codon optimization[343]. To avoid this, the RSV helper plasmids were designed for cytoplasmic expression using a T7 promoter. The RSV antigenome is also transcribed using a T7 promoter, with ribozymes encoded on the 5′ and 3′ ends to cleave the resulting RNA and enable it to be recognized by the RSV polymerase complex[340]. Typically, the RSV reverse genetics system uses modified vaccinia Ankara encoding the T7 polymerase (MVA-T7). Due to lack of immediate availability, I replaced MVA-T7 with a plasmid encoding a codon optimized T7 polymerase which has previously been used for the reverse genetic rescue of Nipah virus[341] (**Figure 4.1**).

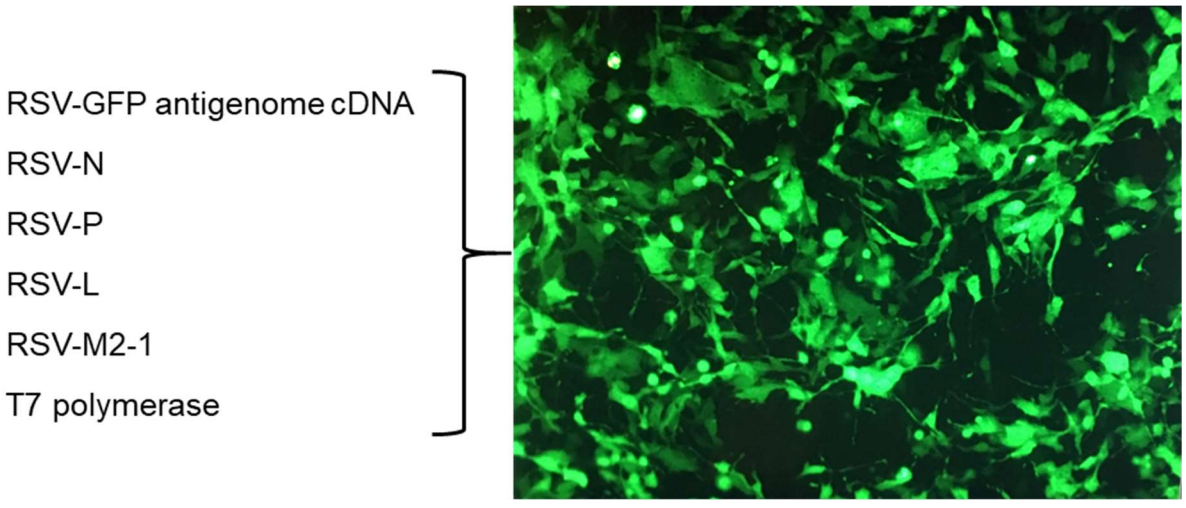

Figure 4.1 Rescue of RSV-GFP from cDNA. RSV-GFP antigenome cDNA, along with 4 helper plasmids (encoding RSV-N, RSV-P, RSV-L, and RSV-M2-1), and a T7 polymerase to drive cytoplasmic gene expression, were transfected into HeLa cells using HeLa MONSTER transfection reagent. Green fluorescence begins to show up at 3 days post transfection. The panel

on the right shows GFP expression at 1 day post-infection of virus on passage 2, after transfection. Cells were imaged using the EVOS FL-auto fluorescent microscope.

4.2.1.2 Deleting the RSV G protein

To test the RSV reverse genetics system and create a tool for future analysis of RSV entry, I deleted the attachment glycoprotein (RSV-G) from the RSV antigenome cDNA. RSV-G has previously been shown to be a non-essential protein that plays a role in the high affinity attachment of RSV to host cells[69]. I then rescued this RSVΔG mutant using the process described in **Figure 4.1**. The successful deletion of RSV-G was then confirmed by western blot (**Figure 4.2**).

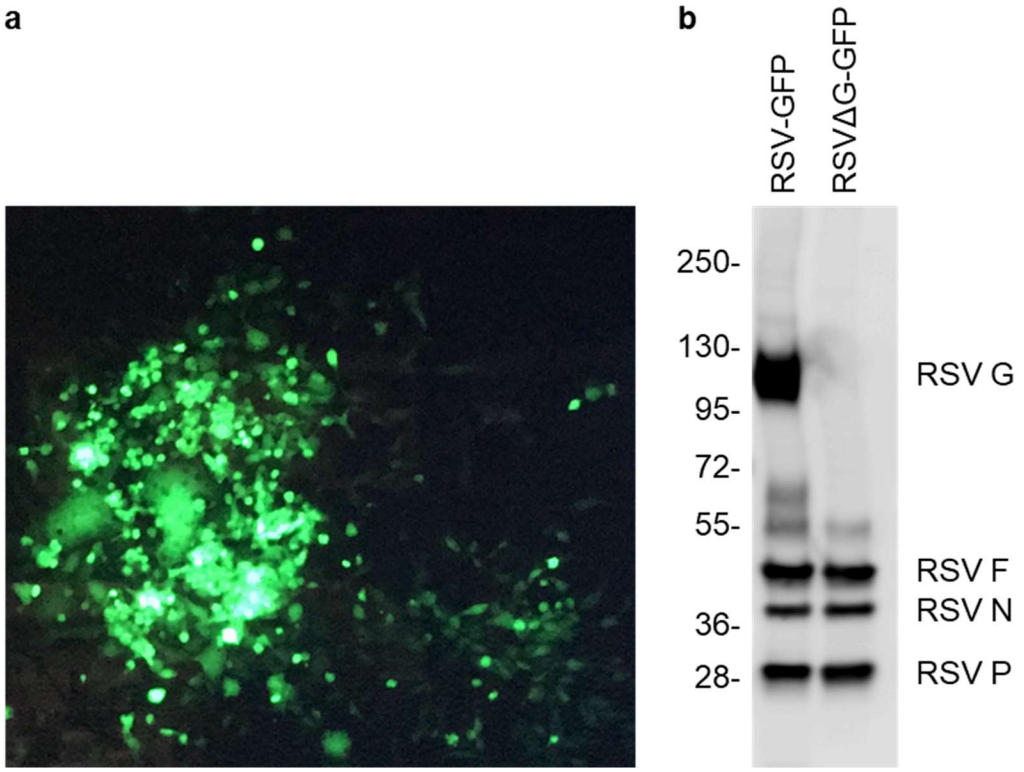

Figure 4.2 Creation of RSVΔG. The RSV-G gene was deleted from the RSV antigenome cDNA. **a)** Green fluorescence of RSVΔG replicating in HeLa cells after rescue from cDNA. **b)** Western blot of sucrose-purified RSV-GFP or RSVΔG-GFP, using a polyclonal antibody raised against RSV. Molecular weight markers shown in kDa and RSV proteins labeled based on approximate size. Panel b performed by Leanne Bilawchuk, with my guidance.

4.2.2 Purifying RSV using the ÄKTA start FPLC

4.2.2.1 Comparison of ÄKTA purified RSV to sucrose purified RSV

When propagating RSV stocks, the virus buds into the conditioned cell media. Viral stocks are then concentrated and purified to remove contaminating cell-derived factors. The typical method for purifying RSV involves using PEG-6000 to precipitate the virus from conditioned media, then loading the precipitate on to a discontinuous sucrose gradient and separating the virus from other constituents via ultracentrifugation[373]. To improve upon this RSV purification process, I examined running the polyethylene glycol viral precipitate though a HiTrap Capto Core 700 column using an ÄKTA Start fast protein liquid chromatography (FPLC) (**Figure 4.3a**). This method was examined because it is faster and requires less sample manipulation that could create variability between stocks. The Capto Core columns contain beads which bind to and remove impurities smaller than 700 kDa. Purifying RSV via FPLC led to similar viral titres compared to sucrose gradient purification (**Figure 4.3b**). Furthermore, similar levels of contaminants were observed between sucrose and FPLC purified RSV. A soluble protein, bovine serum albumin (BSA), and an exosome associated protein, superoxide dismutase (SOD1), are shown as example contaminants (**Figure 4.3c and d**).

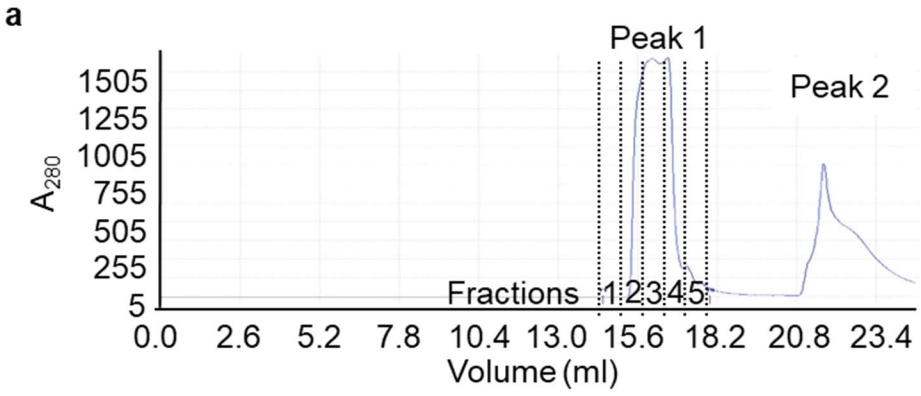

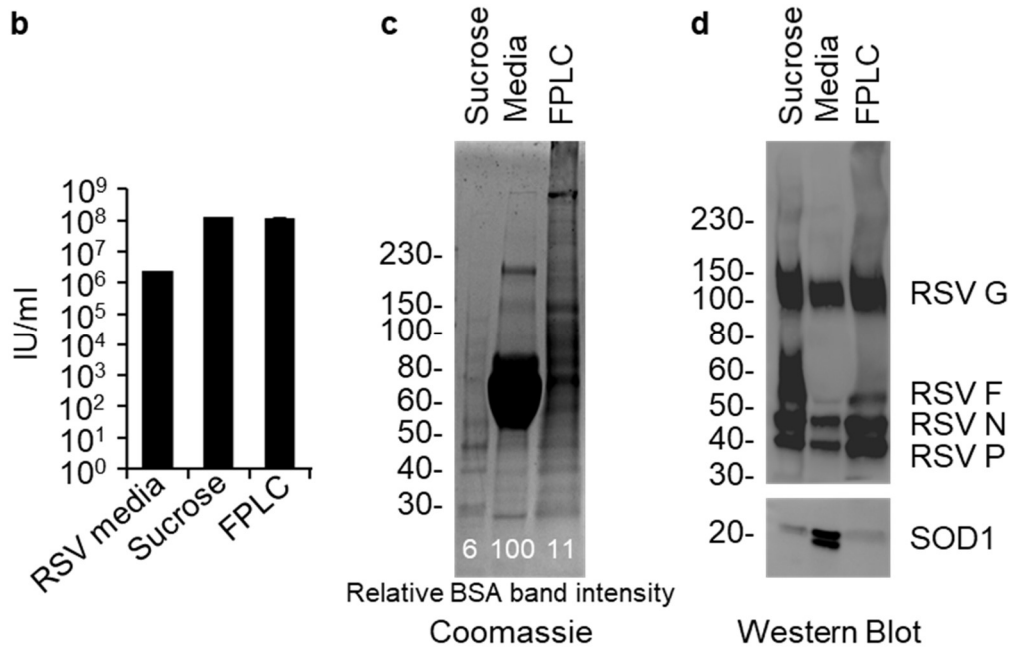

Figure 4.3 Purification of RSV stocks using FPLC. a) Polyethylene glycol-6000 precipitated RSV particles were purified by FPLC using a HiTrap Capto Core 700 column. The flow-through of virus occurred throughout the peak at 280 nm absorbance (peak 1) and was separated into five fractions. The column contaminants were eluted and appear in the second absorbance peak (peak 2). **b)** RSV was titrated on HeLa cells, which were fixed and stained for RSV protein 20 h later using a polyclonal anti-RSV antibody. A secondary antibody conjugated to β-galactosidase is then added, followed by X-Gal substrate. X-Gal substrate cleavage by β-galactosidase creates an insoluble blue color, indicating RSV infection. RSV infected cells were manually counted and the titre of each virus preparation in infectious units per mL (IU/mL) is shown. Bars represent three biological replicates. Five independent experiments were performed, with similar results. **c)** Coomassie blue staining of RSV stock preparations separated by SDS-PAGE. The relative bovine serum albumin (BSA) band intensity was measured by densitometry of the 65 kDa band. **d)** RSV proteins and superoxide dismutase 1 (SOD1) were detected by western blot. Molecular weight markers shown in kDa. Figure adapted from Bilawchuk *et al.*[2]. Panels b, c, and d performed by Leanne Bilawchuk.

Although FPLC-based RSV purification was fast and efficient, we later observed that FPLC-purified RSV had an altered appearance when examined by electron microscopy and was less susceptible to antibody neutralization when compared to sucrose-purified RSV[2]. For consistency with the published literature[120,121,127,138,373], sucrose-purified RSV was used in all remaining experiments and FPLC as a method of RSV purification was not pursued further.

4.2.3 NCL translocates to the cell surface during RSV entry

4.2.3.1 Bronchial epithelial cells express low levels of surface NCL

In 2011, cell surface NCL was identified as an RSV entry receptor that is required for optimal infection of bronchial epithelial cells[128]. However, in Tayyari *et al.* there was little characterization of NCL expression, surface trafficking, or kinetics of its interaction with RSV during the entry phase of viral replication[128]. Within human cells, the majority of NCL is typically located within the nucleus. Studies describing cell surface NCL typically report it as being present at low levels in non-cancerous cells[188]. Therefore, we detected cell surface NCL by antibody staining on non-permeabilized normal human bronchial epithelial (NHBE) cells, the primary host cell type for RSV replication. Cell surface NCL was measured using flow cytometry (**Figure 4.4**). Isotype primary antibody was used as a control for the specificity of staining. Despite bronchial epithelial cells being the primary host cells for RSV replication[22,151], we only measured 6-10% of the cells expressing detectable levels of NCL protein on the external leaflet of the plasma membrane.

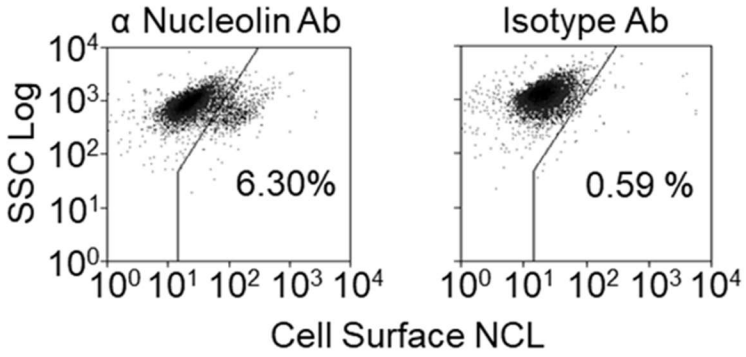

Figure 4.4 Bronchial epithelial cells express low levels of surface NCL. Expression of NCL on the surface of non-permeabilized NHBE cells by flow cytometry (left). Isotype control antibody (right) shows specificity of anti-NCL antibody staining. Experiment performed by David Marchant.

NCL is an RSV receptor that is required for optimal infection[128], which led to a disconnect wherein the question arises of how RSV is infecting cells without readily detectable cell surface NCL. To reconcile the disconnect, we tested whether NCL expression increased during a timecourse of RSV entry. We infected 1HAEo- cells with RSV, then detected NCL by western blot and qRT-PCR at the time points indicated in **Figure 4.5**. We did not observe a significant change in the consistently high levels of NCL protein by immunoblot or mRNA transcripts by qRT-PCR. These observations

led us to postulate that there may be significant trafficking of NCL from inside the cell to the cell surface during RSV entry.

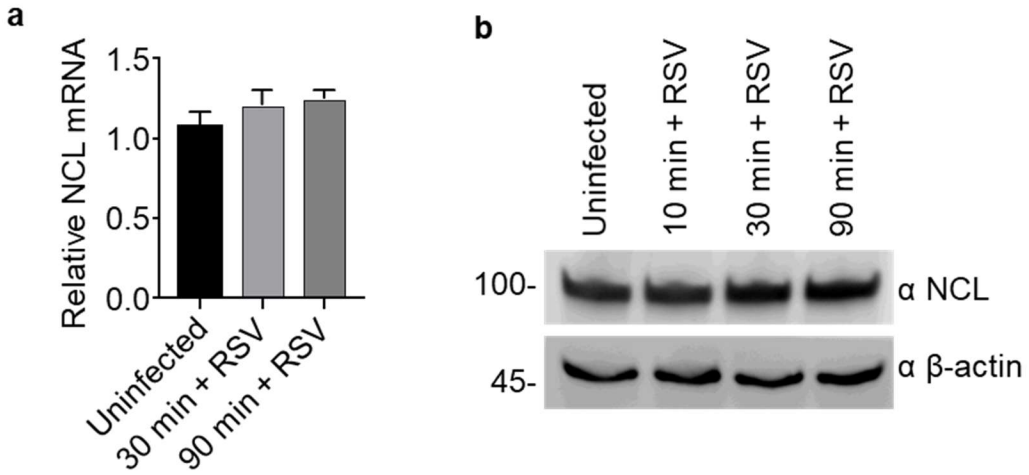

Figure 4.5 NCL mRNA and protein levels are unchanged during RSV entry. a) *NCL* mRNA transcript levels measured by qRT-PCR 0, 30, and 90 min after RSV infection in 1HAEo- cells. All transcript levels normalized to the sample with highest *NCL* expression and raw data was compared using a one-way ANOVA, with Tukey's post hoc test individually comparing each timepoint to 0 min. The timepoints were not statistically different from one another, $p > 0.05$. The data was derived from three biological replicates. Two independent experiments were performed, with similar results. **b)** Western blot of total NCL protein levels at 0, 10, 30, and 90 min after RSV infection in 1HAEo- cells. Actin is stained as a loading control. Experiment was performed by Leanne Bilawchuk.

4.2.3.3 Cell surface NCL levels increase during RSV entry

To investigate if NCL was translocating to the cell surface during RSV entry, we first quantified cell surface NCL on 1HAEo- cells by flow cytometry, during an RSV entry timecourse. We found that the proportion of surface NCL positive cells significantly increased ($p < 0.05$) 30 min post-infection and began decreasing 60 and 90 min after infection (**Figure 4.6a**). Since no change in NCL mRNA or protein levels could be detected (**Figure 4.5**), we hypothesized that the increase in surface NCL was the result of its redistribution within the cell. To test this hypothesis, we infected 1HAEo- cells with RSV and performed subcellular fractionations 0, 30, and 60 min post-infection. NCL in the nuclear, cytoplasmic, and membrane fractions were detected by western blot. During RSV entry, we observed a decrease in the amount of nuclear NCL and increases in the amounts of cytoplasmic and membrane associated NCL (**Figure 4.6b**).

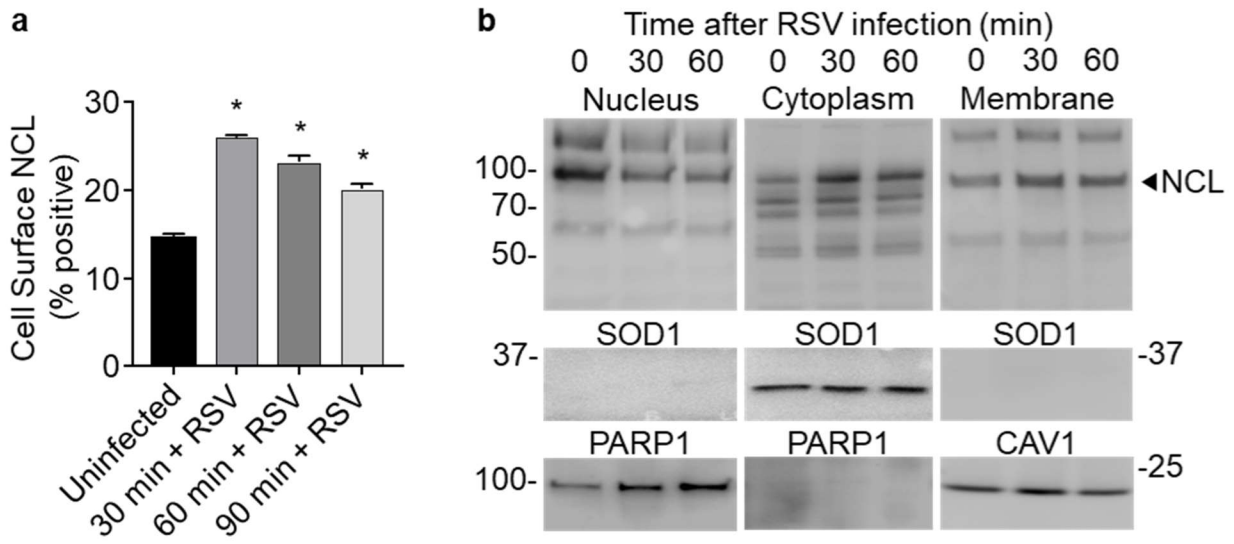

Figure 4.6 RSV entry process triggers NCL redistribution. RSV was bound to 1HAEo- cells for 1 hour on ice to synchronize infection, which is referred to as 0 min. The cells were then warmed to 37ºC to permit RSV entry to proceed for the indicated times in the timecourse. **a)** Cell surface expression of NCL on non-permeabilized 1HAEo- cells during a timecourse of RSV infection, measured by flow cytometry and compared using a one-way ANOVA, with Tukey's post hoc test individually comparing each timepoint to 0 min. *; $p < 0.05$. Four independent experiments were performed, with similar results. **b)** Western blot analysis of NCL from subcellular fractions of 1HAEo- cells during an RSV infection timecourse. Poly (ADP-ribose) polymerase (PARP -nucleus), superoxide dismutase 1 (SOD1 - cytoplasm), and caveolin-1 (CAV1 - membrane) are used as controls for contamination between subcellular fractions. Experiment performed by Leanne Bilawchuk, with my guidance.

4.2.4 RSV-NCL colocalization increases during RSV entry

4.2.4.1 Images of NCL during RSV infection timecourse

To test if the increased surface NCL was interacting with RSV particles, we examined fixed NHBE cells using immunofluorescence confocal microscopy in a series of timepoints during RSV entry. We observed a trend of increasing NCL surrounding RSV particles after 30 min post-infection, which we have termed "patching" (**Figure 4.7**). By 90 min post-infection, we observed a distortion in some RSV particles associated with NCL, which suggested a successful fusion event had occurred.

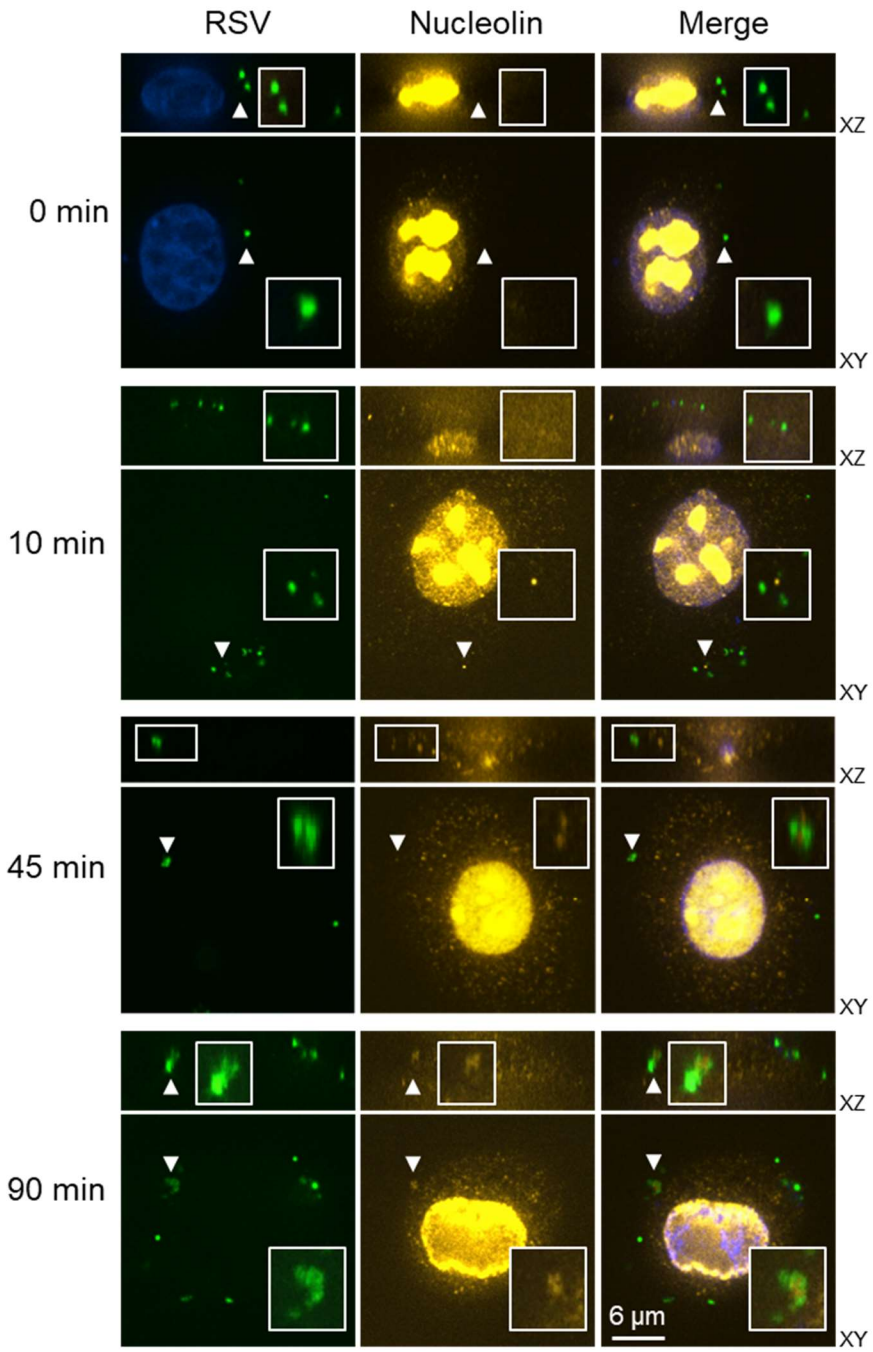

Figure 4.7 NCL colocalizes with RSV particles during a timecourse of viral entry. RSV was bound to NHBE cells on ice for 1 hour (0 min). Confocal immunofluorescence images of permeabilized NHBE cells at 0, 10, 45, and 90 min post warming were taken, showing nuclei (DAPI, blue), NCL (yellow), and RSV (green). Arrowheads indicate RSV particles and RSV-NCL colocalization at timepoints 45 and 90 min after infection. Time (minutes) after infection is shown on the left. Inset boxes show zoom images of viral particles indicated by arrowheads. Two independent experiments were performed, with similar results. Experiments performed by Leanne Bilawchuk, with my guidance.

4.2.4.3 Live cell imaging of DiD-RSV infecting NCL-GFP transfected cells

Since more NCL appeared to cluster around RSV particles as time progressed, I sought to examine the dynamics of RSV-NCL colocalization during the RSV entry process. To do this, I performed live cell imaging using RSV particles labelled with a lipophilic dye. Using a similar system, with two lipophilic dyes, San-Juan-Vergara and colleagues showed that RSV docks on lipid raft domains on NHBE cells and fusion occurs at the cell surface[65]. In order to image NCL in living cells, I used the full length NCL-GFP construct from **Chapter 3**, section 3.2.1. To directly observe the interaction of RSV with NCL-GFP in real-time, I labelled sucrose purified RSV particles with a lipophilic fluorescent dye, 1,1′-dioctadecyl-3,3,3′,3′-tetramethylindodicarbocyanine perchlorate (DiD). The close apposition of DiD in enveloped viral particles results in dim (quenched) DiD fluorescence[374]. Upon fusion of the viral membrane with the host cell plasma membrane, DiD is dispersed throughout the fused viral and host cell membranes. DiD becomes unquenched and its fluorescence increases (**Figure 4.8**)[374]. After fusion, the DiD signal progressively decreases as it diffuses throughout the much larger cellular membrane.

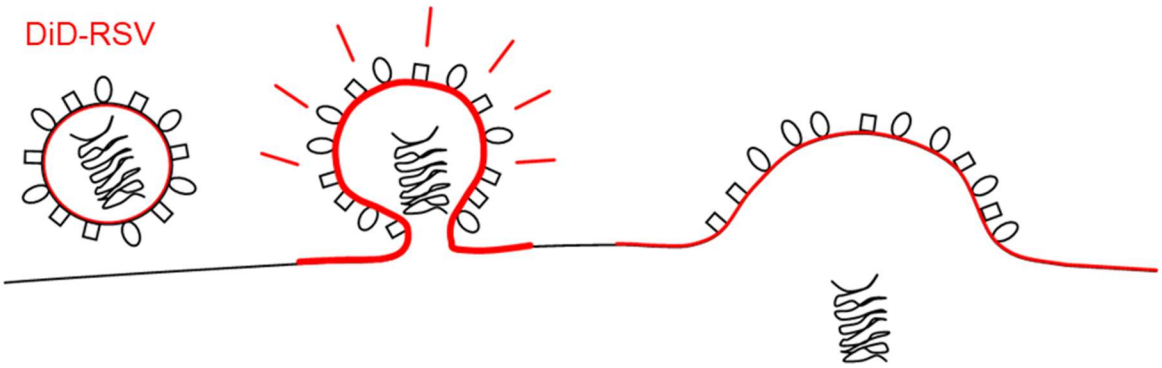

Figure 4.8 Schematic of DiD labelled RSV fusing with a host cell membrane. Initially, DiD-labelled RSV particles are dim because the DiD is quenched in the virus particle. The DiD signal increases in intensity during fusion of the virus and host cell membranes. This system allows tracking of viral particle fusion in unfixed, living cells.

For live cell imaging of RSV interactions with NCL, it is important that NCL-GFP is able to interact with RSV-F, in a manner that is similar to endogenous NCL[128]. To test the binding between NCL-GFP and RSV-F, I transfected HEK-293T cells with NCL-GFP, then lysed the cells. I subsequently mixed the cell lysate with sucrose-purified RSV. I then used antibodies to immunoprecipitate RSV-F and performed western blots for NCL and GFP. I observed both

endogenous NCL and NCL-GFP co-immunoprecipitate with RSV-F, which suggested that adding the GFP tag did not interrupt the ability of NCL to bind RSV-F (**Figure 4.9**).

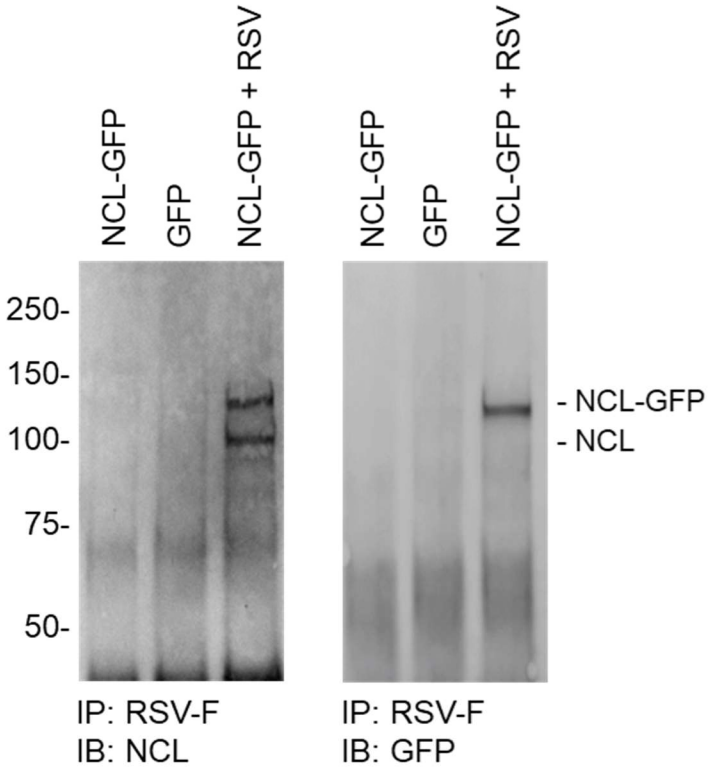

Figure 4.9 NCL-GFP co-immunoprecipitation with RSV-F. HEK-293T cells were transiently transfected with NCL-GFP or GFP, after 48 hours the cells were lysed, and RSV was combined with the cell lysate. Three independent experiments were performed, with similar results. Western blot analysis of immunoprecipitations using anti-RSV-F antibodies shows NCL (left) and GFP (right).

To ensure that the RSV particles were indeed labelled with DiD, cells were infected with DiD-RSV on ice, fixed and stained for RSV-F without warming, then imaged by fluorescence microscopy (**Figure 4.10a**). Several small DiD-labelled particles were observed without RSV-F staining, which were likely exosomes or residual cell membrane debris from viral propagation. However, all particles observed containing RSV-F were also labelled with DiD. The infectivity of DiD-RSV was then measured to ensure that the virus was still viable and that the fusion events observed could lead to productive infections (**Figure 4.10b**). I found that DiD-RSV was still infectious, but less than unlabeled virus (Sucrose Purified). Unlabeled virus that was run though

the column had an intermediate level of infectivity, which was not statistically different from DiD-RSV.

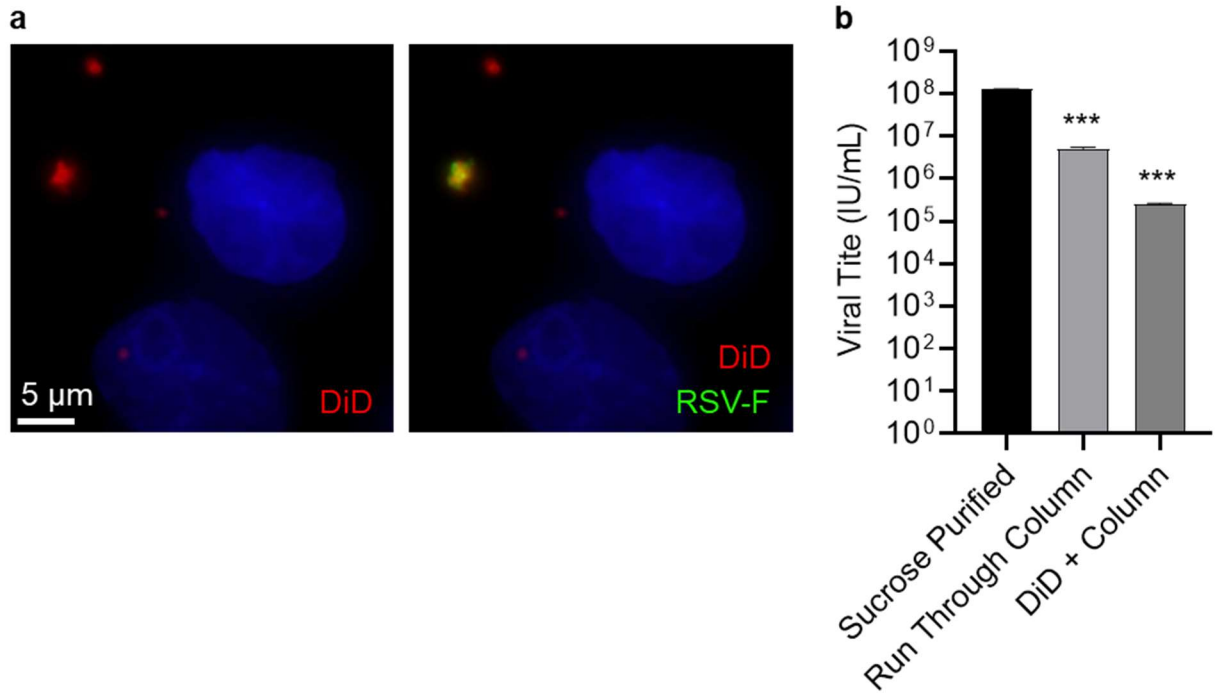

Figure 4.10 Characterization of DiD-RSV. a) RSV was labelled with DiD (red), then used to infect 1HAEo- cells for 1 hour on ice. The cells were then fixed, stained for RSV-F (green) and imaged using fluorescence microscopy. DAPI counterstain shows blue cell nuclei. **b)** Comparison of the viral titres of unlabeled sucrose purified RSV, unlabeled RSV run though the column, and DiD-labelled RSV that was run through the column. The column was used to remove excess DiD from the cell free virus particle suspension. HeLa cells were infected with the viruses, fixed the next day, then stained with an anti-RSV polyclonal antibody, followed by a secondary antibody conjugated to β-galactosidase. Addition of X-Gal substrate then produced a blue color in RSV-infected cells, which were manually counted as RSV infectious units (IU). The data was derived from two biological replicates. The RSV IU per mL were statistically analyzed by one-way ANOVA, with Tukey's post hoc test of significance, comparing all treatments. "Sucrose Purified" compared to "Run Through Column" or "DiD + Column": ***; $p < 0.001$. "Run Through Column" and "DiD + Column" were not statistically different, $p > 0.05$.

I then transiently transfected 1HAEo- bronchial epithelial cells with NCL-GFP and infected them with DiD-RSV. During the infection, I imaged a time course of RSV entry in live cells, with frames taken every 2 minutes. From the first detected increase in DiD signal to the subsequent decrease in signal, I found that most RSV fusion events took approximately 6-8 minutes to occur. Prior to each fusion event, I observed a small amount of NCL-GFP in proximity to quenched DiD-RSV. During viral fusion, NCL-GFP accumulated around the viral particle and continued to accumulate

after de-quenching (**Figure 4.11a**). When 1HAEo- cells, transfected with GFP only, were infected with DiD-RSV, no accumulation of GFP signal was detected around the fusing RSV particle (**Figure 4.11b**). This suggested that the GFP signal in **Figure 4.11a** was the product of NCL-GFP fusion protein, and not autonomous GFP proteins. In summary, the interaction of quenched DiD-labelled RSV particles with patches of NCL-GFP prior to DiD-RSV de-quenching (fusion) suggested that DiD-RSV interacted with NCL prior to fusion.

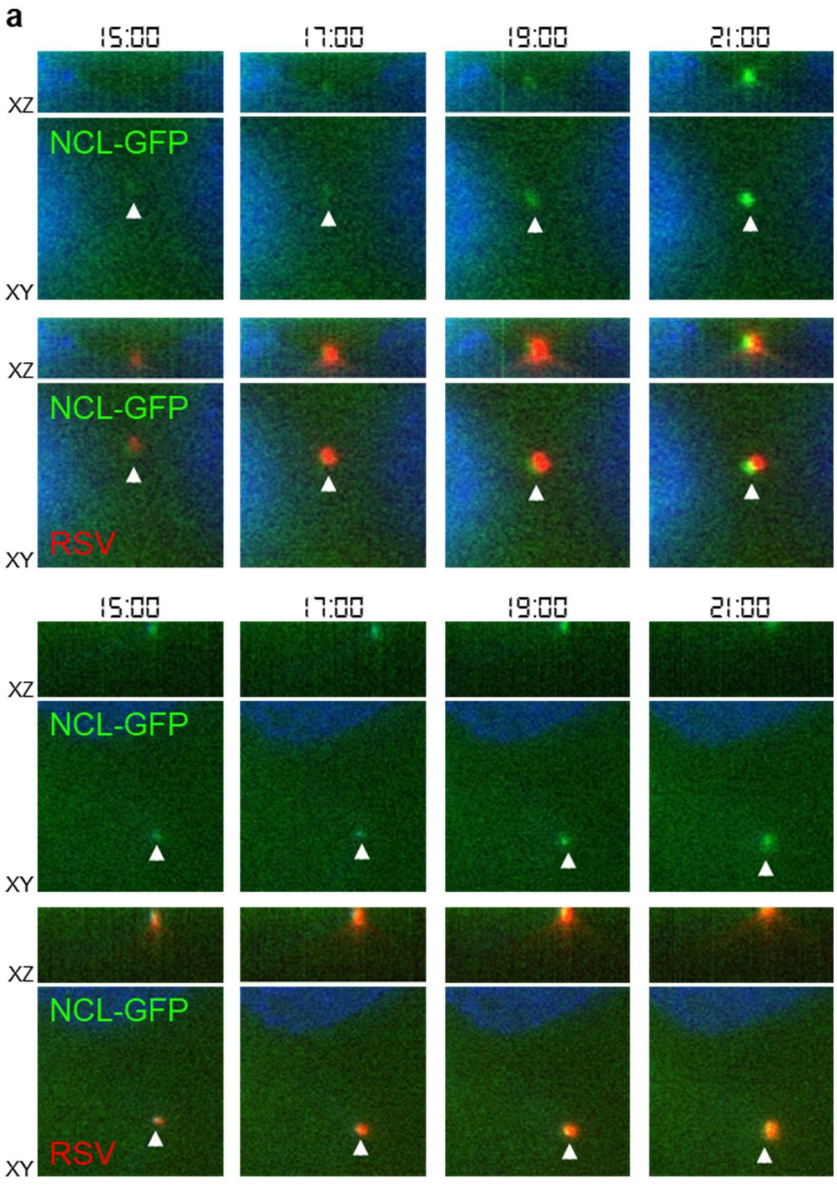

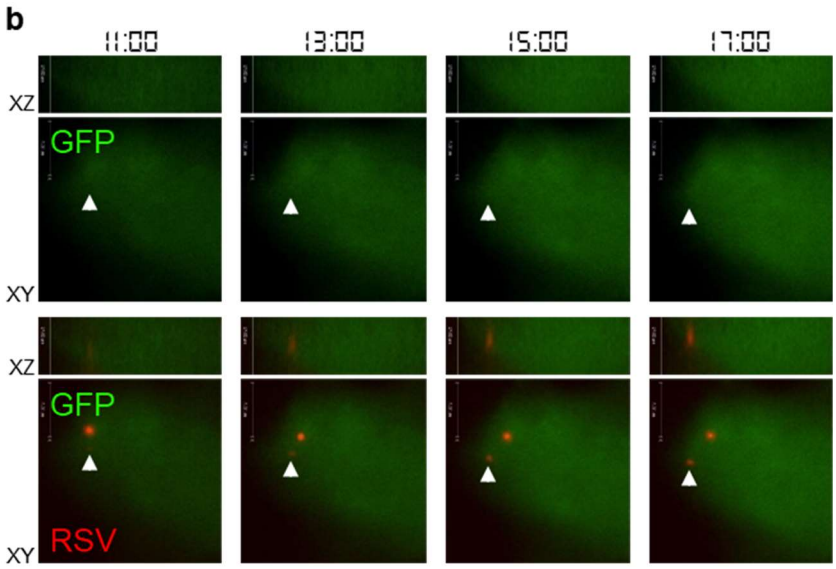

Figure 4.11 NCL-GFP colocalizes with DiD-RSV before and during viral fusion. 1HAEo- cells were transfected with either NCL-GFP (two examples shown) **(a)** or GFP **(b)** then DiD-RSV (red) was bound to the cells for 1 hour on ice. The cells were then warmed, and images were taken every two minutes during infection by live cell imaging at 37°C, with 5% CO_2. Time (mm:ss) is shown above each column. Arrowheads mark RSV particles in the process of fusing with the cell membrane, indicated by an increase in DiD fluorescence (schematic shown in **Figure 4.8**). NCL-GFP, but not GFP, is observed accumulating around fusing DiD-RSV particles. Five independent experiments were performed, with similar results. This experiment was performed with the assistance of Leanne Bilawchuk.

4.2.5 Quantifying RSV-NCL colocalization using imaging flow cytometry

4.2.5.1 Optimization and gating strategy

In **Figures 4.7** and **4.11**, I observed an increase in colocalization between RSV and NCL during viral entry. To quantify this increased colocalization, I established an imaging flow cytometry method. This method enabled detection of RSV particles and NCL patches on the cell surface of thousands of non-permeabilized 1HAEo- cells, which allowed me to measure RSV and NCL colocalization in an unbiased manner. In a typical imaging flow cytometry experiment, I would collect 100 000 – 150 000 cells per timepoint/treatment. To analyze this large dataset, I worked with Aja Rieger (Flow Cytometry Core Manager) and Brian Hall (Amnis/EMD-Millipore) to develop an algorithm, in IDEAS software, that specifically measured NCL colocalizing with RSV on the surface of cells. To do this, standard gates were used to collect single cells and cells that are out of focus (**Figure 4.12a**). Since NCL is abundant within the cell nucleus and cytoplasm, permeabilized cells show bright NCL staining throughout the cell. Therefore, cells with a high area

of NCL fluorescence were removed to keep only non-permeabilized cells (**Figure 4.12b**). To avoid potential outliers in NCL-RSV colocalization intensity, the populations were then gated for cells with 1-5 virions bound. An example of a cell with more than 5 virions bound is shown in **Figure 4.12c**. For specific analysis of RSV-NCL colocalization intensity, cells without an RSV-NCL patching event were removed (**Figure 4.12d**). In a typical experiment, 1000 – 3000 cells with an RSV-NCL colocalization event would remain after all gating.

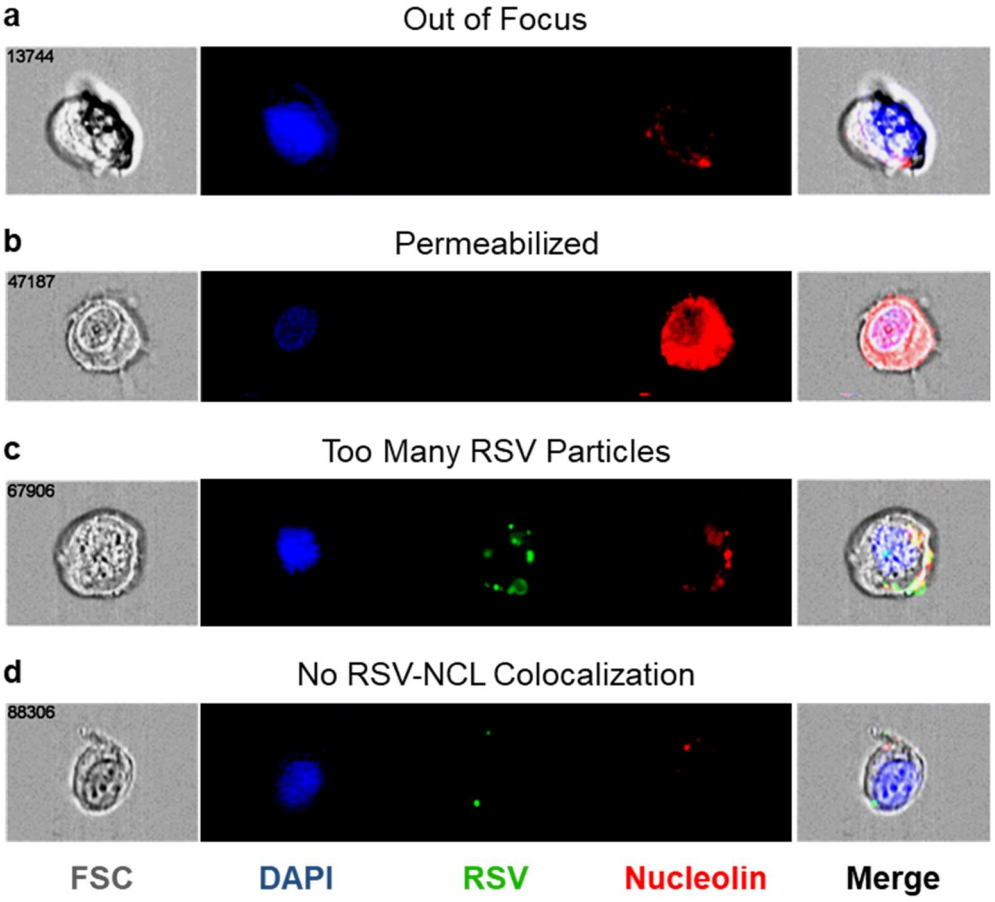

Figure 4.12 Cell populations removed during imaging flow cytometry analysis. RSV was bound to 1HAEo- cells for 1 hour on ice to synchronize infection, then the cells were warmed for 60 min and analyzed by imaging flow cytometry. Example imaging flow cytometry pictures of cells gated out during analysis are shown. **a)** Out of focus cells were removed based on low Gradient RMS in the brightfield channel. **b)** Permeabilized cells were removed based on high NCL area and fluorescence intensity. **c)** Cells with more than 5 RSV particles were removed. **d)** Cells without RSV-NCL colocalization were removed for analysis of NCL patching intensity (**Figure 4.14b**).

To aid with analysis, I created masks within the IDEAS software to pick out patches of cell surface NCL and RSV particles (**Figure 4.13a**). The NCL mask utilized the threshold feature within the software to only include pixels above background, with a minimum intensity. The RSV mask employed the spot count feature, including only small spots, with a minimum intensity. The RSV particle mask was then expanded 2 pixels in every direction, to include NCL that is adjacent but not directly overlapping the RSV particle. The two masks were then overlaid, and cell surface NCL specifically overlapping and surrounding RSV particles was counted as patching with the viral particle (**Figure 4.13b**).

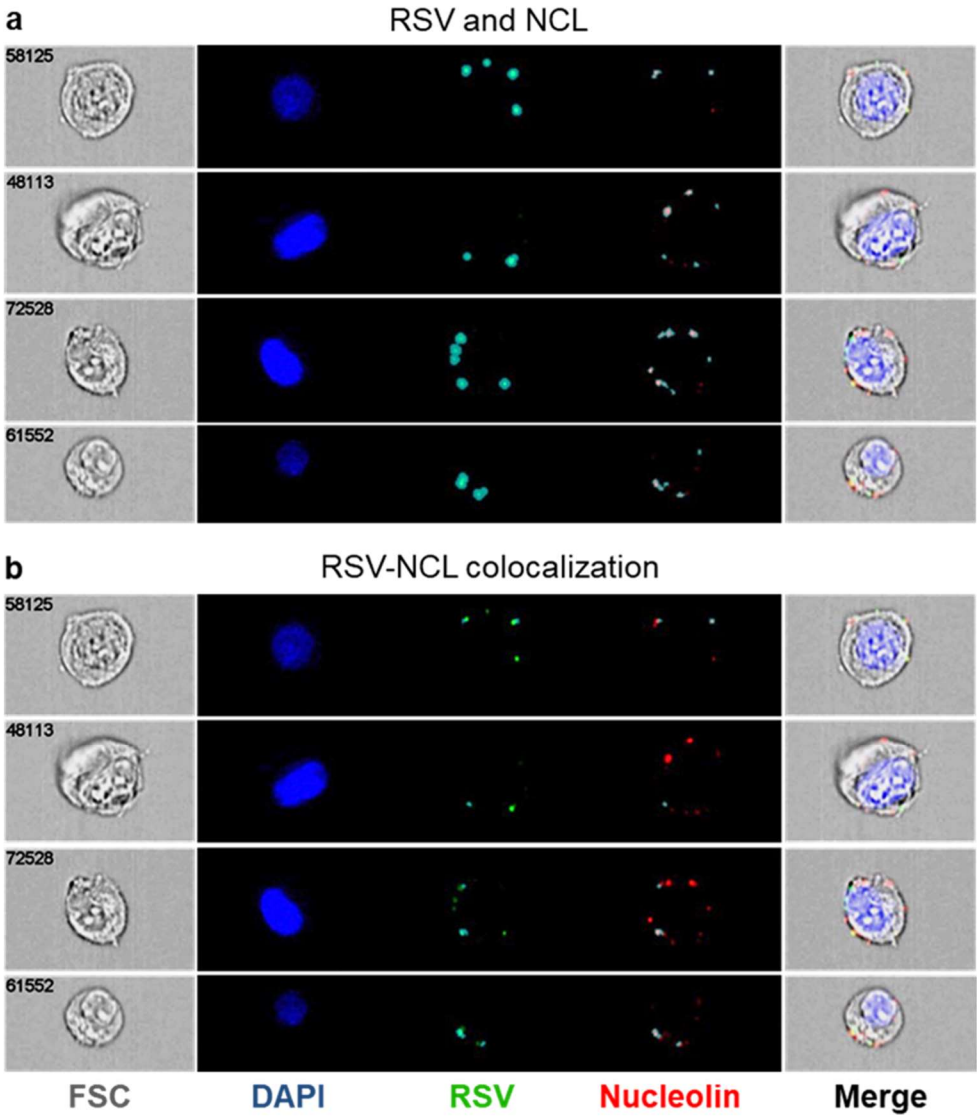

Figure 4.13 Detection of RSV-NCL colocalization using imaging flow cytometry. RSV was bound to 1HAEo- cells for 1 hour on ice to synchronize infection. The cells were warmed for 60

min and analyzed by imaging flow cytometry. Example imaging flow cytometry pictures of non-permeabilized 1HAEo- cells are shown. **a)** Automated detection of RSV particles and NCL patches on the cell surface using IDEAS software (highlighted in light blue). **b)** Detection of overlap between RSV particles and NCL patches using IDEAS software. Areas that overlap between RSV and NCL are highlighted in light blue. Intensity of NCL overlapping with RSV is quantified in **Figure 4.14**.

4.2.5.2 Timecourse of RSV infection

To quantify the colocalization between RSV and NCL observed in **Figures 4.7** and **4.11**, 1HAEo- cells were infected with RSV and fixed at a series of time points from 0 – 90 min after infection. The cells were then analyzed using the imaging flow cytometry method described in section 4.2.5.1. A statistically significant increase in NCL patching with RSV particles was observed from 0 to 60 min post-infection ($p = 0.0054$), which starts to decrease by 90 min (**Figure 4.14a**). The increase in patching directly coincides with an overall increase in cell surface NCL (**Figure 4.6** and **Figure 4.14b**). This implies that the accumulation of NCL around virus particles is at least in part due to active translocation of NCL to the cell surface, rather than only simple diffusion of pre-existing cell surface NCL to viral particles. During this timeframe, a progressive decrease in cell surface RSV intensity is also detected, which is consistent with the internalization of the virus as entry events occur (**Figure 4.14b**). In summary, these results indicate that NCL translocates to the cell surface and colocalizes with viral particles during RSV entry.

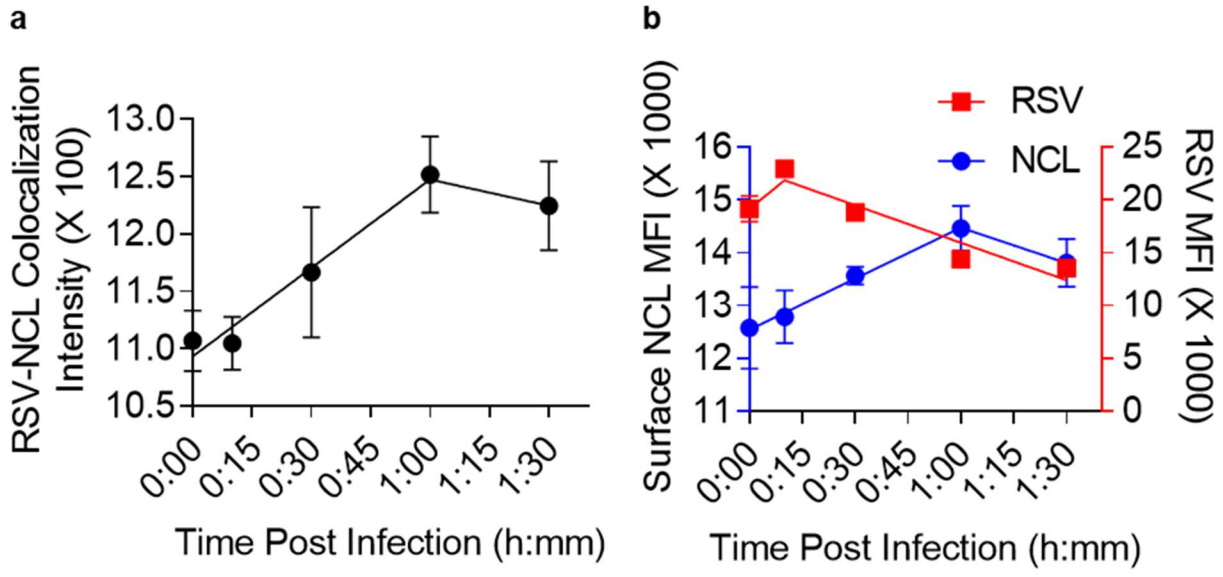

Figure 4.14 Imaging flow cytometry quantification of RSV-NCL colocalization during RSV entry. a) MFI of NCL colocalizing with RSV particles on the surface of 1HAEo- cells measured

by imaging flow cytometry. The data was statistically analyzed by linear regression comparing the slope of the line (0 min to 60 min) to 0, p = 0.0054. **b)** Cell surface MFI of NCL (blue) and RSV (red) in non-permeabilized 1HAEo- cells during a time course of RSV infection, measured by imaging flow cytometry. The data was statistically analyzed by linear regression comparing the slope of the line to 0. Cell surface NCL (blue) 0 min to 60 min, p = 0.0075. RSV (red) 10 min to 90 min, p <0.0001. Each point represents three biological replicates. Four independent experiments were performed, with similar results.

The patching of cell surface NCL around RSV particles that I observed is similar to what has been reported by Hovanessian and colleagues using different NCL-binding ligands[220,248]. Furthermore, they observed that incubating cells at room temperature, instead of 37ºC, prevented cell surface NCL levels from increasing after stimulation with fresh serum[220]. To test if a similar situation occurs during RSV entry, I infected 1HAEo- cells with RSV for 60 min at room temperature (20ºC) instead of 37ºC. Consistent with the previous report, surface NCL levels and the proportion of cells with an RSV-NCL colocalization event were both lower in cells infected at 20ºC (**Figure 4.15a** and **b**). As an additional control, I examined the background rate of cells showing RSV-NCL colocalization in the absence of virus. I determined the background rate to be 0.43%, compared to 11.12% of cells showing RSV-NCL colocalization 60 min after infection (**Figure 4.15c**).

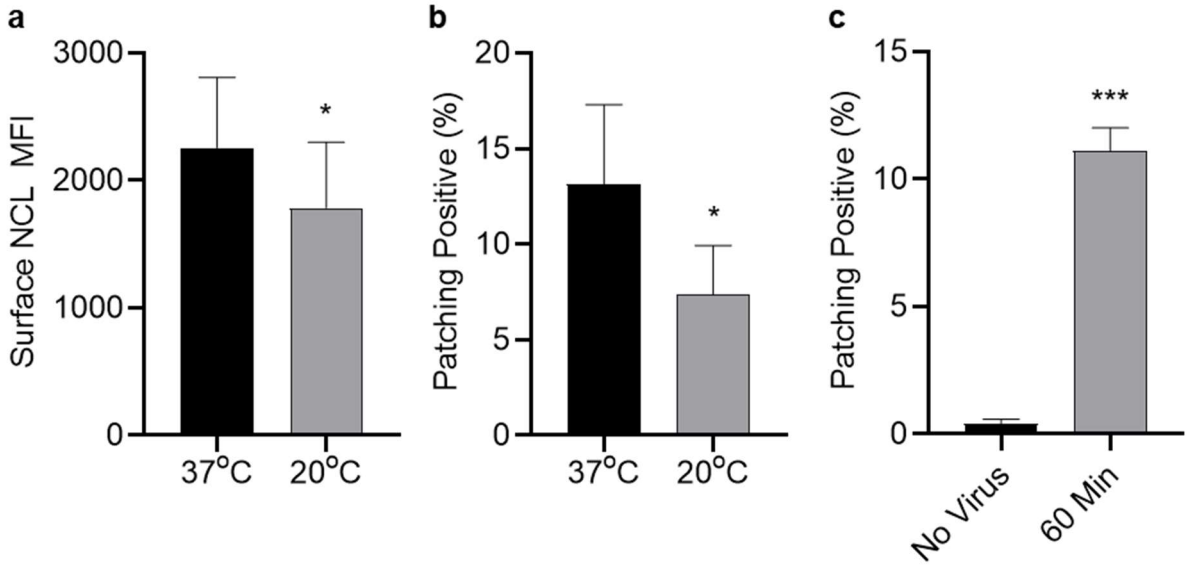

Figure 4.15 Effects of temperature on RSV-NCL patching. RSV was bound to 1HAEo- cells on ice for 1 hour, then the cells were warmed for 60 min at 20ºC or 37ºC. The cells were then harvested and analyzed by imaging flow cytometry for MFI of surface NCL **(a)** or the proportion of cells with an RSV-NCL colocalization event **(b)**. Panels **a** and **b** were derived from two

independent experiments. The data was then statistically compared by paired t-test. **c)** 1HAEo- cells were infected with RSV or treated with sucrose for 60 min at 37°C, then harvested and analyzed by imaging flow cytometry. The data was derived from four independent experiments. The proportion of cells showing an RSV-NCL colocalization event was graphed and statistically analyzed by t-test. *; $p < 0.05$, ***; $p < 0.001$.

4.2.5.3 Preventing RSV-NCL colocalization with an anti-NCL aptamer

To validate imaging flow cytometry as a method of examining RSV-NCL interactions, I tested if blocking cell surface NCL reduced RSV binding and the colocalization between RSV and NCL. I utilized a guanosine-rich DNA aptamer (AS1411) that binds to cell surface NCL[257,258]. When used to treat cells, AS1411 prevents ligands from binding to NCL on the cell surface[375]. Treating cells with AS1411 prior to RSV infection blocks the RSV-NCL interaction and reduces RSV infection[2,127]. 1HAEo- cells were treated with AS1411, or a cytosine-rich control DNA aptamer (CRO), which does not bind NCL. The cells were then infected with RSV for 60 min and analyzed by imaging flow cytometry. When compared to the control treated cells, fewer AS1411-treated cells had RSV bound to the surface (% positive for RSV staining) (**Figure 4.16a**). Of the cells that were RSV positive, the average area of NCL associated with RSV particles was also significantly reduced (**Figure 4.16b**).

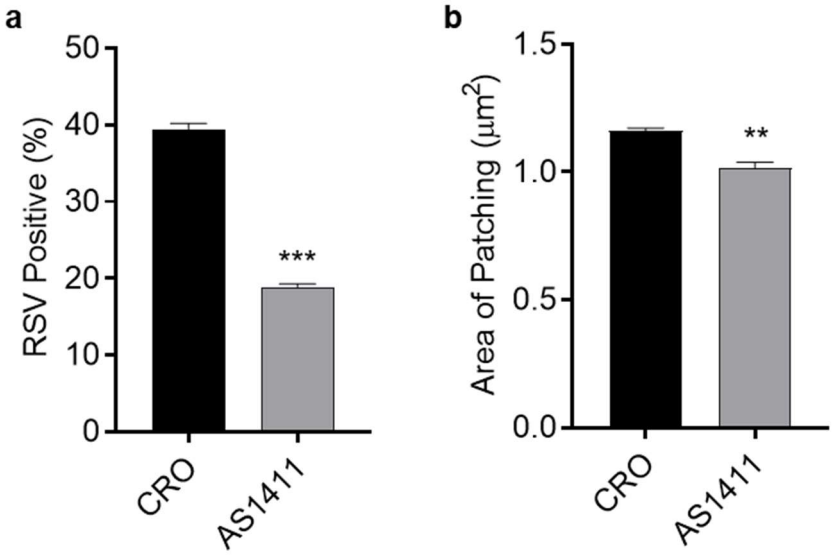

Figure 4.16 Anti-NCL aptamer reduces RSV binding and the area of NCL associated with RSV. 1HAEo- cells were treated with anti-NCL aptamer (AS1411) or control aptamer (CRO) for 1 hour, then RSV was bound to the cells for 1 hour on ice and the cells were warmed to 37°C for 1 hour. The cells were then harvested and analyzed by imaging flow cytometry. **a)** The proportion of cells staining positive for RSV antigen on the cell surface (% positive) was graphed. **b)** Within

the group of cells positive for RSV staining, the average area of NCL associated with RSV particles was graphed. The bars represent three biological replicates. Two independent experiments were performed, with similar results. The data was statistically analyzed by t-test. **; $p < 0.01$, ***; $p < 0.001$. Figure adapted from Bilawchuk *et al.*[2].

4.3 Discussion

In this chapter, I investigated NCL translocation to the cell surface during RSV entry, where it acts as a viral receptor. I found that the normally low levels of NCL on the surface of resting cells increased early during RSV infection. Furthermore, NCL was found to form patches surrounding bound RSV particles on the cell surface during viral fusion. The NCL surface patches were found exclusively colocalized with RSV at the cell surface. This suggested that NCL trafficking to RSV particles was directional and focused to the site of virus particle attachment. These experiments were supported by generation of RSV from a reverse genetics system, which I modified to more easily grow stocks of RSV. Finally, I tested new methods of RSV virus stock purification. This included comparing sucrose ultracentrifugation to FPLC-based methods of RSV purification.

4.3.1 RSV reverse genetic modification and purification

In order to create a new laboratory stock of RSV, I utilized the RSV-GFP reverse genetics system. To make the system more convenient, I replaced the MVA-T7 with a plasmid encoding a codon-optimized T7 polymerase, similar to what has been done for Nipah virus[340,341]. I then used this system to create an RSV mutant lacking the attachment (G) glycoprotein. The wildtype RSV-GFP produced using this system was used for all subsequent experiments involving RSV in **Chapters 4** and **5**.

Next, I sought to investigate methods of purifying RSV. RSV purification plays an important role in removing potentially confounding cell-derived products that arise during RSV infection, such as damage-associated molecular patterns (DAMPs). The traditional method of RSV purification is ultracentrifugation on a sucrose gradient[373]. I also examined an FPLC-based purification method that utilized a column designed to bind impurities smaller than 700 kDa. A comparison of chromatography and ultracentrifugation for the purification of an enveloped virus has been done previously[376]. McGrath *et al.* reported that sepharose column filtration is less time consuming and is superior in preserving the glycoprotein integrity of Moloney Sarcoma Virus[376]. Similarly, I found that FPLC-based RSV purification was a fast and efficient method to preserve infectivity and remove contaminants. However, when viewed by electron microscopy, FPLC-purified RSV

appears to have a matrix of debris surrounding viral particles that was absent in sucrose-purified viral stocks[2]. Furthermore, FPLC-purified RSV is less susceptible to antibody neutralization[2]. Overall, FPLC was a comparable method of RSV purification to sucrose ultracentrifugation in terms of viral yield and removal of impurities, however, the purified virus had a different morphology and neutralization profile compared to sucrose-purified RSV. Considering these differences, and that sucrose ultracentrifugation is the gold standard for RSV purification[120,121,127,138,373], I used sucrose-purified RSV for all of my other experiments. This decision allowed my experiments to be better compared to published RSV literature.

4.3.2 RSV recruits NCL to the cell surface from the nucleus

Bronchial epithelial cells expressed detectable levels of cell surface NCL on a minority of cells. However, bronchial epithelial cells are the primary target of RSV infection *in vivo*[22,151]. This posed the question of how a protein with low surface expression was acting as a viral receptor[128]. We found that surface levels of NCL increased during RSV entry. To explain this increase in surface NCL, I hypothesized that NCL expression was being upregulated or that NCL was translocating to the surface from a pre-existing cellular pool. Constitutively high amounts of NCL protein in cells and unaltered mRNA expression levels suggested that changes in NCL expression were not a factor. Conversely, I found that there was a redistribution of NCL within the cell. Early during RSV infection, the amount of nuclear NCL decreased, while the cytoplasmic and membrane associated NCL levels increased.

4.3.3 NCL recruitment is focused to the site of RSV particle attachment on the cell surface

To gain a better understanding of the interplay between NCL and RSV, confocal microscopy images were taken during a timecourse of RSV entry. The binding of RSV particles to the cell surface caused an increased amount of NCL to be detected surrounding the bound virions. I have termed this phenomenon ‘patching’. Similar accumulation around bound virions has been observed for other RSV entry factors, including TLR4[123] and ATP1A1[121]. Since the increased association of NCL with RSV particles seemed to be a dynamic process, I established a live cell imaging system to investigate when the NCL patching occurs in relation to RSV fusion. The system involved using RSV, stained with a fluorescent lipophilic dye, to infect cells that expressed NCL-GFP. The fluorescence in the stained RSV particles was quenched prior to fusion, and an increase in fluorescent intensity was observed during a fusion event[374]. Here, I observed that a

small amount of NCL colocalized with RSV particles prior to fusion, which appeared to be focused to the site of viral particle attachment. However, the amount of NCL surrounding the RSV particle dramatically increased, concurrent with viral fusion. It is important to note that endogenous NCL is also present in this system and therefore the fluorescent signal does not represent all of the NCL present. It is unlikely that a single fusing DiD-RSV particle contains sufficient DiD to stain an entire macropinosome, given the approximate 500-fold difference in surface area between an average RSV-induced macropinosome (5.7 μm diameter[121]) and a spherical RSV particle (100 nm diameter[60]). Therefore, this DiD-RSV system is not amenable to distinguishing between RSV fusion at the cell surface and within macropinosomes, since DiD-RSV fusing with either would result in dilution of the DiD to an undetectable level. Furthermore, since this lipophilic dye system relies on the mixing of membranes to indicate a fusion event has occurred, I am unable to differentiate between viral hemi-fusion and complete fusion, including nucleocapsid delivery[65]. However, both hemi-fusion and complete fusion are membrane mixing events that would require RSV-F to trigger from the pre-fusion to post-fusion state. Taken together, these results provide support for an association between increased RSV-NCL patching and RSV-F being triggered, with resulting viral-cellular membrane mixing.

4.3.4 Quantification of NCL recruitment by RSV during entry

Next, I sought to quantify NCL patching with RSV particles in an unbiased manner. To do this, I established an imaging flow cytometry assay where cells were harvested at a series of time points after RSV infection, then the intensity of NCL surrounding RSV particles was measured. This technique combined microscopic analysis of subcellular localization with the power of flow cytometry, examining thousands of patching events for each time point. Using this assay, I noted that NCL patching with RSV particles increased up to 60 min after infection, then began to decrease. During the same timeframe, I observed the amount of RSV antigen on the surface of cells progressively decrease. This decrease in RSV staining could be due to macropinocytosis of bound virions[120,121,139] or endocytosis of RSV surface proteins after fusion has occurred[64-66,136]. The kinetics of NCL patching with RSV particles are similar to those of total surface NCL levels increasing during RSV entry. These results support the live cell imaging observation of increased NCL surrounding RSV particles during fusion. Furthermore, the results provide a potential explanation as to why RSV takes a long time to enter host cells[90,120,123,138], where the virus must wait for sufficient recruitment of NCL to the cell surface before fusion can occur.

It is likely that the NCL patching with RSV particles is a result of active transport of NCL to the cell surface, as opposed to passive diffusion of NCL within the plane of the membrane. This is because passive diffusion of membrane proteins is still able to occur at 4ºC[377,378], and the imaging flow cytometry staining protocol requires cells to be kept alive on ice for approximately 4-5 hours. Therefore, if the accumulation of NCL around RSV particles was only a result of diffusion, no difference would be observed throughout the timecourse. The reduced NCL patching during an RSV infection at room temperature also supports this notion of NCL being actively transported. Previous studies have shown surface expression of NCL to be temperature dependent, where less surface NCL is detected when cells are incubated at lower temperatures[188,220]. It is likely that decreasing the temperature prevented the translocation of NCL to the cell surface but would not have prevented NCL already on the surface from accumulating around bound virions[377,378].

4.3.5 The ability of NCL to patch with RSV is associated with infection

After establishing imaging flow cytometry to examine RSV-NCL interactions during viral entry, I validated the method as a means to test compounds that may inhibit the RSV-NCL interaction. I used a previously described DNA aptamer that binds to NCL[257,258,375] and inhibits RSV infection[2,127]. Pre-treatment with the DNA aptamer was effective in reducing the number of cells bound by RSV particles by approximately 50%, indicating that NCL plays a role in stable RSV binding to host cells. However, the decrease in RSV binding observed is not sufficient to account for the entire decrease in RSV infection caused by the DNA aptamer[2,127]. This may suggest that NCL plays other roles in viral entry beyond viral attachment, which is examined in **Chapter 5**. Furthermore, aptamer treatment reduced the area of NCL associated with RSV particles in those cells that were bound by virus. Using imaging flow cytometry to test for compounds that inhibit the RSV-NCL interaction is explored further in **Chapter 5**.

4.3.6 Implications of other receptors that recruit NCL to the cell surface

During RSV entry, the increase in NCL levels on the cell surface and decrease in nuclear NCL implies that NCL is actively translocated from the nucleus to the cell surface. Similar recruitment of NCL to the cell surface has been observed after stimulating cells with VEGF[194,227], HDGF[229], or pleiotrophin[228], which sets a precedent for outside-in signaling to induce translocation of NCL to the cell surface. These published findings on the cell surface recruitment of NCL by growth factors led me to explore growth factor receptors as receptors used by RSV to recruit NCL to the

surface. The discovery of signaling receptors and the cell signals that mediate NCL recruitment to the cell surface are explored further in **Chapter 5**. This trafficking of NCL to the cell surface during RSV entry helps reconcile how a primarily nuclear protein can act as an essential viral receptor on the cell surface, especially considering that only 5-10% of bronchial epithelial cells express detectable levels of cell surface NCL. Taken as a whole, this work represents a novel concept in virology. Typical viral receptors are abundant on the surface of susceptible cells[60], while in this chapter, I described a virus that recruits its receptor to the cell surface during the process of entry.

Chapter 5: RSV Receptors and Signaling

5.1 Introduction

In **Chapter 4**, I described an RSV-induced active translocation of NCL from the nucleus to viral particles on the cell surface. For RSV to induce this active NCL translocation prior to viral fusion, it would need to send a signal through a cell surface receptor, followed by a secondary messenger or signaling cascade to trigger the movement of nuclear NCL. Finally, the movement of NCL to the cell surface would require participation of some components of the cellular cytoskeleton. The idea of an RSV signaling receptor has been proposed before[1,120,123], although never in the context of NCL trafficking. The three main surface receptors that have been the focus of study for RSV-induced cellular signals are EGFR[119-121], TLR4[122-124], and CX3CR1[106,107,111,118].

As an alternative to EGFR, TLR4, and CX3CR1, IGF1R is investigated in this chapter as a candidate signaling receptor. IGF1R is a dimeric growth factor receptor that is highly related to the insulin receptor (IR), with which it can form heterodimers[326]. IGF1R is typically stimulated by IGF1, though much higher concentrations of insulin and IGF2 can also stimulate IGF1R[327]. Upon ligand binding, each IGF1R monomer within the dimer transactivates the other monomer by first phosphorylating tyrosine 1135, followed by tyrosine 1131, then tyrosine 1136[328]. Typical downstream signaling molecules of IGF1R are Ras/Raf/MEK/ERK and PI3K/Akt[296,329], though PKCζ is also activated by IGF1R[295,296].

Downstream of the viral signaling receptor, a secondary messenger or signaling cascade is required to trigger effector functions induced by the virus. In the case of my project, the final function that I am examining is the translocation of NCL to RSV particles. Several kinases are activated during RSV entry, including p38, ERK1/2, PI3K, and several PKC isoforms[123,142,143,147]. Inhibiting p38[123,144], ERK1/2[123,145], or PI3K[120] reduces RSV replication, indicating that they each play a role in viral replication. However, the studies examining each kinase kept the kinase inhibitors present throughout the RSV replication cycle, which does not exclude the kinases from playing a role in other viral processes, such as transcription or genome replication, as opposed to entry. This is of particular importance since PI3K remains activated by RSV up to 6-hours post-infection[147] and p38 and ERK1/2 MAPKs exhibit biphasic activation by RSV, with the second activation peak starting around 6-8 hours post-infection[123,142,146]. The second peak of ERK1/2 activation has been tied to RSV budding and assembly[146], which is essential for the formation of viral plaques (a

common output for measuring RSV infection). Non-specific PKC inhibitors and PKCα inhibitors also reduce RSV infection[120,148,149], but the roles of the other PKC isoforms have not been thoroughly investigated.

In this chapter, I examined the role of one specific PKC isoform, PKCζ, during RSV entry. PKCζ was chosen because it is capable of entering the nucleus and directly phosphorylating NCL[192]. Furthermore, PKCζ activity has been tied to NCL cell surface expression[176]. In a resting state, PKCζ activity is inhibited by a pseudosubstrate domain, which binds to the catalytic site and prevents other substrates from binding[286] (**Figure 1.4**). PKCζ activation relies on the phosphorylation of threonine 410 by PDPK1, downstream of PI3K[300,301], which reduces the affinity of the psuedosubstrate for the catalytic site[286]. Recently, a large pool of constitutively phosphorylated PKCζ (~50% of total PKCζ) has been observed in resting cells[289]. As an alternative to PI3K, this study proposed that PKCζ activity is instead regulated by protein binding partners that stabilize PKCζ in an open conformation, with the pseudosubstrate away from the catalytic domain[286,287]. The open conformation of PKCζ was demonstrated experimentally by showing that bound scaffolding proteins make PKCζ sensitive to a specific protease. Par-6 and p62 are both scaffolding proteins that bind to and activate PKCζ by stabilizing it in an active form[286,287,302]. Acidic proteins, such as 14-3-3, are also able to bind PKCζ and increase its activity[307].

Throughout this chapter, I investigated the cellular signals behind the RSV-induced trafficking of NCL to the cell surface. This was accomplished by testing the effects of inhibiting various kinases, cellular processes, and cell surface receptors on RSV entry. These inhibitors identified IGF1R as an RSV receptor and PKCζ as a crucial downstream kinase that is activated by RSV and necessary for optimal viral replication. PKCζ activity was attributed to IGF1R activation using an *in vitro* kinase assay, while NCL trafficking was attributed to PKCζ activity using imaging flow cytometry. IGF1R was subsequently validated as an RSV receptor using microscopy and determining the binding affinity between purified IGF1R and RSV glycoproteins. Together, these experiments characterized an RSV-induced signaling cascade starting with IGF1R, involving PKCζ, and ending with NCL trafficking to the cell surface.

5.2 Results

5.2.1 RSV glycoproteins fused to Fc

5.2.1.1 Fusing an Fc region to RSV-F

To investigate the interactions between RSV-F and NCL in the absence of whole virus, I sought to create a recombinant form of RSV-F. To do this, we collaborated with Dr. Thomas Grunwald (Ruhr-Universität Bochum, Germany), who provided us with a codon optimized version of RSV-F, derived from the RSV A2 Long Strain. Due to the accumulation of polyadenylation signals and cryptic splice sites, codon optimization was required to enable nuclear expression of RSV-F under a CMV promoter[343]. I cloned this RSV-F into the pCMV6-AC-FC-S vector from Origene, which replaced the RSV-F signal peptide with an IL-2 signal peptide and enabled me to replace the C-terminal RSV-F transmembrane domain[93] with a murine Fc region (RSVF-Fc) to maintain stability of the protein in solution. The IL-2 signal peptide is efficient at driving extracellular secretion was provided as part of the pCMV6-AC-FC-S vector. The Fc region contains the mouse IgG heavy chain CH2 and CH3 domains, along with the hinge region. I transfected RSVF-Fc or the pCMV6-AC-FC-S vector alone into HEK-293T cells, then examined the cell lysate and conditioned media for Fc-containing proteins by western blot, using an anti-mouse antibody that is typically used as a secondary antibody (**Figure 5.1**). To test the functionality of the Fc region, I included each sample after immunoprecipitation using protein G conjugated beads. I observed two bands in each RSVF-Fc lysate, corresponding to the immature RSV-F_0 (that has not yet undergone cleavage during maturation) and the mature RSV-F_1, after accounting for the increased molecular weight due to the addition of the Fc region. RSV-F maturation involves cleavage at two sites, 27 amino acids apart, which separates the RSV-F_2 fragment (with the signal peptide still attached) from the RSV-F_1 fragment. The 27 amino acid fragment (p27) dissociates during maturation. The RSV-F_2 fragment alone was not observed, because the Fc region is attached to the RSV-F_1 C-terminus. Furthermore, the RSV-F_2 fragment normally remains attached to RSV-F_1 via disulphide bonds[95], which are reduced during the western blot. In the conditioned media from RSVF-Fc transfected cells, only the mature RSV-F_1 fragment is observed. No Fc-containing proteins were observed from the vector control (pCMV6-AC-FC-S) transfected cells. Upon closer examination, I discovered that the pCMV6-AC-FC-S multiple cloning site contains a stop codon (upstream of the Fc region), which prevented expression of the Fc region on its own.

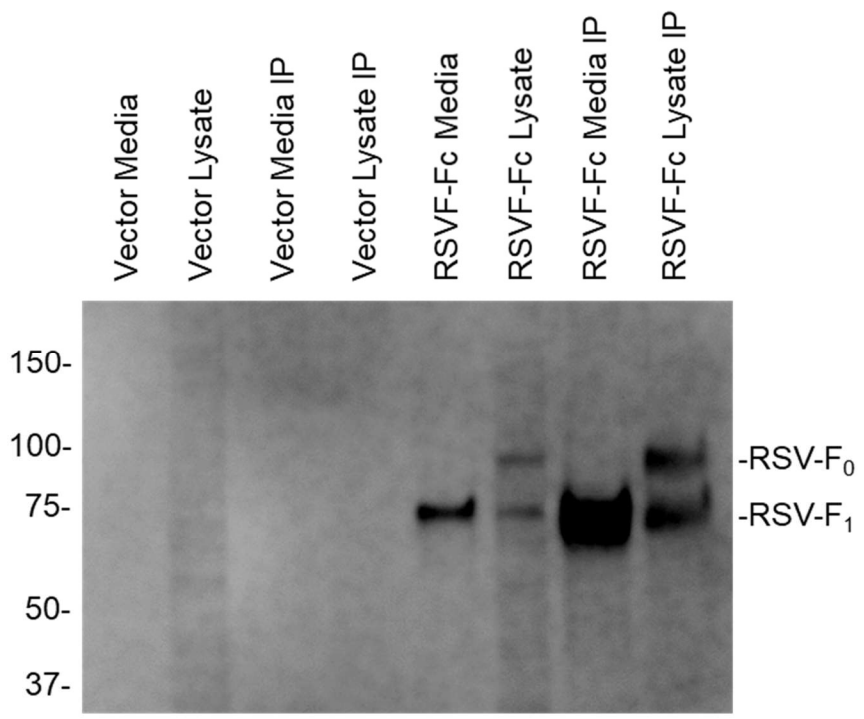

Figure 5.1 Expression and secretion of RSVF-Fc. RSVF-Fc or pCMV6-AC-FC-S (empty vector) were transfected into HEK-293T cells. 24 hours after transfection, the media on each well was replaced with serum free media. 48 hours after transfection, the conditioned media was collected, and the cells were lysed using MOSLB. The conditioned media and lysate from each sample also underwent an immunoprecipitation (IP) by binding Fc-containing proteins to protein G conjugated beads. The samples were then analyzed by western blot using HRP-conjugated anti-mouse antibodies. Molecular weight markers are in kDa.

5.2.1.2 RSVF-Fc binds NCL and blocks RSV infection

To examine if RSVF-Fc functions similarly to unmodified RSV-F, I tested the binding between RSVF-Fc and NCL. I bound RSVF-Fc in conditioned media to protein G-conjugated beads, then used the RSVF-Fc-bound beads to pull down from HEK-293T cell lysates. Proteins bound to the beads were eluted and NCL was detected by western blot (**Figure 5.2a**). I observed NCL co-immunoprecipitate with RSVF-Fc, indicating that RSVF-Fc is able to interact with NCL, like RSV-F on viral particles. However, the binding between RSVF-Fc and NCL was not as strong as observed between RSV-F on virus particles and NCL (**Figure 4.9** and [128]). This could be explained by the dilute, unpurified nature of RSVF-Fc tested in this experiment, compared to the concentrated, sucrose-purified RSV particles used in **Figure 4.9**.

Since RSVF-Fc was able to bind to NCL, I hypothesized that RSVF-Fc would be able to prevent RSV infection by binding to cell surface NCL, thereby preventing infectious RSV particles from interacting with it. To test this hypothesis, I pre-treated 1HAEo- cells with RSVF-Fc, infected with RSV, then examined the number of infected cells after one round of infection (**Figure 5.2b**). In support of the hypothesis, I observed reduced RSV infection in cells pre-treated with RSVF-Fc compared to untreated cells.

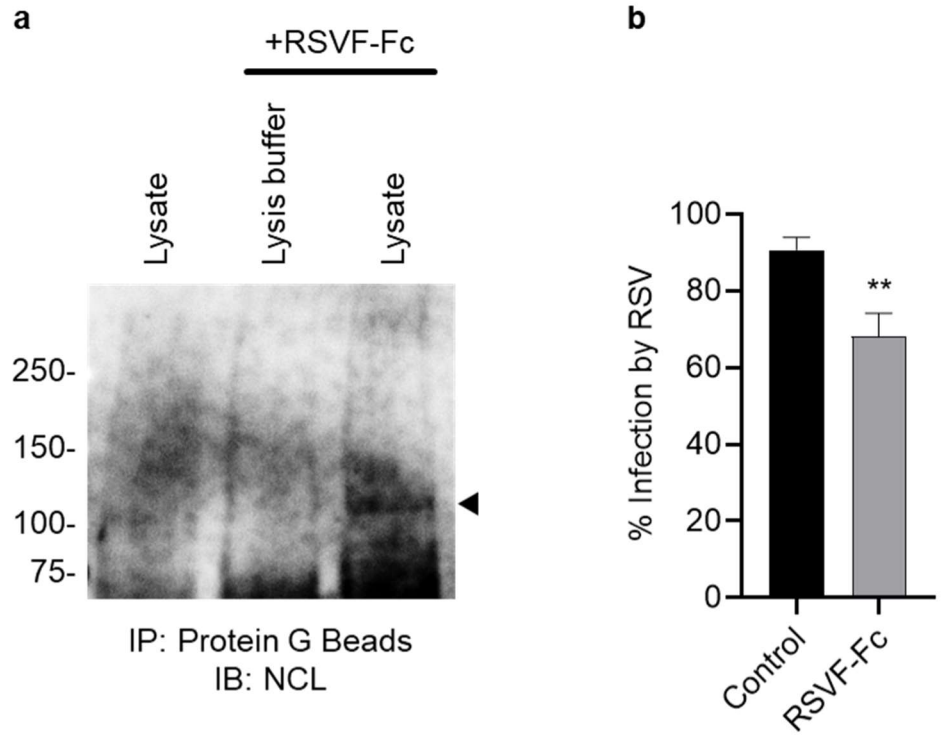

Figure 5.2 RSVF-Fc binds to NCL and inhibits RSV infection. a) Conditioned media containing RSVF-Fc or conditioned media from untransfected cells was bound to protein G beads (see **Figure 5.1**). HEK-293T cells were lysed with MOSLB, then cell lysate or lysis buffer was then combined with the beads to pull down any proteins that interact with RSVF-Fc. Bound proteins were eluted, and a western blot was performed using anti-NCL antibodies. The arrowhead indicates the NCL protein band. **b)** 1HAEo- cells were pre-treated with RSVF-Fc for 1 hour, then infected with RSV. After 3 hours, the cells were acid washed to inactivate any RSV that has not yet entered. 24 hours post-infection, the cells were fixed and stained using a polyclonal anti-RSV antibody followed by a secondary antibody conjugated to β-galactosidase. X-Gal substrate was then added to produce a blue color in RSV-infected cells, which were manually counted as RSV infectious units (IU). The number of RSV IU were then normalized, with the well containing the most infected cells within each experiment set at 100%. The data was derived from two independent experiments, with three biological replicates. The data was compared using an unpaired Student's t-test. **; $p < 0.01$. Molecular weight markers are in kDa. Panel b performed by Leanne Bilawchuk, with my guidance.

5.2.1.3 Cloning and purifying FcV2 and Fc-RSVG

In addition to RSV-F, the other major entry-related glycoprotein on the surface of viral particles is RSV-G, which plays a role in viral attachment to host cells[69]. To create another tool for examining RSV entry, I sought to also attach an Fc region to RSV-G. However, the transmembrane domain of RSV-G is on the N-terminus[109], as opposed to the C-terminus in the case of RSV-F[93]. This prevented me from using pCMV6-AC-FC-S to directly attach an Fc region to RSV-G. Furthermore, the Fc region within pCMV6-AC-FC-S cannot be expressed on its own (**Figure 5.1**), which would be a useful control protein to compare to RSVF-Fc or Fc-RSVG. To overcome both of these problems, I re-designed pCMV6-AC-FC-S using site directed mutagenesis to remove the stop codon in the multiple cloning site and add an additional small multiple cloning site on the C-terminus of the Fc region. The IL-2 signal peptide was not altered, to ensure secretion of the expressed proteins. This new vector, named pCMV6-FcV2-S, can express the Fc region on its own and has two multiple cloning sites to enable the Fc region to be attached to either the N or C terminus of the target protein (**Figure 5.3**).

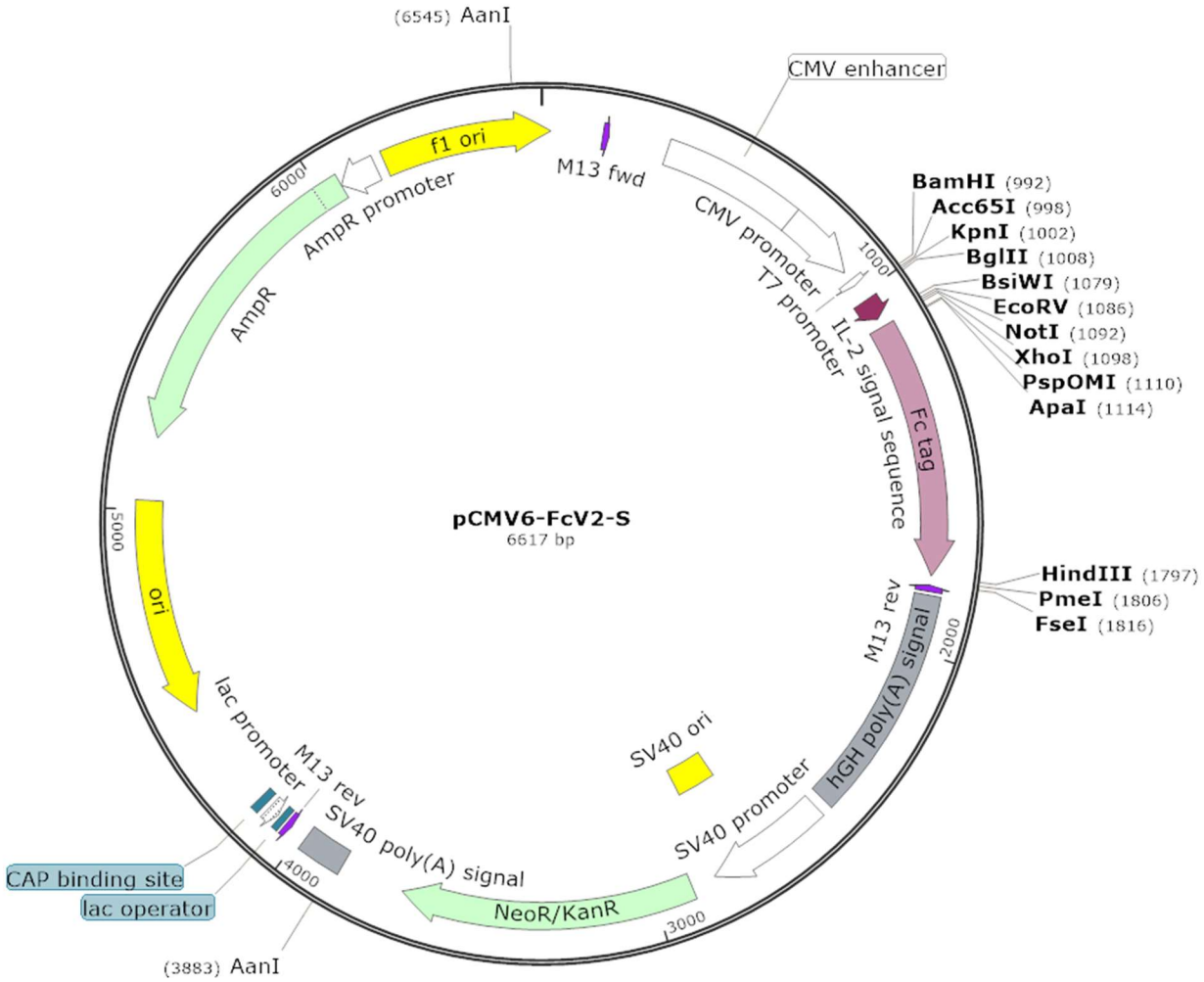

Figure 5.3 pCMV6-FcV2-S vector map. Vector map of pCMV6-FcV2-S, which was created from pCMV6-AC-FC-S to include an additional multiple cloning site at the 3′ end of the Fc region. pCMV6-FcV2-S also has a stop codon in the 5′ multiple cloning site removed to enable expression of the Fc region on its own. Map created using SnapGene Viewer.

I then cloned a codon optimized version of RSV-G, obtained from Dr. Thomas Grunwald, into pCMV6-FcV2-S. Similar to RSVF-Fc, the Fc domain was used to replace the RSV-G transmembrane domain, creating Fc-RSVG. This orientation of the Fc region, in relation to an inserted protein, is also used by the commercially available pCMV6-AN-FC-S vector from Origene. To purify RSVF-Fc, Fc-RSVG, and Fc proteins, I transfected each construct into HEK-293T cells and collected the culture supernatant every 12 hours from 36 to 120 hours post transfection. I then ran the conditioned media containing secreted Fc proteins over a HiTrap Protein G column using an ÄKTA Start FPLC and eluted bound Fc-containing proteins using a

low pH buffer. For each protein, the input media, flow through media, and elution fractions, showing a spike in ultraviolet (UV) absorbance (280 nm), were then analyzed by western blot (**Figure 5.4**). Similar to before (**Figure 5.1**), the F_1 fragment of RSVF-Fc was observed around 80 kDa. Due to glycosylation of RSV-G[108], Fc-RSVG was observed as a smear around 100 kDa. As expected, Fc alone was observed around 30 kDa. The similar level of each Fc protein in input and flow though lanes indicates incomplete binding to the protein G column, especially since the amount of each eluted protein (RSVF-Fc = 71.8 µg, Fc-RSVG = 22 µg, and Fc = 128.4 µg) was not near the reported binding capacity of 25 mg per column.

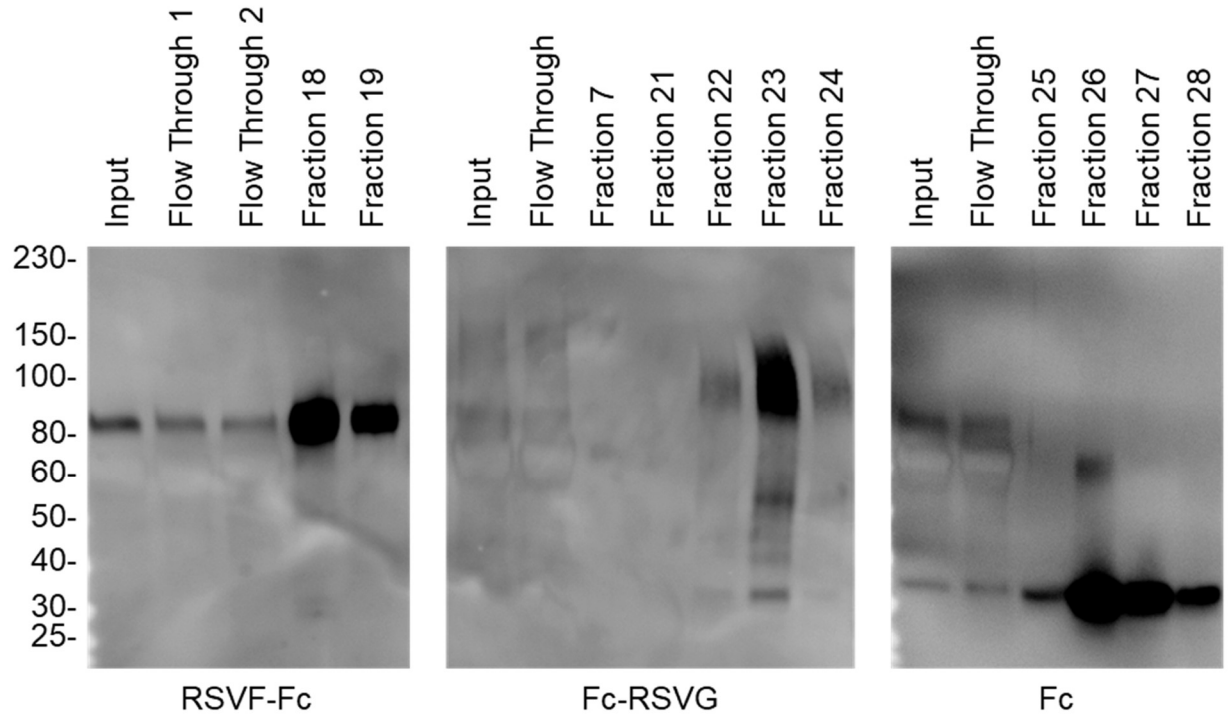

Figure 5.4 Purification of Fc proteins. HEK-293T cells were transfected with RSVF-Fc, Fc-RSVG, or Fc alone. The next day, the media on all cells was replaced with media containing 2% FBS, which the cells were maintained in for the remainder of the experiment. Conditioned media was harvested every 12 hours from 36 to 120 hours post transfection and pooled. The conditioned media was then bound to a HiTrap Protein G column using an ÄKTA Start FPLC and eluted using an increasing linear gradient of pH 2.7 glycine-HCl buffer. 0.5 mL fractions were collected during elution and the pH of eluted fractions was neutralized by adding Tris-HCl pH 9. The RSVF-Fc flow through was run past the same column again to create "Flow Through 2", no noticeable UV absorbance peaks were observed during the second elution of RSVF-Fc from the column. The input conditioned media, flow through(s), and fractions with observable UV absorbance peaks from each protein were then analyzed by western blot using anti-mouse antibodies conjugated to HRP. Molecular weight markers are in kDa.

5.2.2 Kinase and cytoskeleton inhibitors block RSV entry

5.2.2.1 Inhibitors block RSV entry

In **Chapter 4**, I observed NCL re-localization from the nucleus to the cell surface, where NCL formed patches around viral particles during the fusion process. Furthermore, RSV activates several kinases during the entry process[123,142,143,147]. Therefore, I hypothesized that kinase-triggered cellular transport pathways were involved in NCL trafficking to RSV particles, during RSV entry. To test this hypothesis, I sought to identify the cytoskeleton component(s) and the kinase(s) involved in NCL surface trafficking.

To identify the cytoskeleton component(s) and kinase(s) involved in the surface trafficking of NCL, we performed an inhibitor screen during RSV entry. 1HAEo- cells were pre-treated with inhibitors of cellular kinases or cellular transport pathways (**Table 5.1**), then infected with RSV. At 3 hours post-infection, the cells were treated with a mild acidic wash to inactivate any RSV particles that remained bound to the cell surface but had not yet entered (**Figure 5.5a**). To ensure that only the RSV entry process was being examined, the inhibitors were not replaced in the media after the acid wash. After 24 hours of infection, the cells were fixed and immunostained for RSV protein, using a β-galactosidase-based colorimetric assay to detect RSV-infected cells. The number of RSV-infected cells was then counted from each treatment and is shown as a percentage of infection, compared to the cognate vehicle control (**Figure 5.5b**). The purpose of this screen was preliminary in nature, to identify potential pathways that play a role in RSV entry. For simplicity, a single concentration of each inhibitor was tested, based on published literature values.

Cell Transport Target	Inhibitor
Actin (inhibitor)	Cytochalasin D
Actin (stabilizer)	Jasplakinolide
Arp 2&3	CK666
Myosin II	Blebbistatin
β-tubulin	Nocodazole
ER-Golgi	Brefeldin A
N-Glycosylation	Tunicamycin
Nuclear Export	Leptomycin B

Target Kinase	Inhibitor
PKCα/β	Go6976
p38 MAPK	SB203580
MEK 1&2	U0126
Ras	Salirasib
Src	PP2
PI3K	LY294002
PKCζ	PKCζ Pseudosubstrate

Table 5.1 List of cell transport and cellular kinase inhibitors used in Figure 5.5. Concentrations of each inhibitor are listed in **Materials and Methods**.

Preventing actin mobilization during RSV entry, by either stabilizing already formed actin filaments (Jasplakinolide) or preventing actin polymerization (Cytochalasin D), significantly inhibited RSV infection (**Figure 5.5b**). The importance of actin mobilization during RSV entry was consistent with what is known about the dependence of NCL trafficking on the actin cytoskeleton[220]. However, RSV infection did not appear to be dependent on actin related proteins 2 and 3 (Arp2/3), since inhibiting Arp2/3 did not reduce infection (**Figure 5.5b**). Inhibiting β-tubulin polymerization also prevented RSV infection, however, inhibiting myosin II did not (**Figure 5.5b**). Since NCL appeared to be redistributed from the nucleus to the cell surface during RSV entry (**Figure 4.6**), inhibitors of Exportin 1 (chromosomal maintenance 1 – CRM1) mediated nuclear export and ER-Golgi trafficking were tested. Preventing ER-Golgi mediated cellular transport during RSV entry was ineffective in preventing RSV infection (**Figure 5.5b**). Consistently, cell surface trafficking of NCL is also insensitive to ER-Golgi inhibitors[220]. However, preventing Exportin 1 mediated nuclear export slightly increased RSV infection (**Figure 5.5b**). Since cell surface NCL has been shown to be N-glycosylated[183], an N-glycosylation inhibitor was tested, and it was effective at reducing RSV infection (**Figure 5.5b**). Together, these results suggested that RSV entry was dependent upon actin and tubulin, but was independent of Exportin 1-mediated nuclear export or ER-Golgi trafficking. These results also support the possibility that an RSV-induced cellular signal may be responsible for the necessary cellular trafficking and NCL translocation.

Inhibiting PKC α/β, p38 MAPK, or Src kinase signaling during RSV entry did not prevent infection (**Figure 5.5b**). Preventing MEK 1/2 activity (directly upstream of ERK1/2) caused a modest, albeit statistically insignificant, reduction in infection (**Figure 5.5b**). Inhibiting Ras or PI3K signaling during RSV entry significantly decreased infection (**Figure 5.5b**). Of the kinase inhibitors tested, the PKCζ inhibitor was the most effective in preventing RSV infection (**Figure 5.5b**).

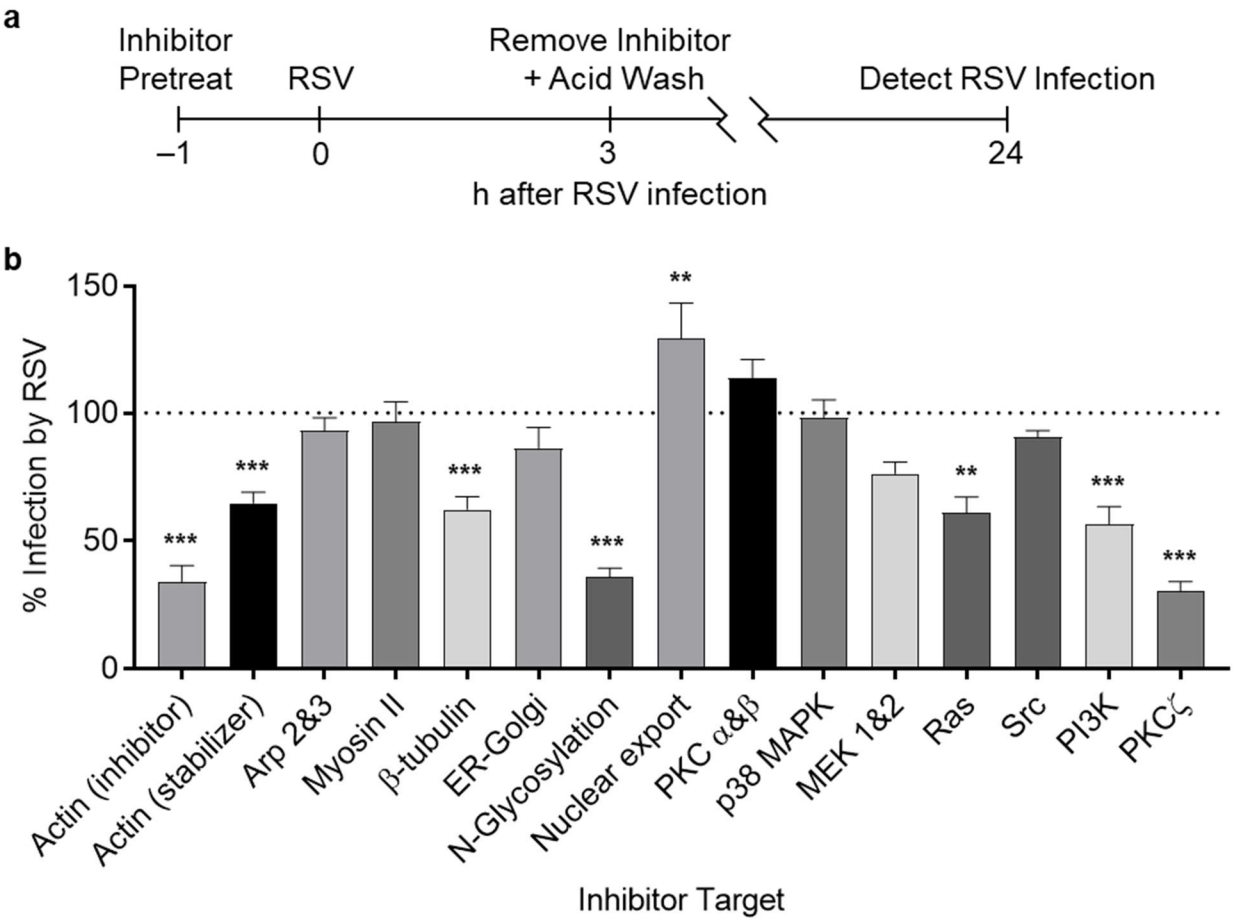

Figure 5.5 Kinase and cellular transport inhibitors block RSV entry. a) Schematic showing the chronology of the RSV entry inhibition assay. 1HAEo- cells were pre-treated with inhibitors for 1 hour, then infected with RSV. 3 hours later, the cells underwent a mild acid wash to inactivate any RSV that had not yet entered, and the inhibitors were removed. At 24 hours after infection, RSV-infected cells were quantified as infectious units using a colorimetric RSV-immunostain assay. **b)** RSV infection in the presence of kinase and cellular transport inhibitors (**Table 5.1**), is shown as a percentage of infectious units, compared to the cognate vehicle control. The x-axis lists the inhibitor target. The dotted line indicates the level of infection in control treated cells (100%). At least two independent experiments, with at least three biological replicates per experiment, were performed for each inhibitor. Representative data from one experiment is shown. Inhibitor treatments were statistically analyzed by one-way ANOVA using raw data, followed by Sidak's post hoc test to compare each inhibitor to its cognate vehicle control. **; $p < 0.01$, ***; $p < 0.001$. Experiment was performed by Leanne Bilawchuk, with my guidance.

5.2.2.2 Inhibitors block increased RSV-NCL colocalization during RSV entry

I wanted to know if the inhibitors that decreased RSV infection were preventing NCL translocation to RSV particles. To test this, I used the imaging flow cytometry assay described in Section 4.2.5 to detect the interaction of RSV particles with NCL in the presence of inhibitors. I pre-treated

1HAEo- cells with the inhibitors, infected with RSV, then measured the change in RSV-NCL colocalization between 0 and 60 min post-infection. Of the kinase inhibitors tested, I found that blocking PKCζ activity caused a decrease in RSV-NCL colocalization as opposed to the characteristic increase observed with antennapedia, the vehicle control (**Figure 5.6a**). A similar decrease in RSV-NCL colocalization was observed when actin polymerization was inhibited (**Figure 5.6b**). Of note, some of the inhibitors that were particularly effective at blocking RSV infection, such as Tunicamycin (N-glycosylation) and LY294002 (PI3K), did not affect the amount of RSV-NCL patching, and so presumably inhibited RSV entry through a mechanism independent of NCL. This indicates that RSV-NCL patching is independent of nascent N-glycosylation, which provides support for a pre-existing pool of NCL in the cell being translocated to the cell surface. This provides evidence that the RSV-NCL patching is functionally important for RSV entry since blocking NCL itself[2,127,128] or preventing the patching from occurring were both effective at preventing viral infection.

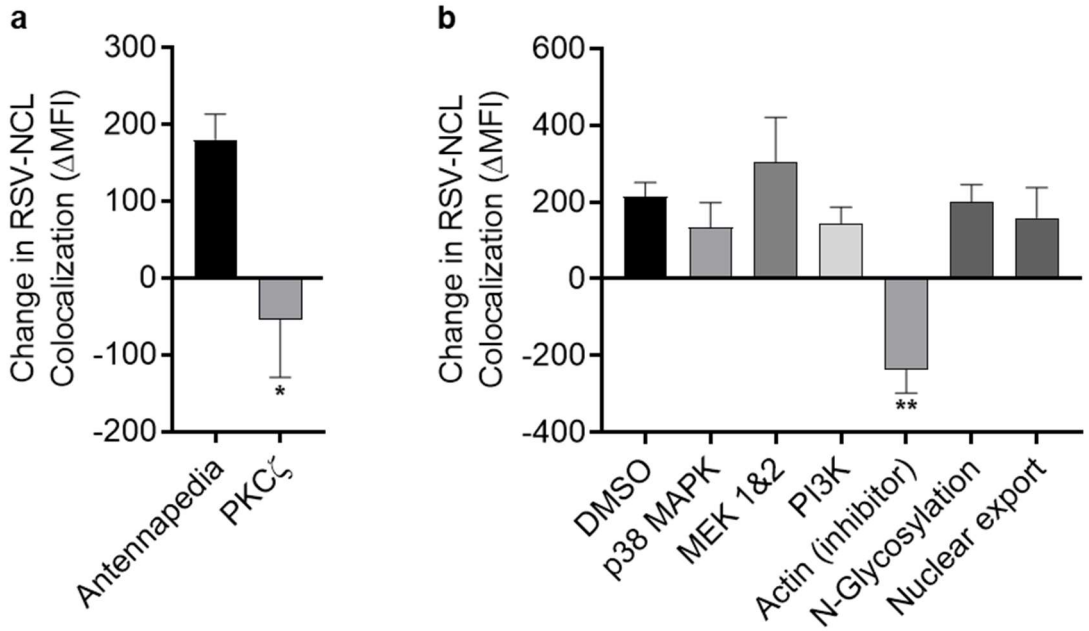

Figure 5.6 Inhibiting PKCζ or actin blocks RSV-NCL patching. 1HAEo- cells were pre-treated with inhibitors for 1 hour, then RSV was bound to the cells for 1 hour on ice. Cells were harvested after binding (0 min) or warmed to 37°C for 60 min, then analyzed by imaging flow cytometry, as described in Section 4.2.5. The difference in intensity of NCL colocalized with RSV between 0 and 60 min post-infection is graphed. A positive number indicates that the intensity of RSV-NCL colocalization increased from 0 to 60 min post-infection. The x-axis lists the inhibitor target. The data was derived from three independent experiments. The peptide inhibitor (PKCζ pseudosubstrate) and its cognate control (antennapedia) are shown in **(a)** and are compared using

a paired t-test. Chemical inhibitors are shown in **(b)** and the data was derived from three independent experiments. The chemical inhibitors were then compared by one-way ANOVA with Dunnett's post hoc test, comparing each inhibitor to DMSO. *; $p < 0.05$, **; $p < 0.01$.

I then compared the intensity of RSV on the surface of cells treated with each inhibitor at 0 min post-infection to determine if the inhibitor treatment altered RSV binding. Blocking either PKCζ activity (**Figure 5.7a**) or actin polymerization (**Figure 5.7b**) caused a reduction in RSV binding, in agreement with their described roles in surface NCL expression[176,220]. None of the other chemical inhibitors tested altered RSV binding. This includes Tunicamycin, which has previously been shown not to alter RSV binding[131]. Together, these data show that inhibiting PKCζ activity or actin mobilization causes a decrease in RSV binding and subsequently prevents an increase in NCL patching with RSV particles.

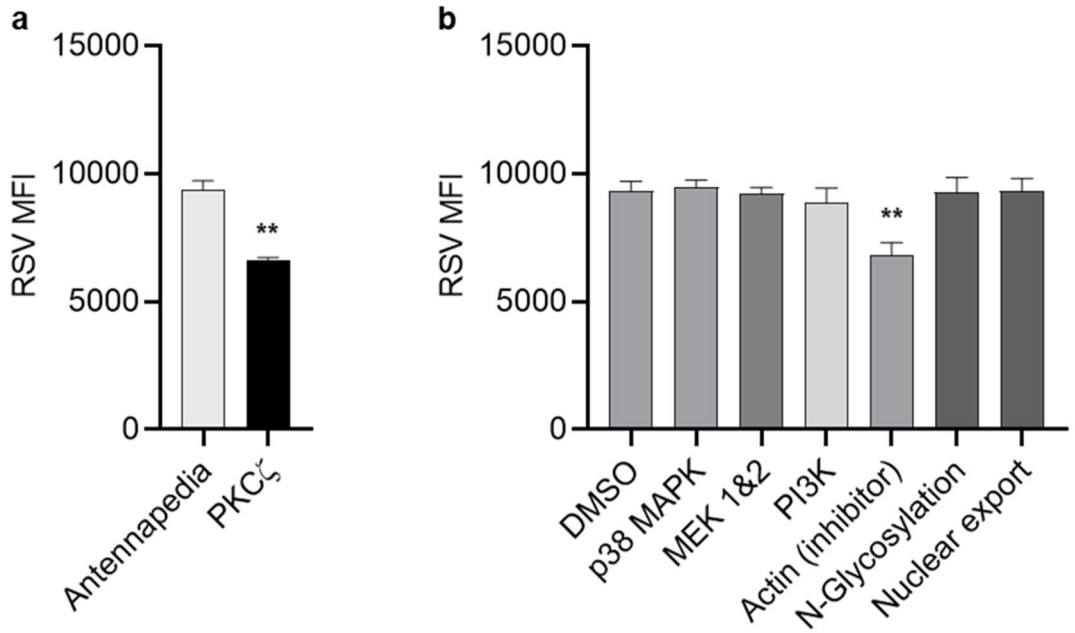

Figure 5.7 Inhibiting PKCζ or actin reduces RSV binding. Using the same experimental data as in **Figure 5.6**, cell surface RSV levels were measured by imaging flow cytometry after RSV binding, but before warming the cells. The x-axis lists the inhibitor target. The peptide inhibitor (PKCζ pseudosubstrate) and its cognate control (antennapedia) are shown in **(a)** and are compared using a Student's t-test. Chemical inhibitors are shown in **(b)** and are compared by one-way ANOVA with Dunnett's post hoc test comparing each inhibitor to DMSO. **; $p < 0.01$. The data was derived from three independent experiments.

5.2.2.3 Cell surface receptor signaling inhibitors block RSV entry

Since kinase activity plays an important role in RSV entry and NCL translocation to viral particles, I hypothesized that this kinase activity was a result of outside-in signaling caused by RSV stimulating cell surface receptors. To investigate this hypothesis, we then inhibited the signaling ability of several known RSV cell surface receptors (**Table 5.2**), using the same RSV entry inhibition assay described in **Figure 5.5**. Consistent with previous research[2,127], blocking cell surface NCL with a DNA aptamer (AS1411) significantly decreases RSV infection (**Figure 5.8**). Blocking TLR4 with an antibody also decreased infection, however, neither blocking nor activating TLR4 signaling altered RSV infection in 1HAEo- cells (**Figure 5.8**). Interestingly, inhibiting EGFR signaling increased RSV infection (**Figure 5.8**), which contrasts with previous reports that described a role for EGFR in RSV entry[119-121]. Blocking CX3CR1 with an antibody or chemical inhibitor did not alter RSV infection (**Figure 5.8**), which agrees with a previous report highlighting that the role CX3CR1 plays is redundant to HSPGs in immortalized cells[106]. Treating cells with an inhibitory peptide for annexin II also did not alter RSV infection (**Figure 5.8**). We then examined several other possible sources for the RSV-induced kinase activity and found that blocking CXCR4 signaling modestly decreased RSV infection (**Figure 5.8**), which is of note since cell surface NCL is known to associate with CXCR4[179,242]. However, inhibiting the Axl and Mer RTKs, which play a critical role in the entry of other enveloped viruses[379-381], each increased RSV infection, with statistical significance obtained for the Axl inhibitor (**Figure 5.8**). Finally, we tested if IGF1R signaling plays a role in RSV entry and we found that inhibiting IGF1R blocked RSV infection, while stimulating IGF1R enhanced RSV infection (**Figure 5.8**). The importance of IGF1R signaling for RSV entry made it a good candidate for the signaling receptor that activates PKCζ, therefore, IGF1R was investigated further.

Target Receptor	Inhibitor
IGF1R (inhibitor)	PQ401
IGF1R (stimulator)	IGF1
Nucleolin (blocking)	AS1411
TLR4 (blocking)	αTLR4 IgA
TLR4 (inhibitor)	C34

Target Receptor	Inhibitor
CX3CR1 (blocking)	αCX3CR1 IgG
CX3CR1 (inhibitor)	AZD8797
CXCR4 (inhibitor)	AMD3465
Axl RTK (inhibitor)	R428
Mer RTK (inhibitor)	UNC569

TLR4 (stimulator)	LPS
EGFR (inhibitor)	AEE788

Annexin II (blocking)	LCKLSL

Table 5.2 List of cell surface receptor inhibitors used in Figure 5.8. Concentrations of each inhibitor are listed in **Materials and Methods**.

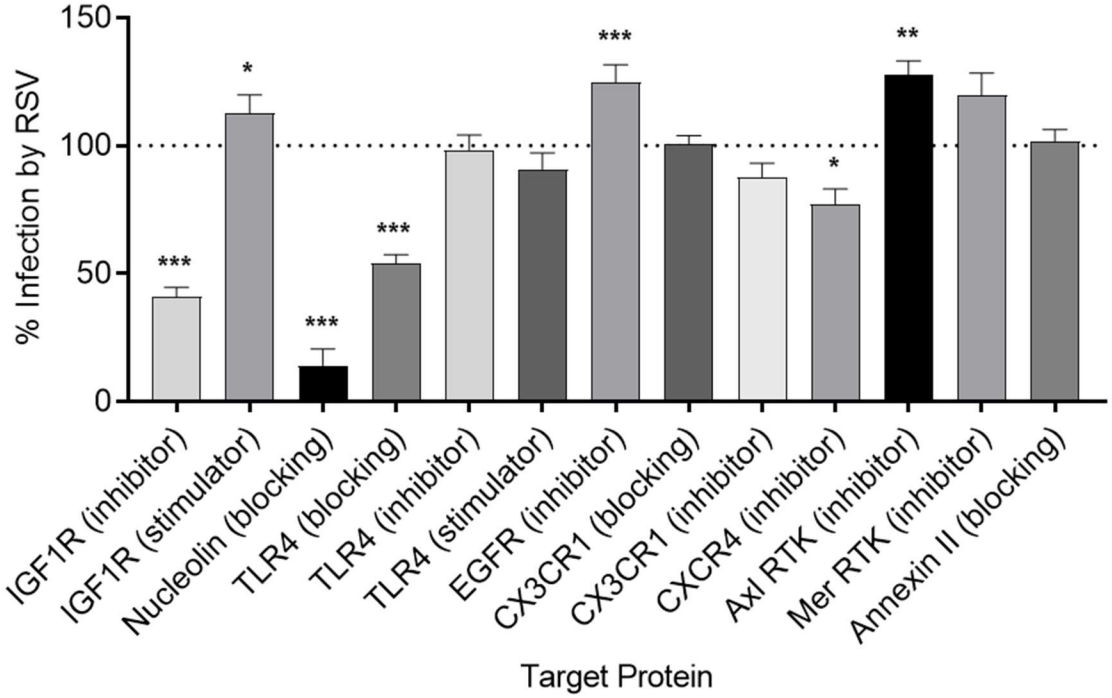

Figure 5.8 Inhibiting cell surface receptors blocks RSV entry. 1HAEo- were pre-treated with inhibitors and infected with RSV as described in **Figure 5.5a**. Graphed are RSV infectious units in the presence of cell surface receptor inhibitors (**Table 5.2)**, as a percentage of the cognate vehicle control. The dotted line indicates the level of infection in control treated cells (100%). The x-axis lists the protein target, with the interaction shown in parenthesis (signaling inhibitor, signaling stimulator, or physical interaction blocker). At least two independent experiments, with at least three biological replicates per experiment, were performed for each inhibitor. Representative data from one experiment is shown. Inhibitor treatments were statistically analyzed by one-way ANOVA using raw data, followed by Sidak's post hoc test to compare each inhibitor to its cognate vehicle control. *; $p < 0.05$, **; $p < 0.01$, ***; $p < 0.001$. Experiment performed by Leanne Bilawchuk, with my guidance.

5.2.3 PKCζ activity during RSV entry

5.2.3.1 PKCζ protein and phosphorylation levels are constant during RSV entry

Since inhibiting PKCζ activity was effective at blocking both RSV infection and RSV-NCL patching, I sought to measure PKCζ activity during a time course of RSV entry. However, when measured by western blot, there were no apparent differences in PKCζ protein levels or phosphorylation within the activation loop (threonine 410) during RSV entry (**Figure 5.9**). Treatment with the PKCζ pseudosubstrate inhibitor was included to test if the inhibitor caused PKCζ degradation or decreased phosphorylation. Neither was observed.

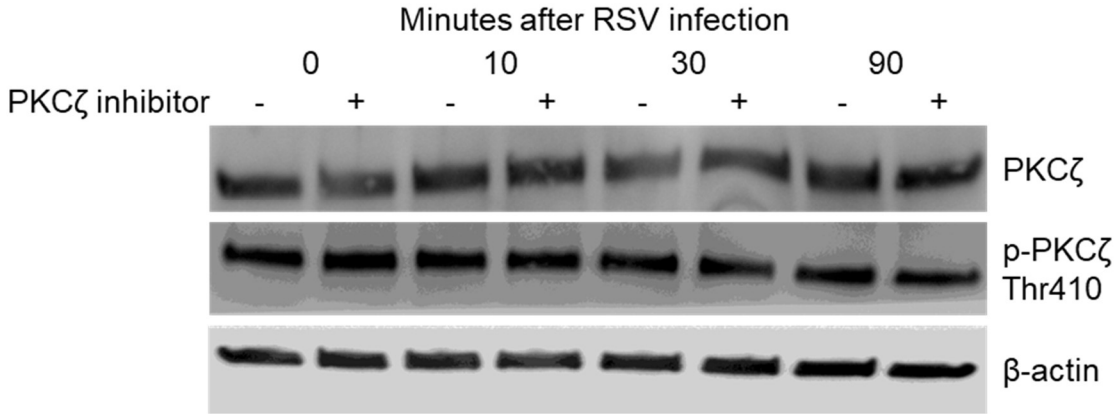

Figure 5.9 Protein levels and phosphorylation of PKCζ are constant during RSV entry. 1HAEo- cells were pre-treated with the PKCζ pseudosubstrate inhibitor (+) or antennapedia control (-), then RSV was bound to the cells for 1 hour on ice. The cells were warmed for the indicated time, lysed using MOSLB, and analyzed by western blot for PKCζ or p-PKCζ (threonine 410). β-actin is used as a loading control. Experiment performed by Leanne Bilawchuk, with my guidance.

5.2.3.2 IGF1R inhibition blocks RSV-induced PKCζ activity

Since PKCζ activity within cells is determined by both phosphorylation and stabilization by binding partners[287], I next measured the activity of PKCζ more directly. To do this, I infected 1HAEo- cells with RSV and harvested them at a series of time points during viral entry. Next, I immunoprecipitated PKCζ (**Figure 5.10a**) and performed an *in vitro* kinase assay using the immunoprecipitated PKCζ, with CREBtide as the substrate. As a result, I observed a large increase in PKCζ activity at 10 min post RSV infection (**Figure 5.10b**), which is consistent with a previous report[143]. Next, I pre-treated cells with either an IGF1R inhibitor (PQ401) or an actin inhibitor (Cytochalasin D), infected with RSV for 10 min, then performed an *in vitro* PKCζ activity assay.

I then compared PKCζ activity between RSV-infected cells and uninfected cells in the presence of each inhibitor. I also included IGF1 on its own (instead of RSV) to determine if stimulating IGF1R is sufficient to induce PKCζ activity in 1HAEo- cells. I also used the PKCζ pseudosubstrate inhibitor, added during the *in vitro* kinase reaction, as a control for specificity of the reaction. Inhibiting IGF1R signaling or actin polymerization blocked the RSV-induced increase in PKCζ activity (**Figure 5.10c**). Adding IGF1 alone for 10 min increased PKCζ activity to a similar degree compared to RSV (**Figure 5.10c**). The ability of IGF1 to increase PKCζ activity is consistent with previous reports[295,296]. Together, these results point to IGF1R as a likely cause for the RSV-induced PKCζ activity and resulting recruitment of NCL to bound RSV particles. Therefore, IGF1R as a signaling receptor for RSV was investigated further.

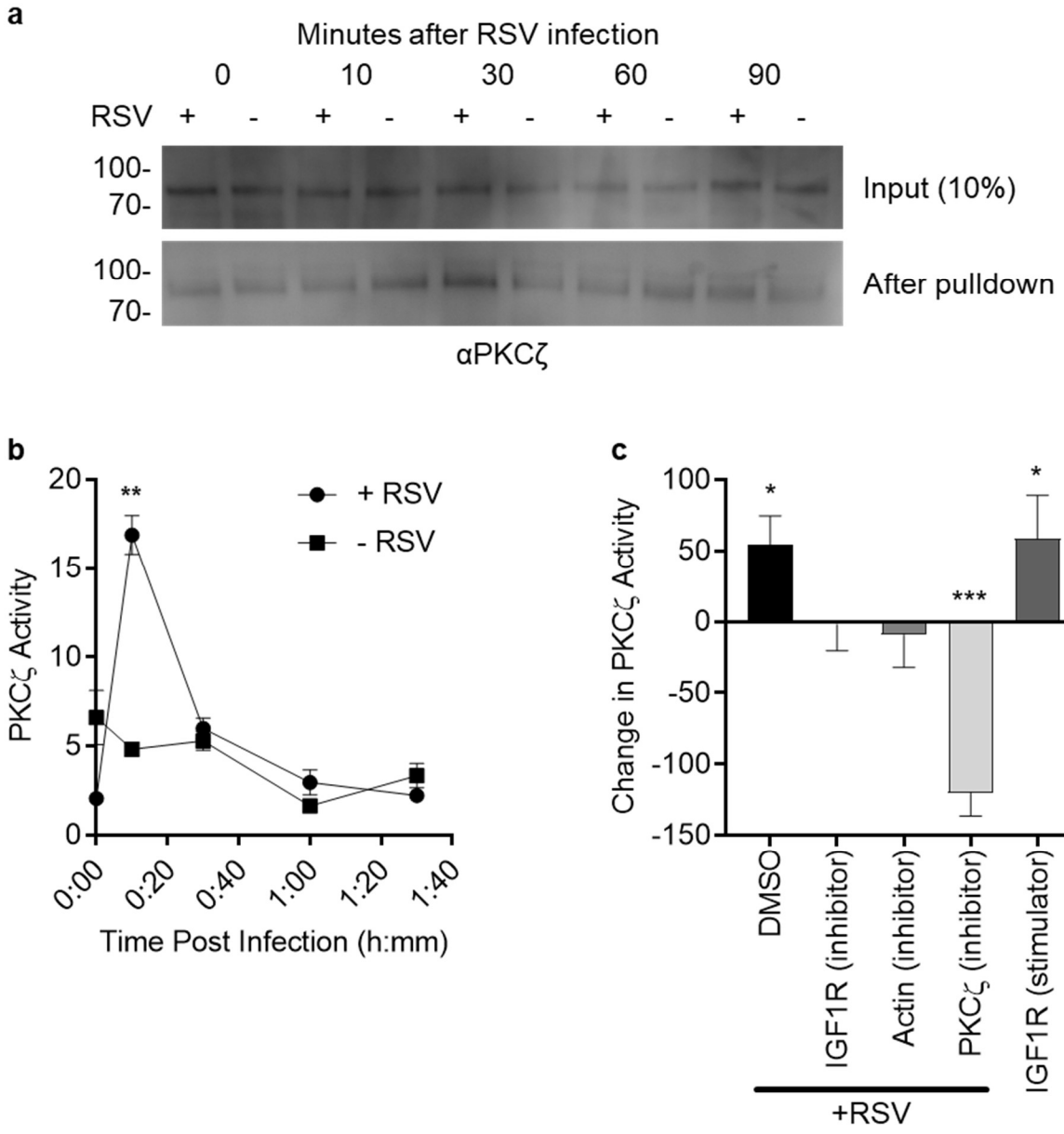

Figure 5.10 RSV activation of PKCζ during entry depends on IGF1R and actin. a) RSV was bound to 1HAEo- cells for 1 hour on ice, then the cells were warmed for the indicated times in the timecourse. The cells were lysed using MOSLB lysis buffer, and the lysates underwent an immunoprecipitation using anti-PKCζ antibodies. The immunoprecipitation eluates (bottom) and input lysates (10% of the volume added to the immunoprecipitation, top) were then analyzed by western blot using anti-PKCζ antibodies. **b)** PKCζ immunoprecipitated in **(a)** underwent an *in vitro* kinase assay for 1 hour at room temperature, using CREBtide as a substrate. The ATP converted to ADP was measured using the ADP-Glo kinase assay as a readout for PKCζ activity. PKCζ activity represents the nmol of ATP converted to ADP by PKCζ. The data points were derived from three technical replicates, with similar results observed in three independent experiments. The data was statistically analyzed by multiple t-tests (one per timepoint), taking into account false discovery rate, using the method by Benjamini, Krieger, and Yekutieli. **c)** 1HAEo- cells were

treated with IGF1R or actin inhibitors (or DMSO) for 1 hour, then treated as above for the PKCζ *in vitro* kinase assay, using only the 10 min timepoint (+/- RSV). Graphed is the difference in PKCζ activity between samples with and without RSV. A positive number indicates that PKCζ activity is higher in RSV-infected cells, compared to uninfected cells. For the IGF1 treatment, cells were cooled on ice for 1 hour (without RSV) and IGF1 was added right before warming. The difference between the IGF1 treated sample and the -RSV sample (without inhibitor) was graphed. For the PKCζ inhibitor treatment, PKCζ pseudosubstrate was added during the *in vitro* kinase reaction for a +RSV sample, as a control for reaction specificity. The difference between PKCζ inhibitor sample and the +RSV sample (without inhibitor) was graphed. The data was derived from five independent experiments. The data was statistically analyzed by one-way repeated measures ANOVA, using Sidak's post hoc test to compare samples used to show the difference graphed (+RSV vs -RSV, IGF1 vs -RSV, and PKCζ vs +RSV). *; $p < 0.05$, **; $p < 0.01$, ***; $p < 0.001$.

5.2.4 The role of IGF1R during RSV entry

5.2.4.1 IGF1R is an RSV receptor

Since IGF1R signaling is important for RSV entry and IGF1R is upstream of PKCζ, I hypothesized that IGF1R is a functional RSV receptor. According to Fields Virology[60], in addition to binding the virus, a receptor must perform at least one of three functions: 1) induce a viral conformational change, such as triggering of a fusion protein, 2) transmit signals to enhance viral entry/replication, or 3) guide bound viral particles to an endocytic pathway. This is in contrast to attachment factors, which assist viral binding, but do not actively promote entry or mediate signals that support viral replication.

To characterize IGF1R as a potential RSV receptor, we first tested if IGF1R and RSV are found in the same location. To do this, we performed immunofluorescence microscopy on 1HAEo- cells and examined IGF1R and RSV colocalization on the cell surface (**Figure 5.11a**). Distinct patches of IGF1R were observed colocalizing with RSV particles above the actin cortical cytoskeleton. Next, we examined if RSV and IGF1R are capable of directly interacting. To do this, we collaborated with Dr. Jason McLellan (University of Texas at Austin) to obtain a recombinant form of RSV-F stabilized in the prefusion state, called DS-Cav1[59]. We then used microscale thermophoresis and observed direct binding between RSV-F and IGF1R (**Figure 5.11b**). No substantial binding between RSV-G and IGF1R was observed. Finally, to validate IGF1R as a signaling receptor, we tested if IGF1R is activated during RSV entry. After ligand binding, the tyrosine kinase domain of IGF1R becomes phosphorylated to activate the receptor's own kinase activities. The first tyrosine to be phosphorylated upon IGF1R activation is at position 1135[328],

which we tested for phosphorylation using western blot. As expected, IGF1R activation is observed as early as 10 min post RSV infection (**Figure 5.11c**), similar to the timeframe of PKCζ activation (**Figure 5.10b**).

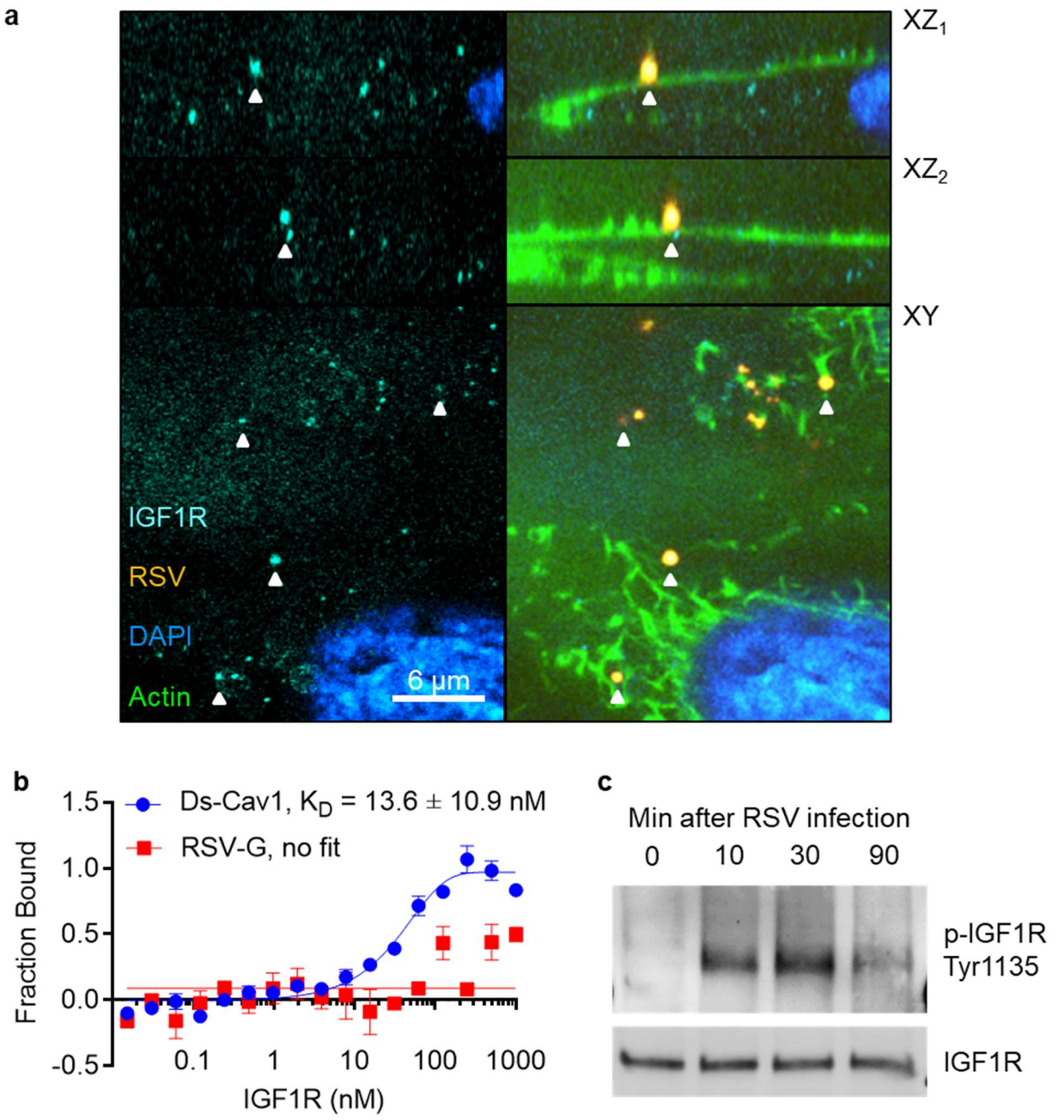

Figure 5.11 IGF1R is an RSV receptor. a) RSV was bound to 1HAEo- cells for 1 hour on ice, then the cells were warmed for 30 min, fixed, permeabilized, and stained for immunofluorescence microscopy. Shown is IGF1R (cyan), RSV (orange), nuclei (DAPI, blue), and actin (green). On the left, only IGF1R and DAPI are shown. On the right, all channels are merged. Arrowheads indicate RSV particles colocalizing with IGF1R. **b)** Microscale thermophoresis measured the

affinity of IGF1R protein with prefusion stabilized RSV-F (DS-Cav1) or RSV-G. 50 nM RSV-F or RSV-G was stained with NT-647, then combined with a dilution series of unlabeled IGF1R, ranging from 1 μM to 15.3 pM. The data points were derived from five independent experiments. The dissociation constant (K_D) is shown ± the standard deviation. **c)** RSV was bound to 1HAEo- cells for 1 hour on ice, then the cells were warmed and lysed at the indicated times using MOSLB lysis buffer. Two independent experiments were performed, with similar results. The lysates were analyzed by western blot using antibodies against IGF1R and p-IGF1R (tyrosine 1135). Experiment performed by Leanne Bilawchuk, with my guidance.

5.2.4.2 IGF1 increases surface NCL

Since RSV-induced IGF1R signaling appears to call NCL to the surface during RSV entry, I hypothesized that treating cells with IGF1 alone would be sufficient to induce a similar increase in surface NCL. Therefore, I transfected HEK-293T cells with NCL-GFP, then treated the cells with IGF1 for 1 hour and examined the surface expression of NCL-GFP by flow cytometry, using a similar method as described in Section 3.2.1.3 (**Figure 5.12**). I observed a modest increase in surface NCL expression on the IGF1-treated cells. The modest nature of this increase is likely a reflection of the transient nature of NCL surface trafficking and the small size of IGF1, compared to a viral particle, which is capable of crosslinking multiple receptors to form a signaling platform[382].

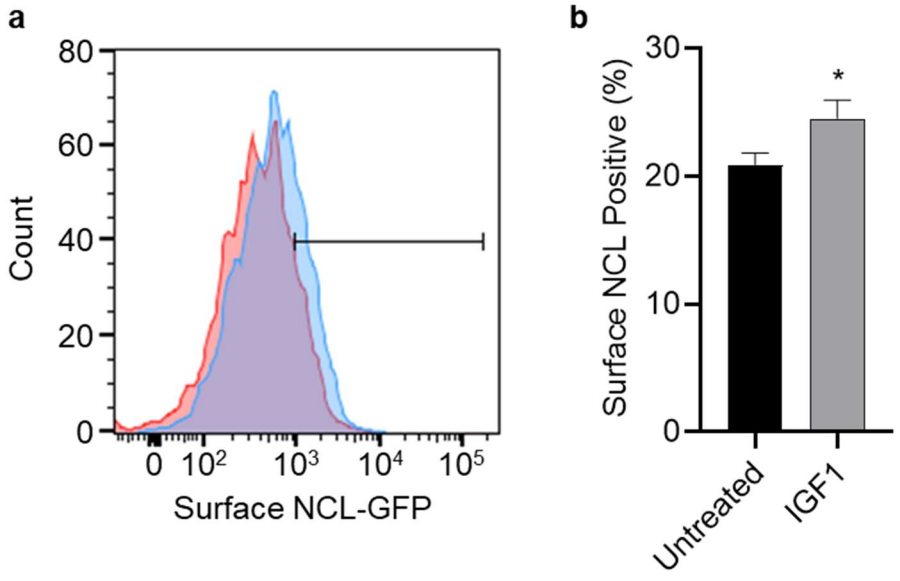

Figure 5.12 IGF1 treatment increases surface NCL expression. HEK-293T cells were transfected with NCL-GFP, then treated with IGF1 for 60 min or left untreated. Surface NCL-GFP levels of GFP-positive cells were detected by immunostaining of non-permeabilized cells using α-GFP antibodies and enumerated by flow cytometry. Overlaid histograms of untreated (red) and

IGF1 treated (blue) cells are shown (**a**) and quantified (**b**). The data was derived from 3 independent experiments, with three biological replicates per experiment (nine data points per bar). Significance was determined by Student's two-tailed t-test *; p = 0.045.

5.2.4.3 IGF1R, NCL, and PKCζ influence the RSV rate of fusion

Next, I wanted to examine if the RSV receptors, IGF1R and NCL, or the intermediary, PKCζ, played a role in the rate of RSV fusion with host cells. To do this, I adapted an assay from Srinivasakumar and colleagues that utilizes RSV stained with a lipophilic dye and examines the increase in fluorescence, due to RSV fusion, on a per-well basis[138]. Based on previous experience with lipophilic dyes, I stained RSV with DiD and infected cells that had been pre-treated with NCL or PKCζ inhibitors. I also included a 1HAEo- cell line that has IGF1R knocked out using CRISPR-Cas9 (courtesy of Dr. Anil Kumar). The DiD fluorescence in each well progressively increased from 30 min post-infection up to 2 hours post-infection, when the assay was stopped. However, the DiD fluorescence increased at a slower rate in cells treated with NCL (**Figure 5.13a**) or PKCζ inhibitors (**Figure 5.13b**), indicating that blocking NCL or PKCζ also directly reduces the rate of RSV fusion with host cells. Similarly, the cells lacking IGF1R also had a slower increase in DiD fluorescence compared to wildtype 1HAEo- cells (**Figure 5.13c**). I then compared the binding of RSV to the cells, based on total DiD fluorescence after unquenching with Trition X-100. I observed that blocking NCL, inhibiting PKCζ, or removing IGF1R all decreased RSV binding (**Figure 5.13d**). This is in agreement with the imaging flow cytometry data for NCL and PKCζ inhibitors (**Figure 4.16** and **Figure 5.7**).

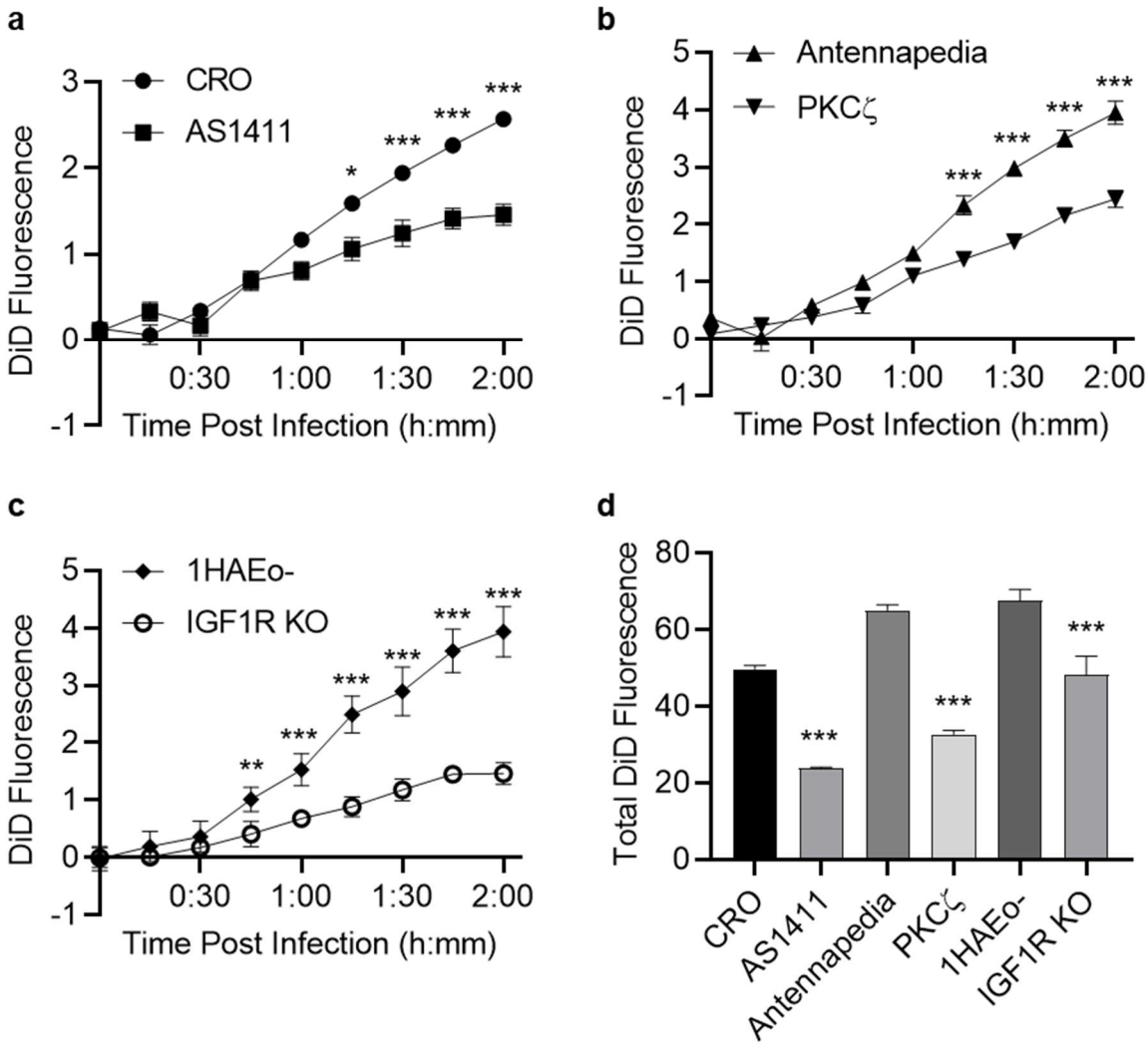

Figure 5.13 The roles of IGF1R, NCL, and PKCζ in RSV binding and fusion. 1HAEo- cells (or IGF1R KO cells) were pre-treated with inhibitors for 1 hour, then DiD-RSV (described in Section 4.2.4) was bound to the cells for 1 hour on ice. Antennapedia and CRO (cytosine rich oligonucleotide) are used as controls for the PKCζ pseudosubstrate and AS1411 respectively. The cells were washed 5x and warmed to 37ºC. **a-c)** At indicated times, the cells were removed from the incubator, DiD fluorescence was measured using a plate reader, and the cells were placed back at 37ºC. The data was statistically analyzed by two-way ANOVA, using Tukey's post hoc test to compare each treatment to its cognate control at every timepoint. **d)** At the end of the experiment, Triton X-100 was added to each well, to a final concentration of 1%, to unquench all remaining DiD. This total fluorescence is representative of all DiD-RSV bound and entered. The data was statistically analyzed by one-way ANOVA, followed by Sidak's post-hoc test, comparing each treatment to the cognate control. *; $p < 0.05$, **; $p < 0.01$, ***; $p < 0.001$. The data points shown were derived from five biological replicates. Two independent experiments were performed, with similar results.

5.3 Discussion

In this chapter, I explored the mechanism behind the NCL trafficking observed in **Chapter 4**. Using a series of kinase and cellular process inhibitors, I found that both PKCζ activity and actin remodeling play a crucial role in the transport of NCL to RSV particles on the cell surface. Furthermore, I identified IGF1R as a novel cell surface receptor for RSV that assists with RSV binding and initiates an RSV-induced signaling cascade, upstream of PKCζ. I also expressed and purified recombinant RSV glycoproteins.

5.3.1 Creation and purification of RSV glycoproteins fused to Fc

To create a tool capable of probing interactions between individual RSV glycoproteins and host cells, I replaced the transmembrane domains of RSV-F and RSV-G with Fc regions. When tested, I found that RSVF-Fc was capable of binding NCL and inhibiting RSV infection when used to pre-treat cells. I then expressed and purified both proteins, in addition to the Fc region alone. Although RSV-SH is also a transmembrane glycoprotein expressed on the virion surface, no entry-related role has been ascribed to this protein[101]. Therefore, I instead focused only on RSV-F and RSV-G when creating recombinant RSV glycoproteins. Although I successfully purified the proteins, I found similar levels of each protein in the input media and flow through, after being run past the column. This indicates inefficient binding of the Fc-proteins to the protein-G columns, especially when comparing the total purified yield of each protein (RSVF-Fc = 71.8 μg, Fc-RSVG = 22 μg, and Fc = 128.4 μg) to the binding capacity of each column (25 mg).

Furthermore, during this project, the importance of the pre-fusion conformation of RSV-F[96], compared to the post-fusion conformation[97] gained prominence within the RSV field[383]. In particular, a high-profile Phase III clinical trial using post-fusion stabilized RSV-F was unsuccessful in inducing a protective response against subsequent RSV challenge (Novavax Trial NCT02608502[384]). This failure caused a dramatic shift in the RSV vaccine field, towards testing pre-fusion stabilized forms of RSV-F. The discovery that approximately 90% of serum neutralizing activity against RSV is mediated by antibodies which bind prefusion RSV-F[383] provides evidence against post-fusion RSV-F playing a major role in viral attachment or entry. Both purified and RSV-associated RSV-F spontaneously triggers over time, which is accelerated by heat, low molarity buffers, or formaldehyde[102-104]. Since my RSVF-Fc protein was not stabilized in the prefusion form, it is highly likely that the protein triggered to the post-fusion form

during my expression and purification. The post-fusion conformation of RSVF-Fc could also be one of the reasons behind the weak binding to NCL and modest reduction in RSV infectivity after pre-treating cells. Due to the purification and stability issues, I chose not to pursue the RSV glycoproteins fused to Fc further. For the experiment involving purified viral glycoproteins binding to IGF1R, we instead collaborated with Dr. Jason McLellan (who created the first pre-fusion stabilized RSV-F[59]) and used commercially available purified RSV-G.

5.3.2 IGF1R is an RSV signaling receptor

The idea of an RSV signaling receptor has been proposed previously[1,120,123]. The three best previously described candidates for RSV signaling receptors are TLR4[122-124], CX3CR1[106,107,111,118], and EGFR[119-121]. However, when tested using an RSV cell entry assay in the 1HAEo- cell model, none of the signaling inhibitors for these receptors blocked RSV infection. Blocking antibodies against CX3CR1 were also ineffective at inhibiting RSV infection, which is not unexpected since the attachment role for CX3CR1 is redundant to HSPGs in immortalized cells[106]. Of note, blocking antibodies against TLR4 were effective in reducing RSV entry, which lends credence to TLR4 playing a role in RSV attachment. Inhibiting CXCR4 caused a 23% reduction in RSV infection, which is intriguing since cell surface NCL interacts with CXCR4[179,242] and PKCζ activation has been observed downstream of CXCR4[291]. However, the modest reduction in RSV infectivity that was observed indicates CXCR4 signaling likely only plays an accessory role during RSV entry. As part of the TAM family (Tyro-3, Axl, and Mer) of RTKs, Axl and Mer signaling plays a role in the entry of a wide range of other enveloped viruses, including Ebola[379], Zika virus[381], and Dengue virus[380]. However, Axl and Mer signaling is unlikely to be involved in RSV entry since inhibiting either receptor slightly increased RSV entry instead of blocking it. Annexin II is a calcium-dependent phospholipid-binding protein that has previously been implicated in RSV entry[117]. Therefore, a peptide inhibitor corresponding to the site where tissue plasminogen activator binds to annexin II[385] was tested to determine if inhibiting annexin II alters RSV entry in 1HAEo- cells. Although the peptide inhibitor did not alter RSV infection, it is possible that RSV binds to a different site on annexin II. Furthermore, annexin II could play a role as a part of an RSV entry receptor complex, since it directly attaches to IGF1R[386].

Of the cell surface receptor signaling inhibitors tested, only inhibiting IGF1R signaling caused a substantial decrease in RSV infection. The role of IGF1R signaling in RSV infection was

supported by IGF1 enhancing RSV entry. IGF1R as an RSV receptor was subsequently characterized by examining RSV-IGF1R colocalization using microscopy, testing direct binding between IGF1R and pre-fusion stabilized RSV-F[59], and showing that IGF1R was activated very early during RSV infection. Furthermore, IGF1R knockout cells had reduced RSV binding and a decreased rate of viral fusion, compared to wildtype cells. Together, these observations show that IGF1R binds directly to RSV and actively promotes viral entry, which means that IGF1R fills the requirements to be an RSV signaling receptor[60]. It is interesting to note that the IGF1R-dependent change in the RSV rate of fusion is reminiscent of a study showing that EGFR enhanced the fusogenicity of a particular strain of RSV-F (2-20)[119]. The study also noted that the A2 strain (used in my project) of RSV-F did not bind as strongly to EGFR, show susceptibility to EGFR signaling inhibitors, or show EGFR-dependent changes in fusogenicity. EGFR and IGF1R are closely related RTKs that are capable of forming heterodimers in some circumstances[324]. It would be interesting to determine the role, if any, that these heterodimers play during RSV entry.

5.3.3 PKCζ is critical for RSV-induced NCL trafficking

In a similar line to investigating potential RSV signaling receptors, I investigated downstream kinases that play a role in RSV entry. During the entry process, RSV activates several kinases including p38, ERK1/2, PI3K, and PKCζ[123,142,143,147]. Similar to what has been observed before, I found that blocking PI3K signaling also reduced RSV entry. In contrast to previous reports, inhibiting p38[123,144], PKCα[148], or Src kinase[121] did not block RSV infection. However, these studies used kinase inhibitors throughout the infection process, as opposed to only during RSV entry, which implies that p38, PKCα, and Src likely play roles in RSV infection after entry has occurred. During infection, RSV activates ERK1/2 in a biphasic manner[123,142,146], and inhibiting early ERK1/2 activity moderately reduces RSV entry[123,145]. Similarly, I observed a reduction in RSV infection when ERK1/2 activity was inhibited by blocking upstream MEK1/2 (though not statistically significant). I also observed that blocking Ras signaling reduced RSV entry. Ras is an important signaling regulator for cellular growth and proliferation (reviewed in [319]), it is possible that the reduction in RSV infection I observed was due to decreased availability of cellular resources. Alternatively, Ras is typically an upstream component for ERK activity and inhibiting Ras could reduce RSV infection indirectly by blocking ERK activation[319]. Ras is also capable of directly binding to PKCζ[299] and NCL[357], so inhibiting Ras may indirectly alter PKCζ activity or NCL localization.

Of the kinases tested, PKCζ played the largest role in the RSV entry process. This is highlighted by the fact that, unlike p38, ERK1/2, or PI3K, blocking PKCζ activity also eliminated NCL trafficking to RSV particles during viral entry. Furthermore, inhibiting PKCζ activity also decreased RSV binding and reduced the RSV rate of fusion to a similar degree as directly inhibiting NCL. This is pertinent because PKCζ is capable of directly phosphorylating NCL in the nucleus[192] and has been proposed to play a role in NCL cell surface expression[176]. Furthermore, cell surface NCL is observed as a phosphoprotein[213]. During RSV entry, PKCζ is likely a crucial part of the link between RSV-induced IGF1R activation and subsequent surface trafficking of NCL. In support of this notion, IGF1 stimulation activated PKCζ (observed by me and others[295,296]), and inhibiting IGF1R blocked RSV-induced PKCζ activity. IGF1 stimulation alone was also sufficient to induce cell surface trafficking of NCL.

5.3.4 Regulation of PKCζ activity

PI3K is typically described as an upstream regulator of PKCζ phosphorylation[300,301], however, there is evidence that PKCζ is constitutively phosphorylated in resting cells[289]. In this case, PKCζ activity is primarily regulated by scaffolding proteins[286,287,302] and interaction with acidic lipids or proteins[285,289,306,307], independent of PI3K. The interaction with binding partners stabilizes PKCζ in an open conformation, with the pseudosubstrate domain away from the catalytic site[286,287]. Since I observed an RSV-induced increase in PKCζ activity, but no change in PKCζ phosphorylation, my observations fit with the idea that binding partners regulate PKCζ activity, independent of PI3K. This also provides an explanation for why inhibiting PI3K did not alter RSV-NCL patching.

Several proteins can alter PKCζ activity. Par-6 is a well-described PKCζ binding partner, that binds the PB1 domain of PKCζ and directly increases kinase activity by stabilizing PKCζ in an open conformation[286,287,303,304,387]. p62 is another protein that binds to the PKCζ PB1 domain and increases activity[287,302]. Of note, p62 can also bind phosphorylated IRS-1, which is directly phosphorylated by IGF1R upon IGF1 stimulation[287,305,388]. After IGF1 stimulation, a functional complex containing p62, phosphorylated IRS-1, and PKCζ has been reported[305], therefore a similar complex could be mediating the RSV-induced PKCζ activity that I observed. Alternatively, 14-3-3 protein and receptor for activated C kinase 1 (RACK1) are scaffolding proteins that are able to interact with both IGF1R[329,389] and PKCζ[291,307,390]. 14-3-3 is also able to directly bind to IRS-1[389]. As an acidic protein, 14-3-3 binding increases PKCζ activity[307].

Since protein scaffolds play a major role in regulating PKCζ activity, it is also important to consider the cellular location of these scaffolds. PKCζ phosphorylation of NCL occurs in the cell nucleus[192], which is consistent with my observation that during RSV infection, nuclear NCL translocated to the cell surface. However, the translocation of NCL from the nucleus to the surface is Exportin 1 independent, since Leptomycin B treatment did not reduce RSV infection or RSV-NCL patching. PKCζ itself is capable of translocating into the nucleus using a non-classical NLS[290]. However, for PKCζ to be active in the nucleus, the scaffolding proteins would also need to be present. Interestingly, p62[391], Par-6[392], 14-3-3[393], IRS-1[394] and RACK1[395] have all been found in the nucleus. In the nucleus, RACK1 and 14-3-3 can act cooperatively[395], implying that a similar situation could occur during regulation of PKCζ activity. In response to IGF1 stimulation, IRS-1 translocates into the nucleus, where it binds directly to NCL[394], which could provide a link between activated PKCζ and NCL.

5.3.5 Role of actin during RSV entry

As the cytoskeleton forms the basis of cellular structure and viral entry is a dynamic process involving protein movement, it is not surprising that inhibitors of cytoskeletal components altered RSV entry. Furthermore, the cortical actin cytoskeleton is a barrier that invading viral particles must pass to infect host cells[60]. I also observed that β-tubulin played a role in RSV entry, while inhibiting myosin II did not have any effect. This contrasts a previous report investigating RSV entry via macropinocytosis, which highlighted an essential role for myosin II, but found no effect when inhibiting β-tubulin[120]. A possible reason for the difference between this report and my data is that the macropinocytosis study used HeLa cells, while I used 1HAEo- cells, which implies that RSV may preferentially enter cells by macropinocytosis or surface fusion in different cell types. An important future step would be to examine the relative contributions of surface fusion and macropinocytosis to RSV entry in ciliated primary bronchial epithelial cells. The presence of host cell cilia likely impacts the route of RSV entry, though it has not been previously explored.

One common point between my project and the macropinocytosis study is the crucial role for actin mobilization[120]. However, instead of macropinocytosis, I identified that actin played a role in RSV binding, along with the subsequent NCL translocation to the cell surface. I also found that actin was essential for RSV-induced PKCζ activation, implying that actin is important for bringing together PKCζ and its scaffolding proteins. However, inhibiting Arp2/3 did not block RSV entry,

in agreement with what has been described previously[139]. Stimulation of cells with IGF1, IGF2, or insulin are all capable of inducing actin mobilization[327,396]. This means that the RSV-induced actin mobilization that I observed may also be downstream of IGF1R. Furthermore, insulin-induced actin remodeling is PI3K-dependent[397], which could explain the role of PI3K that I observed during RSV entry. Interestingly, another study also described Arp2/3 independent actin mobilization downstream of IGF1R signaling[335].

5.3.6 Model of RSV entry

Together, my observations from **Chapter 4** and **Chapter 5** provide evidence toward an updated model of RSV entry (**Figure 5.14**). First, RSV binds to IGF1R on the surface of a host cell, docking on a lipid raft. RSV binding activates IGF1R, which initiates a signal cascade to activate PKCζ, potentially via p62, Par-6, IRS-1, 14-3-3, and/or RACK1. PKCζ then translocates to the nucleus, where it phosphorylates NCL and NCL translocates to RSV particles on the cell surface. RSV then fuses on the cell surface or is internalized by macropinocytosis, followed by fusion (**Figure 1.2**). Using the accepted terminology for viral receptors[60], IGF1R would be the primary receptor for RSV, while NCL would be a co-receptor. Other receptors, such as EGFR, TLR4, CX3CR1, and HSPGs also likely play a role in RSV entry, though they have been excluded from my model for simplicity.

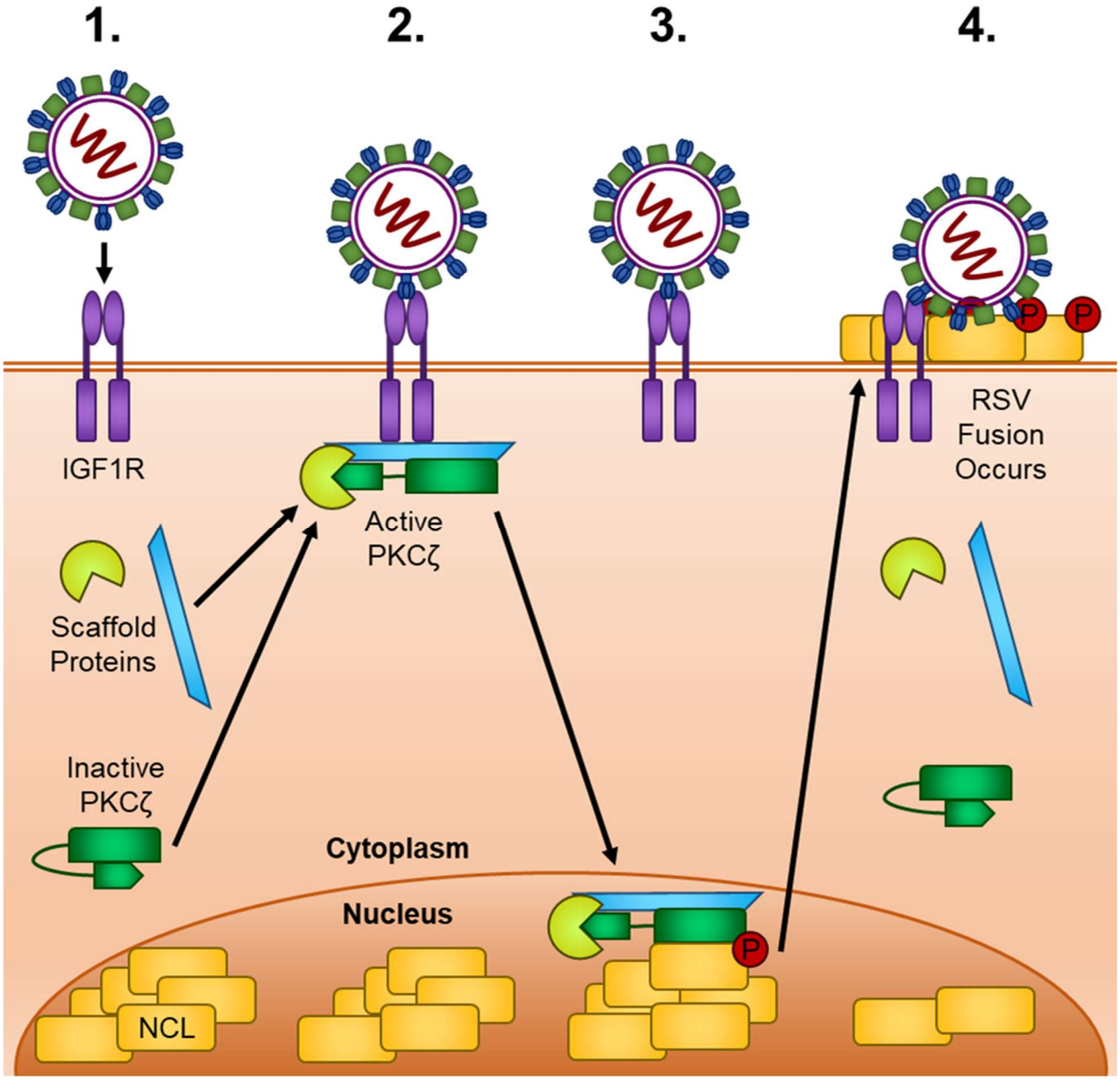

Figure 5.14 RSV receptor binding and recruitment schematic. 1. Before RSV binding, PKCζ is inactive, with the pseudosubstrate bound to the catalytic site. **2.** RSV binds to IGF1R on the cell surface, which causes scaffolding proteins to stabilize PKCζ in an active conformation. **3.** Active PKCζ translocates to the nucleus and phosphorylates NCL. **4.** Phosphorylated NCL traffics to the bound RSV particle and RSV enters the host cell. See **Figure 1.2** for possible RSV fusion mechanisms. Actin was not included in this model for simplicity.

In addition to being an RSV receptor, IGF1R may have further influence on RSV infection. For instance, the exogenous treatment of cells with IGF1 increased NCL surface expression and made cells more susceptible to RSV infection. This is important because alveolar macrophages secrete

IGF1 into the airway lumen when they sense the presence of IL-4, IL-13, or apoptotic cells[335]. Furthermore, IL-4 levels in children are correlated with severity of RSV infection[24] and RSV itself induces IL-13 secretion from infected bronchial epithelial cells[156]. This indicates that a positive feedback loop of IGF1 signaling may occur in infected lungs, where RSV infection induces IGF1 secretion, which subsequently enhances the susceptibility of uninfected cells to RSV infection.

5.3.7 Implications of IGF1R and PKCζ in cell surface NCL biology

When my findings are considered within a wider perspective, they have implications on basic cell biology. A recent study examining the PKCζ interactome[398] identified that the top three signaling pathways related to PKCζ are the EGF, fibroblast growth factor (FGF), and PDGF pathways. The VEGF signaling pathway was also identified as a major PKCζ related pathway. In support of PKCζ being a downstream effector of multiple growth factor pathways, stimulation by EGF[294], IGF1[295,296], insulin[297], VEGF[298], PDGF[299], or nerve growth factor (NGF)[192], can each cause PKCζ activation. Similarly, NCL phosphorylation is increased by stimulation with VEGF[194], NGF[192], or EGF and insulin together[195]. Coupled with the knowledge that IGF1, HDGF[229], or VEGF[194,227] stimulation each cause NCL surface trafficking, this opens the possibility that the translocation of NCL to the surface may be a general response to growth factor stimulation. If this is the case, it would point to scaffolding proteins that are shared between multiple growth factor receptors, such as 14-3-3 and RACK1, as likely effectors for my observed increase in PKCζ activity and NCL surface trafficking. It is also interesting to consider potential implications that the transfer of cell surface NCL, observed in **Chapter 3**, has on the induction of cell surface expression by RSV or growth factors. For instance, it is possible that the increased surface NCL on an RSV-infected cell could spread to neighboring cells and increase their susceptibility to infection.

Chapter 6: Summary and Future Directions

6.1 Summary

RSV is an important human pathogen that is a leading cause of infant hospitalization in North America[19]. Due to its prevalence and severity, RSV has been a priority for vaccine and antiviral development over the past decade[101]. However, our understanding of the RSV infection process is not yet complete. In particular, many questions remain regarding the mechanism RSV uses to enter host cells. Understanding this cell-entry mechanism is of great importance to ongoing vaccine efforts, since a primary goal of vaccination is to induce the production of antibodies that neutralize the virus and prevent entry[101]. In this thesis, I examined the interaction between RSV and a critical cell surface receptor, NCL. In the process of examining this interaction, I discovered a new RSV receptor that induces a signaling cascade needed for optimal viral entry. I also shed light on the mechanisms behind NCL cell surface expression.

In **Chapter 3**, I used a NCL-GFP overexpression model, with a series of truncation mutants, to test the domains of NCL involved in cell surface expression. Using this system, I observed that the NCL RRM and GAR domains are required for efficient expression of NCL on the cell surface. However, the AB domain has an opposing role that reduces cell surface expression when present, possibly by interacting with nuclear proteins. Unexpectedly, mutating the NCL NLS did not substantially alter cell surface expression. These findings give insight into the basic cell biology of NCL, by providing insight into potential protein-protein interactions or post-translational modifications involved in surface trafficking, based on what is already known about the interactions of NCL with other proteins. From a health-related perspective, protein-protein interactions or post-translational modifications that are identified in the future could translate into druggable targets to prevent cell surface expression of NCL. A targeted reduction of cell surface NCL would reduce susceptibility to RSV infection, along with several other pathogens that NCL serves as a receptor for. Cell surface NCL also plays a role in cancer progression, so therapeutic reduction of NCL surface expression could lead to new anti-cancer drugs. During the experiments in **Chapter 3**, I also discovered and characterized a novel process of intercellular cell surface NCL transfer. I found that NCL was freely transferred between the surface of cells in a cell contact-dependent manner. Although this intercellular transfer is an exciting new cell biological phenomenon, the full *in vivo* relevance of the finding is yet to be determined.

Chapter 4 investigates the nature of NCL as an RSV receptor. In particular, how NCL acts as a critical cell surface receptor when only expressed to low levels at the cell surface of a minority of cells. However, during RSV entry, I observed that NCL exited the nucleus and translocated to the cell surface, while total NCL protein and mRNA levels remained constant. Using microscopy to take a closer look at the interaction between cell surface NCL and RSV, I found that NCL accumulated around RSV particles prior to and during RSV fusion with the host cell plasma membrane. I then used imaging flow cytometry to quantify the patching of NCL around RSV particles and found that the maximum colocalization between RSV and NCL occurred 60 min after infection. The active translocation of NCL to the cell surface helps to reconcile how NCL acts as an RSV receptor on cells that normally express low levels of surface NCL and may provide insight into NCL as a cell surface receptor for other pathogens. The RSV-induced NCL transport also represents a novel concept in virology, where a virus directs its own receptor to the cell surface to trigger fusion.

After identifying the active translocation of NCL to viral particles on the cell surface, I examined the mechanism behind the process in **Chapter 5**. This was accomplished by first screening chemical inhibitors of cell surface receptors, cellular kinases, and cellular transport pathways for their effects on RSV entry. From examining the cell surface receptor inhibitors, I found that inhibiting IGF1R signaling blocked RSV entry, while inhibiting previously described RSV receptor signaling (EGFR, TLR4, or CX3CR1) had no effect. In agreement with the literature, inhibiting PI3K blocked RSV entry. The inhibitor screen also identified PKCζ and Ras as novel signaling factors that mediate RSV entry. Furthermore, actin, β-tubulin, and N-glycosylation were all found to be important cellular processes during RSV entry. After identifying these kinases and cellular processes that were important for RSV entry, I used imaging flow cytometry to examine if they played a role in the RSV-induced NCL translocation to viral particles, observed in **Chapter 4**. I found that both actin mobilization and PKCζ activity played a critical role in NCL translocation. I then used an *in vitro* PKCζ kinase assay, in combination with IGF1R inhibitors, to show that RSV-induced PKCζ activity was downstream of IGF1R and required actin mobilization.

IGF1R signaling activates PKCζ and together they play an important role in RSV entry. Since IGF1R has not been described as an RSV receptor previously, I next examined if it fulfilled the requirements of being a viral receptor. RSV-F bound to IGF1R, confirming that the interaction

between RSV and IGF1R was direct. Furthermore, RSV colocalized with IGF1R on the cell surface and caused IGF1R activation in the same timeframe as PKCζ activation. I then tested the role each component of the cascade played during RSV binding and fusion. Inhibiting or removing IGF1R, PKCζ, or NCL each reduced RSV binding to host cells and decreased the rate of fusion. To study this signaling cascade in the absence of RSV, I showed that IGF1 alone was capable of activating PKCζ and inducing cell surface translocation of NCL. Together, this work describes a novel mechanism where RSV usurps a host signaling cascade from IGF1R, through PKCζ, to call NCL to the cell surface for viral fusion to occur. Identifying this sequential signaling cascade opens new targets for therapeutic intervention against RSV infection, where each step in the cascade could potentially be targeted. This is of particular importance considering the large burden of disease posed by RSV infection and the lack of effective treatments against the virus.

6.2 Future Directions

One of the important questions yet to be fully answered is the mechanism NCL uses to reach the cell surface. NCL lacks a signal peptide and translocates to the cell surface in an unconventional manner, independent of the Golgi apparatus[220]. Furthermore, NCL is relatively large (110 kDa) and highly charged, meaning that it would require specialized proteins, such as a pore or ATP-binding cassette (ABC) transporter, to flip it across the plasma membrane, to the extracellular leaflet of the membrane[219]. However, if these flipping proteins exist, they are unlikely to normally reside on the plasma membrane since increasing the cytoplasmic expression of NCL (with the NLS reverse mutant in **Chapter 3**) doesn't increase surface expression. An approach that could provide insight into this problem would be to screen a large panel of inhibitors for cell trafficking proteins, using the NCL-GFP overexpression system that I developed, which provides a more robust readout of cell surface NCL, compared to measuring endogenous NCL. Another option would be to take a proteomic approach and compare proteins that interact with the NCL ΔAB and NCL ΔGAR mutant proteins. Although these two mutant proteins share the same structured central domain, they had opposite phenotypes for surface expression. Removal of the N-terminal AB domain in NCL enhanced cell surface expression, whereas removal of the C-terminal GAR domain abrogated cell surface expression. It is presumable that NCL ΔAB preferentially interacts with proteins involved in surface expression (via the GAR domain), while NCL ΔGAR interacts less with these proteins. Therefore, subtracting the NCL ΔGAR interacting proteins from the NCL ΔAB interactome should

enrich for proteins involved in surface trafficking. This approach may also provide insight into the mechanism NCL uses to tether to cells once on the cell surface.

An important method used to study the function of a protein or system is to knock it out and examine the phenotype. Since NCL is essential for cell survival[201,202], it cannot be completely knocked out of cells, which has made studying cell surface NCL difficult. To overcome this, it is possible to replace endogenous NCL with a mutant lacking three RRM domains using CRISPR-Cas9. Since the RRM domains are redundant to one another for cell survival[201], but important for NCL surface trafficking, this cell line would be viable and would not express surface NCL. One possible limitation to this cell line is that cells with only one NCL RRM grow very slowly[201]. As a compromise, a cell line lacking only two RRMs could be created. Once created, this cell line lacking surface NCL would be a perfect recipient cell line to answer functional questions about surface NCL that is swapped between cells, such as whether transferred NCL enhances cellular proliferation or susceptibility to RSV infection.

As an alternative to creating a cell surface NCL knockout cell line, using siRNA to knock down NCL could work to create recipient cells[128], albeit with a less complete phenotype. Previously it was shown that siRNA silencing of *NCL* depleted surface NCL levels while preserving critical nuclear levels of NCL protein that are required for cell survival[345]. Studying expressed NCL mutant constructs in cells where endogenous *NCL* has been silenced is therefore also a desirable strategy. However, RNA interference rarely results in 100% silencing of gene expression which could cause complication of mutant protein phenotypes by the remaining endogenous protein.

In regard to the RSV-induced PKCζ activation observed in **Chapter 5**, an important future direction will be to determine which scaffolding proteins stabilize PKCζ in an active conformation. To test this, proteins known to associate with PKCζ, such as p62[287,302], Par-6[286,287,303,304,387], IRS-1[287,305], 14-3-3[307,390] and RACK1[291] could be knocked down with siRNA and the resulting effects on RSV infection and NCL surface trafficking could be measured. PKCζ has been shown to enter the nucleus and phosphorylate NCL after NGF stimulation[192]. PKCζ itself has also been implicated in the surface expression of NCL[176]. However, the two processes have never been linked. In other words, is NCL phosphorylation actually necessary for its recruitment to the cell surface? If phosphorylation is indeed necessary, as I hypothesize that it is (**Figure 5.14**), it would be interesting to determine what residue is phosphorylated. Identifying the phosphorylated residue

could be accomplished using an *in vitro* PKCζ kinase assay with peptides derived from the NCL sequence as substrates. Since PKCζ phosphorylates NCL on a serine, this would narrow down the substrates to 26 serine residues with the RRM domains. The serine residues within the AB domain can be excluded since it is not necessary for surface expression and the GAR domain contains no serine residues. Once the phosphorylation site is identified, the NCL-GFP overexpression system could be used to test the surface expression of mutant proteins with phospho-dead and phospho-mimetic mutations at this site.

In **Chapter 5**, I identified IGF1R as a novel RSV receptor. An important future direction to follow this discovery would be to determine the regions of RSV-F and IGF1R that interact. I also observed that IGF1R is an upstream mediator of RSV-induced PKCζ activity. However, an interesting future direction would be to examine the upstream regulators for the other kinases activated during RSV entry. In other words, which cell surface receptors activate p38, ERK1/2, PI3K, and other PKC isoforms[123,142,143,147]? An obvious place to start would be to test the relative roles of known RSV receptors IGF1R, CXCR4, CX3CR1, TLR4, and EGFR in RSV-induced activation of these kinases. Though, it would be worthwhile to expand the examination to include more lipid-raft associated cell surface receptors. This investigation would elucidate if RSV has multiple active signaling receptors, what the role of each receptor is, and if there is any redundancy between receptors. An interesting possibility is that RSV engages different signaling receptors depending on the cell type being infected, since RSV also infects alveolar pneumocytes, epithelial cells in the lower respiratory tract, and nasal epithelial cells in the upper respiratory tract. In line with expanding upon our understanding of RSV-induced cellular signaling, it would also be interesting to follow up on the role Ras plays during RSV entry. As one of the top three hits during the kinase inhibitor screen, Ras plays an important role in efficient RSV entry. Therefore, it would be pertinent to study the upstream regulators and downstream effectors of Ras that are at play during RSV entry.

Works Cited

1 Griffiths, C., Drews, S. J. & Marchant, D. J. Respiratory Syncytial Virus: Infection, Detection, and New Options for Prevention and Treatment. *Clin Microbiol Rev* **30**, 277-319, doi:10.1128/CMR.00010-16 (2017).

2 Bilawchuk, L. M., Griffiths, C. D., Jensen, L. D., Elawar, F. & Marchant, D. J. The Susceptibilities of Respiratory Syncytial Virus to Nucleolin Receptor Blocking and Antibody Neutralization are Dependent upon the Method of Virus Purification. *Viruses* **9**, doi:10.3390/v9080207 (2017).

3 Blount, R. E., Jr., Morris, J. A. & Savage, R. E. Recovery of cytopathogenic agent from chimpanzees with coryza. *Proc Soc Exp Biol Med* **92**, 544-549 (1956).

4 Chanock, R., Roizman, B. & Myers, R. Recovery from infants with respiratory illness of a virus related to chimpanzee coryza agent (CCA). I. Isolation, properties and characterization. *Am J Hyg* **66**, 281-290 (1957).

5 Chanock, R. & Finberg, L. Recovery from infants with respiratory illness of a virus related to chimpanzee coryza agent (CCA). II. Epidemiologic aspects of infection in infants and young children. *Am J Hyg* **66**, 291-300, doi:10.1093/oxfordjournals.aje.a119902 (1957).

6 Falsey, A. R., Hennessey, P. A., Formica, M. A., Cox, C. & Walsh, E. E. Respiratory syncytial virus infection in elderly and high-risk adults. *N Engl J Med* **352**, 1749-1759, doi:10.1056/NEJMoa043951 (2005).

7 Morales, F., Calder, M. A., Inglis, J. M., Murdoch, P. S. & Williamson, J. A study of respiratory infections in the elderly to assess the role of respiratory syncytial virus. *J Infect* **7**, 236-247 (1983).

8 Chatzis, O., Darbre, S., Pasquier, J., Meylan, P., Manuel, O., Aubert, J. D., Beck-Popovic, M., Masouridi-Levrat, S., Ansari, M., Kaiser, L., Posfay-Barbe, K. M. & Asner, S. A. Burden of severe RSV disease among immunocompromised children and adults: a 10 year retrospective study. *BMC Infect Dis* **18**, 111, doi:10.1186/s12879-018-3002-3 (2018).

9 Neilson, K. A. & Yunis, E. J. Demonstration of respiratory syncytial virus in an autopsy series. *Pediatr Pathol* **10**, 491-502, doi:10.3109/15513819009067138 (1990).

10 *Virus Taxonomy: 2018b Release*, <https://talk.ictvonline.org/taxonomy/> (2018).

11 Mufson, M. A., Orvell, C., Rafnar, B. & Norrby, E. Two distinct subtypes of human respiratory syncytial virus. *J Gen Virol* **66 (Pt 10)**, 2111-2124, doi:10.1099/0022-1317-66-10-2111 (1985).

12 Anderson, L. J., Hierholzer, J. C., Tsou, C., Hendry, R. M., Fernie, B. F., Stone, Y. & McIntosh, K. Antigenic characterization of respiratory syncytial virus strains with monoclonal antibodies. *J Infect Dis* **151**, 626-633 (1985).

13 Eshaghi, A., Duvvuri, V. R., Lai, R., Nadarajah, J. T., Li, A., Patel, S. N., Low, D. E. & Gubbay, J. B. Genetic variability of human respiratory syncytial virus A strains circulating in Ontario: a novel genotype with a 72 nucleotide G gene duplication. *PLoS One* **7**, e32807, doi:10.1371/journal.pone.0032807 (2012).

14 Hall, C. B., Walsh, E. E., Schnabel, K. C., Long, C. E., McConnochie, K. M., Hildreth, S. W. & Anderson, L. J. Occurrence of groups A and B of respiratory syncytial virus over 15 years: associated epidemiologic and clinical characteristics in hospitalized and ambulatory children. *J Infect Dis* **162**, 1283-1290, doi:10.1093/infdis/162.6.1283 (1990).

15 Kim, Y. I., Murphy, R., Majumdar, S., Harrison, L. G., Aitken, J. & DeVincenzo, J. P. Relating plaque morphology to respiratory syncytial virus subgroup, viral load, and disease severity in children. *Pediatr Res* **78**, 380-388, doi:10.1038/pr.2015.122 (2015).
16 Glezen, W. P., Taber, L. H., Frank, A. L. & Kasel, J. A. Risk of primary infection and reinfection with respiratory syncytial virus. *Am J Dis Child* **140**, 543-546, doi:10.1001/archpedi.1986.02140200053026 (1986).
17 Hall, C. B., Walsh, E. E., Long, C. E. & Schnabel, K. C. Immunity to and frequency of reinfection with respiratory syncytial virus. *J Infect Dis* **163**, 693-698 (1991).
18 Xiang, Z., Gonzalez, R., Ren, L., Xiao, Y., Chen, L., Zhang, J., Wang, W., Yang, Q., Li, J., Zhou, H., Vernet, G., Paranhos-Baccala, G., Wang, Z. & Wang, J. Prevalence and clinical characteristics of human respiratory syncytial virus in Chinese adults with acute respiratory tract infection. *J Med Virol* **85**, 348-353, doi:10.1002/jmv.23467 (2013).
19 Hall, C. B., Weinberg, G. A., Iwane, M. K., Blumkin, A. K., Edwards, K. M., Staat, M. A., Auinger, P., Griffin, M. R., Poehling, K. A., Erdman, D., Grijalva, C. G., Zhu, Y. & Szilagyi, P. The burden of respiratory syncytial virus infection in young children. *N Engl J Med* **360**, 588-598, doi:10.1056/NEJMoa0804877 (2009).
20 Hislop, A. A. Airway and blood vessel interaction during lung development. *J Anat* **201**, 325-334, doi:10.1046/j.1469-7580.2002.00097.x (2002).
21 Aherne, W., Bird, T., Court, S. D., Gardner, P. S. & McQuillin, J. Pathological changes in virus infections of the lower respiratory tract in children. *J Clin Pathol* **23**, 7-18, doi:10.1136/jcp.23.1.7 (1970).
22 Johnson, J. E., Gonzales, R. A., Olson, S. J., Wright, P. F. & Graham, B. S. The histopathology of fatal untreated human respiratory syncytial virus infection. *Mod Pathol* **20**, 108-119, doi:10.1038/modpathol.3800725 (2007).
23 Welliver, T. P., Reed, J. L. & Welliver, R. C., Sr. Respiratory syncytial virus and influenza virus infections: observations from tissues of fatal infant cases. *Pediatr Infect Dis J* **27**, S92-96, doi:10.1097/INF.0b013e318168b706 (2008).
24 Caballero, M. T., Serra, M. E., Acosta, P. L., Marzec, J., Gibbons, L., Salim, M., Rodriguez, A., Reynaldi, A., Garcia, A., Bado, D., Buchholz, U. J., Hijano, D. R., Coviello, S., Newcomb, D., Bellabarba, M., Ferolla, F. M., Libster, R., Berenstein, A., Siniawaski, S., Blumetti, V., Echavarria, M., Pinto, L., Lawrence, A., Ossorio, M. F., Grosman, A., Mateu, C. G., Bayle, C., Dericco, A., Pellegrini, M., Igarza, I., Repetto, H. A., Grimaldi, L. A., Gudapati, P., Polack, N. R., Althabe, F., Shi, M., Ferrero, F., Bergel, E., Stein, R. T., Peebles, R. S., Boothby, M., Kleeberger, S. R. & Polack, F. P. TLR4 genotype and environmental LPS mediate RSV bronchiolitis through Th2 polarization. *J Clin Invest* **125**, 571-582, doi:10.1172/JCI75183 (2015).
25 Cilla, G., Sarasua, A., Montes, M., Arostegui, N., Vicente, D., Perez-Yarza, E. & Perez-Trallero, E. Risk factors for hospitalization due to respiratory syncytial virus infection among infants in the Basque Country, Spain. *Epidemiol Infect* **134**, 506-513, doi:10.1017/S0950268805005571 (2006).
26 Okiro, E. A., Ngama, M., Bett, A., Cane, P. A., Medley, G. F. & James Nokes, D. Factors associated with increased risk of progression to respiratory syncytial virus-associated pneumonia in young Kenyan children. *Trop Med Int Health* **13**, 914-926, doi:10.1111/j.1365-3156.2008.02092.x (2008).
27 Weber, M. W., Milligan, P., Hilton, S., Lahai, G., Whittle, H., Mulholland, E. K. & Greenwood, B. M. Risk factors for severe respiratory syncytial virus infection leading to

hospital admission in children in the Western Region of The Gambia. *Int J Epidemiol* **28**, 157-162, doi:10.1093/ije/28.1.157 (1999).

28 Wu, A., Budge, P. J., Williams, J., Griffin, M. R., Edwards, K. M., Johnson, M., Zhu, Y., Hartinger, S., Verastegui, H., Gil, A. I., Lanata, C. F. & Grijalva, C. G. Incidence and Risk Factors for Respiratory Syncytial Virus and Human Metapneumovirus Infections among Children in the Remote Highlands of Peru. *PLoS One* **10**, e0130233, doi:10.1371/journal.pone.0130233 (2015).

29 Thorburn, K. Pre-existing disease is associated with a significantly higher risk of death in severe respiratory syncytial virus infection. *Arch Dis Child* **94**, 99-103, doi:10.1136/adc.2008.139188 (2009).

30 Falsey, A. R., McElhaney, J. E., Beran, J., van Essen, G. A., Duval, X., Esen, M., Galtier, F., Gervais, P., Hwang, S. J., Kremsner, P., Launay, O., Leroux-Roels, G., McNeil, S. A., Nowakowski, A., Richardus, J. H., Ruiz-Palacios, G., St Rose, S., Devaster, J. M., Oostvogels, L., Durviaux, S. & Taylor, S. Respiratory syncytial virus and other respiratory viral infections in older adults with moderate to severe influenza-like illness. *J Infect Dis* **209**, 1873-1881, doi:10.1093/infdis/jit839 (2014).

31 Falsey, A. R. & Walsh, E. E. Relationship of serum antibody to risk of respiratory syncytial virus infection in elderly adults. *J Infect Dis* **177**, 463-466, doi:10.1086/517376 (1998).

32 Walsh, E. E. & Falsey, A. R. Humoral and mucosal immunity in protection from natural respiratory syncytial virus infection in adults. *J Infect Dis* **190**, 373-378, doi:10.1086/421524 (2004).

33 Li, Y., Reeves, R. M., Wang, X., Bassat, Q., Brooks, W. A., Cohen, C., Moore, D. P., Nunes, M., Rath, B., Campbell, H., Nair, H., Network, R. S. V. G. E. & investigators, R. Global patterns in monthly activity of influenza virus, respiratory syncytial virus, parainfluenza virus, and metapneumovirus: a systematic analysis. *Lancet Glob Health* **7**, e1031-e1045, doi:10.1016/S2214-109X(19)30264-5 (2019).

34 Broor, S., Campbell, H., Hirve, S., Hague, S., Jackson, S., Moen, A., Nair, H., Palekar, R., Rajatonirina, S., Smith, P. G., Venter, M., Wairagkar, N., Zambon, M., Ziegler, T. & Zhang, W. Leveraging the Global Influenza Surveillance and Response System for global respiratory syncytial virus surveillance-opportunities and challenges. *Influenza Other Respir Viruses*, doi:10.1111/irv.12672 (2019).

35 Foxman, E. F., Storer, J. A., Fitzgerald, M. E., Wasik, B. R., Hou, L., Zhao, H., Turner, P. E., Pyle, A. M. & Iwasaki, A. Temperature-dependent innate defense against the common cold virus limits viral replication at warm temperature in mouse airway cells. *Proc Natl Acad Sci U S A* **112**, 827-832, doi:10.1073/pnas.1411030112 (2015).

36 Hall, C. B., Douglas, R. G., Jr. & Geiman, J. M. Possible transmission by fomites of respiratory syncytial virus. *J Infect Dis* **141**, 98-102 (1980).

37 Kulkarni, H., Smith, C. M., Lee Ddo, H., Hirst, R. A., Easton, A. J. & O'Callaghan, C. Evidence of Respiratory Syncytial Virus Spread by Aerosol. Time to Revisit Infection Control Strategies? *Am J Respir Crit Care Med* **194**, 308-316, doi:10.1164/rccm.201509-1833OC (2016).

38 Bennett, C. R., Jr. & Hamre, D. Growth and serological characteristics of respiratory syncytial virus. *J Infect Dis* **110**, 8-16, doi:10.1093/infdis/110.1.8 (1962).

39 Hall, C. B., Douglas, R. G., Jr., Schnabel, K. C. & Geiman, J. M. Infectivity of respiratory syncytial virus by various routes of inoculation. *Infect Immun* **33**, 779-783 (1981).

40 Liesman, R. M., Buchholz, U. J., Luongo, C. L., Yang, L., Proia, A. D., DeVincenzo, J. P., Collins, P. L. & Pickles, R. J. RSV-encoded NS2 promotes epithelial cell shedding and distal airway obstruction. *J Clin Invest* **124**, 2219-2233, doi:10.1172/JCI72948 (2014).

41 Yu, C. P. & Diu, C. K. Total and Regional Deposition of Inhaled Aerosols in Humans. *J Aerosol Sci* **14**, 599-609, doi:Doi 10.1016/0021-8502(83)90065-4 (1983).

42 Leader, S. & Kohlhase, K. Recent trends in severe respiratory syncytial virus (RSV) among US infants, 1997 to 2000. *J Pediatr* **143**, S127-132, doi:10.1067/s0022-3476(03)00510-9 (2003).

43 Shi, T., McAllister, D. A., O'Brien, K. L., Simoes, E. A. F., Madhi, S. A., Gessner, B. D., Polack, F. P., Balsells, E., Acacio, S., Aguayo, C., Alassani, I., Ali, A., Antonio, M., Awasthi, S., Awori, J. O., Azziz-Baumgartner, E., Baggett, H. C., Baillie, V. L., Balmaseda, A., Barahona, A., Basnet, S., Bassat, Q., Basualdo, W., Bigogo, G., Bont, L., Breiman, R. F., Brooks, W. A., Broor, S., Bruce, N., Bruden, D., Buchy, P., Campbell, S., Carosone-Link, P., Chadha, M., Chipeta, J., Chou, M., Clara, W., Cohen, C., de Cuellar, E., Dang, D. A., Dash-Yandag, B., Deloria-Knoll, M., Dherani, M., Eap, T., Ebruke, B. E., Echavarria, M., de Freitas Lazaro Emediato, C. C., Fasce, R. A., Feikin, D. R., Feng, L., Gentile, A., Gordon, A., Goswami, D., Goyet, S., Groome, M., Halasa, N., Hirve, S., Homaira, N., Howie, S. R. C., Jara, J., Jroundi, I., Kartasasmita, C. B., Khuri-Bulos, N., Kotloff, K. L., Krishnan, A., Libster, R., Lopez, O., Lucero, M. G., Lucion, F., Lupisan, S. P., Marcone, D. N., McCracken, J. P., Mejia, M., Moisi, J. C., Montgomery, J. M., Moore, D. P., Moraleda, C., Moyes, J., Munywoki, P., Mutyara, K., Nicol, M. P., Nokes, D. J., Nymadawa, P., da Costa Oliveira, M. T., Oshitani, H., Pandey, N., Paranhos-Baccala, G., Phillips, L. N., Picot, V. S., Rahman, M., Rakoto-Andrianarivelo, M., Rasmussen, Z. A., Rath, B. A., Robinson, A., Romero, C., Russomando, G., Salimi, V., Sawatwong, P., Scheltema, N., Schweiger, B., Scott, J. A. G., Seidenberg, P., Shen, K., Singleton, R., Sotomayor, V., Strand, T. A., Sutanto, A., Sylla, M., Tapia, M. D., Thamthitiwat, S., Thomas, E. D., Tokarz, R., Turner, C., Venter, M., Waicharoen, S., Wang, J., Watthanaworawit, W., Yoshida, L. M., Yu, H., Zar, H. J., Campbell, H., Nair, H. & Network, R. S. V. G. E. Global, regional, and national disease burden estimates of acute lower respiratory infections due to respiratory syncytial virus in young children in 2015: a systematic review and modelling study. *Lancet* **390**, 946-958, doi:10.1016/S0140-6736(17)30938-8 (2017).

44 Langley, J. M., Wang, E. E., Law, B. J., Stephens, D., Boucher, F. D., Dobson, S., McDonald, J., MacDonald, N. E., Mitchell, I. & Robinson, J. L. Economic evaluation of respiratory syncytial virus infection in Canadian children: a Pediatric Investigators Collaborative Network on Infections in Canada (PICNIC) study. *J Pediatr* **131**, 113-117, doi:10.1016/s0022-3476(97)70133-1 (1997).

45 Paramore, L. C., Ciuryla, V., Ciesla, G. & Liu, L. Economic impact of respiratory syncytial virus-related illness in the US: an analysis of national databases. *Pharmacoeconomics* **22**, 275-284, doi:10.2165/00019053-200422050-00001 (2004).

46 Shi, T., Denouel, A., Tietjen, A. K., Campbell, I., Moran, E., Li, X., Campbell, H., Demont, C., Nyawanda, B. O., Chu, H. Y., Stoszek, S. K., Krishnan, A., Openshaw, P., Falsey, A. R., Nair, H. & Investigators, R. Global Disease Burden Estimates of Respiratory Syncytial Virus-Associated Acute Respiratory Infection in Older Adults in 2015: A Systematic Review and Meta-Analysis. *J Infect Dis*, doi:10.1093/infdis/jiz059 (2019).

47 Shi, T., Ooi, Y., Zaw, E. M., Utjesanovic, N., Campbell, H., Cunningham, S., Bont, L., Nair, H. & Investigators, R. Association Between Respiratory Syncytial Virus-Associated Acute Lower Respiratory Infection in Early Life and Recurrent Wheeze and Asthma in Later Childhood. *J Infect Dis*, doi:10.1093/infdis/jiz311 (2019).

48 Korppi, M., Piippo-Savolainen, E., Korhonen, K. & Remes, S. Respiratory morbidity 20 years after RSV infection in infancy. *Pediatr Pulmonol* **38**, 155-160, doi:10.1002/ppul.20058 (2004).

49 Sigurs, N., Aljassim, F., Kjellman, B., Robinson, P. D., Sigurbergsson, F., Bjarnason, R. & Gustafsson, P. M. Asthma and allergy patterns over 18 years after severe RSV bronchiolitis in the first year of life. *Thorax* **65**, 1045-1052, doi:10.1136/thx.2009.121582 (2010).

50 Stein, R. T., Sherrill, D., Morgan, W. J., Holberg, C. J., Halonen, M., Taussig, L. M., Wright, A. L. & Martinez, F. D. Respiratory syncytial virus in early life and risk of wheeze and allergy by age 13 years. *Lancet* **354**, 541-545, doi:10.1016/S0140-6736(98)10321-5 (1999).

51 Hirsch, H. H., Martino, R., Ward, K. N., Boeckh, M., Einsele, H. & Ljungman, P. Fourth European Conference on Infections in Leukaemia (ECIL-4): guidelines for diagnosis and treatment of human respiratory syncytial virus, parainfluenza virus, metapneumovirus, rhinovirus, and coronavirus. *Clin Infect Dis* **56**, 258-266, doi:10.1093/cid/cis844 (2013).

52 Saez-Llorens, X., Castano, E., Null, D., Steichen, J., Sanchez, P. J., Ramilo, O., Top, F. H., Jr. & Connor, E. Safety and pharmacokinetics of an intramuscular humanized monoclonal antibody to respiratory syncytial virus in premature infants and infants with bronchopulmonary dysplasia. The MEDI-493 Study Group. *Pediatr Infect Dis J* **17**, 787-791, doi:10.1097/00006454-199809000-00007 (1998).

53 Palivizumab, a Humanized Respiratory Syncytial Virus Monoclonal Antibody, Reduces Hospitalization From Respiratory Syncytial Virus Infection in High-risk Infants. *Pediatrics* **102**, 531-537 (1998).

54 Hampp, C., Kauf, T. L., Saidi, A. S. & Winterstein, A. G. Cost-effectiveness of respiratory syncytial virus prophylaxis in various indications. *Arch Pediatr Adolesc Med* **165**, 498-505, doi:10.1001/archpediatrics.2010.298 (2011).

55 American Academy of Pediatrics Committee on Infectious, D. & American Academy of Pediatrics Bronchiolitis Guidelines, C. Updated guidance for palivizumab prophylaxis among infants and young children at increased risk of hospitalization for respiratory syncytial virus infection. *Pediatrics* **134**, 415-420, doi:10.1542/peds.2014-1665 (2014).

56 Blanken, M. O., Rovers, M. M., Molenaar, J. M., Winkler-Seinstra, P. L., Meijer, A., Kimpen, J. L., Bont, L. & Dutch, R. S. V. N. N. Respiratory syncytial virus and recurrent wheeze in healthy preterm infants. *N Engl J Med* **368**, 1791-1799, doi:10.1056/NEJMoa1211917 (2013).

57 Simoes, E. A. F., Bont, L., Manzoni, P., Fauroux, B., Paes, B., Figueras-Aloy, J., Checchia, P. A. & Carbonell-Estrany, X. Past, Present and Future Approaches to the Prevention and Treatment of Respiratory Syncytial Virus Infection in Children. *Infect Dis Ther* **7**, 87-120, doi:10.1007/s40121-018-0188-z (2018).

58 *RSV Vaccine and mAb Snapshot*, <https://path.org/resources/rsv-vaccine-and-mab-snapshot/> (2019).

59 McLellan, J. S., Chen, M., Joyce, M. G., Sastry, M., Stewart-Jones, G. B., Yang, Y., Zhang, B., Chen, L., Srivatsan, S., Zheng, A., Zhou, T., Graepel, K. W., Kumar, A., Moin, S.,

Boyington, J. C., Chuang, G. Y., Soto, C., Baxa, U., Bakker, A. Q., Spits, H., Beaumont, T., Zheng, Z., Xia, N., Ko, S. Y., Todd, J. P., Rao, S., Graham, B. S. & Kwong, P. D. Structure-based design of a fusion glycoprotein vaccine for respiratory syncytial virus. *Science* **342**, 592-598, doi:10.1126/science.1243283 (2013).

60 Fields, B. N., Knipe, D. M. & Howley, P. M. *Fields virology*. 6th edn, (Wolters Kluwer Health/Lippincott Williams & Wilkins, 2013).

61 Samal, S. K. & Collins, P. L. RNA replication by a respiratory syncytial virus RNA analog does not obey the rule of six and retains a nonviral trinucleotide extension at the leader end. *J Virol* **70**, 5075-5082 (1996).

62 Liljeroos, L., Krzyzaniak, M. A., Helenius, A. & Butcher, S. J. Architecture of respiratory syncytial virus revealed by electron cryotomography. *Proc Natl Acad Sci U S A* **110**, 11133-11138, doi:10.1073/pnas.1309070110 (2013).

63 Kiss, G., Holl, J. M., Williams, G. M., Alonas, E., Vanover, D., Lifland, A. W., Gudheti, M., Guerrero-Ferreira, R. C., Nair, V., Yi, H., Graham, B. S., Santangelo, P. J. & Wright, E. R. Structural analysis of respiratory syncytial virus reveals the position of M2-1 between the matrix protein and the ribonucleoprotein complex. *J Virol* **88**, 7602-7617, doi:10.1128/JVI.00256-14 (2014).

64 Alonas, E., Lifland, A. W., Gudheti, M., Vanover, D., Jung, J., Zurla, C., Kirschman, J., Fiore, V. F., Douglas, A., Barker, T. H., Yi, H., Wright, E. R., Crowe, J. E., Jr. & Santangelo, P. J. Combining single RNA sensitive probes with subdiffraction-limited and live-cell imaging enables the characterization of virus dynamics in cells. *ACS Nano* **8**, 302-315, doi:10.1021/nn405998v (2014).

65 San-Juan-Vergara, H., Sampayo-Escobar, V., Reyes, N., Cha, B., Pacheco-Lugo, L., Wong, T., Peeples, M. E., Collins, P. L., Castano, M. E. & Mohapatra, S. S. Cholesterol-rich microdomains as docking platforms for respiratory syncytial virus in normal human bronchial epithelial cells. *J Virol* **86**, 1832-1843, doi:10.1128/JVI.06274-11 (2012).

66 Zheng, L. L., Yang, X. X., Liu, Y., Wan, X. Y., Wu, W. B., Wang, T. T., Wang, Q., Zhen, S. J. & Huang, C. Z. In situ labelling chemistry of respiratory syncytial viruses by employing the biotinylated host-cell membrane protein for tracking the early stage of virus entry. *Chem Commun (Camb)* **50**, 15776-15779, doi:10.1039/c4cc06264g (2014).

67 Ke, Z., Dillard, R. S., Chirkova, T., Leon, F., Stobart, C. C., Hampton, C. M., Strauss, J. D., Rajan, D., Rostad, C. A., Taylor, J. V., Yi, H., Shah, R., Jin, M., Hartert, T. V., Peebles, R. S., Jr., Graham, B. S., Moore, M. L., Anderson, L. J. & Wright, E. R. The Morphology and Assembly of Respiratory Syncytial Virus Revealed by Cryo-Electron Tomography. *Viruses* **10**, doi:10.3390/v10080446 (2018).

68 Karron, R. A., Buonagurio, D. A., Georgiu, A. F., Whitehead, S. S., Adamus, J. E., Clements-Mann, M. L., Harris, D. O., Randolph, V. B., Udem, S. A., Murphy, B. R. & Sidhu, M. S. Respiratory syncytial virus (RSV) SH and G proteins are not essential for viral replication in vitro: clinical evaluation and molecular characterization of a cold-passaged, attenuated RSV subgroup B mutant. *Proc Natl Acad Sci U S A* **94**, 13961-13966 (1997).

69 Techaarpornkul, S., Barretto, N. & Peeples, M. E. Functional analysis of recombinant respiratory syncytial virus deletion mutants lacking the small hydrophobic and/or attachment glycoprotein gene. *J Virol* **75**, 6825-6834, doi:10.1128/JVI.75.15.6825-6834.2001 (2001).

70 Gan, S. W., Tan, E., Lin, X., Yu, D., Wang, J., Tan, G. M., Vararattanavech, A., Yeo, C. Y., Soon, C. H., Soong, T. W., Pervushin, K. & Torres, J. The small hydrophobic protein of the human respiratory syncytial virus forms pentameric ion channels. *J Biol Chem* **287**, 24671-24689, doi:10.1074/jbc.M111.332791 (2012).

71 Mitra, R., Baviskar, P., Duncan-Decocq, R. R., Patel, D. & Oomens, A. G. The human respiratory syncytial virus matrix protein is required for maturation of viral filaments. *J Virol* **86**, 4432-4443, doi:10.1128/JVI.06744-11 (2012).

72 Tawar, R. G., Duquerroy, S., Vonrhein, C., Varela, P. F., Damier-Piolle, L., Castagne, N., MacLellan, K., Bedouelle, H., Bricogne, G., Bhella, D., Eleouet, J. F. & Rey, F. A. Crystal structure of a nucleocapsid-like nucleoprotein-RNA complex of respiratory syncytial virus. *Science* **326**, 1279-1283, doi:10.1126/science.1177634 (2009).

73 Cowton, V. M. & Fearns, R. Evidence that the respiratory syncytial virus polymerase is recruited to nucleotides 1 to 11 at the 3' end of the nucleocapsid and can scan to access internal signals. *J Virol* **79**, 11311-11322, doi:10.1128/JVI.79.17.11311-11322.2005 (2005).

74 Fearns, R., Peeples, M. E. & Collins, P. L. Mapping the transcription and replication promoters of respiratory syncytial virus. *J Virol* **76**, 1663-1672, doi:10.1128/jvi.76.4.1663-1672.2002 (2002).

75 Gilman, M. S. A., Liu, C., Fung, A., Behera, I., Jordan, P., Rigaux, P., Ysebaert, N., Tcherniuk, S., Sourimant, J., Eleouet, J. F., Sutto-Ortiz, P., Decroly, E., Roymans, D., Jin, Z. & McLellan, J. S. Structure of the Respiratory Syncytial Virus Polymerase Complex. *Cell* **179**, 193-204 e114, doi:10.1016/j.cell.2019.08.014 (2019).

76 Collins, P. L., Hill, M. G., Cristina, J. & Grosfeld, H. Transcription elongation factor of respiratory syncytial virus, a nonsegmented negative-strand RNA virus. *Proc Natl Acad Sci U S A* **93**, 81-85 (1996).

77 Bermingham, A. & Collins, P. L. The M2-2 protein of human respiratory syncytial virus is a regulatory factor involved in the balance between RNA replication and transcription. *Proc Natl Acad Sci U S A* **96**, 11259-11264, doi:10.1073/pnas.96.20.11259 (1999).

78 Sedeyn, K., Schepens, B. & Saelens, X. Respiratory syncytial virus nonstructural proteins 1 and 2: Exceptional disrupters of innate immune responses. *PLoS Pathog* **15**, e1007984, doi:10.1371/journal.ppat.1007984 (2019).

79 Chatterjee, S., Luthra, P., Esaulova, E., Agapov, E., Yen, B. C., Borek, D. M., Edwards, M. R., Mittal, A., Jordan, D. S., Ramanan, P., Moore, M. L., Pappu, R. V., Holtzman, M. J., Artyomov, M. N., Basler, C. F., Amarasinghe, G. K. & Leung, D. W. Structural basis for human respiratory syncytial virus NS1-mediated modulation of host responses. *Nat Microbiol* **2**, 17101, doi:10.1038/nmicrobiol.2017.101 (2017).

80 McDonald, T. P., Pitt, A. R., Brown, G., Rixon, H. W. & Sugrue, R. J. Evidence that the respiratory syncytial virus polymerase complex associates with lipid rafts in virus-infected cells: a proteomic analysis. *Virology* **330**, 147-157, doi:10.1016/j.virol.2004.09.034 (2004).

81 Munday, D. C., Wu, W., Smith, N., Fix, J., Noton, S. L., Galloux, M., Touzelet, O., Armstrong, S. D., Dawson, J. M., Aljabr, W., Easton, A. J., Rameix-Welti, M. A., de Oliveira, A. P., Simabuco, F. M., Ventura, A. M., Hughes, D. J., Barr, J. N., Fearns, R., Digard, P., Eleouet, J. F. & Hiscox, J. A. Interactome analysis of the human respiratory syncytial virus RNA polymerase complex identifies protein chaperones as important

cofactors that promote L-protein stability and RNA synthesis. *J Virol* **89**, 917-930, doi:10.1128/JVI.01783-14 (2015).

82 Radhakrishnan, A., Yeo, D., Brown, G., Myaing, M. Z., Iyer, L. R., Fleck, R., Tan, B. H., Aitken, J., Sanmun, D., Tang, K., Yarwood, A., Brink, J. & Sugrue, R. J. Protein analysis of purified respiratory syncytial virus particles reveals an important role for heat shock protein 90 in virus particle assembly. *Mol Cell Proteomics* **9**, 1829-1848, doi:10.1074/mcp.M110.001651 (2010).

83 Boyer, J. C. & Haenni, A. L. Infectious transcripts and cDNA clones of RNA viruses. *Virology* **198**, 415-426, doi:10.1006/viro.1994.1053 (1994).

84 McGivern, D. R., Collins, P. L. & Fearns, R. Identification of internal sequences in the 3' leader region of human respiratory syncytial virus that enhance transcription and confer replication processivity. *J Virol* **79**, 2449-2460, doi:10.1128/JVI.79.4.2449-2460.2005 (2005).

85 Hanley, L. L., McGivern, D. R., Teng, M. N., Djang, R., Collins, P. L. & Fearns, R. Roles of the respiratory syncytial virus trailer region: effects of mutations on genome production and stress granule formation. *Virology* **406**, 241-252, doi:10.1016/j.virol.2010.07.006 (2010).

86 Fearns, R., Collins, P. L. & Peeples, M. E. Functional analysis of the genomic and antigenomic promoters of human respiratory syncytial virus. *J Virol* **74**, 6006-6014, doi:10.1128/jvi.74.13.6006-6014.2000 (2000).

87 Dickens, L. E., Collins, P. L. & Wertz, G. W. Transcriptional mapping of human respiratory syncytial virus. *J Virol* **52**, 364-369 (1984).

88 Kuo, L., Grosfeld, H., Cristina, J., Hill, M. G. & Collins, P. L. Effects of mutations in the gene-start and gene-end sequence motifs on transcription of monocistronic and dicistronic minigenomes of respiratory syncytial virus. *J Virol* **70**, 6892-6901 (1996).

89 Drake, J. W. Rates of spontaneous mutation among RNA viruses. *Proc Natl Acad Sci U S A* **90**, 4171-4175 (1993).

90 Levine, S. & Hamilton, R. Kinetics of the respiratory syncytial virus growth cycle in HeLa cells. *Arch Gesamte Virusforsch* **28**, 122-132, doi:10.1007/bf01249378 (1969).

91 Zheng, X., Gao, L., Wang, L., Liang, C., Wang, B., Liu, Y., Feng, S., Zhang, B., Zhou, M., Yu, X., Xiang, K., Chen, L., Guo, T., Shen, H. C., Zou, G., Wu, J. Z. & Yun, H. Discovery of Ziresovir as a Potent, Selective, and Orally Bioavailable Respiratory Syncytial Virus Fusion Protein Inhibitor. *J Med Chem* **62**, 6003-6014, doi:10.1021/acs.jmedchem.9b00654 (2019).

92 Battles, M. B., Langedijk, J. P., Furmanova-Hollenstein, P., Chaiwatpongsakorn, S., Costello, H. M., Kwanten, L., Vranckx, L., Vink, P., Jaensch, S., Jonckers, T. H., Koul, A., Arnoult, E., Peeples, M. E., Roymans, D. & McLellan, J. S. Molecular mechanism of respiratory syncytial virus fusion inhibitors. *Nat Chem Biol* **12**, 87-93, doi:10.1038/nchembio.1982 (2016).

93 Collins, P. L., Huang, Y. T. & Wertz, G. W. Nucleotide sequence of the gene encoding the fusion (F) glycoprotein of human respiratory syncytial virus. *Proc Natl Acad Sci U S A* **81**, 7683-7687, doi:10.1073/pnas.81.24.7683 (1984).

94 Zimmer, G., Budz, L. & Herrler, G. Proteolytic activation of respiratory syncytial virus fusion protein. Cleavage at two furin consensus sequences. *J Biol Chem* **276**, 31642-31650, doi:10.1074/jbc.M102633200 (2001).

95 Day, N. D., Branigan, P. J., Liu, C., Gutshall, L. L., Luo, J., Melero, J. A., Sarisky, R. T. & Del Vecchio, A. M. Contribution of cysteine residues in the extracellular domain of the F protein of human respiratory syncytial virus to its function. *Virol J* **3**, 34, doi:10.1186/1743-422X-3-34 (2006).
96 McLellan, J. S., Chen, M., Leung, S., Graepel, K. W., Du, X., Yang, Y., Zhou, T., Baxa, U., Yasuda, E., Beaumont, T., Kumar, A., Modjarrad, K., Zheng, Z., Zhao, M., Xia, N., Kwong, P. D. & Graham, B. S. Structure of RSV fusion glycoprotein trimer bound to a prefusion-specific neutralizing antibody. *Science* **340**, 1113-1117, doi:10.1126/science.1234914 (2013).
97 McLellan, J. S., Yang, Y., Graham, B. S. & Kwong, P. D. Structure of respiratory syncytial virus fusion glycoprotein in the postfusion conformation reveals preservation of neutralizing epitopes. *J Virol* **85**, 7788-7796, doi:10.1128/JVI.00555-11 (2011).
98 Kahn, J. S., Schnell, M. J., Buonocore, L. & Rose, J. K. Recombinant vesicular stomatitis virus expressing respiratory syncytial virus (RSV) glycoproteins: RSV fusion protein can mediate infection and cell fusion. *Virology* **254**, 81-91, doi:10.1006/viro.1998.9535 (1999).
99 Helm, C. A., Israelachvili, J. N. & McGuiggan, P. M. Molecular mechanisms and forces involved in the adhesion and fusion of amphiphilic bilayers. *Science* **246**, 919-922, doi:10.1126/science.2814514 (1989).
100 Hughson, F. M. Structural characterization of viral fusion proteins. *Curr Biol* **5**, 265-274, doi:10.1016/s0960-9822(95)00057-1 (1995).
101 Battles, M. B. & McLellan, J. S. Respiratory syncytial virus entry and how to block it. *Nat Rev Microbiol* **17**, 233-245, doi:10.1038/s41579-019-0149-x (2019).
102 Chaiwatpongsakorn, S., Epand, R. F., Collins, P. L., Epand, R. M. & Peeples, M. E. Soluble respiratory syncytial virus fusion protein in the fully cleaved, pretriggered state is triggered by exposure to low-molarity buffer. *J Virol* **85**, 3968-3977, doi:10.1128/JVI.01813-10 (2011).
103 Killikelly, A. M., Kanekiyo, M. & Graham, B. S. Pre-fusion F is absent on the surface of formalin-inactivated respiratory syncytial virus. *Sci Rep* **6**, 34108, doi:10.1038/srep34108 (2016).
104 Yunus, A. S., Jackson, T. P., Crisafi, K., Burimski, I., Kilgore, N. R., Zoumplis, D., Allaway, G. P., Wild, C. T. & Salzwedel, K. Elevated temperature triggers human respiratory syncytial virus F protein six-helix bundle formation. *Virology* **396**, 226-237, doi:10.1016/j.virol.2009.10.040 (2010).
105 Mousa, J. J., Sauer, M. F., Sevy, A. M., Finn, J. A., Bates, J. T., Alvarado, G., King, H. G., Loerinc, L. B., Fong, R. H., Doranz, B. J., Correia, B. E., Kalyuzhniy, O., Wen, X., Jardetzky, T. S., Schief, W. R., Ohi, M. D., Meiler, J. & Crowe, J. E., Jr. Structural basis for nonneutralizing antibody competition at antigenic site II of the respiratory syncytial virus fusion protein. *Proc Natl Acad Sci U S A* **113**, E6849-E6858, doi:10.1073/pnas.1609449113 (2016).
106 Johnson, S. M., McNally, B. A., Ioannidis, I., Flano, E., Teng, M. N., Oomens, A. G., Walsh, E. E. & Peeples, M. E. Respiratory Syncytial Virus Uses CX3CR1 as a Receptor on Primary Human Airway Epithelial Cultures. *PLoS Pathog* **11**, e1005318, doi:10.1371/journal.ppat.1005318 (2015).
107 Chirkova, T., Lin, S., Oomens, A. G., Gaston, K. A., Boyoglu-Barnum, S., Meng, J., Stobart, C. C., Cotton, C. U., Hartert, T. V., Moore, M. L., Ziady, A. G. & Anderson, L. J. CX3CR1 is an important surface molecule for respiratory syncytial virus infection in

human airway epithelial cells. *J Gen Virol* **96**, 2543-2556, doi:10.1099/vir.0.000218 (2015).
108 Kwilas, S., Liesman, R. M., Zhang, L., Walsh, E., Pickles, R. J. & Peeples, M. E. Respiratory syncytial virus grown in Vero cells contains a truncated attachment protein that alters its infectivity and dependence on glycosaminoglycans. *J Virol* **83**, 10710-10718, doi:10.1128/JVI.00986-09 (2009).
109 Wertz, G. W., Collins, P. L., Huang, Y., Gruber, C., Levine, S. & Ball, L. A. Nucleotide sequence of the G protein gene of human respiratory syncytial virus reveals an unusual type of viral membrane protein. *Proc Natl Acad Sci U S A* **82**, 4075-4079, doi:10.1073/pnas.82.12.4075 (1985).
110 Gorman, J. J., Ferguson, B. L., Speelman, D. & Mills, J. Determination of the disulfide bond arrangement of human respiratory syncytial virus attachment (G) protein by matrix-assisted laser desorption/ionization time-of-flight mass spectrometry. *Protein Sci* **6**, 1308-1315, doi:10.1002/pro.5560060619 (1997).
111 Tripp, R. A., Jones, L. P., Haynes, L. M., Zheng, H., Murphy, P. M. & Anderson, L. J. CX3C chemokine mimicry by respiratory syncytial virus G glycoprotein. *Nat Immunol* **2**, 732-738, doi:10.1038/90675 (2001).
112 Feldman, S. A., Hendry, R. M. & Beeler, J. A. Identification of a linear heparin binding domain for human respiratory syncytial virus attachment glycoprotein G. *J Virol* **73**, 6610-6617 (1999).
113 Trento, A., Galiano, M., Videla, C., Carballal, G., Garcia-Barreno, B., Melero, J. A. & Palomo, C. Major changes in the G protein of human respiratory syncytial virus isolates introduced by a duplication of 60 nucleotides. *J Gen Virol* **84**, 3115-3120, doi:10.1099/vir.0.19357-0 (2003).
114 Roberts, S. R., Lichtenstein, D., Ball, L. A. & Wertz, G. W. The membrane-associated and secreted forms of the respiratory syncytial virus attachment glycoprotein G are synthesized from alternative initiation codons. *J Virol* **68**, 4538-4546 (1994).
115 Hendricks, D. A., McIntosh, K. & Patterson, J. L. Further characterization of the soluble form of the G glycoprotein of respiratory syncytial virus. *J Virol* **62**, 2228-2233 (1988).
116 Bukreyev, A., Yang, L., Fricke, J., Cheng, L., Ward, J. M., Murphy, B. R. & Collins, P. L. The secreted form of respiratory syncytial virus G glycoprotein helps the virus evade antibody-mediated restriction of replication by acting as an antigen decoy and through effects on Fc receptor-bearing leukocytes. *J Virol* **82**, 12191-12204, doi:10.1128/JVI.01604-08 (2008).
117 Malhotra, R., Ward, M., Bright, H., Priest, R., Foster, M. R., Hurle, M., Blair, E. & Bird, M. Isolation and characterisation of potential respiratory syncytial virus receptor(s) on epithelial cells. *Microbes Infect* **5**, 123-133, doi:10.1016/s1286-4579(02)00079-5 (2003).
118 Anderson, C. S., Chu, C. Y., Wang, Q., Mereness, J. A., Ren, Y., Donlon, K., Bhattacharya, S., Misra, R. S., Walsh, E. E., Pryhuber, G. S. & Mariani, T. J. CX3CR1 as a respiratory syncytial virus receptor in pediatric human lung. *Pediatr Res*, doi:10.1038/s41390-019-0677-0 (2019).
119 Currier, M. G., Lee, S., Stobart, C. C., Hotard, A. L., Villenave, R., Meng, J., Pretto, C. D., Shields, M. D., Nguyen, M. T., Todd, S. O., Chi, M. H., Hammonds, J., Krumm, S. A., Spearman, P., Plemper, R. K., Sakamoto, K., Peebles, R. S., Jr., Power, U. F. & Moore, M. L. EGFR Interacts with the Fusion Protein of Respiratory Syncytial Virus Strain 2-20 and

Mediates Infection and Mucin Expression. *PLoS Pathog* **12**, e1005622, doi:10.1371/journal.ppat.1005622 (2016).
120 Krzyzaniak, M. A., Zumstein, M. T., Gerez, J. A., Picotti, P. & Helenius, A. Host cell entry of respiratory syncytial virus involves macropinocytosis followed by proteolytic activation of the F protein. *PLoS Pathog* **9**, e1003309, doi:10.1371/journal.ppat.1003309 (2013).
121 Lingemann, M., McCarty, T., Liu, X., Buchholz, U. J., Surman, S., Martin, S. E., Collins, P. L. & Munir, S. The alpha-1 subunit of the Na+,K+-ATPase (ATP1A1) is required for macropinocytic entry of respiratory syncytial virus (RSV) in human respiratory epithelial cells. *PLoS Pathog* **15**, e1007963, doi:10.1371/journal.ppat.1007963 (2019).
122 Kurt-Jones, E. A., Popova, L., Kwinn, L., Haynes, L. M., Jones, L. P., Tripp, R. A., Walsh, E. E., Freeman, M. W., Golenbock, D. T., Anderson, L. J. & Finberg, R. W. Pattern recognition receptors TLR4 and CD14 mediate response to respiratory syncytial virus. *Nat Immunol* **1**, 398-401, doi:10.1038/80833 (2000).
123 Marchant, D., Singhera, G. K., Utokaparch, S., Hackett, T. L., Boyd, J. H., Luo, Z., Si, X., Dorscheid, D. R., McManus, B. M. & Hegele, R. G. Toll-like receptor 4-mediated activation of p38 mitogen-activated protein kinase is a determinant of respiratory virus entry and tropism. *J Virol* **84**, 11359-11373, doi:10.1128/JVI.00804-10 (2010).
124 Ajamian, F., Wu, Y., Ebeling, C., Ilarraza, R., Odemuyiwa, S. O., Moqbel, R. & Adamko, D. J. Respiratory syncytial virus induces indoleamine 2,3-dioxygenase activity: a potential novel role in the development of allergic disease. *Clin Exp Allergy* **45**, 644-659, doi:10.1111/cea.12498 (2015).
125 Behera, A. K., Matsuse, H., Kumar, M., Kong, X., Lockey, R. F. & Mohapatra, S. S. Blocking intercellular adhesion molecule-1 on human epithelial cells decreases respiratory syncytial virus infection. *Biochem Biophys Res Commun* **280**, 188-195, doi:10.1006/bbrc.2000.4093 (2001).
126 Holguera, J., Villar, E. & Munoz-Barroso, I. Identification of cellular proteins that interact with Newcastle Disease Virus and human Respiratory Syncytial Virus by a two-dimensional virus overlay protein binding assay (VOPBA). *Virus Res* **191**, 138-142, doi:10.1016/j.virusres.2014.07.031 (2014).
127 Mastrangelo, P., Norris, M. J., Duan, W., Barrett, E. G., Moraes, T. J. & Hegele, R. G. Targeting Host Cell Surface Nucleolin for RSV Therapy: Challenges and Opportunities. *Vaccines (Basel)* **5**, doi:10.3390/vaccines5030027 (2017).
128 Tayyari, F., Marchant, D., Moraes, T. J., Duan, W., Mastrangelo, P. & Hegele, R. G. Identification of nucleolin as a cellular receptor for human respiratory syncytial virus. *Nat Med* **17**, 1132-1135, doi:10.1038/nm.2444 (2011).
129 Feldman, S. A., Audet, S. & Beeler, J. A. The fusion glycoprotein of human respiratory syncytial virus facilitates virus attachment and infectivity via an interaction with cellular heparan sulfate. *J Virol* **74**, 6442-6447, doi:10.1128/jvi.74.14.6442-6447.2000 (2000).
130 Krusat, T. & Streckert, H. J. Heparin-dependent attachment of respiratory syncytial virus (RSV) to host cells. *Arch Virol* **142**, 1247-1254, doi:10.1007/s007050050156 (1997).
131 Martinez, I. & Melero, J. A. Binding of human respiratory syncytial virus to cells: implication of sulfated cell surface proteoglycans. *J Gen Virol* **81**, 2715-2722, doi:10.1099/0022-1317-81-11-2715 (2000).
132 Derscheid, R. J., van Geelen, A., McGill, J. L., Gallup, J. M., Cihlar, T., Sacco, R. E. & Ackermann, M. R. Human respiratory syncytial virus Memphis 37 grown in HEp-2 cells

causes more severe disease in lambs than virus grown in Vero cells. *Viruses* **5**, 2881-2897, doi:10.3390/v5112881 (2013).
133 Rixon, H. W., Brown, C., Brown, G. & Sugrue, R. J. Multiple glycosylated forms of the respiratory syncytial virus fusion protein are expressed in virus-infected cells. *J Gen Virol* **83**, 61-66, doi:10.1099/0022-1317-83-1-61 (2002).
134 Pfeifle, J. & Anderer, F. A. Isolation and characterization of phosphoprotein pp 105 from simian virus 40-transformed mouse fibroblasts. *Biochim Biophys Acta* **762**, 86-93, doi:10.1016/0167-4889(83)90120-9 (1983).
135 Shakeri, A., Mastrangelo, P., Griffin, J. K., Moraes, T. J. & Hegele, R. G. Respiratory syncytial virus receptor expression in the mouse and viral tropism. *Histol Histopathol* **30**, 401-411, doi:10.14670/HH-30.401 (2015).
136 Zheng, L. L., Li, C. M., Zhen, S. J., Li, Y. F. & Huang, C. Z. A dynamic cell entry pathway of respiratory syncytial virus revealed by tracking the quantum dot-labeled single virus. *Nanoscale* **9**, 7880-7887, doi:10.1039/c7nr02162c (2017).
137 Kolokoltsov, A. A., Deniger, D., Fleming, E. H., Roberts, N. J., Jr., Karpilow, J. M. & Davey, R. A. Small interfering RNA profiling reveals key role of clathrin-mediated endocytosis and early endosome formation for infection by respiratory syncytial virus. *J Virol* **81**, 7786-7800, doi:10.1128/JVI.02780-06 (2007).
138 Srinivasakumar, N., Ogra, P. L. & Flanagan, T. D. Characteristics of fusion of respiratory syncytial virus with HEp-2 cells as measured by R18 fluorescence dequenching assay. *J Virol* **65**, 4063-4069 (1991).
139 Mehedi, M., McCarty, T., Martin, S. E., Le Nouen, C., Buehler, E., Chen, Y. C., Smelkinson, M., Ganesan, S., Fischer, E. R., Brock, L. G., Liang, B., Munir, S., Collins, P. L. & Buchholz, U. J. Actin-Related Protein 2 (ARP2) and Virus-Induced Filopodia Facilitate Human Respiratory Syncytial Virus Spread. *PLoS Pathog* **12**, e1006062, doi:10.1371/journal.ppat.1006062 (2016).
140 Miyauchi, K., Kim, Y., Latinovic, O., Morozov, V. & Melikyan, G. B. HIV enters cells via endocytosis and dynamin-dependent fusion with endosomes. *Cell* **137**, 433-444, doi:10.1016/j.cell.2009.02.046 (2009).
141 Greber, U. F. Signalling in viral entry. *Cell Mol Life Sci* **59**, 608-626, doi:10.1007/s00018-002-8453-3 (2002).
142 Dickey, L. L., Duncan, J. K., Hanley, T. M. & Fearns, R. Decapping protein 1 phosphorylation modulates IL-8 expression during respiratory syncytial virus infection. *Virology* **481**, 199-209, doi:10.1016/j.virol.2015.02.043 (2015).
143 Monick, M., Staber, J., Thomas, K. & Hunninghake, G. Respiratory syncytial virus infection results in activation of multiple protein kinase C isoforms leading to activation of mitogen-activated protein kinase. *J Immunol* **166**, 2681-2687 (2001).
144 Choi, M. S., Heo, J., Yi, C. M., Ban, J., Lee, N. J., Lee, N. R., Kim, S. W., Kim, N. J. & Inn, K. S. A novel p38 mitogen activated protein kinase (MAPK) specific inhibitor suppresses respiratory syncytial virus and influenza A virus replication by inhibiting virus-induced p38 MAPK activation. *Biochem Biophys Res Commun* **477**, 311-316, doi:10.1016/j.bbrc.2016.06.111 (2016).
145 Kong, X., San Juan, H., Behera, A., Peeples, M. E., Wu, J., Lockey, R. F. & Mohapatra, S. S. ERK-1/2 activity is required for efficient RSV infection. *FEBS Lett* **559**, 33-38, doi:10.1016/S0014-5793(04)00002-X (2004).

146 Preugschas, H. F., Hrincius, E. R., Mewis, C., Tran, G. V. Q., Ludwig, S. & Ehrhardt, C. Late activation of the Raf/MEK/ERK pathway is required for translocation of the respiratory syncytial virus F protein to the plasma membrane and efficient viral replication. *Cell Microbiol* **21**, e12955, doi:10.1111/cmi.12955 (2019).
147 Thomas, K. W., Monick, M. M., Staber, J. M., Yarovinsky, T., Carter, A. B. & Hunninghake, G. W. Respiratory syncytial virus inhibits apoptosis and induces NF-kappa B activity through a phosphatidylinositol 3-kinase-dependent pathway. *J Biol Chem* **277**, 492-501, doi:10.1074/jbc.M108107200 (2002).
148 San-Juan-Vergara, H., Peeples, M. E., Lockey, R. F. & Mohapatra, S. S. Protein kinase C-alpha activity is required for respiratory syncytial virus fusion to human bronchial epithelial cells. *J Virol* **78**, 13717-13726, doi:10.1128/JVI.78.24.13717-13726.2004 (2004).
149 Masaki, T., Kojima, T., Okabayashi, T., Ogasawara, N., Ohkuni, T., Obata, K., Takasawa, A., Murata, M., Tanaka, S., Hirakawa, S., Fuchimoto, J., Ninomiya, T., Fujii, N., Tsutsumi, H., Himi, T. & Sawada, N. A nuclear factor-kappaB signaling pathway via protein kinase C delta regulates replication of respiratory syncytial virus in polarized normal human nasal epithelial cells. *Mol Biol Cell* **22**, 2144-2156, doi:10.1091/mbc.E10-11-0875 (2011).
150 Zhang, L., Bukreyev, A., Thompson, C. I., Watson, B., Peeples, M. E., Collins, P. L. & Pickles, R. J. Infection of ciliated cells by human parainfluenza virus type 3 in an in vitro model of human airway epithelium. *J Virol* **79**, 1113-1124, doi:10.1128/JVI.79.2.1113-1124.2005 (2005).
151 Zhang, L., Peeples, M. E., Boucher, R. C., Collins, P. L. & Pickles, R. J. Respiratory syncytial virus infection of human airway epithelial cells is polarized, specific to ciliated cells, and without obvious cytopathology. *J Virol* **76**, 5654-5666, doi:10.1128/jvi.76.11.5654-5666.2002 (2002).
152 Wee, P. & Wang, Z. Epidermal Growth Factor Receptor Cell Proliferation Signaling Pathways. *Cancers (Basel)* **9**, doi:10.3390/cancers9050052 (2017).
153 Monick, M. M., Cameron, K., Staber, J., Powers, L. S., Yarovinsky, T. O., Koland, J. G. & Hunninghake, G. W. Activation of the epidermal growth factor receptor by respiratory syncytial virus results in increased inflammation and delayed apoptosis. *J Biol Chem* **280**, 2147-2158, doi:10.1074/jbc.M408745200 (2005).
154 Tan, Y. & Kagan, J. C. A cross-disciplinary perspective on the innate immune responses to bacterial lipopolysaccharide. *Mol Cell* **54**, 212-223, doi:10.1016/j.molcel.2014.03.012 (2014).
155 Rallabhandi, P., Phillips, R. L., Boukhvalova, M. S., Pletneva, L. M., Shirey, K. A., Gioannini, T. L., Weiss, J. P., Chow, J. C., Hawkins, L. D., Vogel, S. N. & Blanco, J. C. Respiratory syncytial virus fusion protein-induced toll-like receptor 4 (TLR4) signaling is inhibited by the TLR4 antagonists Rhodobacter sphaeroides lipopolysaccharide and eritoran (E5564) and requires direct interaction with MD-2. *MBio* **3**, doi:10.1128/mBio.00218-12 (2012).
156 Tulic, M. K., Hurrelbrink, R. J., Prele, C. M., Laing, I. A., Upham, J. W., Le Souef, P., Sly, P. D. & Holt, P. G. TLR4 polymorphisms mediate impaired responses to respiratory syncytial virus and lipopolysaccharide. *J Immunol* **179**, 132-140, doi:10.4049/jimmunol.179.1.132 (2007).
157 Funchal, G. A., Jaeger, N., Czepielewski, R. S., Machado, M. S., Muraro, S. P., Stein, R. T., Bonorino, C. B. & Porto, B. N. Respiratory syncytial virus fusion protein promotes

TLR-4-dependent neutrophil extracellular trap formation by human neutrophils. *PLoS One* **10**, e0124082, doi:10.1371/journal.pone.0124082 (2015).

158 Cortjens, B., de Boer, O. J., de Jong, R., Antonis, A. F., Sabogal Pineros, Y. S., Lutter, R., van Woensel, J. B. & Bem, R. A. Neutrophil extracellular traps cause airway obstruction during respiratory syncytial virus disease. *J Pathol* **238**, 401-411, doi:10.1002/path.4660 (2016).

159 Haeberle, H. A., Takizawa, R., Casola, A., Brasier, A. R., Dieterich, H. J., Van Rooijen, N., Gatalica, Z. & Garofalo, R. P. Respiratory syncytial virus-induced activation of nuclear factor-kappaB in the lung involves alveolar macrophages and toll-like receptor 4-dependent pathways. *J Infect Dis* **186**, 1199-1206, doi:10.1086/344644 (2002).

160 Imai, T., Hieshima, K., Haskell, C., Baba, M., Nagira, M., Nishimura, M., Kakizaki, M., Takagi, S., Nomiyama, H., Schall, T. J. & Yoshie, O. Identification and molecular characterization of fractalkine receptor CX3CR1, which mediates both leukocyte migration and adhesion. *Cell* **91**, 521-530, doi:10.1016/s0092-8674(00)80438-9 (1997).

161 Jeong, K. I., Piepenhagen, P. A., Kishko, M., DiNapoli, J. M., Groppo, R. P., Zhang, L., Almond, J., Kleanthous, H., Delagrave, S. & Parrington, M. CX3CR1 Is Expressed in Differentiated Human Ciliated Airway Cells and Co-Localizes with Respiratory Syncytial Virus on Cilia in a G Protein-Dependent Manner. *PLoS One* **10**, e0130517, doi:10.1371/journal.pone.0130517 (2015).

162 Boyoglu-Barnum, S., Todd, S. O., Meng, J., Barnum, T. R., Chirkova, T., Haynes, L. M., Jadhao, S. J., Tripp, R. A., Oomens, A. G., Moore, M. L. & Anderson, L. J. Mutating the CX3C Motif in the G Protein Should Make a Live Respiratory Syncytial Virus Vaccine Safer and More Effective. *J Virol* **91**, doi:10.1128/JVI.02059-16 (2017).

163 Pike, L. J. Rafts defined: a report on the Keystone Symposium on Lipid Rafts and Cell Function. *J Lipid Res* **47**, 1597-1598, doi:10.1194/jlr.E600002-JLR200 (2006).

164 Mollinedo, F. & Gajate, C. Lipid rafts as major platforms for signaling regulation in cancer. *Adv Biol Regul* **57**, 130-146, doi:10.1016/j.jbior.2014.10.003 (2015).

165 Triantafilou, M., Miyake, K., Golenbock, D. T. & Triantafilou, K. Mediators of innate immune recognition of bacteria concentrate in lipid rafts and facilitate lipopolysaccharide-induced cell activation. *J Cell Sci* **115**, 2603-2611 (2002).

166 Mineo, C., James, G. L., Smart, E. J. & Anderson, R. G. Localization of epidermal growth factor-stimulated Ras/Raf-1 interaction to caveolae membrane. *J Biol Chem* **271**, 11930-11935, doi:10.1074/jbc.271.20.11930 (1996).

167 Zhuang, L., Lin, J., Lu, M. L., Solomon, K. R. & Freeman, M. R. Cholesterol-rich lipid rafts mediate akt-regulated survival in prostate cancer cells. *Cancer Res* **62**, 2227-2231 (2002).

168 Huo, H., Guo, X., Hong, S., Jiang, M., Liu, X. & Liao, K. Lipid rafts/caveolae are essential for insulin-like growth factor-1 receptor signaling during 3T3-L1 preadipocyte differentiation induction. *J Biol Chem* **278**, 11561-11569, doi:10.1074/jbc.M211785200 (2003).

169 Orrick, L. R., Olson, M. O. & Busch, H. Comparison of nucleolar proteins of normal rat liver and Novikoff hepatoma ascites cells by two-dimensional polyacrylamide gel electrophoresis. *Proc Natl Acad Sci U S A* **70**, 1316-1320, doi:10.1073/pnas.70.5.1316 (1973).

170 Lapeyre, B., Amalric, F., Ghaffari, S. H., Rao, S. V., Dumbar, T. S. & Olson, M. O. Protein and cDNA sequence of a glycine-rich, dimethylarginine-containing region located near the

carboxyl-terminal end of nucleolin (C23 and 100 kDa). *J Biol Chem* **261**, 9167-9173 (1986).
171 Tajrishi, M. M., Tuteja, R. & Tuteja, N. Nucleolin: The most abundant multifunctional phosphoprotein of nucleolus. *Commun Integr Biol* **4**, 267-275, doi:10.4161/cib.4.3.14884 (2011).
172 Mamrack, M. D., Olson, M. O. & Busch, H. Amino acid sequence and sites of phosphorylation in a highly acidic region of nucleolar nonhistone protein C23. *Biochemistry* **18**, 3381-3386, doi:10.1021/bi00582a026 (1979).
173 Allain, F. H., Bouvet, P., Dieckmann, T. & Feigon, J. Molecular basis of sequence-specific recognition of pre-ribosomal RNA by nucleolin. *EMBO J* **19**, 6870-6881, doi:10.1093/emboj/19.24.6870 (2000).
174 Ginisty, H., Amalric, F. & Bouvet, P. Two different combinations of RNA-binding domains determine the RNA binding specificity of nucleolin. *J Biol Chem* **276**, 14338-14343, doi:10.1074/jbc.M011120200 (2001).
175 Schmidt-Zachmann, M. S. & Nigg, E. A. Protein localization to the nucleolus: a search for targeting domains in nucleolin. *J Cell Sci* **105 (Pt 3)**, 799-806 (1993).
176 Ding, Y., Song, N., Liu, C., He, T., Zhuo, W., He, X., Chen, Y., Song, X., Fu, Y. & Luo, Y. Heat shock cognate 70 regulates the translocation and angiogenic function of nucleolin. *Arterioscler Thromb Vasc Biol* **32**, e126-134, doi:10.1161/ATVBAHA.112.247502 (2012).
177 Erard, M. S., Belenguer, P., Caizergues-Ferrer, M., Pantaloni, A. & Amalric, F. A major nucleolar protein, nucleolin, induces chromatin decondensation by binding to histone H1. *Eur J Biochem* **175**, 525-530, doi:10.1111/j.1432-1033.1988.tb14224.x (1988).
178 Farin, K., Di Segni, A., Mor, A. & Pinkas-Kramarski, R. Structure-function analysis of nucleolin and ErbB receptors interactions. *PLoS One* **4**, e6128, doi:10.1371/journal.pone.0006128 (2009).
179 Niu, H., Yang, X., Xu, Z., Du, T. & Wang, R. Cell surface nucleolin interacts with CXCR4 receptor via the 212 c-terminal portion. *Tumour Biol* **36**, 1099-1104, doi:10.1007/s13277-014-2734-y (2015).
180 Song, N., Ding, Y., Zhuo, W., He, T., Fu, Z., Chen, Y., Song, X., Fu, Y. & Luo, Y. The nuclear translocation of endostatin is mediated by its receptor nucleolin in endothelial cells. *Angiogenesis* **15**, 697-711, doi:10.1007/s10456-012-9284-y (2012).
181 Ghisolfi, L., Kharrat, A., Joseph, G., Amalric, F. & Erard, M. Concerted activities of the RNA recognition and the glycine-rich C-terminal domains of nucleolin are required for efficient complex formation with pre-ribosomal RNA. *Eur J Biochem* **209**, 541-548, doi:10.1111/j.1432-1033.1992.tb17318.x (1992).
182 Olson, M. O., Orrick, L. R., Jones, C. & Busch, H. Phosphorylation of acid-soluble nucleolar proteins of Novikoff hepatoma ascites cells in vivo. *J Biol Chem* **249**, 2823-2827 (1974).
183 Carpentier, M., Morelle, W., Coddeville, B., Pons, A., Masson, M., Mazurier, J. & Legrand, D. Nucleolin undergoes partial N- and O-glycosylations in the extranuclear cell compartment. *Biochemistry* **44**, 5804-5815, doi:10.1021/bi047831s (2005).
184 Losfeld, M. E., Leroy, A., Coddeville, B., Carpentier, M., Mazurier, J. & Legrand, D. N-Glycosylation influences the structure and self-association abilities of recombinant nucleolin. *FEBS J* **278**, 2552-2564, doi:10.1111/j.1742-4658.2011.08180.x (2011).

185 Lischwe, M. A., Roberts, K. D., Yeoman, L. C. & Busch, H. Nucleolar specific acidic phosphoprotein C23 is highly methylated. *J Biol Chem* **257**, 14600-14602 (1982).
186 Leitinger, N. & Wesierska-Gadek, J. ADP-ribosylation of nucleolar proteins in HeLa tumor cells. *J Cell Biochem* **52**, 153-158, doi:10.1002/jcb.240520207 (1993).
187 Raman, B., Guarnaccia, C., Nadassy, K., Zakhariev, S., Pintar, A., Zanuttin, F., Frigyes, D., Acatrinei, C., Vindigni, A., Pongor, G. & Pongor, S. N(omega)-arginine dimethylation modulates the interaction between a Gly/Arg-rich peptide from human nucleolin and nucleic acids. *Nucleic Acids Res* **29**, 3377-3384, doi:10.1093/nar/29.16.3377 (2001).
188 Hovanessian, A. G., Soundaramourty, C., El Khoury, D., Nondier, I., Svab, J. & Krust, B. Surface expressed nucleolin is constantly induced in tumor cells to mediate calcium-dependent ligand internalization. *PLoS One* **5**, e15787, doi:10.1371/journal.pone.0015787 (2010).
189 Losfeld, M. E., Khoury, D. E., Mariot, P., Carpentier, M., Krust, B., Briand, J. P., Mazurier, J., Hovanessian, A. G. & Legrand, D. The cell surface expressed nucleolin is a glycoprotein that triggers calcium entry into mammalian cells. *Exp Cell Res* **315**, 357-369, doi:10.1016/j.yexcr.2008.10.039 (2009).
190 Schwab, M. S. & Dreyer, C. Protein phosphorylation sites regulate the function of the bipartite NLS of nucleolin. *Eur J Cell Biol* **73**, 287-297 (1997).
191 Caizergues-Ferrer, M., Belenguer, P., Lapeyre, B., Amalric, F., Wallace, M. O. & Olson, M. O. Phosphorylation of nucleolin by a nucleolar type NII protein kinase. *Biochemistry* **26**, 7876-7883, doi:10.1021/bi00398a051 (1987).
192 Zhou, G., Seibenhener, M. L. & Wooten, M. W. Nucleolin is a protein kinase C-zeta substrate. Connection between cell surface signaling and nucleus in PC12 cells. *J Biol Chem* **272**, 31130-31137, doi:10.1074/jbc.272.49.31130 (1997).
193 Jordan, P., Heid, H., Kinzel, V. & Kubler, D. Major cell surface-located protein substrates of an ecto-protein kinase are homologs of known nuclear proteins. *Biochemistry* **33**, 14696-14706, doi:10.1021/bi00253a007 (1994).
194 Wu, D. M., Zhang, P., Liu, R. Y., Sang, Y. X., Zhou, C., Xu, G. C., Yang, J. L., Tong, A. P. & Wang, C. T. Phosphorylation and changes in the distribution of nucleolin promote tumor metastasis via the PI3K/Akt pathway in colorectal carcinoma. *FEBS Lett* **588**, 1921-1929, doi:10.1016/j.febslet.2014.03.047 (2014).
195 Suzuki, N., Kobayashi, M., Sakata, K., Suzuki, T. & Hosoya, T. Synergistic stimulatory effect of glucocorticoid, EGF and insulin on the synthesis of ribosomal RNA and phosphorylation of nucleolin in primary cultured rat hepatocytes. *Biochim Biophys Acta* **1092**, 367-375, doi:10.1016/s0167-4889(97)90014-8 (1991).
196 Ballal, N. R., Kang, Y. J., Olson, M. O. & Busch, H. Changes in nucleolar proteins and their phosphorylation patterns during liver regeneration. *J Biol Chem* **250**, 5921-5925 (1975).
197 Kang, Y. J., Olson, M. O., Jones, C. & Busch, H. Nucleolar phosphoproteins of normal rat liver and Novikoff hepatoma ascites cells. *Cancer Res* **35**, 1470-1475 (1975).
198 Spector, D. L., Ochs, R. L. & Busch, H. Silver staining, immunofluorescence, and immunoelectron microscopic localization of nucleolar phosphoproteins B23 and C23. *Chromosoma* **90**, 139-148, doi:10.1007/bf00292451 (1984).
199 Reeder, R. H. rRNA synthesis in the nucleolus. *Trends Genet* **6**, 390-395, doi:10.1016/0168-9525(90)90298-k (1990).

200 Ginisty, H., Amalric, F. & Bouvet, P. Nucleolin functions in the first step of ribosomal RNA processing. *EMBO J* **17**, 1476-1486, doi:10.1093/emboj/17.5.1476 (1998).
201 Storck, S., Thiry, M. & Bouvet, P. Conditional knockout of nucleolin in DT40 cells reveals the functional redundancy of its RNA-binding domains. *Biol Cell* **101**, 153-167, doi:10.1042/BC20080054 (2009).
202 Ugrinova, I., Monier, K., Ivaldi, C., Thiry, M., Storck, S., Mongelard, F. & Bouvet, P. Inactivation of nucleolin leads to nucleolar disruption, cell cycle arrest and defects in centrosome duplication. *BMC Mol Biol* **8**, 66, doi:10.1186/1471-2199-8-66 (2007).
203 Angelov, D., Bondarenko, V. A., Almagro, S., Menoni, H., Mongelard, F., Hans, F., Mietton, F., Studitsky, V. M., Hamiche, A., Dimitrov, S. & Bouvet, P. Nucleolin is a histone chaperone with FACT-like activity and assists remodeling of nucleosomes. *EMBO J* **25**, 1669-1679, doi:10.1038/sj.emboj.7601046 (2006).
204 Ma, N., Matsunaga, S., Takata, H., Ono-Maniwa, R., Uchiyama, S. & Fukui, K. Nucleolin functions in nucleolus formation and chromosome congression. *J Cell Sci* **120**, 2091-2105, doi:10.1242/jcs.008771 (2007).
205 Miranda, G. A., Chokler, I. & Aguilera, R. J. The murine nucleolin protein is an inducible DNA and ATP binding protein which is readily detected in nuclear extracts of lipopolysaccharide-treated splenocytes. *Exp Cell Res* **217**, 294-308, doi:10.1006/excr.1995.1090 (1995).
206 Bates, P. J., Reyes-Reyes, E. M., Malik, M. T., Murphy, E. M., O'Toole, M. G. & Trent, J. O. G-quadruplex oligonucleotide AS1411 as a cancer-targeting agent: Uses and mechanisms. *Biochim Biophys Acta Gen Subj* **1861**, 1414-1428, doi:10.1016/j.bbagen.2016.12.015 (2017).
207 Rosenberg, J. E., Bambury, R. M., Van Allen, E. M., Drabkin, H. A., Lara, P. N., Jr., Harzstark, A. L., Wagle, N., Figlin, R. A., Smith, G. W., Garraway, L. A., Choueiri, T., Erlandsson, F. & Laber, D. A. A phase II trial of AS1411 (a novel nucleolin-targeted DNA aptamer) in metastatic renal cell carcinoma. *Invest New Drugs* **32**, 178-187, doi:10.1007/s10637-013-0045-6 (2014).
208 Borer, R. A., Lehner, C. F., Eppenberger, H. M. & Nigg, E. A. Major nucleolar proteins shuttle between nucleus and cytoplasm. *Cell* **56**, 379-390, doi:10.1016/0092-8674(89)90241-9 (1989).
209 Ishimaru, D., Zuraw, L., Ramalingam, S., Sengupta, T. K., Bandyopadhyay, S., Reuben, A., Fernandes, D. J. & Spicer, E. K. Mechanism of regulation of bcl-2 mRNA by nucleolin and A+U-rich element-binding factor 1 (AUF1). *J Biol Chem* **285**, 27182-27191, doi:10.1074/jbc.M109.098830 (2010).
210 Jiang, Y., Xu, X. S. & Russell, J. E. A nucleolin-binding 3' untranslated region element stabilizes beta-globin mRNA in vivo. *Mol Cell Biol* **26**, 2419-2429, doi:10.1128/MCB.26.6.2419-2429.2006 (2006).
211 Zhang, D., Liang, Y., Xie, Q., Gao, G., Wei, J., Huang, H., Li, J., Gao, J. & Huang, C. A novel post-translational modification of nucleolin, SUMOylation at Lys-294, mediates arsenite-induced cell death by regulating gadd45alpha mRNA stability. *J Biol Chem* **290**, 4784-4800, doi:10.1074/jbc.M114.598219 (2015).
212 Takagi, M., Absalon, M. J., McLure, K. G. & Kastan, M. B. Regulation of p53 translation and induction after DNA damage by ribosomal protein L26 and nucleolin. *Cell* **123**, 49-63, doi:10.1016/j.cell.2005.07.034 (2005).

213 Pfeifle, J., Hagmann, W. & Anderer, F. A. Cell adhesion-dependent differences in endogenous protein phosphorylation on the surface of various cell lines. *Biochim Biophys Acta* **670**, 274-284, doi:10.1016/0005-2795(81)90020-9 (1981).
214 Semenkovich, C. F., Ostlund, R. E., Jr., Olson, M. O. & Yang, J. W. A protein partially expressed on the surface of HepG2 cells that binds lipoproteins specifically is nucleolin. *Biochemistry* **29**, 9708-9713, doi:10.1021/bi00493a028 (1990).
215 Christian, S., Pilch, J., Akerman, M. E., Porkka, K., Laakkonen, P. & Ruoslahti, E. Nucleolin expressed at the cell surface is a marker of endothelial cells in angiogenic blood vessels. *J Cell Biol* **163**, 871-878, doi:10.1083/jcb.200304132 (2003).
216 Pfeifle, J. & Anderer, F. A. Localization of phosphoprotein PP 105 in cell lines of various species. *Biochem Biophys Res Commun* **116**, 106-112, doi:10.1016/0006-291x(83)90387-x (1983).
217 Bi, J., Wang, R., Zhang, Y., Han, X., Ampah, K. K., Liu, W. & Zeng, X. Identification of nucleolin as a lipid-raft-dependent beta1-integrin-interacting protein in A375 cell migration. *Mol Cells* **36**, 507-517, doi:10.1007/s10059-013-0149-z (2013).
218 Krust, B., El Khoury, D., Nondier, I., Soundaramourty, C. & Hovanessian, A. G. Targeting surface nucleolin with multivalent HB-19 and related Nucant pseudopeptides results in distinct inhibitory mechanisms depending on the malignant tumor cell type. *BMC Cancer* **11**, 333, doi:10.1186/1471-2407-11-333 (2011).
219 Rabouille, C. Pathways of Unconventional Protein Secretion. *Trends Cell Biol* **27**, 230-240, doi:10.1016/j.tcb.2016.11.007 (2017).
220 Hovanessian, A. G., Puvion-Dutilleul, F., Nisole, S., Svab, J., Perret, E., Deng, J. S. & Krust, B. The cell-surface-expressed nucleolin is associated with the actin cytoskeleton. *Exp Cell Res* **261**, 312-328, doi:10.1006/excr.2000.5071 (2000).
221 Watowich, S. S. & Morimoto, R. I. Complex regulation of heat shock- and glucose-responsive genes in human cells. *Mol Cell Biol* **8**, 393-405, doi:10.1128/mcb.8.1.393 (1988).
222 Zhang, M., Kenny, S. J., Ge, L., Xu, K. & Schekman, R. Translocation of interleukin-1beta into a vesicle intermediate in autophagy-mediated secretion. *Elife* **4**, doi:10.7554/eLife.11205 (2015).
223 Buschow, S. I., van Balkom, B. W., Aalberts, M., Heck, A. J., Wauben, M. & Stoorvogel, W. MHC class II-associated proteins in B-cell exosomes and potential functional implications for exosome biogenesis. *Immunol Cell Biol* **88**, 851-856, doi:10.1038/icb.2010.64 (2010).
224 Liang, B., Peng, P., Chen, S., Li, L., Zhang, M., Cao, D., Yang, J., Li, H., Gui, T., Li, X. & Shen, K. Characterization and proteomic analysis of ovarian cancer-derived exosomes. *J Proteomics* **80**, 171-182, doi:10.1016/j.jprot.2012.12.029 (2013).
225 Skogberg, G., Gudmundsdottir, J., van der Post, S., Sandstrom, K., Bruhn, S., Benson, M., Mincheva-Nilsson, L., Baranov, V., Telemo, E. & Ekwall, O. Characterization of human thymic exosomes. *PLoS One* **8**, e67554, doi:10.1371/journal.pone.0067554 (2013).
226 Grinstein, E., Shan, Y., Karawajew, L., Snijders, P. J., Meijer, C. J., Royer, H. D. & Wernet, P. Cell cycle-controlled interaction of nucleolin with the retinoblastoma protein and cancerous cell transformation. *J Biol Chem* **281**, 22223-22235, doi:10.1074/jbc.M513335200 (2006).

227 Huang, Y., Shi, H., Zhou, H., Song, X., Yuan, S. & Luo, Y. The angiogenic function of nucleolin is mediated by vascular endothelial growth factor and nonmuscle myosin. *Blood* **107**, 3564-3571, doi:10.1182/blood-2005-07-2961 (2006).
228 Koutsioumpa, M., Polytarchou, C., Courty, J., Zhang, Y., Kieffer, N., Mikelis, C., Skandalis, S. S., Hellman, U., Iliopoulos, D. & Papadimitriou, E. Interplay between alphavbeta3 integrin and nucleolin regulates human endothelial and glioma cell migration. *J Biol Chem* **288**, 343-354, doi:10.1074/jbc.M112.387076 (2013).
229 Chen, S. C., Hu, T. H., Huang, C. C., Kung, M. L., Chu, T. H., Yi, L. N., Huang, S. T., Chan, H. H., Chuang, J. H., Liu, L. F., Wu, H. C., Wu, D. C., Chang, M. C. & Tai, M. H. Hepatoma-derived growth factor/nucleolin axis as a novel oncogenic pathway in liver carcinogenesis. *Oncotarget* **6**, 16253-16270, doi:10.18632/oncotarget.3608 (2015).
230 Shibata, Y., Muramatsu, T., Hirai, M., Inui, T., Kimura, T., Saito, H., McCormick, L. M., Bu, G. & Kadomatsu, K. Nuclear targeting by the growth factor midkine. *Mol Cell Biol* **22**, 6788-6796, doi:10.1128/mcb.22.19.6788-6796.2002 (2002).
231 Stepanova, V., Lebedeva, T., Kuo, A., Yarovoi, S., Tkachuk, S., Zaitsev, S., Bdeir, K., Dumler, I., Marks, M. S., Parfyonova, Y., Tkachuk, V. A., Higazi, A. A. & Cines, D. B. Nuclear translocation of urokinase-type plasminogen activator. *Blood* **112**, 100-110, doi:10.1182/blood-2007-07-104455 (2008).
232 Deng, J. S., Ballou, B. & Hofmeister, J. K. Internalization of anti-nucleolin antibody into viable HEp-2 cells. *Mol Biol Rep* **23**, 191-195, doi:10.1007/bf00351168 (1996).
233 Shi, H., Huang, Y., Zhou, H., Song, X., Yuan, S., Fu, Y. & Luo, Y. Nucleolin is a receptor that mediates antiangiogenic and antitumor activity of endostatin. *Blood* **110**, 2899-2906, doi:10.1182/blood-2007-01-064428 (2007).
234 Tate, A., Isotani, S., Bradley, M. J., Sikes, R. A., Davis, R., Chung, L. W. & Edlund, M. Met-Independent Hepatocyte Growth Factor-mediated regulation of cell adhesion in human prostate cancer cells. *BMC Cancer* **6**, 197, doi:10.1186/1471-2407-6-197 (2006).
235 Reyes-Reyes, E. M. & Akiyama, S. K. Cell-surface nucleolin is a signal transducing P-selectin binding protein for human colon carcinoma cells. *Exp Cell Res* **314**, 2212-2223, doi:10.1016/j.yexcr.2008.03.016 (2008).
236 Larrucea, S., Gonzalez-Rubio, C., Cambronero, R., Ballou, B., Bonay, P., Lopez-Granados, E., Bouvet, P., Fontan, G., Fresno, M. & Lopez-Trascasa, M. Cellular adhesion mediated by factor J, a complement inhibitor. Evidence for nucleolin involvement. *J Biol Chem* **273**, 31718-31725, doi:10.1074/jbc.273.48.31718 (1998).
237 Said, E. A., Krust, B., Nisole, S., Svab, J., Briand, J. P. & Hovanessian, A. G. The anti-HIV cytokine midkine binds the cell surface-expressed nucleolin as a low affinity receptor. *J Biol Chem* **277**, 37492-37502, doi:10.1074/jbc.M201194200 (2002).
238 Legrand, D., Vigie, K., Said, E. A., Elass, E., Masson, M., Slomianny, M. C., Carpentier, M., Briand, J. P., Mazurier, J. & Hovanessian, A. G. Surface nucleolin participates in both the binding and endocytosis of lactoferrin in target cells. *Eur J Biochem* **271**, 303-317, doi:10.1046/j.1432-1033.2003.03929.x (2004).
239 Lv, S., Dai, C., Liu, Y., Sun, B., Shi, R., Han, M., Bian, R. & Wang, R. Cell surface protein C23 affects EGF-EGFR induced activation of ERK and PI3K-AKT pathways. *J Mol Neurosci* **55**, 519-524, doi:10.1007/s12031-014-0375-7 (2015).
240 Qi, J., Li, H., Liu, N., Xing, Y., Zhou, G., Wu, Y., Liu, Y., Chen, W., Yue, J., Han, B., Kang, S. & Wu, X. The implications and mechanisms of the extra-nuclear nucleolin in the

esophageal squamous cell carcinomas. *Med Oncol* **32**, 45, doi:10.1007/s12032-015-0484-3 (2015).

241 Wang, Y., Mao, M. & Xu, J. C. Cell-surface nucleolin is involved in lipopolysaccharide internalization and signalling in alveolar macrophages. *Cell Biol Int* **35**, 677-685, doi:10.1042/CBI20100625 (2011).

242 Yang, X., Xu, Z., Li, D., Cheng, S., Fan, K., Li, C., Li, A., Zhang, J. & Feng, M. Cell surface nucleolin is crucial in the activation of the CXCL12/CXCR4 signaling pathway. *Tumour Biol* **35**, 333-338, doi:10.1007/s13277-013-1044-0 (2014).

243 Di Segni, A., Farin, K. & Pinkas-Kramarski, R. Identification of nucleolin as new ErbB receptors- interacting protein. *PLoS One* **3**, e2310, doi:10.1371/journal.pone.0002310 (2008).

244 Bose, S., Basu, M. & Banerjee, A. K. Role of nucleolin in human parainfluenza virus type 3 infection of human lung epithelial cells. *J Virol* **78**, 8146-8158, doi:10.1128/JVI.78.15.8146-8158.2004 (2004).

245 Chan, C. M., Chu, H., Zhang, A. J., Leung, L. H., Sze, K. H., Kao, R. Y., Chik, K. K., To, K. K., Chan, J. F., Chen, H., Jin, D. Y., Liu, L. & Yuen, K. Y. Hemagglutinin of influenza A virus binds specifically to cell surface nucleolin and plays a role in virus internalization. *Virology* **494**, 78-88, doi:10.1016/j.virol.2016.04.008 (2016).

246 Xiao, X., Feng, Y., Zhu, Z. & Dimitrov, D. S. Identification of a putative Crimean-Congo hemorrhagic fever virus entry factor. *Biochem Biophys Res Commun* **411**, 253-258, doi:10.1016/j.bbrc.2011.06.109 (2011).

247 Callebaut, C., Blanco, J., Benkirane, N., Krust, B., Jacotot, E., Guichard, G., Seddiki, N., Svab, J., Dam, E., Muller, S., Briand, J. P. & Hovanessian, A. G. Identification of V3 loop-binding proteins as potential receptors implicated in the binding of HIV particles to CD4(+) cells. *J Biol Chem* **273**, 21988-21997, doi:10.1074/jbc.273.34.21988 (1998).

248 Nisole, S., Krust, B. & Hovanessian, A. G. Anchorage of HIV on permissive cells leads to coaggregation of viral particles with surface nucleolin at membrane raft microdomains. *Exp Cell Res* **276**, 155-173, doi:10.1006/excr.2002.5522 (2002).

249 de Verdugo, U. R., Selinka, H. C., Huber, M., Kramer, B., Kellermann, J., Hofschneider, P. H. & Kandolf, R. Characterization of a 100-kilodalton binding protein for the six serotypes of coxsackie B viruses. *J Virol* **69**, 6751-6757 (1995).

250 Qiu, J. & Brown, K. E. A 110-kDa nuclear shuttle protein, nucleolin, specifically binds to adeno-associated virus type 2 (AAV-2) capsid. *Virology* **257**, 373-382, doi:10.1006/viro.1999.9664 (1999).

251 Su, P. Y., Wang, Y. F., Huang, S. W., Lo, Y. C., Wang, Y. H., Wu, S. R., Shieh, D. B., Chen, S. H., Wang, J. R., Lai, M. D. & Chang, C. F. Cell surface nucleolin facilitates enterovirus 71 binding and infection. *J Virol* **89**, 4527-4538, doi:10.1128/JVI.03498-14 (2015).

252 Barel, M., Hovanessian, A. G., Meibom, K., Briand, J. P., Dupuis, M. & Charbit, A. A novel receptor - ligand pathway for entry of Francisella tularensis in monocyte-like THP-1 cells: interaction between surface nucleolin and bacterial elongation factor Tu. *BMC Microbiol* **8**, 145, doi:10.1186/1471-2180-8-145 (2008).

253 Sinclair, J. F. & O'Brien, A. D. Cell surface-localized nucleolin is a eukaryotic receptor for the adhesin intimin-gamma of enterohemorrhagic Escherichia coli O157:H7. *J Biol Chem* **277**, 2876-2885, doi:10.1074/jbc.M110230200 (2002).

254 Hanahan, D. & Weinberg, R. A. The hallmarks of cancer. *Cell* **100**, 57-70, doi:10.1016/s0092-8674(00)81683-9 (2000).
255 Destouches, D., El Khoury, D., Hamma-Kourbali, Y., Krust, B., Albanese, P., Katsoris, P., Guichard, G., Briand, J. P., Courty, J. & Hovanessian, A. G. Suppression of tumor growth and angiogenesis by a specific antagonist of the cell-surface expressed nucleolin. *PLoS One* **3**, e2518, doi:10.1371/journal.pone.0002518 (2008).
256 Dailey, M. M., Miller, M. C., Bates, P. J., Lane, A. N. & Trent, J. O. Resolution and characterization of the structural polymorphism of a single quadruplex-forming sequence. *Nucleic Acids Res* **38**, 4877-4888, doi:10.1093/nar/gkq166 (2010).
257 Reyes-Reyes, E. M., Teng, Y. & Bates, P. J. A new paradigm for aptamer therapeutic AS1411 action: uptake by macropinocytosis and its stimulation by a nucleolin-dependent mechanism. *Cancer Res* **70**, 8617-8629, doi:10.1158/0008-5472.CAN-10-0920 (2010).
258 Soundararajan, S., Wang, L., Sridharan, V., Chen, W., Courtenay-Luck, N., Jones, D., Spicer, E. K. & Fernandes, D. J. Plasma membrane nucleolin is a receptor for the anticancer aptamer AS1411 in MV4-11 leukemia cells. *Mol Pharmacol* **76**, 984-991, doi:10.1124/mol.109.055947 (2009).
259 Manning, G., Whyte, D. B., Martinez, R., Hunter, T. & Sudarsanam, S. The protein kinase complement of the human genome. *Science* **298**, 1912-1934, doi:10.1126/science.1075762 (2002).
260 Rosse, C., Linch, M., Kermorgant, S., Cameron, A. J., Boeckeler, K. & Parker, P. J. PKC and the control of localized signal dynamics. *Nat Rev Mol Cell Biol* **11**, 103-112, doi:10.1038/nrm2847 (2010).
261 Isakov, N. Protein kinase C (PKC) isoforms in cancer, tumor promotion and tumor suppression. *Semin Cancer Biol* **48**, 36-52, doi:10.1016/j.semcancer.2017.04.012 (2018).
262 Coussens, L., Parker, P. J., Rhee, L., Yang-Feng, T. L., Chen, E., Waterfield, M. D., Francke, U. & Ullrich, A. Multiple, distinct forms of bovine and human protein kinase C suggest diversity in cellular signaling pathways. *Science* **233**, 859-866, doi:10.1126/science.3755548 (1986).
263 Takai, Y., Kishimoto, A., Iwasa, Y., Kawahara, Y., Mori, T. & Nishizuka, Y. Calcium-dependent activation of a multifunctional protein kinase by membrane phospholipids. *J Biol Chem* **254**, 3692-3695 (1979).
264 Ohno, S., Akita, Y., Konno, Y., Imajoh, S. & Suzuki, K. A novel phorbol ester receptor/protein kinase, nPKC, distantly related to the protein kinase C family. *Cell* **53**, 731-741, doi:10.1016/0092-8674(88)90091-8 (1988).
265 Ono, Y., Fujii, T., Ogita, K., Kikkawa, U., Igarashi, K. & Nishizuka, Y. Identification of three additional members of rat protein kinase C family: delta-, epsilon- and zeta-subspecies. *FEBS Lett* **226**, 125-128, doi:10.1016/0014-5793(87)80564-1 (1987).
266 Osada, S., Mizuno, K., Saido, T. C., Akita, Y., Suzuki, K., Kuroki, T. & Ohno, S. A phorbol ester receptor/protein kinase, nPKC eta, a new member of the protein kinase C family predominantly expressed in lung and skin. *J Biol Chem* **265**, 22434-22440 (1990).
267 Osada, S., Mizuno, K., Saido, T. C., Suzuki, K., Kuroki, T. & Ohno, S. A new member of the protein kinase C family, nPKC theta, predominantly expressed in skeletal muscle. *Mol Cell Biol* **12**, 3930-3938, doi:10.1128/mcb.12.9.3930 (1992).
268 Akimoto, K., Mizuno, K., Osada, S., Hirai, S., Tanuma, S., Suzuki, K. & Ohno, S. A new member of the third class in the protein kinase C family, PKC lambda, expressed

dominantly in an undifferentiated mouse embryonal carcinoma cell line and also in many tissues and cells. *J Biol Chem* **269**, 12677-12683 (1994).

269 Selbie, L. A., Schmitz-Peiffer, C., Sheng, Y. & Biden, T. J. Molecular cloning and characterization of PKC iota, an atypical isoform of protein kinase C derived from insulin-secreting cells. *J Biol Chem* **268**, 24296-24302 (1993).

270 Ono, Y., Kurokawa, T., Fujii, T., Kawahara, K., Igarashi, K., Kikkawa, U., Ogita, K. & Nishizuka, Y. Two types of complementary DNAs of rat brain protein kinase C. Heterogeneity determined by alternative splicing. *FEBS Lett* **206**, 347-352, doi:10.1016/0014-5793(86)81010-9 (1986).

271 Kawaguchi, T., Niino, Y., Ohtaki, H., Kikuyama, S. & Shioda, S. New PKCdelta family members, PKCdeltaIV, deltaV, deltaVI, and deltaVII are specifically expressed in mouse testis. *FEBS Lett* **580**, 2458-2464, doi:10.1016/j.febslet.2006.03.084 (2006).

272 Ono, Y., Fujii, T., Igarashi, K., Kuno, T., Tanaka, C., Kikkawa, U. & Nishizuka, Y. Phorbol ester binding to protein kinase C requires a cysteine-rich zinc-finger-like sequence. *Proc Natl Acad Sci U S A* **86**, 4868-4871, doi:10.1073/pnas.86.13.4868 (1989).

273 House, C. & Kemp, B. E. Protein kinase C contains a pseudosubstrate prototope in its regulatory domain. *Science* **238**, 1726-1728, doi:10.1126/science.3686012 (1987).

274 Parker, P. J., Coussens, L., Totty, N., Rhee, L., Young, S., Chen, E., Stabel, S., Waterfield, M. D. & Ullrich, A. The complete primary structure of protein kinase C--the major phorbol ester receptor. *Science* **233**, 853-859, doi:10.1126/science.3755547 (1986).

275 Sossin, W. S. & Schwartz, J. H. Ca(2+)-independent protein kinase Cs contain an amino-terminal domain similar to the C2 consensus sequence. *Trends Biochem Sci* **18**, 207-208, doi:10.1016/0968-0004(93)90189-t (1993).

276 Dries, D. R., Gallegos, L. L. & Newton, A. C. A single residue in the C1 domain sensitizes novel protein kinase C isoforms to cellular diacylglycerol production. *J Biol Chem* **282**, 826-830, doi:10.1074/jbc.C600268200 (2007).

277 Cenni, V., Doppler, H., Sonnenburg, E. D., Maraldi, N., Newton, A. C. & Toker, A. Regulation of novel protein kinase C epsilon by phosphorylation. *Biochem J* **363**, 537-545, doi:10.1042/0264-6021:3630537 (2002).

278 Dutil, E. M., Toker, A. & Newton, A. C. Regulation of conventional protein kinase C isozymes by phosphoinositide-dependent kinase 1 (PDK-1). *Curr Biol* **8**, 1366-1375, doi:10.1016/s0960-9822(98)00017-7 (1998).

279 Ikenoue, T., Inoki, K., Yang, Q., Zhou, X. & Guan, K. L. Essential function of TORC2 in PKC and Akt turn motif phosphorylation, maturation and signalling. *EMBO J* **27**, 1919-1931, doi:10.1038/emboj.2008.119 (2008).

280 Facchinetti, V., Ouyang, W., Wei, H., Soto, N., Lazorchak, A., Gould, C., Lowry, C., Newton, A. C., Mao, Y., Miao, R. Q., Sessa, W. C., Qin, J., Zhang, P., Su, B. & Jacinto, E. The mammalian target of rapamycin complex 2 controls folding and stability of Akt and protein kinase C. *EMBO J* **27**, 1932-1943, doi:10.1038/emboj.2008.120 (2008).

281 Hecker, E. Cocarcinogenic principles from the seed oil of Croton tiglium and from other Euphorbiaceae. *Cancer Res* **28**, 2338-2349 (1968).

282 Young, S., Parker, P. J., Ullrich, A. & Stabel, S. Down-regulation of protein kinase C is due to an increased rate of degradation. *Biochem J* **244**, 775-779, doi:10.1042/bj2440775 (1987).

283 Berenblum, I. The cocarcinogenic action of croton resin. *Cancer Research* **1**, 44-48 (1941).

284 Newton, A. C. Protein kinase C as a tumor suppressor. *Semin Cancer Biol* **48**, 18-26, doi:10.1016/j.semcancer.2017.04.017 (2018).
285 Nakanishi, H. & Exton, J. H. Purification and characterization of the zeta isoform of protein kinase C from bovine kidney. *J Biol Chem* **267**, 16347-16354 (1992).
286 Graybill, C., Wee, B., Atwood, S. X. & Prehoda, K. E. Partitioning-defective protein 6 (Par-6) activates atypical protein kinase C (aPKC) by pseudosubstrate displacement. *J Biol Chem* **287**, 21003-21011, doi:10.1074/jbc.M112.360495 (2012).
287 Tobias, I. S. & Newton, A. C. Protein Scaffolds Control Localized Protein Kinase Czeta Activity. *J Biol Chem* **291**, 13809-13822, doi:10.1074/jbc.M116.729483 (2016).
288 Reina-Campos, M., Diaz-Meco, M. T. & Moscat, J. The Dual Roles of the Atypical Protein Kinase Cs in Cancer. *Cancer Cell* **36**, 218-235, doi:10.1016/j.ccell.2019.07.010 (2019).
289 Tobias, I. S., Kaulich, M., Kim, P. K., Simon, N., Jacinto, E., Dowdy, S. F., King, C. C. & Newton, A. C. Protein kinase Czeta exhibits constitutive phosphorylation and phosphatidylinositol-3,4,5-triphosphate-independent regulation. *Biochem J* **473**, 509-523, doi:10.1042/BJ20151013 (2016).
290 Perander, M., Bjorkoy, G. & Johansen, T. Nuclear import and export signals enable rapid nucleocytoplasmic shuttling of the atypical protein kinase C lambda. *J Biol Chem* **276**, 13015-13024, doi:10.1074/jbc.M010356200 (2001).
291 Chen, S., Lin, F., Shin, M. E., Wang, F., Shen, L. & Hamm, H. E. RACK1 regulates directional cell migration by acting on G betagamma at the interface with its effectors PLC beta and PI3K gamma. *Mol Biol Cell* **19**, 3909-3922, doi:10.1091/mbc.E08-04-0433 (2008).
292 Sanz, L., Sanchez, P., Lallena, M. J., Diaz-Meco, M. T. & Moscat, J. The interaction of p62 with RIP links the atypical PKCs to NF-kappaB activation. *EMBO J* **18**, 3044-3053, doi:10.1093/emboj/18.11.3044 (1999).
293 Monick, M. M., Carter, A. B., Flaherty, D. M., Peterson, M. W. & Hunninghake, G. W. Protein kinase C zeta plays a central role in activation of the p42/44 mitogen-activated protein kinase by endotoxin in alveolar macrophages. *J Immunol* **165**, 4632-4639, doi:10.4049/jimmunol.165.8.4632 (2000).
294 Liu, Y., Wang, B., Wang, J., Wan, W., Sun, R., Zhao, Y. & Zhang, N. Down-regulation of PKCzeta expression inhibits chemotaxis signal transduction in human lung cancer cells. *Lung Cancer* **63**, 210-218, doi:10.1016/j.lungcan.2008.05.010 (2009).
295 Liu, Q., Ning, W., Dantzer, R., Freund, G. G. & Kelley, K. W. Activation of protein kinase C-zeta and phosphatidylinositol 3'-kinase and promotion of macrophage differentiation by insulin-like growth factor-I. *J Immunol* **160**, 1393-1401 (1998).
296 Yano, K., Bauchat, J. R., Liimatta, M. B., Clemmons, D. R. & Duan, C. Down-regulation of protein kinase C inhibits insulin-like growth factor I-induced vascular smooth muscle cell proliferation, migration, and gene expression. *Endocrinology* **140**, 4622-4632, doi:10.1210/endo.140.10.7035 (1999).
297 Bandyopadhyay, G., Standaert, M. L., Zhao, L., Yu, B., Avignon, A., Galloway, L., Karnam, P., Moscat, J. & Farese, R. V. Activation of protein kinase C (alpha, beta, and zeta) by insulin in 3T3/L1 cells. Transfection studies suggest a role for PKC-zeta in glucose transport. *J Biol Chem* **272**, 2551-2558, doi:10.1074/jbc.272.4.2551 (1997).
298 Wellner, M., Maasch, C., Kupprion, C., Lindschau, C., Luft, F. C. & Haller, H. The proliferative effect of vascular endothelial growth factor requires protein kinase C-alpha

and protein kinase C-zeta. *Arterioscler Thromb Vasc Biol* **19**, 178-185, doi:10.1161/01.atv.19.1.178 (1999).

299 Diaz-Meco, M. T., Lozano, J., Municio, M. M., Berra, E., Frutos, S., Sanz, L. & Moscat, J. Evidence for the in vitro and in vivo interaction of Ras with protein kinase C zeta. *J Biol Chem* **269**, 31706-31710 (1994).

300 Chou, M. M., Hou, W., Johnson, J., Graham, L. K., Lee, M. H., Chen, C. S., Newton, A. C., Schaffhausen, B. S. & Toker, A. Regulation of protein kinase C zeta by PI 3-kinase and PDK-1. *Curr Biol* **8**, 1069-1077, doi:10.1016/s0960-9822(98)70444-0 (1998).

301 Le Good, J. A., Ziegler, W. H., Parekh, D. B., Alessi, D. R., Cohen, P. & Parker, P. J. Protein kinase C isotypes controlled by phosphoinositide 3-kinase through the protein kinase PDK1. *Science* **281**, 2042-2045, doi:10.1126/science.281.5385.2042 (1998).

302 Chang, S., Kim, J. H. & Shin, J. p62 forms a ternary complex with PKCzeta and PAR-4 and antagonizes PAR-4-induced PKCzeta inhibition. *FEBS Lett* **510**, 57-61, doi:10.1016/s0014-5793(01)03224-0 (2002).

303 Joberty, G., Petersen, C., Gao, L. & Macara, I. G. The cell-polarity protein Par6 links Par3 and atypical protein kinase C to Cdc42. *Nat Cell Biol* **2**, 531-539, doi:10.1038/35019573 (2000).

304 Qiu, R. G., Abo, A. & Steven Martin, G. A human homolog of the C. elegans polarity determinant Par-6 links Rac and Cdc42 to PKCzeta signaling and cell transformation. *Curr Biol* **10**, 697-707, doi:10.1016/s0960-9822(00)00535-2 (2000).

305 Xi, G., Shen, X., Rosen, C. J. & Clemmons, D. R. IRS-1 Functions as a Molecular Scaffold to Coordinate IGF-I/IGFBP-2 Signaling During Osteoblast Differentiation. *J Bone Miner Res* **31**, 1300-1314, doi:10.1002/jbmr.2791 (2016).

306 Nakanishi, H., Brewer, K. A. & Exton, J. H. Activation of the zeta isozyme of protein kinase C by phosphatidylinositol 3,4,5-trisphosphate. *J Biol Chem* **268**, 13-16 (1993).

307 Van Der Hoeven, P. C., Van Der Wal, J. C., Ruurs, P. & Van Blitterswijk, W. J. Protein kinase C activation by acidic proteins including 14-3-3. *Biochem J* **347 Pt 3**, 781-785, doi:10.1042/0264-6021:3470781 (2000).

308 Hong, Y. aPKC: the Kinase that Phosphorylates Cell Polarity. *F1000Res* **7**, doi:10.12688/f1000research.14427.1 (2018).

309 Schonwasser, D. C., Marais, R. M., Marshall, C. J. & Parker, P. J. Activation of the mitogen-activated protein kinase/extracellular signal-regulated kinase pathway by conventional, novel, and atypical protein kinase C isotypes. *Mol Cell Biol* **18**, 790-798, doi:10.1128/mcb.18.2.790 (1998).

310 Lemmon, M. A. & Schlessinger, J. Cell signaling by receptor tyrosine kinases. *Cell* **141**, 1117-1134, doi:10.1016/j.cell.2010.06.011 (2010).

311 Yarden, Y. & Schlessinger, J. Epidermal growth factor induces rapid, reversible aggregation of the purified epidermal growth factor receptor. *Biochemistry* **26**, 1443-1451, doi:10.1021/bi00379a035 (1987).

312 Singh, B., Carpenter, G. & Coffey, R. J. EGF receptor ligands: recent advances. *F1000Res* **5**, doi:10.12688/f1000research.9025.1 (2016).

313 Zhang, X., Gureasko, J., Shen, K., Cole, P. A. & Kuriyan, J. An allosteric mechanism for activation of the kinase domain of epidermal growth factor receptor. *Cell* **125**, 1137-1149, doi:10.1016/j.cell.2006.05.013 (2006).

314 Waters, K. M., Liu, T., Quesenberry, R. D., Willse, A. R., Bandyopadhyay, S., Kathmann, L. E., Weber, T. J., Smith, R. D., Wiley, H. S. & Thrall, B. D. Network analysis of

epidermal growth factor signaling using integrated genomic, proteomic and phosphorylation data. *PLoS One* **7**, e34515, doi:10.1371/journal.pone.0034515 (2012).

315 Goi, T., Shipitsin, M., Lu, Z., Foster, D. A., Klinz, S. G. & Feig, L. A. An EGF receptor/Ral-GTPase signaling cascade regulates c-Src activity and substrate specificity. *EMBO J* **19**, 623-630, doi:10.1093/emboj/19.4.623 (2000).

316 Batzer, A. G., Rotin, D., Urena, J. M., Skolnik, E. Y. & Schlessinger, J. Hierarchy of binding sites for Grb2 and Shc on the epidermal growth factor receptor. *Mol Cell Biol* **14**, 5192-5201, doi:10.1128/mcb.14.8.5192 (1994).

317 Pelicci, G., Lanfrancone, L., Grignani, F., McGlade, J., Cavallo, F., Forni, G., Nicoletti, I., Grignani, F., Pawson, T. & Pelicci, P. G. A novel transforming protein (SHC) with an SH2 domain is implicated in mitogenic signal transduction. *Cell* **70**, 93-104, doi:10.1016/0092-8674(92)90536-l (1992).

318 Chardin, P., Camonis, J. H., Gale, N. W., van Aelst, L., Schlessinger, J., Wigler, M. H. & Bar-Sagi, D. Human Sos1: a guanine nucleotide exchange factor for Ras that binds to GRB2. *Science* **260**, 1338-1343, doi:10.1126/science.8493579 (1993).

319 Terrell, E. M. & Morrison, D. K. Ras-Mediated Activation of the Raf Family Kinases. *Cold Spring Harb Perspect Med* **9**, doi:10.1101/cshperspect.a033746 (2019).

320 Mattoon, D. R., Lamothe, B., Lax, I. & Schlessinger, J. The docking protein Gab1 is the primary mediator of EGF-stimulated activation of the PI-3K/Akt cell survival pathway. *BMC Biol* **2**, 24, doi:10.1186/1741-7007-2-24 (2004).

321 Alessi, D. R., James, S. R., Downes, C. P., Holmes, A. B., Gaffney, P. R., Reese, C. B. & Cohen, P. Characterization of a 3-phosphoinositide-dependent protein kinase which phosphorylates and activates protein kinase Balpha. *Curr Biol* **7**, 261-269, doi:10.1016/s0960-9822(06)00122-9 (1997).

322 Stokoe, D., Stephens, L. R., Copeland, T., Gaffney, P. R., Reese, C. B., Painter, G. F., Holmes, A. B., McCormick, F. & Hawkins, P. T. Dual role of phosphatidylinositol-3,4,5-trisphosphate in the activation of protein kinase B. *Science* **277**, 567-570, doi:10.1126/science.277.5325.567 (1997).

323 Miettinen, P. J., Berger, J. E., Meneses, J., Phung, Y., Pedersen, R. A., Werb, Z. & Derynck, R. Epithelial immaturity and multiorgan failure in mice lacking epidermal growth factor receptor. *Nature* **376**, 337-341, doi:10.1038/376337a0 (1995).

324 Nahta, R., Yuan, L. X., Zhang, B., Kobayashi, R. & Esteva, F. J. Insulin-like growth factor-I receptor/human epidermal growth factor receptor 2 heterodimerization contributes to trastuzumab resistance of breast cancer cells. *Cancer Res* **65**, 11118-11128, doi:10.1158/0008-5472.CAN-04-3841 (2005).

325 Kull, F. C., Jr., Jacobs, S., Su, Y. F., Svoboda, M. E., Van Wyk, J. J. & Cuatrecasas, P. Monoclonal antibodies to receptors for insulin and somatomedin-C. *J Biol Chem* **258**, 6561-6566 (1983).

326 Seely, B. L., Reichart, D. R., Takata, Y., Yip, C. & Olefsky, J. M. A functional assessment of insulin/insulin-like growth factor-I hybrid receptors. *Endocrinology* **136**, 1635-1641, doi:10.1210/endo.136.4.7895674 (1995).

327 Kadowaki, T., Koyasu, S., Nishida, E., Sakai, H., Takaku, F., Yahara, I. & Kasuga, M. Insulin-like growth factors, insulin, and epidermal growth factor cause rapid cytoskeletal reorganization in KB cells. Clarification of the roles of type I insulin-like growth factor receptors and insulin receptors. *J Biol Chem* **261**, 16141-16147 (1986).

328 Favelyukis, S., Till, J. H., Hubbard, S. R. & Miller, W. T. Structure and autoregulation of the insulin-like growth factor 1 receptor kinase. *Nat Struct Biol* **8**, 1058-1063, doi:10.1038/nsb721 (2001).
329 Kiely, P. A., Sant, A. & O'Connor, R. RACK1 is an insulin-like growth factor 1 (IGF-1) receptor-interacting protein that can regulate IGF-1-mediated Akt activation and protection from cell death. *J Biol Chem* **277**, 22581-22589, doi:10.1074/jbc.M201758200 (2002).
330 Sasaoka, T., Ishiki, M., Sawa, T., Ishihara, H., Takata, Y., Imamura, T., Usui, I., Olefsky, J. M. & Kobayashi, M. Comparison of the insulin and insulin-like growth factor 1 mitogenic intracellular signaling pathways. *Endocrinology* **137**, 4427-4434, doi:10.1210/endo.137.10.8828504 (1996).
331 Tartare-Deckert, S., Sawka-Verhelle, D., Murdaca, J. & Van Obberghen, E. Evidence for a differential interaction of SHC and the insulin receptor substrate-1 (IRS-1) with the insulin-like growth factor-I (IGF-I) receptor in the yeast two-hybrid system. *J Biol Chem* **270**, 23456-23460, doi:10.1074/jbc.270.40.23456 (1995).
332 Giorgetti, S., Ballotti, R., Kowalski-Chauvel, A., Tartare, S. & Van Obberghen, E. The insulin and insulin-like growth factor-I receptor substrate IRS-1 associates with and activates phosphatidylinositol 3-kinase in vitro. *J Biol Chem* **268**, 7358-7364 (1993).
333 Liu, J. P., Baker, J., Perkins, A. S., Robertson, E. J. & Efstratiadis, A. Mice carrying null mutations of the genes encoding insulin-like growth factor I (Igf-1) and type 1 IGF receptor (Igf1r). *Cell* **75**, 59-72 (1993).
334 Yakar, S., Liu, J. L., Stannard, B., Butler, A., Accili, D., Sauer, B. & LeRoith, D. Normal growth and development in the absence of hepatic insulin-like growth factor I. *Proc Natl Acad Sci U S A* **96**, 7324-7329, doi:10.1073/pnas.96.13.7324 (1999).
335 Han, C. Z., Juncadella, I. J., Kinchen, J. M., Buckley, M. W., Klibanov, A. L., Dryden, K., Onengut-Gumuscu, S., Erdbrugger, U., Turner, S. D., Shim, Y. M., Tung, K. S. & Ravichandran, K. S. Macrophages redirect phagocytosis by non-professional phagocytes and influence inflammation. *Nature* **539**, 570-574, doi:10.1038/nature20141 (2016).
336 Girnita, L., Worrall, C., Takahashi, S., Seregard, S. & Girnita, A. Something old, something new and something borrowed: emerging paradigm of insulin-like growth factor type 1 receptor (IGF-1R) signaling regulation. *Cell Mol Life Sci* **71**, 2403-2427, doi:10.1007/s00018-013-1514-y (2014).
337 Cozens, A. L., Yezzi, M. J., Yamaya, M., Steiger, D., Wagner, J. A., Garber, S. S., Chin, L., Simon, E. M., Cutting, G. R., Gardner, P. & et al. A transformed human epithelial cell line that retains tight junctions post crisis. *In Vitro Cell Dev Biol* **28A**, 735-744 (1992).
338 DuBridge, R. B., Tang, P., Hsia, H. C., Leong, P. M., Miller, J. H. & Calos, M. P. Analysis of mutation in human cells by using an Epstein-Barr virus shuttle system. *Mol Cell Biol* **7**, 379-387 (1987).
339 Gey, G. O., Coffman, W. D. & Kubicek, M. T. Tissue Culture Studies of the Proliferative Capacity of Cervical Carcinoma and Normal Epithelium. *Cancer Research* **12**, 264-265 (1952).
340 Kwilas, A. R., Yednak, M. A., Zhang, L., Liesman, R., Collins, P. L., Pickles, R. J. & Peeples, M. E. Respiratory syncytial virus engineered to express the cystic fibrosis transmembrane conductance regulator corrects the bioelectric phenotype of human cystic fibrosis airway epithelium in vitro. *J Virol* **84**, 7770-7781, doi:10.1128/JVI.00346-10 (2010).

341 Yun, T., Park, A., Hill, T. E., Pernet, O., Beaty, S. M., Juelich, T. L., Smith, J. K., Zhang, L., Wang, Y. E., Vigant, F., Gao, J., Wu, P., Lee, B. & Freiberg, A. N. Efficient reverse genetics reveals genetic determinants of budding and fusogenic differences between Nipah and Hendra viruses and enables real-time monitoring of viral spread in small animal models of henipavirus infection. *J Virol* **89**, 1242-1253, doi:10.1128/JVI.02583-14 (2015).
342 Shen, Y., Rosendale, M., Campbell, R. E. & Perrais, D. pHuji, a pH-sensitive red fluorescent protein for imaging of exo- and endocytosis. *J Cell Biol* **207**, 419-432, doi:10.1083/jcb.201404107 (2014).
343 Ternette, N., Stefanou, D., Kuate, S., Uberla, K. & Grunwald, T. Expression of RNA virus proteins by RNA polymerase II dependent expression plasmids is hindered at multiple steps. *Virol J* **4**, 51, doi:10.1186/1743-422X-4-51 (2007).
344 Cong, R., Das, S. & Bouvet, P. in *The Nucleolus* (ed Mark O. J. Olson) 185-212 (Springer New York, 2011).
345 Fujiki, H., Watanabe, T. & Suganuma, M. Cell-surface nucleolin acts as a central mediator for carcinogenic, anti-carcinogenic, and disease-related ligands. *J Cancer Res Clin Oncol* **140**, 689-699, doi:10.1007/s00432-014-1587-5 (2014).
346 Denny, P. W., Gokool, S., Russell, D. G., Field, M. C. & Smith, D. F. Acylation-dependent protein export in Leishmania. *J Biol Chem* **275**, 11017-11025, doi:10.1074/jbc.275.15.11017 (2000).
347 Nadolski, M. J. & Linder, M. E. Protein lipidation. *FEBS J* **274**, 5202-5210, doi:10.1111/j.1742-4658.2007.06056.x (2007).
348 Hernandez, J. L., Davda, D., Majmudar, J. D., Won, S. J., Prakash, A., Choi, A. I. & Martin, B. R. Correlated S-palmitoylation profiling of Snail-induced epithelial to mesenchymal transition. *Mol Biosyst* **12**, 1799-1808, doi:10.1039/c6mb00019c (2016).
349 Serwa, R. A., Abaitua, F., Krause, E., Tate, E. W. & O'Hare, P. Systems Analysis of Protein Fatty Acylation in Herpes Simplex Virus-Infected Cells Using Chemical Proteomics. *Chem Biol* **22**, 1008-1017, doi:10.1016/j.chembiol.2015.06.024 (2015).
350 Thinon, E., Fernandez, J. P., Molina, H. & Hang, H. C. Selective Enrichment and Direct Analysis of Protein S-Palmitoylation Sites. *J Proteome Res* **17**, 1907-1922, doi:10.1021/acs.jproteome.8b00002 (2018).
351 Wilson, J. P., Raghavan, A. S., Yang, Y. Y., Charron, G. & Hang, H. C. Proteomic analysis of fatty-acylated proteins in mammalian cells with chemical reporters reveals S-acylation of histone H3 variants. *Mol Cell Proteomics* **10**, M110 001198, doi:10.1074/mcp.M110.001198 (2011).
352 Won, S. J. & Martin, B. R. Temporal Profiling Establishes a Dynamic S-Palmitoylation Cycle. *ACS Chem Biol* **13**, 1560-1568, doi:10.1021/acschembio.8b00157 (2018).
353 Towler, D. A., Adams, S. P., Eubanks, S. R., Towery, D. S., Jackson-Machelski, E., Glaser, L. & Gordon, J. I. Purification and characterization of yeast myristoyl CoA:protein N-myristoyltransferase. *Proc Natl Acad Sci U S A* **84**, 2708-2712, doi:10.1073/pnas.84.9.2708 (1987).
354 Wu, X. S., Martina, J. A. & Hammer, J. A., 3rd. Melanoregulin is stably targeted to the melanosome membrane by palmitoylation. *Biochem Biophys Res Commun* **426**, 209-214, doi:10.1016/j.bbrc.2012.08.064 (2012).
355 Gammella, E., Buratti, P., Cairo, G. & Recalcati, S. The transferrin receptor: the cellular iron gate. *Metallomics* **9**, 1367-1375, doi:10.1039/c7mt00143f (2017).

356 Yap, M. C., Kostiuk, M. A., Martin, D. D., Perinpanayagam, M. A., Hak, P. G., Siddam, A., Majjigapu, J. R., Rajaiah, G., Keller, B. O., Prescher, J. A., Wu, P., Bertozzi, C. R., Falck, J. R. & Berthiaume, L. G. Rapid and selective detection of fatty acylated proteins using omega-alkynyl-fatty acids and click chemistry. *J Lipid Res* **51**, 1566-1580, doi:10.1194/jlr.D002790 (2010).

357 Farin, K., Schokoroy, S., Haklai, R., Cohen-Or, I., Elad-Sfadia, G., Reyes-Reyes, M. E., Bates, P. J., Cox, A. D., Kloog, Y. & Pinkas-Kramarski, R. Oncogenic synergism between ErbB1, nucleolin, and mutant Ras. *Cancer Res* **71**, 2140-2151, doi:10.1158/0008-5472.CAN-10-2887 (2011).

358 Warrener, P. & Petryshyn, R. Phosphorylation and proteolytic degradation of nucleolin from 3T3-F442A cells. *Biochem Biophys Res Commun* **180**, 716-723, doi:10.1016/s0006-291x(05)81124-6 (1991).

359 Davis, D. M. Intercellular transfer of cell-surface proteins is common and can affect many stages of an immune response. *Nat Rev Immunol* **7**, 238-243, doi:10.1038/nri2020 (2007).

360 Pasquier, J., Guerrouahen, B. S., Al Thawadi, H., Ghiabi, P., Maleki, M., Abu-Kaoud, N., Jacob, A., Mirshahi, M., Galas, L., Rafii, S., Le Foll, F. & Rafii, A. Preferential transfer of mitochondria from endothelial to cancer cells through tunneling nanotubes modulates chemoresistance. *J Transl Med* **11**, 94, doi:10.1186/1479-5876-11-94 (2013).

361 Burtey, A., Wagner, M., Hodneland, E., Skaftnesmo, K. O., Schoelermann, J., Mondragon, I. R., Espedal, H., Golebiewska, A., Niclou, S. P., Bjerkvig, R., Kogel, T. & Gerdes, H. H. Intercellular transfer of transferrin receptor by a contact-, Rab8-dependent mechanism involving tunneling nanotubes. *FASEB J* **29**, 4695-4712, doi:10.1096/fj.14-268615 (2015).

362 Dance, A. Core Concept: Cells nibble one another via the under-appreciated process of trogocytosis. *Proc Natl Acad Sci U S A* **116**, 17608-17610, doi:10.1073/pnas.1912252116 (2019).

363 Vanherberghen, B., Andersson, K., Carlin, L. M., Nolte-'t Hoen, E. N., Williams, G. S., Hoglund, P. & Davis, D. M. Human and murine inhibitory natural killer cell receptors transfer from natural killer cells to target cells. *Proc Natl Acad Sci U S A* **101**, 16873-16878, doi:10.1073/pnas.0406240101 (2004).

364 Abdu, Y., Maniscalco, C., Heddleston, J. M., Chew, T. L. & Nance, J. Developmentally programmed germ cell remodelling by endodermal cell cannibalism. *Nat Cell Biol* **18**, 1302-1310, doi:10.1038/ncb3439 (2016).

365 Thurlbeck, W. M. Postnatal human lung growth. *Thorax* **37**, 564-571, doi:10.1136/thx.37.8.564 (1982).

366 Techaarpornkul, S., Collins, P. L. & Peeples, M. E. Respiratory syncytial virus with the fusion protein as its only viral glycoprotein is less dependent on cellular glycosaminoglycans for attachment than complete virus. *Virology* **294**, 296-304, doi:10.1006/viro.2001.1340 (2002).

367 Hewlett, L. J., Prescott, A. R. & Watts, C. The coated pit and macropinocytic pathways serve distinct endosome populations. *J Cell Biol* **124**, 689-703, doi:10.1083/jcb.124.5.689 (1994).

368 Schanzer, D. L., Langley, J. M. & Tam, T. W. Hospitalization attributable to influenza and other viral respiratory illnesses in Canadian children. *Pediatr Infect Dis J* **25**, 795-800, doi:10.1097/01.inf.0000232632.86800.8c (2006).

369 Collins, P. L., Hill, M. G., Camargo, E., Grosfeld, H., Chanock, R. M. & Murphy, B. R. Production of infectious human respiratory syncytial virus from cloned cDNA confirms an

essential role for the transcription elongation factor from the 5' proximal open reading frame of the M2 mRNA in gene expression and provides a capability for vaccine development. *Proc Natl Acad Sci U S A* **92**, 11563-11567 (1995).

370 Hallak, L. K., Collins, P. L., Knudson, W. & Peeples, M. E. Iduronic acid-containing glycosaminoglycans on target cells are required for efficient respiratory syncytial virus infection. *Virology* **271**, 264-275, doi:10.1006/viro.2000.0293 (2000).

371 Hallak, L. K., Spillmann, D., Collins, P. L. & Peeples, M. E. Glycosaminoglycan sulfation requirements for respiratory syncytial virus infection. *J Virol* **74**, 10508-10513, doi:10.1128/jvi.74.22.10508-10513.2000 (2000).

372 Grosfeld, H., Hill, M. G. & Collins, P. L. RNA replication by respiratory syncytial virus (RSV) is directed by the N, P, and L proteins; transcription also occurs under these conditions but requires RSV superinfection for efficient synthesis of full-length mRNA. *J Virol* **69**, 5677-5686 (1995).

373 Ueba, O. Respiratory syncytial virus. I. Concentration and purification of the infectious virus. *Acta Med Okayama* **32**, 265-272 (1978).

374 Ayala-Nunez, N. V., Wilschut, J. & Smit, J. M. Monitoring virus entry into living cells using DiD-labeled dengue virus particles. *Methods* **55**, 137-143, doi:10.1016/j.ymeth.2011.07.009 (2011).

375 Perrone, R., Butovskaya, E., Lago, S., Garzino-Demo, A., Pannecouque, C., Palu, G. & Richter, S. N. The G-quadruplex-forming aptamer AS1411 potently inhibits HIV-1 attachment to the host cell. *Int J Antimicrob Agents* **47**, 311-316, doi:10.1016/j.ijantimicag.2016.01.016 (2016).

376 McGrath, M., Witte, O., Pincus, T. & Weissman, I. L. Retrovirus purification: method that conserves envelope glycoprotein and maximizes infectivity. *J Virol* **25**, 923-927 (1978).

377 Anderson, C. M., Georgiou, G. N., Morrison, I. E., Stevenson, G. V. & Cherry, R. J. Tracking of cell surface receptors by fluorescence digital imaging microscopy using a charge-coupled device camera. Low-density lipoprotein and influenza virus receptor mobility at 4 degrees C. *J Cell Sci* **101 (Pt 2)**, 415-425 (1992).

378 Morrison, I. E., Anderson, C. M., Georgiou, G. N., Stevenson, G. V. & Cherry, R. J. Analysis of receptor clustering on cell surfaces by imaging fluorescent particles. *Biophys J* **67**, 1280-1290, doi:10.1016/S0006-3495(94)80600-9 (1994).

379 Brindley, M. A., Hunt, C. L., Kondratowicz, A. S., Bowman, J., Sinn, P. L., McCray, P. B., Jr., Quinn, K., Weller, M. L., Chiorini, J. A. & Maury, W. Tyrosine kinase receptor Axl enhances entry of Zaire ebolavirus without direct interactions with the viral glycoprotein. *Virology* **415**, 83-94, doi:10.1016/j.virol.2011.04.002 (2011).

380 Meertens, L., Carnec, X., Lecoin, M. P., Ramdasi, R., Guivel-Benhassine, F., Lew, E., Lemke, G., Schwartz, O. & Amara, A. The TIM and TAM families of phosphatidylserine receptors mediate dengue virus entry. *Cell Host Microbe* **12**, 544-557, doi:10.1016/j.chom.2012.08.009 (2012).

381 Strange, D. P., Jiyarom, B., Pourhabibi Zarandi, N., Xie, X., Baker, C., Sadri-Ardekani, H., Shi, P. Y. & Verma, S. Axl Promotes Zika Virus Entry and Modulates the Antiviral State of Human Sertoli Cells. *MBio* **10**, doi:10.1128/mBio.01372-19 (2019).

382 English, T. J. & Hammer, D. A. The effect of cellular receptor diffusion on receptor-mediated viral binding using Brownian adhesive dynamics (BRAD) simulations. *Biophys J* **88**, 1666-1675, doi:10.1529/biophysj.104.047043 (2005).

383 Ngwuta, J. O., Chen, M., Modjarrad, K., Joyce, M. G., Kanekiyo, M., Kumar, A., Yassine, H. M., Moin, S. M., Killikelly, A. M., Chuang, G. Y., Druz, A., Georgiev, I. S., Rundlet, E. J., Sastry, M., Stewart-Jones, G. B., Yang, Y., Zhang, B., Nason, M. C., Capella, C., Peeples, M. E., Ledgerwood, J. E., McLellan, J. S., Kwong, P. D. & Graham, B. S. Prefusion F-specific antibodies determine the magnitude of RSV neutralizing activity in human sera. *Sci Transl Med* **7**, 309ra162, doi:10.1126/scitranslmed.aac4241 (2015).

384 Novavax. *A Study to Evaluate the Efficacy of an RSV F Vaccine in Older Adults*, <https://clinicaltrials.gov/ct2/show/NCT02608502> (2015).

385 Hajjar, K. A., Mauri, L., Jacovina, A. T., Zhong, F., Mirza, U. A., Padovan, J. C. & Chait, B. T. Tissue plasminogen activator binding to the annexin II tail domain. Direct modulation by homocysteine. *J Biol Chem* **273**, 9987-9993, doi:10.1074/jbc.273.16.9987 (1998).

386 Zhao, W. Q., Chen, G. H., Chen, H., Pascale, A., Ravindranath, L., Quon, M. J. & Alkon, D. L. Secretion of Annexin II via activation of insulin receptor and insulin-like growth factor receptor. *J Biol Chem* **278**, 4205-4215, doi:10.1074/jbc.M210545200 (2003).

387 Lin, D., Edwards, A. S., Fawcett, J. P., Mbamalu, G., Scott, J. D. & Pawson, T. A mammalian PAR-3-PAR-6 complex implicated in Cdc42/Rac1 and aPKC signalling and cell polarity. *Nat Cell Biol* **2**, 540-547, doi:10.1038/35019582 (2000).

388 Geetha, T., Zheng, C., Vishwaprakash, N., Broderick, T. L. & Babu, J. R. Sequestosome 1/p62, a scaffolding protein, is a newly identified partner of IRS-1 protein. *J Biol Chem* **287**, 29672-29678, doi:10.1074/jbc.M111.322404 (2012).

389 Craparo, A., Freund, R. & Gustafson, T. A. 14-3-3 (epsilon) interacts with the insulin-like growth factor I receptor and insulin receptor substrate I in a phosphoserine-dependent manner. *J Biol Chem* **272**, 11663-11669, doi:10.1074/jbc.272.17.11663 (1997).

390 Gannon-Murakami, L. & Murakami, K. Selective association of protein kinase C with 14-3-3 zeta in neuronally differentiated PC12 Cells. Stimulatory and inhibitory effect of 14-3-3 zeta in vivo. *J Biol Chem* **277**, 23116-23122, doi:10.1074/jbc.M201478200 (2002).

391 Pankiv, S., Lamark, T., Bruun, J. A., Overvatn, A., Bjorkoy, G. & Johansen, T. Nucleocytoplasmic shuttling of p62/SQSTM1 and its role in recruitment of nuclear polyubiquitinated proteins to promyelocytic leukemia bodies. *J Biol Chem* **285**, 5941-5953, doi:10.1074/jbc.M109.039925 (2010).

392 Cline, E. G. & Nelson, W. J. Characterization of mammalian Par 6 as a dual-location protein. *Mol Cell Biol* **27**, 4431-4443, doi:10.1128/MCB.02235-06 (2007).

393 Brunet, A., Kanai, F., Stehn, J., Xu, J., Sarbassova, D., Frangioni, J. V., Dalal, S. N., DeCaprio, J. A., Greenberg, M. E. & Yaffe, M. B. 14-3-3 transits to the nucleus and participates in dynamic nucleocytoplasmic transport. *J Cell Biol* **156**, 817-828, doi:10.1083/jcb.200112059 (2002).

394 Tu, X., Batta, P., Innocent, N., Prisco, M., Casaburi, I., Belletti, B. & Baserga, R. Nuclear translocation of insulin receptor substrate-1 by oncogenes and Igf-I. Effect on ribosomal RNA synthesis. *J Biol Chem* **277**, 44357-44365, doi:10.1074/jbc.M208001200 (2002).

395 Neasta, J., Kiely, P. A., He, D. Y., Adams, D. R., O'Connor, R. & Ron, D. Direct interaction between scaffolding proteins RACK1 and 14-3-3zeta regulates brain-derived neurotrophic factor (BDNF) transcription. *J Biol Chem* **287**, 322-336, doi:10.1074/jbc.M111.272195 (2012).

396 Miyata, Y., Nishida, E., Koyasu, S., Yahara, I. & Sakai, H. Protein kinase C-dependent and -independent pathways in the growth factor-induced cytoskeletal reorganization. *J Biol Chem* **264**, 15565-15568 (1989).

397 Martin, S. S., Rose, D. W., Saltiel, A. R., Klippel, A., Williams, L. T. & Olefsky, J. M. Phosphatidylinositol 3-kinase is necessary and sufficient for insulin-stimulated stress fiber breakdown. *Endocrinology* **137**, 5045-5054, doi:10.1210/endo.137.11.8895379 (1996).
398 Hou, C., Li, Y., Liu, H., Dang, M., Qin, G., Zhang, N. & Chen, R. Profiling the interactome of protein kinase C zeta by proteomics and bioinformatics. *Proteome Sci* **16**, 5, doi:10.1186/s12953-018-0134-8 (2018).